# An evaluation of safety assessment methods for a reinforced concrete frame using non-linear finite element analyses

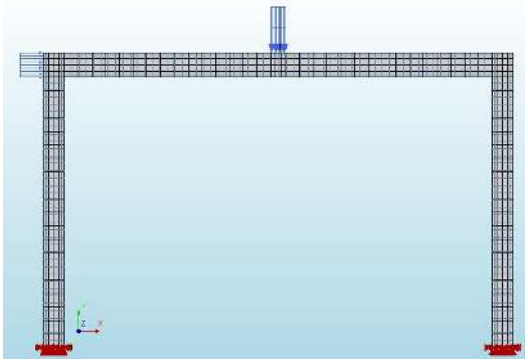

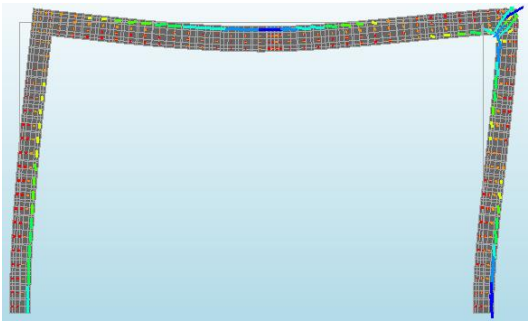

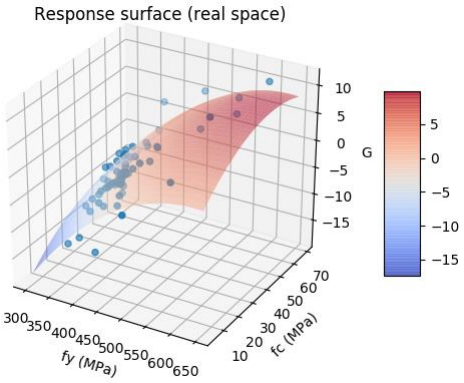


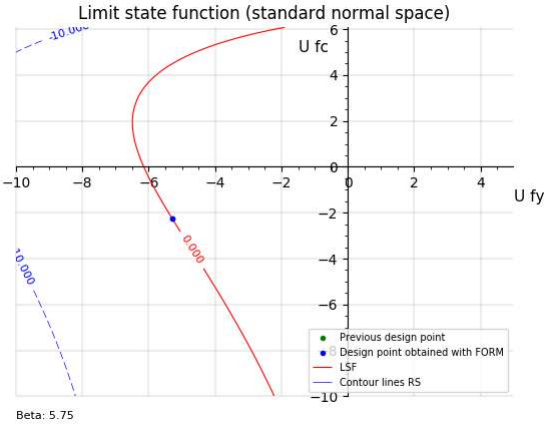


**Master of Science Thesis**

Pieter Dolron
Delft University of Technology
20 March 2018

# An evaluation of safety assessment methods for a reinforced concrete frame using non-linear finite element analyses

Master of Science Thesis

For obtaining the degree of Master of Science in Civil Engineering
at Delft University of Technology

Pieter Dolron

20 March 2018

**Graduation Committee:**

Dr. ir. M.A.N. Hendriks
Prof. dr. ir. J.G. Rots
Dr. ir. Y. Yang
Prof. dr. ir. R.D.J.M. Steenbergen

# Abstract

In order to perform a reassessment of existing structures or design new structures in a more efficient and economical way non-linear finite element (NLFE) models are used to take into account all non-linear behavior in reinforced concrete structures. The Model Code 2010 (fib, 2012) suggest several safety formats to perform non-linear finite element analyses with an intended reliability index $\beta_R = 3.04$. The safety formats seems to be safe for statically determinate structures with a predictable failure mode. For instance a bending failure in a simply supported reinforced concrete beam. However it is unclear if the intended safety level is met for statically indeterminate structures. Since the redundancy of the structural system and the several possibilities to redistribute the internal forces could lead to unpredictable failure modes.

In this thesis three reinforced concrete portal frame designs are used to evaluate the probability of failure of the structural resistance determined with the safety formats i.e. the safety of the safety formats will be assessed. The ductility of the portal frame designs determines the degree of redistribution of the internal forces. Therefore this case study will focus on three portal frame designs with all a different ductile behavior. The global design resistance is determined according to the following safety formats: the global resistance factor method (GRFm), the estimation of a coefficient of variation (ECOV) method and the partial factor method (PFm). A comparison is made with the local design resistance of the portal frame designs according to the Eurocode 2 using partial safety factors.

The reliability level of the structural design resistance according to the least conservative safety formats is determined for each portal frame design. Several response surfaces were constructed and the first order reliability method (FORM) was used to determine the reliability level. In case of relatively low material and geometrical uncertainties the safety formats lead to a structural resistance that can safely be used i.e. the intended reliability level is met. However when the detailing uncertainties in concrete frame corners are relatively large these uncertainties should be implemented in the safety formats. Further research and more experimental results are needed to make a better estimation of the (model) uncertainties possible.

Finally, the used methods are evaluated and several comments are given on the difficulties of using those methods. Constructing a response surface in combination with the FORM in order to find the design point is definitely not an automated process as the mathematical procedures seems to indicate.

# Contents

# Preface

This thesis concludes my master program Structural Engineering at the faculty Civil Engineering and Geosciences at Delft University of Technology.

I would like to express my gratitude towards my graduation committee: Dr. ir. M.A.N. Hendriks, Prof. dr. ir. J.G. Rots, Dr. ir. Y. Yang and Prof. dr. ir. R.D.J.M. Steenbergen. I especially would like to thank my first supervisor Max Hendriks for sharing much knowledge and being available to discuss the progress during the project.

Last but not least, I would like to thank my family and friends for their support.

Delft, March 2018

Pieter Dolron

# 1 Introduction

The infrastructure is growing old and the traffic load will increase in the coming years. According to the classic design procedure old concrete bridges are not safe anymore and have to be replaced. The classic design procedure, which is mainly used in the past for structural concrete elements, is based on local safety evaluation. This means that the safety condition is evaluated for each element at each critical cross-section individually. This is a quite conservative approach due to simplified models and less redistribution of the internal forces, which lead to a conservative load carrying capacity of the structure.

More sophisticated models, namely non-linear finite element (NLFE) models, can be used to take into account the redundancy of the structural system and the capacity to redistribute the internal forces. The failure of one element does not automatically mean that the whole structural system fails. Therefore a global safety evaluation is needed to evaluate the structural system. In order to extent the lifespan of the existing concrete bridges, a reassessment using non-linear finite element analyses can be used to reveal any additional 'hidden' load carrying capacity. Therefore existing concrete structures can still be safe enough to resists the increasing traffic load.

This thesis will focus on a case study of a portal frame, which can for instance be used to support a bridge. The reinforced concrete portal frame is loaded with a vertical load $F_v$ and a horizontal load $F_h$. The vertical load $F_v$ can be seen as the sum of the self-weight of the bridge and the traffic load. The horizontal load $F_h$ represent the wind load on the bridge. The loading model is a huge simplification from reality but it is only meant to place the portal frame in a context. The portal frame discussed in this thesis is a small scale design in order to compare the NLFE model with experimental results. The portal frame is designed using a local safety approach to resist the vertical and horizontal load $F_v$ and $F_h$. Any additional capacity of the portal frame can be found using the safety formats for NLFE analysis, which are described in the Model Code 2010 (fib, 2012). In this case additional capacity means additional vertical loading on top of the already present vertical and horizontal load $F_v$ and $F_h$. In order to verify the safety level of the maximum structural resistance according to the safety formats a safety assessment will be performed in this thesis. The safety level will be verified using a global safety approach.

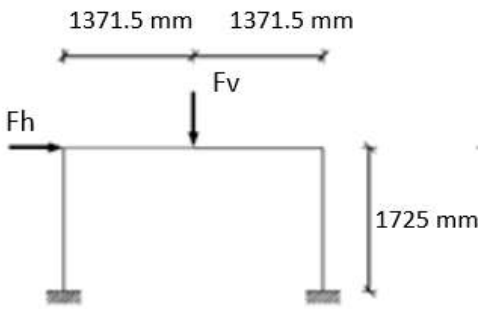


*Figure 1. Reinforced concrete portal frame with loads determined by a local safety evaluation.*

This thesis will deepen the work of Blomfors (2014) and Blomfors et al. (2016) where a large scale NLFE model of a reinforced concrete frame was analyzed. The safety of two loading histories was assessed. In one of the cases the safety level of the ECOV method was lower than the intended safety level, which lead to an unsafe situation. This thesis will focus on the safety of three reinforced concrete portal frame designs. Each design has a different influence on the ductility of the structure and therefore the capacity to redistribute the internal forces. In this case the ductility means the ability of a frame to form a plastic mechanism. A ductile frame can form a plastic mechanism and is more able to redistribute the internal forces compared to a brittle frame, where a brittle failure almost immediately lead to the total collapse of the frame.

## 1.1 Background

### 1.1.1 Local safety evaluation

The classic design approach for reinforced concrete structures is based on a linear elastic model to determine the internal forces $E$ resulting from an external load $F$. The critical section of each component is designed to resist (resistance: $R$) the internal forces using a local non-linear model or empirical model. Subsequently the safety of each element is evaluated using a local safety evaluation. A local safety evaluation leads often to conservative and uneconomic reinforced concrete structures. According to the Eurocode 0 (NEN-EN 1990, 2011) the reliability level is met when the following local safety check is fulfilled:

$$E_d \leq R_d, \tag{1.1}$$

where $E_d$ is the design value of the load effects e.g. internal forces, stresses, etc. resulting from the external load $F_d$ and $R_d$ is the corresponding design resistance at the critical section of an element. The design value of the load effects is defined as (NEN-EN 1990, 2011):

$$E_d = E(\gamma_{F,i}\, F_{rep}, \boldsymbol{X_d}, \boldsymbol{a_d}) \qquad i \geq 1, \tag{1.1a}$$

where:

| | |
|---|---|
| $\gamma_{Sd}$ | is the partial factor that accounts for model uncertainties; |
| $\gamma_{F,i} = \gamma_{f,i}\, \gamma_{Sd}$ | is the partial factor for the load, with $\gamma_{f,i}$ the partial factor for unfavorable fluctuations of $F$ compared to $F_{rep}$; |
| $F_{d,i} = \gamma_{F,i}\, F_{rep,i}$ | is the design value of the external load; |
| $F_{rep} = \psi\, F_k$ | is the representative load with $\psi$ is the combination factor and $F_k$ the characteristic load; |
| $\boldsymbol{X_d}$ | is the vector with the design material values; |
| $\boldsymbol{a_d}$ | is the vector with the design values of the geometrical variables, mostly equal to the nominal value and in case of significant influence on the structural safety $\pm\, \Delta a$. |

The design value of resistance is defined as (NEN-EN 1990, 2011):

$$R_d = R\left(\frac{X_{k,i}}{\gamma_{M,i}}; \boldsymbol{a_d}\right) \qquad i \geq 1, \tag{1.1b}$$

where:

| | |
|---|---|
| $\gamma_{Rd}$ | is the partial factor that accounts for model uncertainties and also includes $\eta_i$ the conversion factor considering volume and scale effects and influences of temperature and humidity; |
| $\gamma_{M,i} = \gamma_{Rd}\,\gamma_{m,i}$ | is the partial factor for the resistance, with $\gamma_m$ the local resistance factor for unfavorable fluctuations of $X$ compared to $X_k$ and the stochastic nature of $\eta$; |
| $X_{d,i} = \frac{X_{k,i}}{\gamma_{M,i}}$ | is the design material value with $X_k$ is the characteristic material value; |
| $\boldsymbol{a_d} = a_{nom}\ (\pm\ \Delta a)$ | is the vector with the design values of the geometrical variables (see equation (1.1a)). |

The partial safety factors for the resistance in a local safety evaluation are related to the characteristic material values.

### 1.1.2 Global safety evaluation

The classical linear elastic approach (local safety evaluation) leads to internal forces that can differ significantly from reality. The stiffness of the structure changes due to the cracking of concrete and yielding of the reinforcement steel. The redundancy of the structural system and the capacity to redistribute the internal forces is especially high for statically indeterminate structures. In order to assess this non-linear material behavior NLFE analyses can be performed, which can account for non-linear material behavior. A NLFE model is the most accurate model to determine the response of a structural reinforced concrete system. Especially for a statically indeterminate structure where the failure of one element does not necessarily lead to the failure of the structural system. Statically indeterminate structures provides several ways to redistribute the internal forces and can find new equilibrium paths. Therefore global safety evaluation is needed to assess the safety of the structural system. The global safety check according to the Model Code 2010 (fib, 2012) is defined as:

$$F_d \leq R_d, \tag{1.2}$$

where: $F_d$ is design value of the external load and $R_d$ is the design resistance of the structural system. The design value of the external load $F_d$ can be found in the same manner as in equation (1.1a). The design resistance $R_d$ is defined as (fib, 2012):

$$R_d = \frac{R_m}{\gamma_R\,\gamma_{Rd}}, \tag{1.2a}$$

where:

| | |
|---|---|
| $R_m$ | is the mean value of resistance (determined with a NLFE analysis with mean material values); |
| $\gamma_R$ | is the global resistance factor; |
| $\gamma_{Rd}$ | is the model uncertainty factor. |

The partial safety factors for the resistance in a global safety evaluation are related to the mean material values. The value of the model uncertainty is related to the uncertainty of the non-linear finite element model. In the Model Code 2010 (fib, 2012) the recommended values are:

$\gamma_{Rd} = 1.0$ for no uncertainties;
$\gamma_{Rd} = 1.06$ for models with low uncertainties;
$\gamma_{Rd} = 1.1$ for models with high uncertainties.

## 1.2 Problem description

The safety formats as presented in the Model Code 2010 (fib, 2012) will be used to determine the design resistance $R_d$ of the reinforced concrete portal frame. The design resistance of the structure according to the corresponding safety format (SF) will be denoted as: $R_{SF}$ and is determined using a global safety approach.

A global safety evaluation of equation (1.2) should result in an overall target reliability of at least: $\beta_t = 3.8$. However, in this thesis only the resistance side of equation (1.2) will be evaluated since the main interest is to determine the safety of the design resistance $R_{SF}$. Therefore the design resistance $R_{SF}$ obtained according to a corresponding safety format should lead to a reliability index of at least: $\beta_R = \alpha_R \, \beta_t = 0.8 \cdot 3.8 = \ 3.04$, which corresponds to a probability of failure of $p_f = \Phi(-\beta_R) = 10^{-3}$. The safety formats seems to be safe for statically determinate structures with a predictable failure mode and will lead to the intended reliability index $\beta_R$ (Blomfors, Engen, & Plos, Evaluation of safety formats for non-linear finite element analyses of statically indeterminate concrete structures subjected to different load paths, 2016). However it is unclear whether the safety formats lead to a safe design resistances for statically indeterminate structures. Redistribution of the internal forces leads to unpredictable failure modes which could influence the safety of the structure.

In this thesis a safety assessment will be performed for a statically indeterminate reinforced concrete frame (figure 1). The goal is to find out whether the target reliability $\beta_R$ of the safety formats is met in order to safely use the safety formats. Furthermore a comparison between a local and a global safety approach will be made in order to find out if a global safety approach could lead to any additional capacity.

### 1.2.1 Global safety evaluation of a portal frame using implicit limit state functions

The reliability level $\beta_R$ and the probability of failure of the safety formats can be determined with the following implicit limit state function (Blomfors, Engen, & Plos, Evaluation of safety formats for non-linear finite element analyses of statically indeterminate concrete structures subjected to different load paths, 2016):

$$G(\boldsymbol{X}) = \theta_m \, R(\boldsymbol{X}) - R_{SF}, \tag{1.3}$$

where $\theta_m$ is the model uncertainty of the NLFE model, $R(\boldsymbol{X})$ is the total resistance of a NLFE analysis using stochastic variables $\boldsymbol{X}$ and $R_{SF}$ is the total resistance of the NLFE model according to the corresponding safety format $R_{SF}$. The measure of the total structural resistance is chosen to be the sum of the vertical and horizontal load (Blomfors, Engen, & Plos, Evaluation of safety formats for non-linear finite element analyses of statically indeterminate concrete structures subjected to different load paths, 2016). The measure of the structural resistance is not a real physical quantity. However, this is not needed since this quantity is only used to determine a possible failure of the portal frame. The limit state function is implicit since there is no analytical model available to assess the failure modes. Therefore a NLFE model will be used. This implicit limit state function will be used to perform a global safety evaluation of the design resistance according to the safety formats.

## 1.3 Aim

The aim of this thesis is to evaluate safety assessment methods for a reinforced concrete frame. A distinction will be made between local and global safety assessment methods. The classical design approach to obtain the structural design resistance of reinforced concrete structures using a local safety assessment method is described in the Eurocode 2 (NEN-EN 1992 -1-1, 2011). A global safety assessment method to obtain the structural design resistance of reinforced concrete structures is proposed in the Model Code 2010 (fib, 2012). A global safety evaluation should be performed using the safety formats (Model Code 2010) in combination with non-linear finite element analyses.

The degree of redistribution can have an influence on the safety level, especially for statically indeterminate structures. The ductility of the portal frame determines the degree of redistribution of the internal forces. Therefore this case study will focus on three portal frame designs with all a different ductile behavior:

- Design 1: basic design
- Design 2: higher longitudinal reinforcement ratio (compared to design 1)
- Design 3: higher concrete strength class (compared to design 1)

The case study of three designs of a reinforced concrete portal frame will be used to determine the structural resistance using a local and a global safety approach. A level II reliability method will be used to determine if the intended reliability level $\beta_R = 3.04$ of the safety formats is met in order to safely use the safety formats. A schematic representation of the safety assessment methods that will be evaluated is given in figure 2. The dotted line stands for the comparison between the local and the global safety approach using a level I reliability method. The arrow represents the verification of the intended reliability level used for the safety formats by means of a level II reliability method.

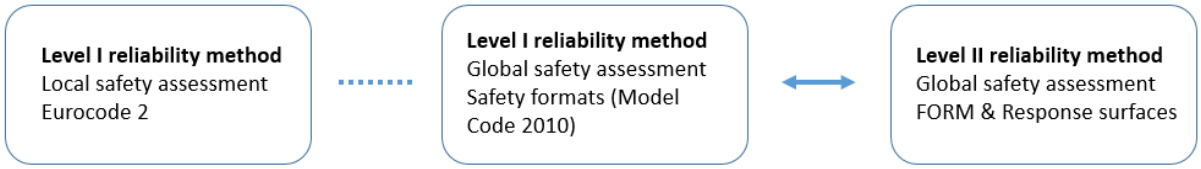


*Figure 2. Schematic representation of the safety assessment methods*

## 1.4 Limitations

- Only the reliability of the structural resistance will be assessed in this thesis
- Only the total load carrying capacity in ULS will be assessed in this thesis.
- Just three portal frame designs are used to evaluate the safety formats.
- Just one loading path will be assed.
- Just two experimental results where available which lead to less information about the model uncertainty.
- Only the first order reliability method (FORM) in combination with a response surface is used to determine the reliability index.

## 1.5 Outline of contents

An introduction to the subject of this thesis is made in chapter 1. The problem is introduced and the aim of this thesis is given. Furthermore the limitations of this thesis are shortly discussed.

Chapter 2 contains a review of reliability theory that is used to calculate the probability of failure of a structural system. A general introduction is made and after that the used reliability methods are described to perform a safety assessment.

In chapter 3 the safety formats are discussed. The safety formats are used to determine the global design resistance of a structural system by means of a NLFE model. Only the safety formats which are presented in the Model code 2010 (fib, 2012) will be discussed in this thesis.

Three different reinforced concrete portal frame designs are presented in chapter 4. The ductility and therefore the ability to redistribute the internal forces is different for each frame. The main uncertainty is the rotational capacity of the corner of a reinforced concrete portal frame. Several detailing possibilities will be elaborated. The three introduced portal frame design have a different structural resistance. The resistance of each frame is evaluated using a local and a global safety approach. The resistance obtained from a local design approach is believed to be conservative. Therefore a global safety approach by means of NLFE analyses in combination with the safety formats is used to determine if there is any additional capacity. Eventually, the main goal of this thesis is to determine the safety of the structural resistance obtained by the safety formats (global safety evaluation). This will be verified in chapter 7.

Chapter 5 contains the structural analysis of an experiment (Seraj, Kotsovos, & Pavlovic, 1995) performed on two different portal frame designs. The portal frame designs used in this experiment are similar to design 1 given in chapter 4. The experiment is used to determine the real structural resistance and to analyze the failure modes of the reinforced concrete portal frames. A local safety approach according to the Eurocode 2 (NEN-EN 1992 -1-1, 2011) will be used to predict the failure modes. This failure modes will be compared to the failure modes obtained from the experiment. Finally, a NLFE model will be created based on the experiment. The structural resistance of the NLFE model and the experiment will be compared to determine the model uncertainty.

In chapter 6 the uncertainties are explained that have an influence on the structural resistance of a portal frame. The dominating uncertainties are taken into account based on the influence on the failure mode.

Chapter 7 contains the global safety assessment of the reinforced concrete portal frame. A level II reliability method is used to determine if the intended reliability of the safety formats is met i.e. the validity of the safety formats will be determined. Three cases are introduced based on the uncertainties defined in chapter 6 and each case has a different influence on the rotational capacity of the corner and therefore the structural resistance of the portal frame.

Chapter 8 contains the conclusions of this thesis. Also suggestions for further work will be given.

# 2 Review of reliability analysis

## 2.1 Principles of limit state design

In general a structure is safe when the structural resistance $R$ is larger than the loads $S$ (solicitation). The limit state function (LSF) is is defined as:

$$G(\boldsymbol{X}) = R - S. \tag{2.1}$$

Where the vector $\boldsymbol{X}$ contains $n$ basic variables. The probability of failure equals: $p_f = P[G < 0]$. Figure 3 shows the variables $S$, $R$ and $G$. If $S$ and $R$ are normally distributed than $G = R - S$ is also normally distributed with the following mean and standard deviation:

$$\mu_G = \mu_R - \mu_S, \tag{2.2}$$

$$\sigma_G = \sqrt{\sigma_R^2 + \sigma_S^2}. \tag{2.3}$$

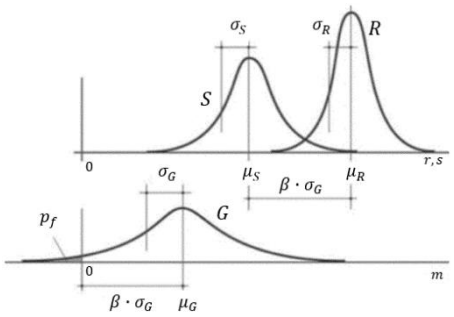


*Figure 3. Probability of failure for normally distributed variables R and S (Schneider, 2006).*

The reliability index is determined as follows:

$$\beta = \frac{\mu_G}{\sigma_G}. \tag{2.4}$$

Assuming normally distributed variables $R$ and $S$ and a linear LSF the failure probability can be calculated according to:

$$p_f = \Phi(-\beta). \tag{2.5}$$

### 2.1.1 Joint probability density function

The problem $G = R - S$ can also represented with a joint probability density function of the variables $R$ and $S$ (figure 4). The limit state function $G = 0$ separates the safe domain $G > 0$ from the failure domain $G < 0$. The probability of failure is equal to volume under the joint probability density function corresponding to the failure domain.

The distribution for the resistance and the load are $f_R(r)$ and $f_S(s)$, respectively. If $R$ and $S$ are independent the joint probability density function is:

$$f_{RS}(r,s) = f_R(r)\, f_S(s). \tag{2.6}$$

The failure probability can be calculated with the following integral:

$$p_f = \iint_{G<0} f_R(r)\, f_S(s) dr ds. \tag{2.7}$$

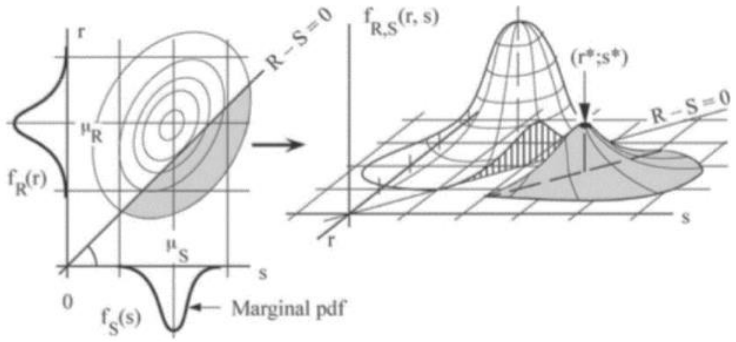


*Figure 4. The limit state function and the joint probability density function (Schneider, 2006).*

### 2.1.2 The reliability index in the normalized space

The linear limit state function $G(\boldsymbol{X})$ for two independent random variables $X_1$ and $X_2$ can be represented in the following general form:

$$G(\boldsymbol{X}) = a_0 + a_1 X_1 + a_2 X_2. \tag{2.8}$$

The normalized variables can be determined according to:

$$U_i = \frac{X_i - \mu_{Xi}}{\sigma_{Xi}}. \tag{2.9}$$

This leads to following LSF with the standard normal variables:

$$G(\boldsymbol{U}) = a_0 + a_1\,\mu_{X1} + a_2\,\mu_{X2} + a_1\,\sigma_{X1}\,U_1 + a_2\,\sigma_{X2}\,U_2, \tag{2.10}$$

with equations (2.2), (2.3) and (2.4) this can be rewritten to:

$$G(\boldsymbol{U}) = \beta - \alpha_1 U_1 - \alpha_2 U_2, \tag{2.11}$$

where:

$\beta = \frac{a_0 + a_1\,\mu_{X1} + a_2\,\mu_{X2}}{\sqrt{(a_1\,\sigma_{X1})^2 + (a_2\,\sigma_{X2})^2}}$ is the shortest distance from the origin to the LSF in standard normal space (figure 5);

$\boldsymbol{\alpha} = \alpha_i = \frac{-a_i\,\sigma_{Xi}}{\sqrt{(a_1\,\sigma_{X1})^2 + (a_2\,\sigma_{X2})^2}}$ is a unit vector normal to the LSF (figure 5).

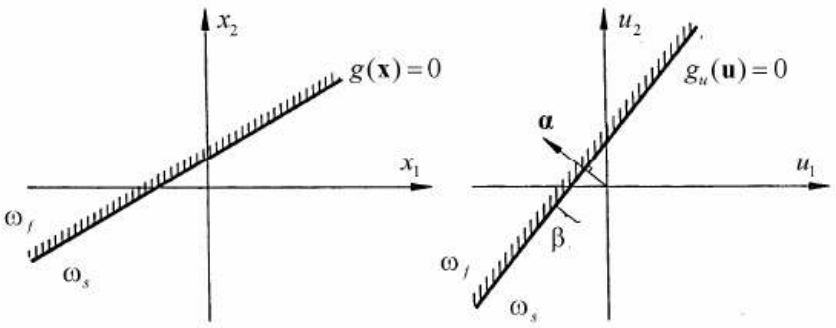


*Figure 5. Linear LSF in real (left) and standard normal (right) space (Sørensen, 2004).*

## 2.2 Reliability methods

The reliability methods can be divided into groups based on the complexity and the time needed to perform a safety assessment. Three groups of reliability methods are discussed in this paper, the level III, level II and level I methods (Jonkman, Steenbergen, Morales-Nápoles, Vrouwenvelder, & Vrijling, 2016).

### 2.2.1 Level III methods

Level III methods determine the probability of failure given by the integral (2.7) exactly. The integral can be calculated analytically, which is only possible in a limited number of simple cases. The integral can also be calculated numerically. This is only possible when the number of random variables $n$ is small. Furthermore Monte Carlo simulations (figure 6) and Importance sampling are possibilities to calculate the probability of failure exactly.

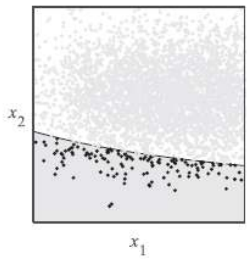


*Figure 6. Level III method: Monte Carlo simulation where the probability of failure is found by dividing the number of outcomes in the unsafe region by the total number of outcomes (Engen, 2017).*

### 2.2.2 Level II methods

Level II methods approximate the probability of failure. The non-linear limit state function will be linearized in the design point, i.e. the point on $G(\boldsymbol{X}) = 0$ with the highest probability density. The design point is also the point on $G(\boldsymbol{U}) = 0$ closest to the origin in the standard normal space (figure 7). In this thesis the first order reliability method (FORM) will be used to determine if the intended safety level of the safety formats is met.

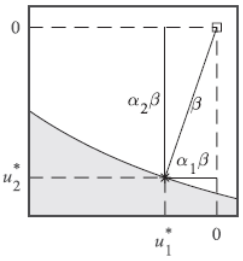


*Figure 7. Level II method: the reliability index is found by locating the point on $g(\boldsymbol{U}) = 0$ closest to the origin in the standard normal space (Engen, 2017).*

### 2.2.3 Level I methods

Level I methods are semi-probabilistic methods. The distributions of the stochastic variables are used to determine the characteristic value of the corresponding variable. The characteristic value for the resistance is a low percentile and for the load a high percentile of the probability density function. Furthermore partial factors $\gamma$'s are used to calculate the design values. The partial factors are derived using a level II method. Therefore the design procedure in the Eurocode according to the local safety evaluation is a level I method. Also the global safety evaluation used for the safety formats as presented in the Model Code 2010 (fib, 2012) is a level I method since a global safety factor is used.

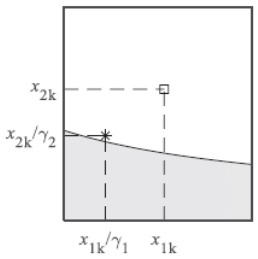


*Figure 8. Level I method: the nominal values for the basic variables $x_{ik}$ are scaled with partial factors $\gamma_i$ in order to impose an intended safety level (Engen, 2017).*

## 2.3 First order reliability method

The first order reliability method (FORM) is a level II approximation method. The explicit limit state function (LSF) should be linear and contain normally distributed variables in order to calculate the probability of failure with equation (2.5). An explicit LSF can be expressed with an analytical model in contrast to an implicit LSF as defined in equation (1.3), which is given by a NLFE model. A non-linear explicit LSF can be linearized in a certain point using a first order Taylor expansion (Jonkman, Steenbergen, Morales-Nápoles, Vrouwenvelder, & Vrijling, 2016):

$$G \approx G(x_i^*) + \sum_{i=1}^{n} \frac{\partial G(x_i^*)}{\partial X_i}(X_i - x_i^*). \tag{2.12}$$

This leads to an approximation of the LSF with the following general form:

$$G = a_0 + \sum_{i=1}^{n} a_i X_i, \tag{2.13}$$

where $a_i = \frac{\partial G(x_i^*)}{\partial X_i}$ and $a_0 = G(x_i^*) - \sum_{i=1}^{n} a_i x_i^*$ are the constant coefficients of the linear equation.

In order to reduce the error, the non-linear LSF should be linearized in the design point, which is the point on the LSF with the highest probability of failure. Therefore, the reliability index is the shortest distance from the LSF (design point) to the origin when the stochastic variables are transformed to the standard normal space:

$$\beta = \min_{z=0} \left( \sqrt{\sum_{i=1}^{n} U_i^2} \right). \tag{2.14}$$

### 2.3.1 FORM real space

The design point, the reliability index and the corresponding probability of failure can be determined using an iterative process with an explicit limit state function in the real space:

1. Estimate the design point $x_i^*$ (start with $\mu_i$).
2. Linearize the LSF $G(X_1, X_2, .., X_n)$ function according to equation (2.13). Therefore the following constants should be determined:
   $a_i = \frac{\partial G(x_i^*)}{\partial X_i}$ and $a_0 = G(x_i^*) - \sum_{i=1}^{n} a_i x_i^*$.
3. Calculate the mean, standard deviation, reliability index , sensitivity factors and the new design point with the following formulas:
   $\mu_G = a_0 + \sum_{i=1}^{n} a_i \ \mu_i,$ (2.15)
   $\sigma_G = [\sum_{i=1}^{n} (a_i \ \sigma_i)^2]^{1/2},$ (2.16)
   $\beta = \frac{\mu_G}{\sigma_G},$ (2.17)
   $\alpha_i = \frac{\sigma_i}{\sigma_G} \ a_i,$ (2.18)
   $x_i = \mu_i - \alpha_i \ \beta \ \sigma_i.$ (2.19)
4. Check convergence with: $|\beta_{i+1} - \beta_i| < \epsilon$ (e.g. $\epsilon = 10^{-3}$). If convergence is not achieved proceed with step 1.
5. Calculate the probability of failure $p_f = \Phi(-\beta)$.

### 2.3.2 FORM standard normal space

The design point, the reliability index and the corresponding probability of failure can be determined using an iterative process with an explicit limit state function in the standard normal space (Sørensen, 2004):

1. Guess $\boldsymbol{u}_0$, (vector containing first guess of the design point)
   set $i = 0$.
2. Calculate $g(\boldsymbol{u}_i)$ (explicit LSF).
3. Calculate $\nabla g(\boldsymbol{u}_i)$ (vector containing partial derivatives $\frac{\delta g}{\delta u^i}$ at place $i$).
4. Calculate an improved guess of the $\beta$ point:
   $\boldsymbol{u}_{i+1} = \nabla g(\boldsymbol{u}_i) \frac{\nabla g(\boldsymbol{u}_i)^T \boldsymbol{u}^i - g(\boldsymbol{u}_i)}{\nabla g(\boldsymbol{u}_i)^T \nabla g(\boldsymbol{u}_i)}.$ (2.20)
5. Calculate the corresponding reliability index:
   $\beta_{i+1} = \sqrt{(\boldsymbol{u}_{i+1})^T \boldsymbol{u}_{i+1}}.$ (2.21)
6. Check convergence with: $|\beta_{i+1} - \beta_i| < \epsilon$ (e.g. $\epsilon = 10^{-3}$). If convergence is not achieved then $i = i + 1$ and proceed with step 2.

When convergence is achieved the reliability index $\beta = \beta_{i+1}$, the probability of failure is $p_f = \Phi(-\beta)$, the design point is $\boldsymbol{u}_* = \boldsymbol{u}_{i+1}$ and the vector $\boldsymbol{\alpha}$ containing the sensitivity factors can be determined with:

$$\boldsymbol{\alpha} = -\frac{\nabla g(\boldsymbol{u}_*)}{|\nabla g(\boldsymbol{u}_*)|}. \quad (2.22)$$

## 2.4 Response surface method in combination with the FORM

The use of a NLFE model results in an implicit limit state function (LSF) since there is no analytical expression available for the LSF. In order to find the design point for an implicit LSF, a response surface can be fitted to the results of the NLFE model. The actual LSF $G(\boldsymbol{X})$ can be replaced by a response surface $\overline{G}(\boldsymbol{X})$, which is usually a quadratic polynomial function with undetermined coefficients (Engen, 2017):

$$G(\boldsymbol{X}) \approx \overline{G}(\boldsymbol{X}) = \boldsymbol{A}\boldsymbol{b} + e, \tag{2.23}$$

where $\overline{G}(\boldsymbol{X})$ is the response surface based on several NLFE analyses with stochastic variables $\boldsymbol{X}$, the matrix $\boldsymbol{A}$ contains the powers of the random variables $\boldsymbol{X}$, the vector $\boldsymbol{b}$ contains the undetermined coefficients and $e$ is error term. The model uncertainty can be included by multiplying equation (2.23) with the model uncertainty $\theta_m$ and can be treated as a stochastic variable.

The error term $e$ is due to an approximation of the NLFE analyses with a polynomial function and is assumed to have a mean equal to zero and an unknown standard deviation i.e. $e \sim N(0, \sigma_e^2)$ (Engen, 2017). In this thesis it is assumed that the coefficient $\boldsymbol{b}$ are deterministic i.e. neglecting the uncertainty introduced by the response surface and the correlation between the coefficients (Engen, 2017). The approximation error in terms of the failure probability will be very small and can be neglected if the experimental points are chosen in a judicious way (Zhao & Qiu, 2013).

The response surface method is often combined with the FORM following an iterative approach (Engen, 2017):

1. Fit the response surface to a set of experimental points. The first set of experimental points are usually centered on the mean values of the random variables.
2. Find the location of the design point by using the FORM.
3. Find a new center for the experimental points based on the design point.
4. Check for convergence.

In order to reduce the number of iterations needed to find the design point (reduction of NLFE analyses) several studies have been performed to optimize step 3 (Engen, 2017). The approaches of Bucher and Bourgund (1990) and Zhao and Qiu (2013) are treated in this thesis.

### 2.4.1 Approach Bucher and Bourgund (1990)

The actual LSF $G(\boldsymbol{X})$ is replaced by the response surface $\overline{G}(\boldsymbol{X})$ which is a usually a quadratic polynomial function without cross terms:

$$\overline{G}(\boldsymbol{X}) = a + \sum_{i=1}^{n} b_i\, x_i + \sum_{i=1}^{n} c_i\, x_i^2, \tag{2.24}$$

where $n$ is the number of random variables $\boldsymbol{X}$ and $a$, $b_i$ and $c_i$ are the $2n+1$ undetermined coefficients. Without cross terms the function basically represents the actual LSF $G(\boldsymbol{X})$ along the coordinate axes. The undetermined coefficients $a$, $b_i$ and $c_i$ can be solved by performing $2n+1$ NLFE analyses of $\overline{G}(\boldsymbol{X})$. The following $2n+1$ experimental points are suggested to perform the NLFE analyses: the mean values $\overline{\boldsymbol{X}}$ and $\boldsymbol{X_i} = \overline{\boldsymbol{X}}_{\boldsymbol{i}} \pm \boldsymbol{f_i}\, \boldsymbol{\sigma_i}$. In which $f_i$ is an arbitrary factor and $\sigma_i$ is the standard deviation of the considered variable. The value $f = 3$ is recommended in several papers (Zhao & Qiu, 2013). The points should also lie along the axes (figure 9) since there are no cross terms used in the RSF (equation (2.24)).

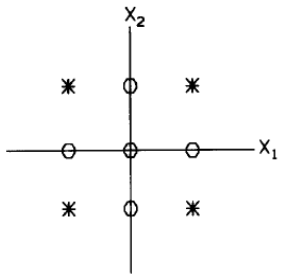


*Figure 9. Example of experimental points to obtain the RSF two random variables are considered: points along the coordinate axes indicated with ○ (mostly used for a RSF without cross terms) and other possible experiment points (could be added for a RSF with cross terms) indicated with * (Rajashekhar & Ellingwood, 1993).*

The response surface can also be written in matrix notation:

$$\overline{G}(\boldsymbol{X}) = \boldsymbol{A}\boldsymbol{b}, \tag{2.25}$$

where $\boldsymbol{A} = [1, x_1, x_2, x_1^2, x_2^2]$ is the matrix that contains the powers of random variables and $\boldsymbol{b} = [a, b_1, b_2, c_1, c_2]^T$ is the vector of undetermined coefficients when only two random variables are considered. The sample space is saturated when the number of undetermined coefficients is equal to the number of sample points. The coefficients can be determined with the following expression:

$$\boldsymbol{b} = \boldsymbol{A}^{-1}\,\boldsymbol{G}, \tag{2.26}$$

where $\boldsymbol{G}$ is a vector with NLFE analyses results of the experimental points. When the sample space is over-saturated. In this case there are more experimental points than undetermined coefficients. The coefficients $\boldsymbol{b}$ can only be determined by means of a least squares approach (Eklund, Skorve, & Strand, 2017):

$$\boldsymbol{b} = (\boldsymbol{A}^T\boldsymbol{A})^{-1}\boldsymbol{A}^T\boldsymbol{G}. \tag{2.27}$$

In order to reduce the number of NLFE analyses an over-saturated sample space should be avoided. When more accuracy is needed the cross terms can be included in the RSF:

$$\overline{G}(\boldsymbol{x}) = a + \sum_{i=1}^{n} b_i\, x_i + \sum_{i=1}^{n} c_i\, x_i^2 + \sum_{i\neq j}\sum d_{ij}\, x_i\, x_j. \tag{2.28}$$

More experimental points in figure 9 should be used to determine all coefficients.

The response surface $\overline{G}(\boldsymbol{X})$ with known coefficients $\boldsymbol{b}$ is used to make a first estimation of the design point $\boldsymbol{X_D}$ with the use of FORM. When $\boldsymbol{X}$ is found, $G(\boldsymbol{X_D})$ is evaluated with a NLFE analysis and the new center point $\boldsymbol{X_M}$ is chosen on a straight line from the mean vector $\overline{\boldsymbol{X}}$ to $\boldsymbol{X_D}$ such that $G(\boldsymbol{X}) = 0$ at the new center point $\boldsymbol{X_M}$ i.e.,

$$\boldsymbol{X_M} = \overline{\boldsymbol{X}} + \left(\boldsymbol{X_D} - \overline{\boldsymbol{X}}\right)\frac{G(\overline{\boldsymbol{X}})}{G(\overline{\boldsymbol{X}}) - G(\boldsymbol{X_D})}. \tag{2.29}$$

The new center point $\boldsymbol{X_M}$ is used instead of $\overline{\boldsymbol{X}}$ to obtain new experimental points and a new RSF can be determined. The process is repeated until $\boldsymbol{X_D}$ is sufficiently stable. The response surface $\overline{G}(\boldsymbol{X})$ and the design point $\boldsymbol{X_D}$ is found.

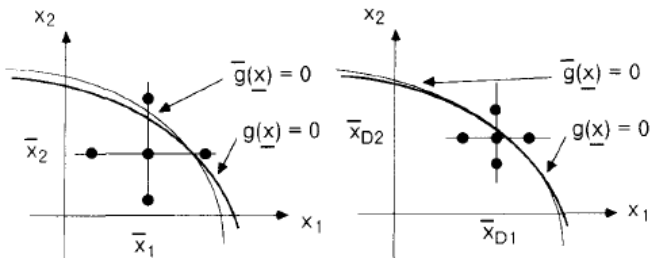


*Figure 10. Schematic sketch of the suggest procedure (Bucher & Bourgund, 1990).*

### 2.4.2 Approach Zhao and Qiu (2013)

Zhao and Qiu (2013) have improved the approach of Bucher and Bourgund (1990) in order to reduce the number of NLFE analyses needed to find the design point. Therefore the control point of experimental points is constructed. The control point is constructed in such a way that the center of the experimental points lies exactly on the failure surface and is close to the actual design point. The control point can be constructed in with the following steps (Zhao & Qiu, 2013):

1. Select $n+1$ experimental points, $\overline{\boldsymbol{X}}$ and $\boldsymbol{X_i} = \overline{\boldsymbol{X}}_{\boldsymbol{i}} - \boldsymbol{f_i}\,\boldsymbol{\sigma_i}$ with $f = 3$.
2. Perform $n+1$ NLFE analyses of the experimental point selected in step 1 and determine $G(\overline{\boldsymbol{X}})$ and $G(\boldsymbol{X_i})$.
3. Calculate the differences between $G(\overline{\boldsymbol{X}})$ and $G(\boldsymbol{X_i})$, as follows:
   $F(\boldsymbol{X_i}) = G(\overline{\boldsymbol{X}}) - G(\boldsymbol{X_i}),\ i = 1,2,..,n.$ (2.30)
4. The weight of each experimental point is determined:
   $w_i = \frac{F(\boldsymbol{X_i})}{\sum_{j=1}^{n}|F(\boldsymbol{X_j})|},\ i = 1,2,..,n.$ (2.31)
5. The control point in the standard normal space is:
   $\boldsymbol{U}_c = \sum_{i=1}^{n} w_i \boldsymbol{U}_i,$ (2.32)
   where:
   $\boldsymbol{U}_i = (\boldsymbol{X}_i - \overline{\boldsymbol{X}})./\boldsymbol{\sigma},$ (2.33)
   where the symbol ./ represents the division of the corresponding component between two vectors.

The control point in the actual space can be calculated with:

$$\boldsymbol{X}_c = \boldsymbol{U}_c .\times \boldsymbol{\sigma} + \overline{\boldsymbol{X}}, \tag{2.34}$$

where the symbol .× represents the product of the corresponding components between two vectors.

The design point and the reliability index can be found using the following iterative procedure (Zhao & Qiu, 2013):

1. Determine the control point with equation (2.34).
2. The new center point $\boldsymbol{X}_M$ can be determined with:
   $$\boldsymbol{X}_{M_{i+1}} = \boldsymbol{X}_{M_i} + (\boldsymbol{X}_{M_{i-1}} - \boldsymbol{X}_{M_i})\frac{G(\boldsymbol{X}_{M_i})}{G(\boldsymbol{X}_{M_i}) - G(\boldsymbol{X}_{M_{i-1}})}.$$ (2.35)
   For the first iteration equation (2.35) is expressed as:
   $$\boldsymbol{X_M} = \overline{\boldsymbol{X}} + (\boldsymbol{X}_c - \overline{\boldsymbol{X}})\frac{G(\overline{\boldsymbol{X}})}{G(\overline{\boldsymbol{X}}) - G(\boldsymbol{X_C})}.$$ (2.36)

Check the convergence. If the convergence is not achieved, repeat equation (2.35) for a new iteration. The convergence criterion is as follows:

$$\left|\frac{G\left(\boldsymbol{X}_{M_{i+1}}\right)}{G(\overline{\boldsymbol{X}})}\right| < \epsilon. \tag{2.37}$$

This criterion with the maximum error e.g. $\epsilon = 0.001$ guarantees that $\boldsymbol{X}_M$ lies on the original limit state surface and does not deviate from the actual design point excessively.

3. Select $2n + 1$ experimental points depending on the center point $\boldsymbol{X}_M$ and $\boldsymbol{X_i} = \overline{\boldsymbol{X}}_{\boldsymbol{M}} \pm \boldsymbol{f_i}\, \boldsymbol{\sigma_i}$, where $f = 1$ since the region close to the design point gives the main contribution to the failure probability.
4. Determine the response surface $\overline{G}(\boldsymbol{X})$ given in (2.25).
5. Apply FORM to determine the design point and calculate the reliability index $\beta$.
6. Delete the old design point. The updated set of experimental points is the new design point as center point in combination with the previously selected experimental points (in total $2n + 1$ experimental points). Go to step 4 for a new iteration.
7. Check convergence.
8. If the convergence is not achieved, go to step 4.

Convergence criteria:

- The reliability indices of two subsequent iterations are almost the same:

$$\left|\frac{\beta^{i+1} - \beta^{i}}{\beta^{i+1}}\right| < \epsilon. \tag{2.38}$$

- The LSF at the design point $\boldsymbol{U}^*$ is close to zero:

$$\left|\frac{G^{i}(\boldsymbol{U}^*)}{G(\overline{\boldsymbol{x}})}\right| < \epsilon. \tag{2.39}$$

The maximum error is for example $\epsilon = 0.001$.

## 2.5 Transformation of log-normal and correlated variables

In order to perform a first order reliability analysis for correlated and non-normal variables they are transformed to their corresponding normal variables. Only the transformation of lognormal to normal distributed variables is presented in this thesis. Normal correlated variables can be transferred to normal uncorrelated variables using Cholesky triangulation (Sørensen, 2004).

### 2.5.1 Transformation of lognormal variables

The lognormal distribution function of variable $X$ with expected value $\mu$ and standard deviation $\sigma$ is presented below (Sørensen, 2004):

$$F_X(x) = \Phi\left(\frac{\ln x - \mu_L}{\sigma_L}\right), \tag{2.40}$$

where:

$$\sigma_L = \sqrt{\ln\left(\frac{\sigma^2}{\mu^2} + 1\right)} \qquad \text{and} \qquad \mu_L = \ln \mu - \frac{1}{2}\,\sigma_L^2. \tag{2.41}$$

The transformation of the lognormal to a normal distribution can be performed by:

$$\Phi(U_i) = F_{X_i}(X_i), \tag{2.42}$$

where: $U_i \sim N(0,1)$ is a standard normal variable and $\Phi(U_i)$ is the corresponding cumulative density function.

$$\Phi(u) = \Phi\left(\frac{\ln x - \mu_L}{\sigma_L}\right), \tag{2.43}$$

$$x = \exp(\sigma_L\, u + \mu_L). \tag{2.44}$$

This leads to a normally distributed variable $Y = \ln(X) \sim N(\mu_L, \sigma_L)$ with expected value $\mu_L$ and standard deviation $\sigma_L$. The mean and the standard deviation can be found with equation (2.41). The transformation of the real $x$ space to the standard normal $u$ space can be obtained using equation (2.44).

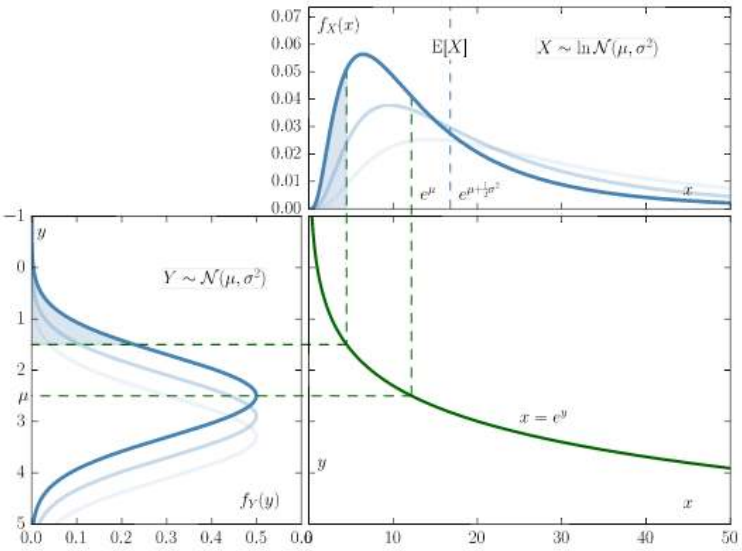


*Figure 11. Relation between normal and log-normal distribution (De Vuyst , 2018).*

### 2.5.2 Transformation of normal correlated variables

Cholesky triangulation is used to transform the correlated normally distributed variables $\boldsymbol{X} = X_i,..,X_n$, with mean values $\mu_{X_i},..,\mu_{X_n}$, standard deviations $\sigma_{X_i},..,\sigma_{X_n}$ and correlation coefficient matrix $\boldsymbol{\rho} = \rho_{ij}, i,j = 1..n$ to uncorrelated normally distributed variables. If the correlated variables are transformed from lognormal to normal the correlation coefficient matrix $\boldsymbol{\rho}$ is transformed to $\boldsymbol{\rho}'$ (difference between $\boldsymbol{\rho}$ and $\boldsymbol{\rho}'$ is negligible for small coefficients of variation). The correlation matrix coefficient matrix is defined as:

$$\boldsymbol{\rho} = \begin{bmatrix} 1 & \rho_{X_1X_2} & \cdots & \rho_{X_1X_n} \\ \rho_{X_1X_2} & 1 & \cdots & \rho_{X_2X_n} \\ \vdots & \vdots & \ddots & \vdots \\ \rho_{X_1X_n} & \rho_{X_2X_n} & \cdots & 1 \end{bmatrix}, \tag{2.45}$$

where:

$$\rho_{X_1X_2} = \frac{Cov[X_1X_2]}{\sigma_{X_1}\sigma_{X_2}} \quad \text{and} \quad Cov[X_1X_2] = E[(X_1 - \mu_{X_1})(X_2 - \mu_{X_2})]. \tag{2.46}$$

The normal variables $X_i$ are transformed to the normalized variables $Y_i = \frac{X_i - \mu_{X_i}}{\sigma_{X_i}}$ to obtain the vector $\boldsymbol{Y}$. The vector $\boldsymbol{Y}$ is transformed to the normalized and uncorrelated variables $\boldsymbol{U}$ with a lower triangular transformation matrix $\boldsymbol{T}$ (i.e. $T_{ij} = 0$ for $j > i$). The covariance matrix $\boldsymbol{C_Y}$ for $\boldsymbol{Y}$ can be written as (Sørensen, 2004):

$$\boldsymbol{C_Y} = E[\boldsymbol{YY}^T] = E[\boldsymbol{TUU}^T\boldsymbol{T}^T] = \boldsymbol{T}E[\boldsymbol{UU}^T]\boldsymbol{T}^T = \boldsymbol{TT}^T = \boldsymbol{\rho}. \tag{2.47}$$

The matrix $\boldsymbol{T}$ can be formed by using $\boldsymbol{TT}^T = \boldsymbol{\rho}$ which results in (Cholesky decomposition):

$$T_{11} = 1$$
$$T_{21} = \rho_{12} \qquad T_{22} = \sqrt{1 - T_{21}^2}$$
$$T_{31} = \rho_{13} \qquad T_{32} = \frac{\rho_{23} - T_{21}T_{31}}{T_{22}} \qquad T_{33} = \sqrt{1 - T_{31}^2 - T_{32}^2}$$
etc. (2.48)

The transformation from $\boldsymbol{X}$ to $\boldsymbol{U}$ is:

$$\boldsymbol{X} = \boldsymbol{\mu_X} + \boldsymbol{DTu}, \tag{2.49}$$

where $\boldsymbol{D}$ is a diagonal matrix with the standard deviations in the diagonal and $\boldsymbol{X} \sim N(\boldsymbol{\mu_X}, \boldsymbol{DT})$ is a normally distributed variable with expected value $\boldsymbol{\mu_X}$ and standard deviation $\boldsymbol{DT}$.

# 3 Review of safety formats for non-linear analysis

In order to determine a safe structural resistance of a structural system by means of the global safety approach using a NLFE model, the Model Code 2010 (fib, 2012) suggest several safety formats. The Safety formats are divided into two groups, namely the global resistance methods and the partial safety method.

## 3.1 General

The general design condition is formulated in equation (1.2):

$$F_d \leq R_d,$$

where $F_d$ is the design value of the external load and $R_d = \frac{R_m}{\gamma_R \gamma_{Rd}}$ is the design resistance. The global resistance factor $\gamma_R$ is dependent from the chosen Safety Format and the value of the model uncertainty is $\gamma_{Rd} = 1.06$ for models with low uncertainties.

## 3.2 Global resistance methods

The global resistance factor method (GRFm) and the estimation of a coefficient of variation of resistance method (ECOV) are the two global resistance methods according to the Model Code 2010 (fib, 2012). Each global resistance method has a different way to determine the global resistance factor.

### 3.2.1 Global resistance factor method (GRFm)

This safety format determines the design resistance $R_d$ with a NLFE analysis with the input of mean GRF material parameters with the same (scaled) global resistance factor for each material (Appendix A.1).

The design resistance is calculated from:

$$R_d = \frac{r(f_m^{GRF}, \dots)}{\gamma_R \gamma_{Rd}}, \tag{3.1}$$

where:

| | |
|---|---|
| $r(f_m^{GRF}, \dots)$ | is the function $r$ calculate the resistance of the NLFE analysis with mean GRF input material; |
| $\gamma_R = 1.2$ | is the partial factor of the resistance (Appendix A.1); |
| $\gamma_{Rd} = 1.06$ | is the model uncertainty. |

The input values for the NLFE analysis for steel and concrete can be calculated with following formulas (Appendix A.1):

$$f_{ym}^{GRF} = 1.1\, f_{yk}, \tag{3.2}$$

$$f_{cm}^{GRF} = 0.85\, f_{ck}. \tag{3.3}$$

### 3.2.2 Estimation of a coefficient of variation of resistance method (ECOV)

Probabilistic studies indicate a log-normal distribution function (fib, 2012) for the resistance of reinforced concrete beams. The mean and characteristic resistance determine the two-parameter lognormal distribution. From this log-normal distribution the global resistance factor $\gamma_R$ can be calculated. The design resistance is defined as:

$$R_d = \frac{R_m}{\gamma_R \gamma_{Rd}}, \tag{3.4}$$

where:

| | |
|---|---|
| $R_m$ | is the mean resistance obtained from NLFE analysis with mean input parameters; |
| $\gamma_R$ | is the global resistance factor; |
| $\gamma_{Rd} = 1.06$ | is the model uncertainty factor. |

To determine the two-parameter lognormal distribution two non-linear finite element analyses should be performed resulting in:

$$R_m = r(f_m, \dots), \tag{3.5}$$
$$R_k = r(f_k, \dots). \tag{3.6}$$

where:

| | |
|---|---|
| $r(f_m, \dots)$ | represents a NLFE analysis with mean input parameters; |
| $r(f_k, \dots)$ | represents a NLFE analysis with characteristic input parameters. |

The coefficient of variation of the resistance can be calculated according to (Appendix A.2):

$$V_R = \frac{1}{1.65} \ln\left(\frac{R_m}{R_k}\right). \tag{3.7}$$

The global resistance factor is defined as (Appendix A.2):

$$\gamma_R = \frac{R_m}{R_d} = e^{\alpha_R \beta V_R} = e^{3.04 V_R}, \tag{3.8}$$

where:

| | |
|---|---|
| $\alpha_R = 0.8$ | is the sensitivity factor (dominant strength parameter); |
| $\beta_t = 3.8$ | is the target reliability index; |
| $V_R$ | is the coefficient of variation. |

The ECOV method has the advantage that the $\beta$ factor could be changed in order to fulfill the required safety level. The reliability of this method depends strongly on the selection of the relevant material parameters for the corresponding failure mode.

## 3.3 Partial factor method (PFm)

The input for the material parameters in the NLFE analysis are the design values. The low material values can cause unrealistic redistribution of the internal forces. This may cause deviations in the structural response. The failure mode of the NLFE analysis could be different from the real failure mode. However case studies indicate that the partial factor method can be used as a safe solution (fib, 2012). The design values of the materials can be obtained with the partial safety factor $\gamma_M$, which consist of a factor for a material property $\gamma_m$ and a factor for the model uncertainty $\gamma_{Rd}$:

$$\gamma_M = \gamma_m \gamma_{Rd}. \tag{3.9}$$

Therefore no global resistance factor is needed for this safety format. The resistance $R_d$ of the NLFE analysis can be calculated according to:

$$R_d = r(f_d, \dots), \tag{3.10}$$

where:

$r(f_d, \dots)$ represents a NLFE analysis with design input parameters.

# 4 Three designs of a concrete frame based on ductility

Three reinforced concrete portal frame designs will be described in this chapter. The three designs are used to determine the influence of ductile behavior and redistribution of internal forces on the structural safety. The structural resistance will be determined using a Level I reliability method on local and a global level. After that there will be determined if there is any additional capacity. This chapter describes the three portal frame designs in detail. The safety of the global structural resistance obtained by the safety formats will be assed in chapter 7 using a global level II reliability method.

First several corner reinforcement detailing possibilities will be presented in chapter 4.1. Secondly chapter 4.2 presents the three portal frame designs i.e. the dimensions, corner reinforcement, the longitudinal reinforcement, the shear reinforcement, steel grade and the concrete strength class of the three reinforced concrete frames by means of a description and technical drawings. Subsequently in chapter 4.3 a level I reliability method is used to perform a local safety check to determine the structural resistance of the three portal frame designs according to the Eurocode 2 (NEN-EN 1992 -1-1, 2011). In chapter 4.4 a Level I reliability method is used on global level to determine the structural resistance of the three portal frame designs according to the Model Code 2010 (fib, 2012). In this way the failure modes predicted with a local and global safety approach can be compared. Finally in chapter 4.5 there will be determined if there is any additional capacity by comparing the structural resistance of a local and a global level approach.

## 4.1 Reinforcement detailing in concrete frame corners

The ductility of the portal frame determines the degree of redistribution of internal forces. The forming of plastic hinges in the plastic frame leads to more or less redistribution of the internal forces. In order to have a ductile frame behavior the bending moment resistance of the corner should be at least equal to the bending moment resistance of the members. Therefore an important part of the frame design is the detailing of the corners. The ductility of the corner is in fact the rotational capacity.

The corner reinforcement is based on a strut and tie model. The corners of a reinforced concrete portal frame should be able to resist an opening and a closing moment. However in this thesis the loading is defined is such a way that corner B is subjected to an opening moment and corner D to a closing moment. The strut and tie models for corner B subjected to an opening moment and corner D subjected to a closing corner are presented in figure 12.

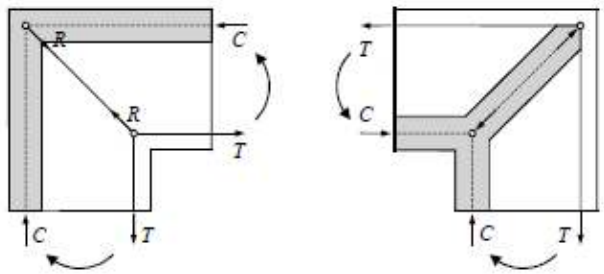


*Figure 12. Strut and tie model for an opening moment (left, corner B) and a closing moment (right, corner D) (Johansson, 2000).*

Both corners B and D can be reinforced according to the longitudinal reinforcement detailing (without the inclined bar, which is only needed for opening moment) presented in figure 13 (a) and (b). Figure 13 (a) shows the detailing with spliced bars, where an inclined bar is used to resist an

opening moment. Figure 13 (b) is the conventional detailing of a corner subjected to a closing moment. The longitudinal reinforcement with spliced bars in figure 13 (a) is easier to place compared to the longitudinal reinforcement of figure 13 (b) (Johansson, 2000).

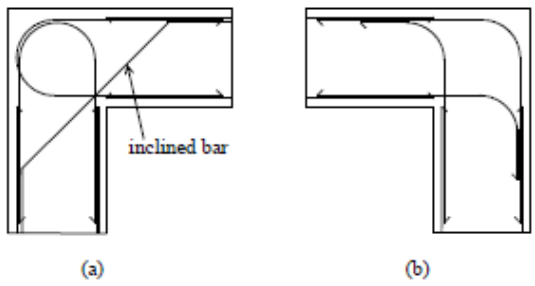


*Figure 13. Reinforcement detailing with spliced bars (inclined bar for opening moment) (a) and the conventional reinforcement detailing (b) (Johansson, 2000).*

The inclined bar (figure 13 (a)) should prevent the occurrence of a diagonal crack (figure 15 (a), crack 1) as result from an opening moment. However the inclined bar is not as effective as was believed in the past and could be replaced by enough longitudinal reinforcement. (Johansson, 2000). This is shown in figure 14.

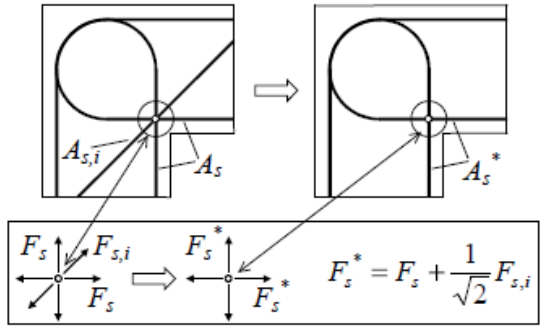


*Figure 14. Replacement inclined bar with enough longitudinal reinforcement to resist an opening moment (Johansson, 2000).*

The failure modes of the corners subjected to an opening and closing moment are presented in figure 15. A corner subjected to an opening moment is sensitive for secondary cracks. Additional radial stirrups can be added perpendicular to the expected secondary crack to increase the corner capacity (figure 15 (b)).

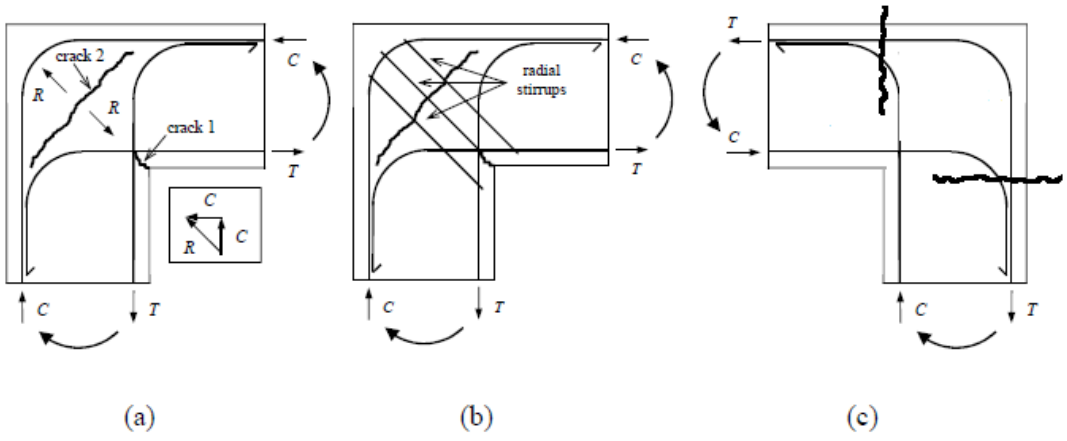


*Figure 15. Failure modes corner subjected to an opening moment without (a) and with radial stirrups (b) and corner subjected to a closing moment (c) (Johansson, 2000).*

## 4.2 Portal Frame designs

The linear elastic moment distribution as result from the external loading is given in figure 16. The reinforced detailing should be able to resist an opening and a closing moment. The opening moment in corner B is relatively low due to the external loading. No additional corner reinforcement, i.e. an inclined bar and/or radial stirrups, is necessary in corner B. In figure 14 is already shown that enough longitudinal reinforcement can replace the inclined bar. Therefore corner B (opening moment) and corner D (closing moment) of the three portal frame designs are equipped with the same reinforcement detailing as presented in figure 15 (a) and (c) for corner B and D, respectively.

The largest linear elastic moments exist in C, D and E (figure 16) as results of the vertical loading $F_v$ in C and the horizontal loading $F_h$ in B. If the plastic hinges show a ductile behavior the frame is capable to resist a larger additional vertical load compared to a frame with a more brittle behavior. Especially corner D is vulnerable to show a brittle behavior due to a large stress concentration.

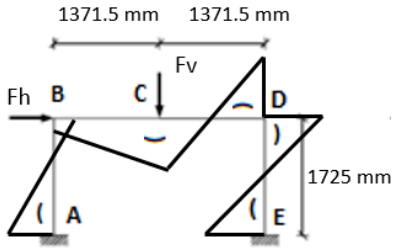


*Figure 16. Linear elastic moment distribution resulting from Fv and Fh.*

The portal frame shows a ductile behavior if the plastic moment resistance of an abutting member is equal or smaller than the plastic moment resistance of the corner (Johansson, 2000). Due to the external loading, corner D is exposed to a closing moment. The failure mode of a corner subjected to a closing moment is mainly determined by a concrete compressive failure (Johansson, 2000). The ductility of corner D can be improved by placing additional longitudinal reinforcement or using a higher concrete strength class. No additional reinforcement is placed in the corners since this mainly improves the ductility of a corner subjected to an opening moment (corner B). This is hardly needed since the loading of the portal frame leads to a very small moment in corner B which is exposed to an opening moment.

The safety of the safety formats will be validated for three portal frame designs. The ductility of the portal frame determines the degree of redistribution of the internal forces. Therefore the case study will focus on three designs with all a different ductile behavior:

- Design 1: basic design
- Design 2: higher longitudinal reinforcement ratio (compared to design 1)
- Design 3: higher concrete strength class (compared to design 1)

### 4.2.1 Design 1

Design 1 is similar to one of the reinforced portal frame designs used in the experiment (Seraj, Kotsovos, & Pavlovic, 1995) discussed in chapter 5. Design 1 is verified using a local safety approach according to the Eurocode 2 and is able to resist a vertical design load in C of $F_v = 18.8$ kN and a horizontal design load in B of $F_h = 15.7$ kN.

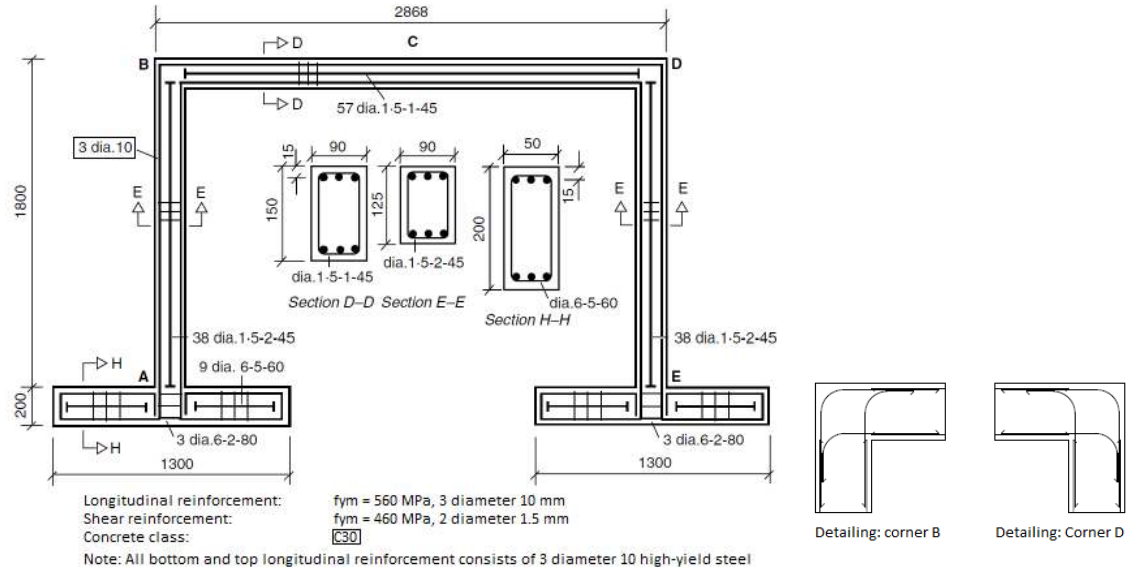


*Figure 17. Design 1: longitudinal reinforcement diameter d=10 mm and concrete strength class: C30 (Blomfors, 2014).*

### 4.2.2 Design 2

The longitudinal reinforcement ratio of design 2 is higher compared to design 1 and the shear reinforcement ratio is still the same as for design 1.

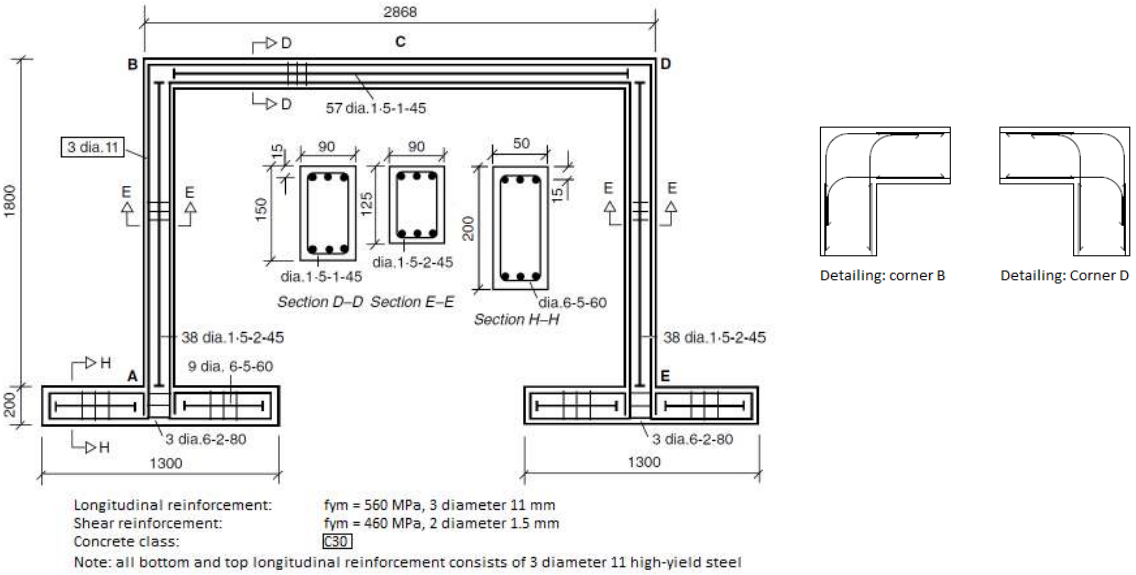


*Figure 18. Design 2: longitudinal reinforcement diameter d=11 mm and concrete strength class: C30.*

### 4.2.3 Design 3

Design 3 is made with a higher concrete class: C40 and the same longitudinal and shear reinforcement ratio is used as for design 1.

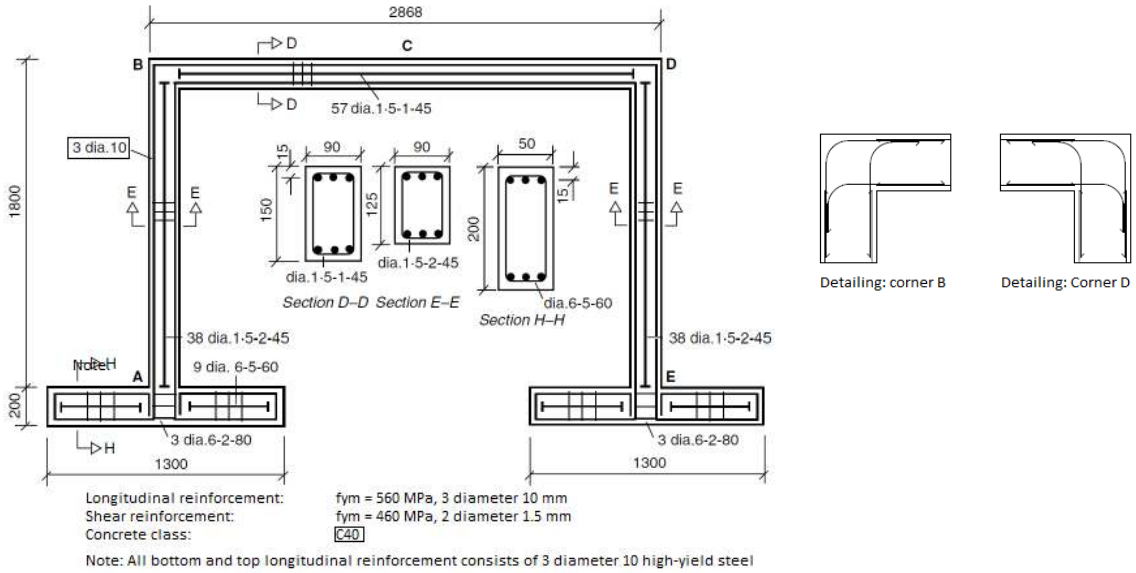


*Figure 19. Design 3: longitudinal reinforcement diameter d=10 mm and concrete strength class: C40.*

## 4.3 Level I reliability method: local design resistance (Eurocode 2)

To perform a local safety evaluation a distinction between the several elements is necessary. Therefore the elements will be numbered from left to right. This leads to the following element numbering: the left column (AB), beam (BD) and the right column (DE) are labeled as element 1, element 2 and element 3, respectively. The element numbering is shown in figure 20.

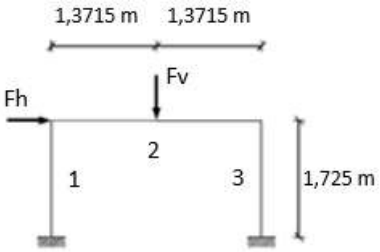


*Figure 20. Element numbering*

The determination of the design resistance for the elements of the three portal frame designs can be found in Appendix C.1. Design 1 is made by Seraj et al. (1995) and is used in an experiment described in chapter 5. Design 1 is provided with only the minimum required shear reinforcement since the shear resistance $V_{Rd,C}$ was found to be sufficient to resist the shear forces $V_E$ resulting from the external load $F_v$ and $F_h$. The shear resistance $V_{Rd,S}$ based on the implemented shear reinforcement is much lower and therefore $V_E$ cannot be higher than $V_{Rd,C}$ (Appendix C.1). The maximum shear resistance of design 2 and 3 is the same since there is not used more shear reinforcement.

The general check for the shear resistance is defined as (NEN-EN 1992 -1-1, 2011):

$V_E < V_{Rd,C}$, no shear reinforcement is needed, otherwise: (4.1)

$V_E < V_{Rd,S}$. (4.2)

The bending moment resistance of the elements in design 2 and 3, is larger than the shear resistance (Appendix C.1.3.2). Therefore a shear failure mode determines the structural resistance of the elements of the three portal frame designs. For simplification all portal frames are assumed to have a local design resistance of:

$F_v = 18.8$ kN, $F_h = 15.7$ kN.

The governing local safety evaluation by means of a unity check (UC) for portal frame design 1, 2 and three is determined below. The unity check is defined as: $UC = \frac{V_E}{V_{Rd,C}}$, when $V_{Rd,C,min} \leq V_{Rd,C}$.

*Table 1. Local safety evaluation for the shear resistance without shear reinforcement.*

| Shear resistance of elements without shear reinforcement | | | | |
|---|---|---|---|---|
| Design 1 | VRd,C,min (kN) | VRd,C (kN) | VE (kN) | UC (-) |
| Element 1 | 6.0 | 10.5 | 4.21 | 0.40 |
| Element 2 | 8.1 | 12.8 | 13.68 | 1.06 |
| Element 3 | 7.2 | 11.7 | 11.48 | 0.98 |
| Design 2 | VRd,C,min (kN) | VRd,C (kN) | VE (kN) | UC (-) |
| Element 1 | 6.0 | 11.2 | 4.21 | 0.4 |
| Element 2 | 8.1 | 13.6 | 13.68 | 1.0 |
| Element 3 | 7.2 | 12.3 | 11.48 | 0.9 |
| Design 3 | VRd,C,min (kN) | VRd,C (kN) | VE (kN) | UC (-) |
| Element 1 | 6.9 | 11.5 | 4.21 | 0.37 |
| Element 2 | 9.2 | 14.0 | 13.68 | 0.98 |
| Element 3 | 8.0 | 12.7 | 11.48 | 0.91 |

### 4.3.1 Strut and tie model corner region

The analyses of the separate elements leads to the conclusion that structural resistance of the portal frame is determined by the shear resistance of element 2. However a detailed analyses of the corner region should be performed to verify this conclusion. The external loading of the portal frame leads to a situation where corner D is exposed to a large closing moment. The resistance of the internal compressive strut in corner D should be determined in order to determine the bending moment capacity of the corner. This should be done based on a strut and tie model as shown in chapter 4.1.

## 4.4 Level I reliability method: global design resistance (Model Code 2010)

The NLFE models of portal frame design 1, 2 and 3 used to determine the design resistance according to the safety formats are presented in Appendix D**.** The model uncertainty is not needed to determine the global design resistance of the portal frame designs 1, 2 and 3 since the safety formats make use of a prescribed model uncertainty.

All settings of the NLFE model are chosen according to the Guidelines for Non-Linear Finite Element analyses of Concrete Structures (Hendriks, de Boer, & Belletti, 2017). Therefore errors in the results due to incorrect user input is minimized. The material input parameters in the NLFE model for the three portal frame designs can be found in Appendix B.2. The safety formats and the NLFE analyses that have to be performed in order to obtain the global design resistance are discussed in chapter 3. The results of the global design resistance according to the safety formats are presented in table 2. The NLFE analyses and the corresponding load displacement diagrams to obtain the global design resistance are presented in the chapters 4.4.1 - 4.4.3.

*Table 2. Results NLFE analyses and calculated global design resistance according to the safety formats.*

| | Result NLFE analyses (kN) | | | | Resistance Safety Format (kN) | | |
|---|---|---|---|---|---|---|---|
| Design 1 | mean | characteristic | mean GRF | design | GRFm | ECOV | PFm |
| Fv (kN) | 28.80 | 25.30 | 26.00 | 19.20 | 17.08 | 20.40 | 19.20 |
| Fh (kN) | 15.70 | 15.70 | 15.70 | 15.70 | 15.70 | 15.70 | 15.70 |
| Design 2 | mean | characteristic | mean GRF | design | GRFm | ECOV | PFm |
| Fv (kN) | 33.10 | 30.60 | 35.60 | 28.00 | 24.63 | 26.09 | 28.00 |
| Fh (kN) | 15.70 | 15.70 | 15.70 | 15.70 | 15.70 | 15.70 | 15.70 |
| Design 3 | mean | characteristic | mean GRF | design | GRFm | ECOV | PFm |
| Fv (kN) | 28.30 | 25.20 | 27.60 | 21.30 | 18.34 | 20.58 | 21.30 |
| Fh (kN) | 15.70 | 15.70 | 15.70 | 15.70 | 15.70 | 15.70 | 15.70 |

The results of the safety formats with the highest probability of failure for each design are: ECOV, PFm and PFm for design 1, 2 and 3, respectively (table 2). The lowest probability of failure is obtained when the lowest design resistance is obtained. For each design the lowest global design resistance is obtained with the GRFm.

### 4.4.1 Design 1: Global design resistance according to the safety formats

In order to calculate the global design resistance according to the GRFm, the ECOV method and the PFm 4 NLFE analyses have been performed. The input material values for the NLFE analyses can be found in Appendix B.2. To obtain the global design resistance according to the GRFm a NLFE analysis with mean GRF material values has been performed. The global design resistance according to the ECOV method can be found after performing two NLFE analyses with mean and characteristic material values. The global design resistance of the PFm is found with a NLFE analyses with design material values. The load is incrementally applied in three phases (figure 21). The load-displacement diagrams of the NLFE analyses are shown in figure 22.

Load phases:

Phase 1: incrementally applied vertical load till $F_v = 18.8$ kN;
Phase 2: incrementally applied horizontal load till $F_h = 15.7$ kN and constant $F_v = 18.8$ kN;
Phase 3: incrementally applied vertical load till failure kN and constant $F_h = 15.7$ kN.

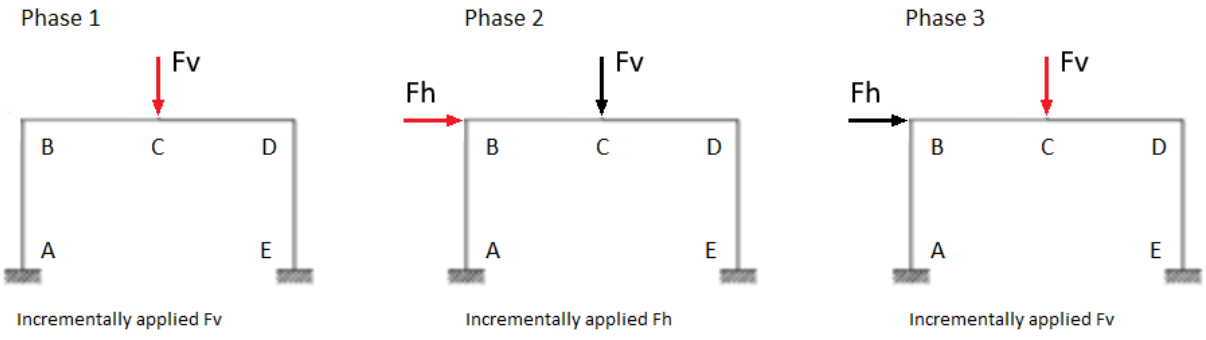


*Figure 21. The three applied load phases.*

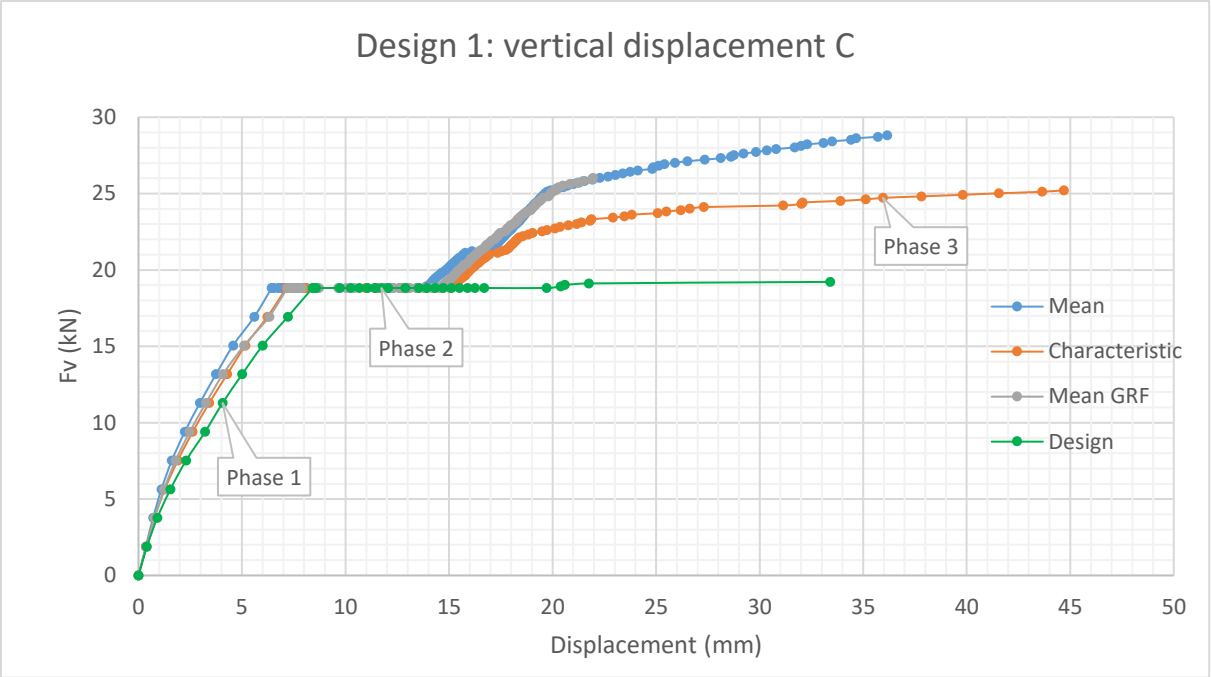


*Figure 22. Load-displacement diagram for the NLFE analyses with mean, characteristic, mean GRF and design material values. The vertical load Fv and the vertical displacement C are shown.*

#### *4.4.1.1 Global design resistance according to the GRFm*

The focus of this thesis is to determine if there is any additional vertical capacity of portal frame. The horizontal load $F_h = 15.7$ kN on the portal frame is therefore always the same and will not be reduced by a safety factor. The resistance of the portal frame obtained with a NLFE analysis with mean GRF material values is:

$F_v = 26.0$ kN and $F_h = 15.7$ kN.

This result is also presented in table 2. The definition of the total structural resistance made by Blomfors (2014) is used to calculate the global design resistance. The total structural resistance is defined as the sum of the vertical and horizontal load. This total structural resistance is not a real physical quantity since the loads are orthogonal. However this definition can be used to implement all safety in the vertical force. This is done since the horizontal load is assumed to be always present on the structure and will not be reduced by a safety factor. Therefore all safety is implemented in the vertical resistance of the structure. This leads to a lower global design resistance compared to a situation where only the vertical load is evaluated and is assumed to be a safe solution. The global design resistance according to the GRFm is determined with equation (3.1):

$$R_d = \frac{r(f_m^{GRF},\dots)}{\gamma_R\,\gamma_{Rd}} = \frac{41.7}{1.2 \cdot 1.06} = 32.78 \text{ kN}.$$

This leads to the following global design resistance according to the GRFm:

$F_v = 17.08$ kN and $F_h = 15.7$ kN.

#### 4.4.1.2 Global design resistance according to the ECOV method

To determine the global design resistance according to the ECOV method two NLFE analyses with mean and characteristic material values have been performed. The resistance of a NLFE analysis with mean material values is:

$F_v = 28.8$ kN and $F_h = 15.7$ kN.

The resistance of a NLFE analysis with characteristic material values is:

$F_v = 25.3$ kN and $F_h = 15.7$ kN.

The coefficient of variation of the resistance can be calculated according to equation (3.7):

$$V_R = \frac{1}{1.65}\ln\left(\frac{R_m}{R_k}\right) = \frac{1}{1.65}\ln\left(\frac{44.5}{41.0}\right) = 0.0496.$$

The global resistance factor is calculated with equation (3.8):

$$\gamma_R = e^{3.04\,V_R} = 1.16.$$

The global design resistance according to the ECOV method is determined with equation (3.4):

$$R_d = \frac{R_m}{\gamma_R\,\gamma_{Rd}} = \frac{44.5}{1.16 \cdot 1.06} = 36.1 \text{ kN}.$$

This leads to the following global design resistance according to the ECOV method:

$F_v = 20.40$ kN and $F_h = 15.7$ kN.

#### 4.4.1.3 Global design resistance according to the PFm

The global design resistance according to the PFm is obtained after performing a NLFE analysis with design material values. The global design resistance is equal to the resistance of a NLFE analysis with design material values is:

$F_v = 19.20$ kN and $F_h = 15.7$ kN.

#### 4.4.1.4 Structural failure of the portal frames

Several elements have to fail before the structural system fails since the portal frame is statically indeterminate. First the concrete compressive strut in closing corner D (right corner) fails partially. In figure 23 the principle stresses in the concrete compressive strut are shown before partial failure. The principle stresses after partial failure of the concrete compressive strut is shown in figure 24. The failure of the concrete compressive strut is also visible in the load-displacement diagram presented in figure 26. In fact the softening behavior of the parabolic concrete compression diagram (figure 25) is used to redistribute the internal forces to the other parts of the portal frame. The middle part of the concrete compressive strut fails and the remaining concrete compressive stresses are redistributed in the lower and upper part of the concrete compressive strut. The stiffness of corner D is decreasing due to the failing compressive strut. The internal forces are redistributed to other parts of the portal frame. Eventually three additional plastic hinges start to appear in locations A, C and E. Now a mechanism starts to develop and lead to the failure of the structural system.

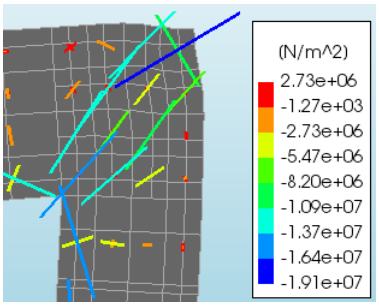


*Figure 23. Principle stresses before partial failure of the compressive strut in corner D (load-step 24).*

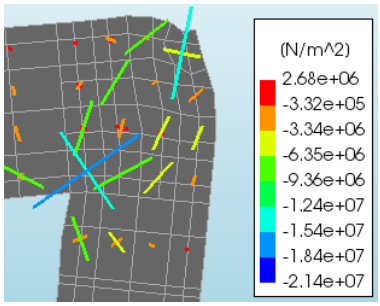


*Figure 24. Principle stresses after partial failure of the compressive strut in corner D (load-step 25).*

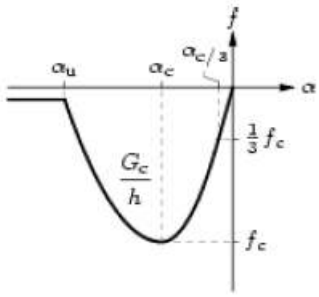


*Figure 25. Parabolic compression diagram concrete (Hendriks, de Boer, & Belletti, 2017).*

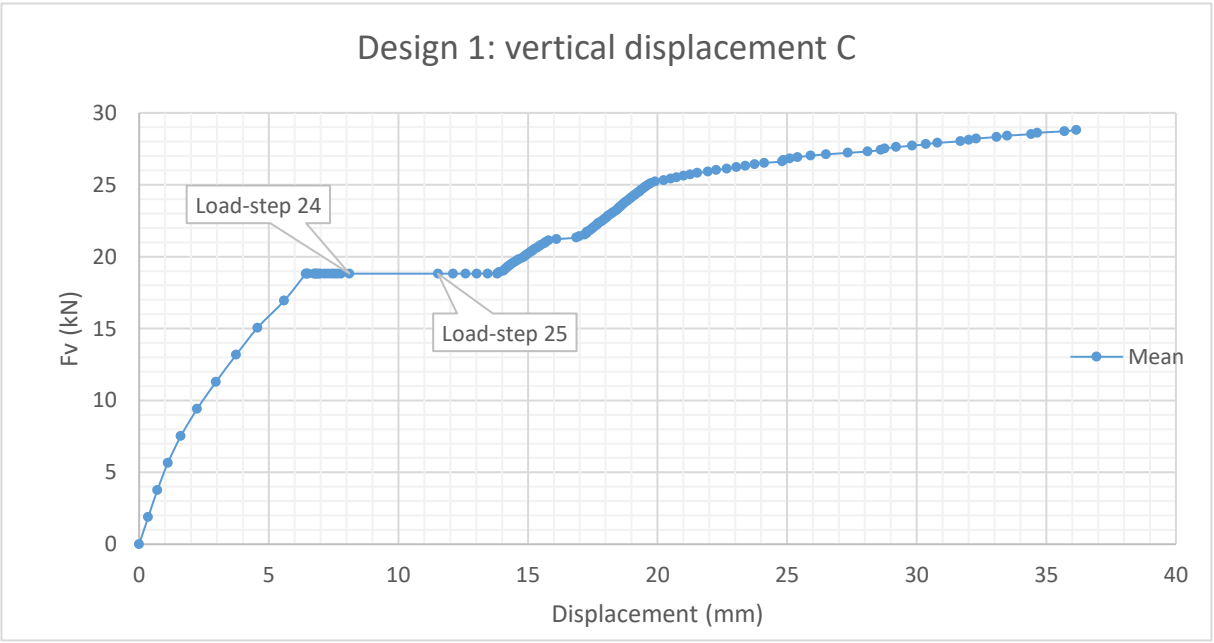


*Figure 26. Load-displacement diagram for a NLFE analysis with mean material values. A lot of additional vertical displacement is shown after the partial failure of the compressive strut in corner D. Partial failure of the compressive strut occurs between load-step.*

Due to the softening behavior of the concrete in corner D the maximum moment capacity of corner D is reached. Composed line elements are included in the NLFE model. This elements can integrate the stresses over the height of the element to determine the moment distribution at a certain position. In figure 27 the moment distribution is shown directly after the failure of the concrete compressive strut (load-step 25). Figure 28 shows the moment distribution before failure of the structural system (load-step 29). The maximum moment capacity of corner D is reached after load-step 25 and cannot increase any more.

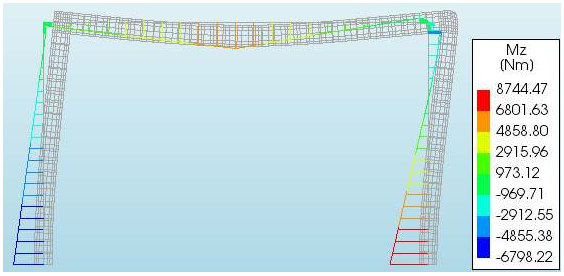


*Figure 27. Moment distribution composed line elements after failure of the concrete compressive strut (load-step 25).*

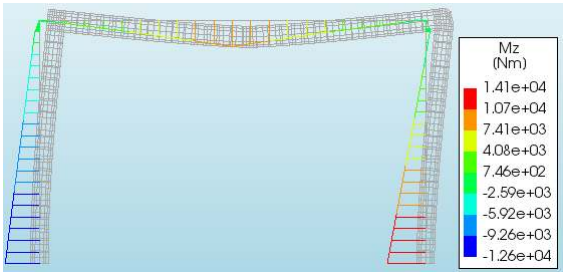


*Figure 28. Moment distribution composed line elements before the structural system failure (load-step 130).*

The failure of the structural system occors after the forming of plastic hinges at midspan C (load-step 89) and the bottom of the left and the right column (load-step 113). The forming of the plastic hinges occurs after the yielding of the reinforcement. This is shown in figure 29 and 30. The partial failure of corner D and the forming of the plastic hinges at location A, C and E lead to a mechanism and eventually to the failure of the structural system at load-step 130.

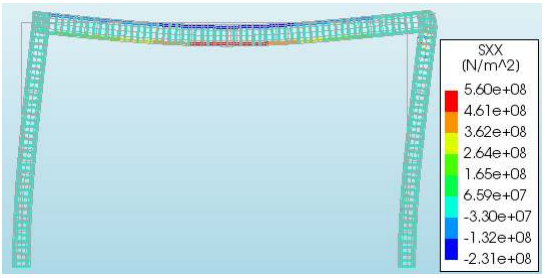


*Figure 29. Yielding of the steel reinforcement at midspan C (load-step 89).*

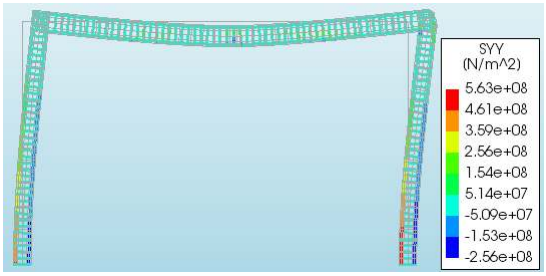


*Figure 30. Yielding of the steel reinforcement at location A and E (load-step 113).*

For the other NLFE analyses with characteristic, mean GRF and design material values a simular partially failure of corner D and the forming of plastic hinges at A, C and E has been found.

### 4.4.2 Design 2: Global design resistance according to the safety formats

The load-displacement diagram of the NLFE analyses with mean, characteristic, mean GRF and design material values for design 2 are presented in figure 31. Design 2 has a larger longitudinal reinforcement ratio compared to design 1. Therefore the stiffness of the portal frame has increased, which results in less vertical displacement of point C, especially in the first two loading phases. A larger stiffness results in a more brittle behavior. The rotational capacity of the corner is decreasing when a higher concrete strength (which leads to a higher stiffness) is used.

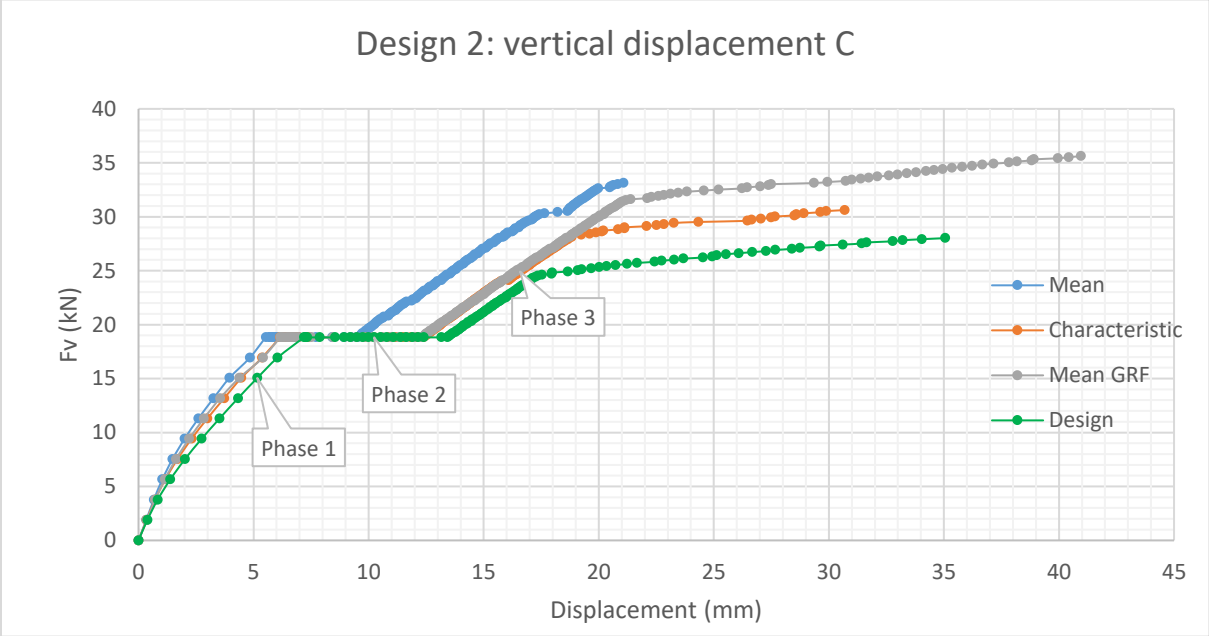


*Figure 31. Load-displacement diagram for the NLFE analyses with mean, characteristic, mean GRF and design material values. The vertical load Fv and the vertical displacement C are shown.*

For example the load-displacement diagrams of a NLFE analysis with mean and mean GRF material values will be compared. The yield strength used in both NLFE analyses is more or less the same (Appendix B.2):

$f_{y,mean} = 560$ MPa and $f_{y,mean\ GRF} = 558$ MPa.

The difference in both NLFE analyses can be found in the used concrete compressive strength (Appendix B.2):

$f_{c,mean} = 38$ MPa and $f_{c,mean\ GRF} = 25.5$ MPa.

The stiffness of the concrete for the portal frame with mean GRF material values is lower and therefore the rotational capacity of corner D is larger. Due to a larger rotational capacity a ductile failure of the portal frame is obtained and this even led to a higher structural resistance of the portal frame with mean GRF values. This example shows clearly that the rotational capacity of the corner is an important factor for a brittle or ductile behavior of the portal frame.

#### 4.4.2.1 Global design resistance according to the GRFm

The resistance of the portal frame obtained with a NLFE analysis with mean GRF material values is:

$F_v = 35.60$ kN and $F_h = 15.7$ kN.

The global design resistance according to the GRFm is determined with equation (3.1):

$$R_d = \frac{r(f_m^{GRF},\ldots)}{\gamma_R \gamma_{Rd}} = \frac{51.3}{1.2 \cdot 1.06} = 40.33 \text{ kN}.$$

This leads to the following global design resistance according to the GRFm:

$F_v = 24.63$ kN and $F_h = 15.7$ kN.

#### 4.4.2.2 Global design resistance according to the ECOV method

To determine the global design resistance according to the ECOV method two NLFE analyses with mean and characteristic material values have been performed. The resistance of a NLFE analysis with mean material values is:

$F_v = 33.1$ kN and $F_h = 15.7$ kN.

The resistance of a NLFE analysis with characteristic material values is:

$F_v = 30.6$ kN and $F_h = 15.7$ kN.

The coefficient of variation of the resistance can be calculated according to equation (3.7):

$$V_R = \frac{1}{1.65} \ln\left(\frac{R_m}{R_k}\right) = \frac{1}{1.65} \ln\left(\frac{48.8}{46.3}\right) = 0.0319.$$

The global resistance factor is calculated with equation (3.8):

$$\gamma_R = e^{3.04\, V_R} = 1.10.$$

The global design resistance according to the ECOV method is determined with equation (3.4):

$$R_d = \frac{R_m}{\gamma_R \gamma_{Rd}} = \frac{48.8}{1.10 \cdot 1.06} = 41.79 \text{ kN}.$$

This leads to the following global design resistance according to the ECOV method:

$F_v = 26.09$ kN and $F_h = 15.7$ kN.

#### 4.4.2.3 Global design resistance according to the PFm

The global design resistance according to the PFm is obtained after performing a NLFE analysis with design material values. The global design resistance is equal to the resistance of a NLFE analysis with design material values is:

$F_v = 28.0$ kN and $F_h = 15.7$ kN.

#### 4.4.2.4 Structural failure of the portal frame

The structural failure of portal frame design 2 is comparable to portal frame design 1. Only the NLFE analysis with mean material values leads to a brittle failure of corner D and the plastic hinges at location A, C and E are not fully formed.

### 4.4.3 Design 3: Global design resistance according to the safety formats

The load-displacement diagram of the NLFE analyses with mean, characteristic, mean GRF and design material values for design 3 are presented in figure 32. Design 2 has a larger concrete compressive strength compared to design 1.

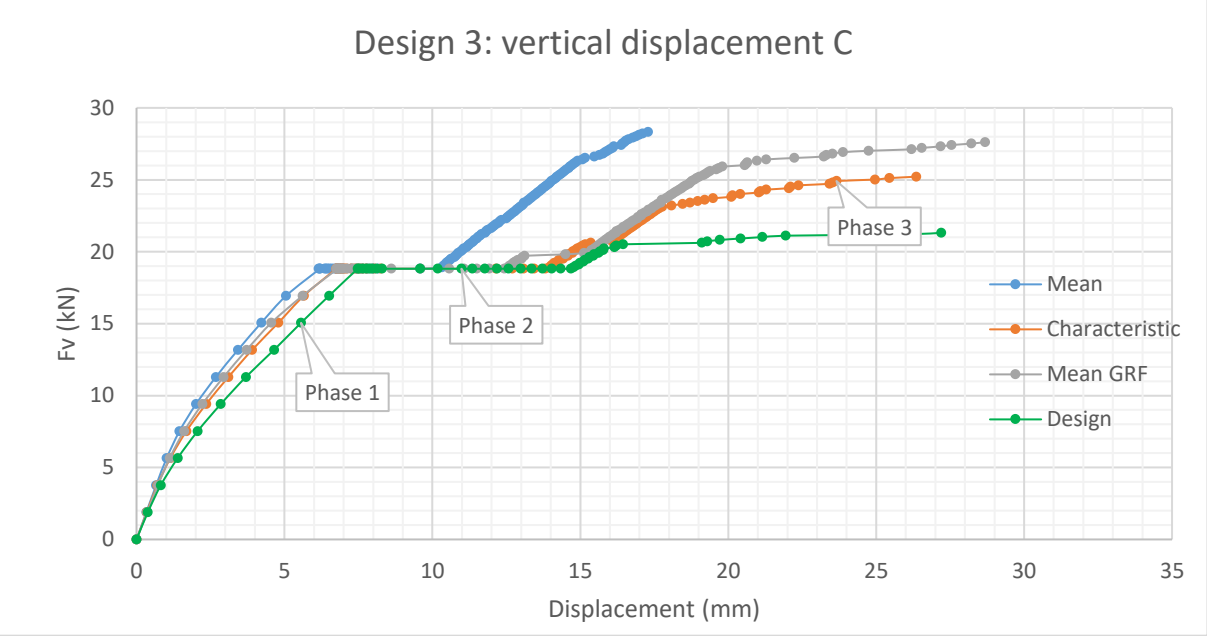


*Figure 32. Load-displacement diagram for the NLFE analyses with mean, characteristic, mean GRF and design material values. The vertical load Fv and the vertical displacement C are shown.*

#### *4.4.3.1 Global design resistance according to the GRFm*

The resistance of the portal frame obtained with a NLFE analysis with mean GRF material values is:

$F_v = 27.6$ kN and $F_h = 15.7$ kN.

The global design resistance according to the GRFm is determined with equation (3.1):

$$R_d = \frac{r(f_m^{GRF},\ldots)}{\gamma_R\,\gamma_{Rd}} = \frac{43.3}{1.2 \cdot 1.06} = 34.04 \text{ kN}.$$

This leads to the following global design resistance according to the GRFm:

$F_v = 18.34$ kN and $F_h = 15.7$ kN.

#### *4.4.3.2 Global design resistance according to the ECOV method*

To determine the global design resistance according to the ECOV method two NLFE analyses with mean and characteristic material values have been performed. The resistance of a NLFE analysis with mean material values is:

$F_v = 28.3$ kN and $F_h = 15.7$ kN.

The resistance of a NLFE analysis with characteristic material values is:

$F_v = 25.2$ kN and $F_h = 15.7$ kN.

The coefficient of variation of the resistance can be calculated according to equation (3.7):

$$V_R = \frac{1}{1.65}\ln\left(\frac{R_m}{R_k}\right) = \frac{1}{1.65}\ln\left(\frac{44.0}{40.9}\right) = 0.0442.$$

The global resistance factor is calculated with equation (3.8):

$$\gamma_R = e^{3.04\,V_R} = 1.14.$$

The global design resistance according to the ECOV method is determined with equation (3.4):

$$R_d = \frac{R_m}{\gamma_R\,\gamma_{Rd}} = \frac{44.0}{1.14 \cdot 1.06} = 36.28 \text{ kN}.$$

This leads to the following global design resistance according to the ECOV method:

$F_v = 20.58$ kN and $F_h = 15.7$ kN.

#### *4.4.3.3 Global design resistance according to the PFm*

The global design resistance according to the PFm is obtained after performing a NLFE analysis with design material values. The global design resistance is equal to the resistance of a NLFE analysis with design material values is:

$F_v = 21.3$ kN and $F_h = 15.7$ kN.

#### *4.4.3.4 Structural failure of the portal frame*

The structural failure of portal frame design 3 is comparable to portal frame design 1. Only the NLFE analysis with mean material values leads to a brittle failure of corner D and the plastic hinges at location A, C and E are not fully formed.

## 4.5 Additional load carrying capacity

The maximum additional vertical capacity is the difference between the global and local design resistance and is presented in table 3. The question that remains is how safe is the global design resistance obtained with a safety format i.e. what is the reliability index $\beta_R$. This will be determined in chapter 7, for the safety formats which obtain the highest global design resistance and therefore lead to the lowest reliability index.

*Table 3. Additional vertical capacity: difference between the least conservative global and local design resistance using a level I reliability method.*

| | Global design resistance (kN) | | | Local design resistance (kN) | Additional vertical capacity (kN) |
|---|---|---|---|---|---|
| Design 1 | **Least conservative safety format (SF)** | | $\beta_R$ | Eurocode 2 (EC2) | Difference SF and EC2 |
| Fv (kN) | ECOV | 20.4 | ? | 18.8 | 1.6 |
| Fh (kN) | | 15.7 | | 15.7 | |
| Design 2 | | | | | |
| Fv (kN) | PFm | 28.0 | ? | 18.8 | 9.2 |
| Fh (kN) | | 15.7 | | 15.7 | |
| Design 3 | | | | | |
| Fv (kN) | PFm | 21.3 | ? | 18.8 | 2.5 |
| Fh (kN) | | 15.7 | | 15.7 | |

The safety formats that leads to the most conservative global design resistance is for al portal frame designs the same, namely the GRFm. This safety format leads to a conservative global design resistance and is for design 1 and 3 even lower than the local design resistance.

*Table 4. Additional vertical capacity: difference between the most conservative global and local design resistance using a level I reliability method.*

| | Global design resistance (kN) | | Local design resistance (kN) | Additional vertical capacity (kN) |
|---|---|---|---|---|
| Design 1 | **Most conservative safety format (SF)** | | Eurocode 2 (EC2) | Difference SF and EC2 |
| Fv (kN) | GRFm | 17.1 | 18.8 | -1.7 |
| Fh (kN) | | 15.7 | 15.7 | |
| Design 2 | | | | |
| Fv (kN) | GRFm | 24.6 | 18.8 | 5.8 |
| Fh (kN) | | 15.7 | 15.7 | |
| Design 3 | | | | |
| Fv (kN) | GRFm | 18.3 | 18.8 | -0.5 |
| Fh (kN) | | 15.7 | 15.7 | |

A more realistic failure mode of the reinforced portal frame design for the defined load situation is a compressive strut failure in the frame corner due to a closing moment followed by the formation of three plastic hinges at location A, C and E (NLFE results indicates this failure mode). A detailed analysis of a strut and tie model according to Eurocode 2 of the concrete frame corner could lead to a lower local design resistance compared to the local element resistance. Therefore the additional vertical capacity could be higher.

# 5 Structural analysis of an experiment of a Portal Frame

In order to perform a safety assessment of a statically indeterminate portal frame by means of NLFE analyses a real experiment (Seraj, Kotsovos, & Pavlovic, 1995) is used to determine the model uncertainty. The model uncertainty involves all uncertainties which are not included in the NLFE model.

The portal frames tested in the experiment are more or less similar compared to the three portal frame designs described in chapter 4.2. Only the loading of the experimental frame is different from the loading described in chapter 1. Unfortunately there are no experimental results available of the three portal frame designs described in chapter 4.2 with the same loading procedure. However, the best way to quantify the model uncertainty is to use the results of the experiment. The model uncertainty can be determined after comparing the structural resistance of the experiment with the structural resistance of the NLFE model (of the experiment).

## 5.1 Experiment by Seraj, Kotsovos & Pavlovic (1995)

### 5.1.1 Frame details experiment

Two portal frames were designed and tested by Seraj et al. (1995). The portal frames have fixed supports and corner connections. The frames were labelled as Portal Frame 1 (PF1) and Portal Frame 2 (PF2). PF1 was designed according to the British Code 8110 (1985) and PF2 was designed according to the compressive-force path (CFP) method.

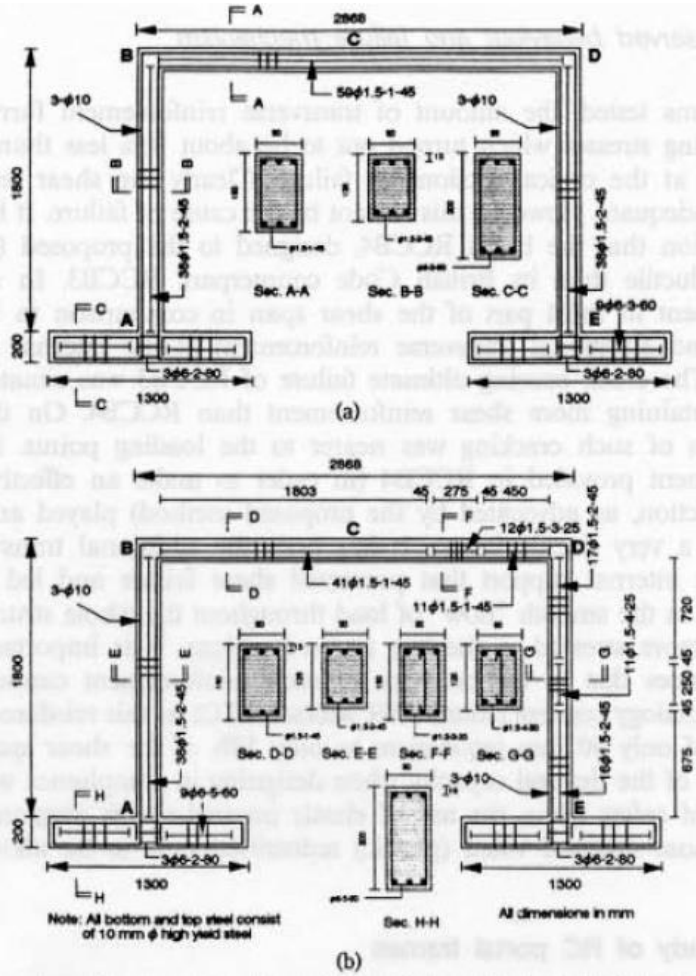


*Figure 33. Dimensional, cross-sectional and design details of the fixed Portal Frames: PF1 (a) and PF2 (b) (Seraj, Kotsovos, & Pavlovic, 1995).*

The CFP method is a force path which follows the compressive side of the frame due to bending moments (figure 34 (c)). If the sign of the bending moment changes the force path goes from the lower side to the upper side of an element. This happens at the location where the moment is zero. The locations are called internal supports (IS1, IS2 and IS3 in figure 34 (c)). The design procedure of the CFP method is not discussed extensively in this thesis since only the load-carrying capacity for this frame design is important and the design method is of less importance. Design details of both frames can be found in figure 33. The fixed supports were made by post-tensioning the footings to the laboratory floor.

Both frames are designed to resist a vertical force of $F_v = 24$ kN and a horizontal force of $F_h = 20$ kN. Linear elastic calculations are performed to design the frames using a local design approach. The linear elastic moment and shear force diagram are shown in figure 34.

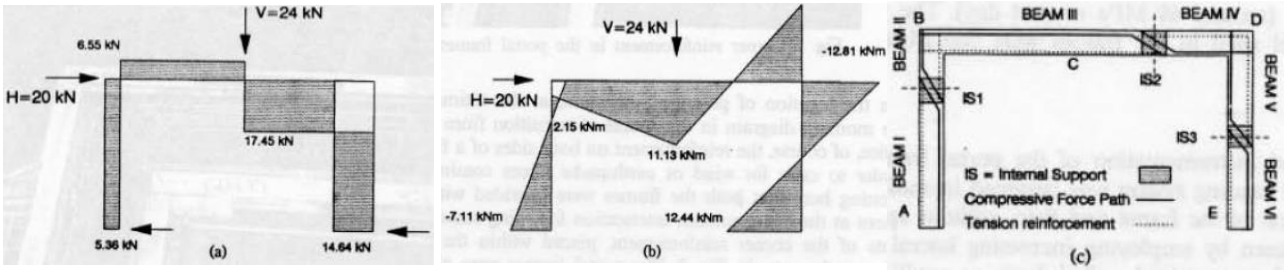


*Figure 34. Linear elastic shear force diagram (a), moment diagram (b) and CFP of PF2 (c) (Seraj, Kotsovos, & Pavlovic, 1995).*

The design is made using a local design approach with mean material strength values in order to design the frame as close as possible to the real structural resistance. The used mean material values are given in Appendix B.3. Only nominal shear reinforcement is placed in PF1 since according to the British Code 8110 (1985) no shear reinforcement is required. In PF2 some additional shear reinforcement was needed in accordance with the CFP method for the sections F-F and G-G. The frames are also provided with the necessary amount of corner reinforcement at the beam-column intersection following standard design practice (no further details given).

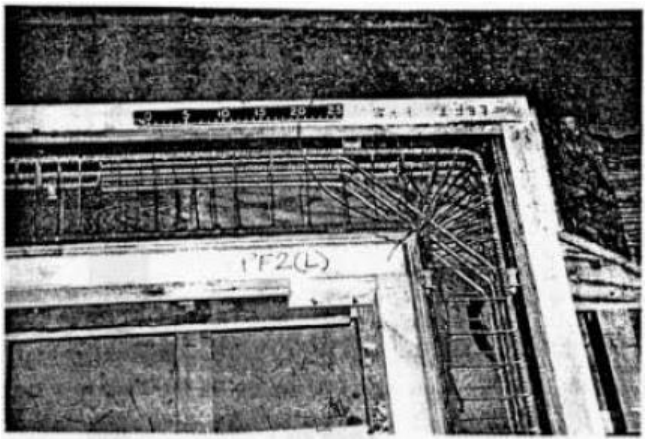


*Figure 35. Corner reinforcement at the beam-column intersection (Seraj, Kotsovos, & Pavlovic, 1995).*

The reinforcement applied in both corners (figure 35) is to prevent a diagonal crack which starts from the inside of the corner as a result of an opening moment (figure 36). The radial stirrups are place to prevent the secondary cracks as explained in chapter 4.1. The most critical corner is corner D which is loaded with a closing moment (figure 37). The inclined bar and the radial stirrups have no use for the closing moment at D and the opening moment stays very low at B. When a closing moment is applied to a corner the concrete needs to resist the compressive stresses in the compression strut (figure 37).

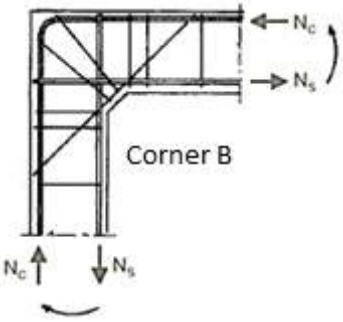


*Figure 36. Opening moment (Walraven, Staafwerkmodellen als basis voor het detailleren van betonconstructies, 1988).*

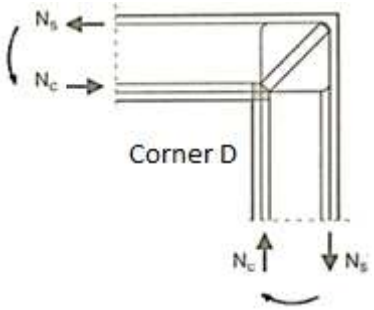


*Figure 37. Closing moment (Walraven & Fennis, Gewapend Beton (CTB2220), 2013).*

### 2.1.2 Test setup

The test setup is shown in figure 38 and the instrumentation in figure 39. The vertical force is applied with a tension jack at location C and the horizontal force with a compression jack at location B. The tension jack was connected to a steel framework which was pulled downward to apply the vertical load. The loads were recorded separately by a data logger. The vertical displacement of C is measured with LVDT 1 and the horizontal displacement of D is measured with LVDT 2. The strain is measured with strain gauges at location C, $\epsilon_4$ and $\epsilon_{11}$ (compression and tension), and at location D, $\epsilon_3$ and location E, $\epsilon_8$. More instrumentation is used during the experiments but the results are not given by Seraj et al. (1995).

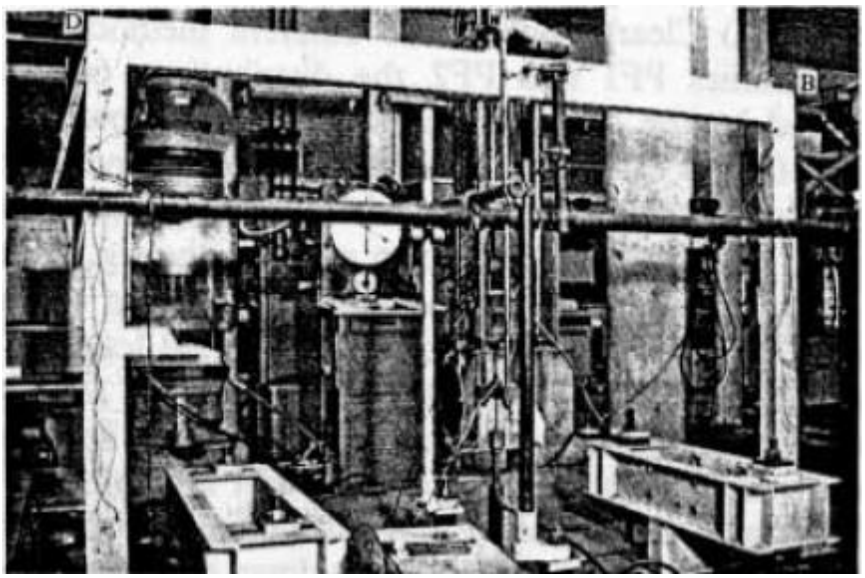


*Figure 38. Test setup (Seraj, Kotsovos, & Pavlovic, 1995).*

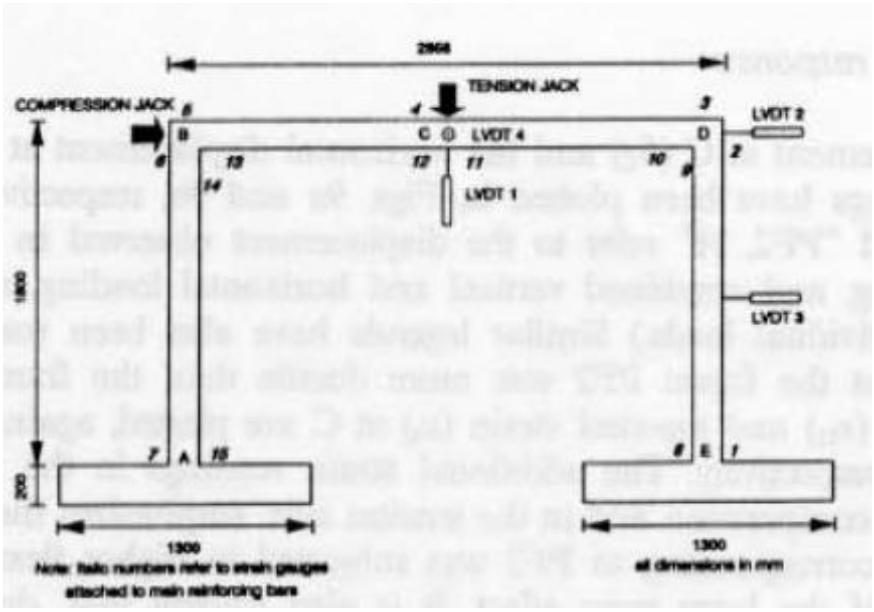


*Figure 39. Instrumentation on the portal frame (Seraj, Kotsovos, & Pavlovic, 1995).*

### 5.1.3 Structural resistance

The theoretical loading procedure is as follows. First the vertical load $F_v = 24$ kN is incrementally applied to the frame. After that the vertical load is kept constant (controlled by the data logger) and the horizontal load $F_h$ is incrementally applied until failure.

During the experiment the loads were recorded and the results will be described here. First the frames PF1 and PF2 were incrementally subjected to a vertical load of 23.72 kN and 23.69 kN, respectively (table 5). Maintaining the vertical loads constant in the loading machines, the frame is now incrementally subjected to a horizontal load. Failure of PF1 and PF2 happened at a horizontal load of 20 kN and 19.95 kN, respectively.

The results are shown in table 5 and in Appendix E.1. After inspecting the results of the experiment. The strain at location C ($\epsilon_{11}$) has been increased after the vertical load was totally applied on the frame (table 5). The horizontal load should theoretically not produce any extra strain at C since the bending moment at C only depends on the vertical force.

*Table 5. Results PF1 and PF2 (Seraj, Kotsovos, & Pavlovic, 1995).*

| Frame | At the end of load $V$ | | | At the end of load $V+H$ | | | | | |
|---|---|---|---|---|---|---|---|---|---|
| | $\varepsilon_{11}\times10^6$ | $\varepsilon_4\times10^6$ | $M_c$, kNm | $\varepsilon_{11}\times10^6$ | $\varepsilon_4\times10^6$ | $M_c$, kNm | Applied $V$, kN | Calculated $V$, kN | Applied $H$, kN |
| PF1 | 1679 | −514 | 9.76 | 2033 | −744 | 11.73 | 23.72 | 28.50 | 20.00 |
| PF2 | 1596 | −584 | 9.32 | 2313 | −892 | 13.26 | 23.69 | 33.68 | 19.95 |

It was concluded that the side sway of the frame leads to an additional vertical force on the frame. This is caused by the steel framework which was fixed after applying the vertical force $F_v = 24$ kN. The side sway of the reinforced concrete frame due to the horizontal force $F_h$ leads to elongation of the steel framework which causes the additional vertical force $F_{v,sway}$.

The length of the steel frame is equal to OC after applying the vertical force (figure 40). The horizontal load on the frame leads to a side sway of the frame. To make this side sway possible the length of the steel frame connected to the tension jack must increase with OC'-OC (figure 40). Since the tension jack is displacement controlled i.e. steel frame is fixed after applying the vertical force,

the elongation of the steel frame leads to an additional vertical force $F_{v,sway}$ on the structure. Theoretically there should also be a horizontal force component but this has a negligible effect the experimental results.

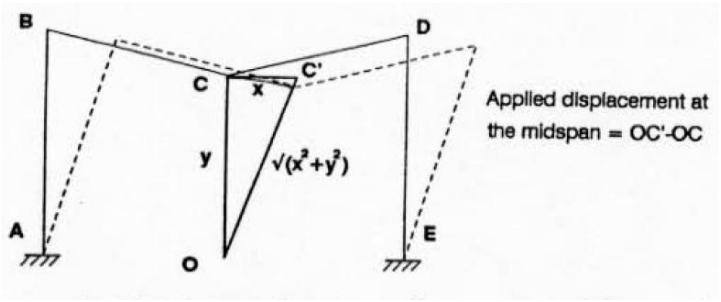


*Figure 40. Pull-down effect due to side sway of the portal frame (Seraj, Kotsovos, & Pavlovic, 1995).*

The measured strain at the midspan of C during failure can be translated using the bending moment resistance of a section at C (local level approach) to the applied total vertical load of 28.50 kN and 33.68 kN for PF1 and PF2, respectively (table 5).

According to the experimental results this additional vertical load due the side sway $F_{v,sway}$ is almost not present at initial sway, but after an applied horizontal force $F_h = 15$ kN, the additional force in more or less linear increasing from 0 to $F_{v,sway} = 28.50 - 23.72 = 4.78$ kN and $F_{v,sway} = 33.68 - 23.69 = 10$ kN for PF1 and PF2, respectively.

The additional vertical load due to the sway effect is described here very accurately. This is needed to simulate the experiments in order to make an accurate assumption of the model uncertainty

### 5.1.4 Deformational response

- The results of the deformational response are shown in the graphs in Appendix E1, figure E1 (a), (b), (c), (d), (e) and (f).
- The results of the vertical and horizontal deformation, figure E1 (a) and (b), show a more ductile behavior for PF2 (more vertical and horizontal deformation).
- The horizontal deformation of PF2 is much larger than the deformation of PF1. This leads to higher strains at midspan C, figure E1 (c) and (d), due to a higher pull down effect.
- The steel strain in corner D is larger for PF1 than in PF2, indicating more rotational deformation in PF1 than in PF2 figure E1 (e).
- At the inner side of the support at E, both frames PF1 and PF2 has reach the yield stress but only frame PF2 was exposed to plastic deformation (indicated by a horizontal upper bound).
- It appears that the rotations at point D and E due to the moments are transferred more uniformly in the case of PF2. For PF1 the rotations are more concentrated in corner D.
- The strain gauges $\epsilon_7$ and $\epsilon_{15}$ at support A show that a plastic hinges was formed in PF2. PF1 nearly reaches its plastic capacity.

### 5.1.5 Cracking process and failure mechanism

The cracks formed near failure of PF1 and PF2 are shown in figures E2 till E7. The crack pattern at B and C for PF1 and PF2 are almost similar. The crack pattern near corner D and E is different for PF1 and PF2. The cracking process and the failure mechanism is described below.

#### 5.1.5.1 *Vertical loading* $\mathrm{F_v}$

The observations during the vertical loading are the same for both frames PF1 and PF2. The first flexural crack was observed at midspan C at a vertical load of $\mathrm{F_v} = 10$ kN. The flexural cracks were gradually propagating upwards and the deepest fissure was found at the end of the vertical loading. Cracks also appeared in the corners B and D when the vertical load $F_v = 18$ kN.

#### 5.1.5.2 *Horizontal loading* $\mathrm{F_h}$ *and additional vertical loading due side sway* $\mathrm{F_{v,sway}}$

In both frames flexural cracks were detected in corner D at a horizontal load $F_h = 2$ kN. When the horizontal load was increased more cracks appeared in the top right half of column DE. The depth of these cracks was less for PF1 than for PF2. The cracks for PF1 were concentrated near corner D in contrast with PF2 were the cracks were more spread over both tension sides of the column. When the failure load was almost reached cracks were visible at the bottom half of column AB in PF2. No cracks were detected in PF1.

#### 5.1.5.3 *Failure mechanism*

The failure of PF1 was caused by excessive cracking at corner D. Wide diagonal cracks and spalling of the concrete lead to the collapse of this frame. A mechanism could not be formed since the corner D already failed.

PF2 failed almost like a mechanism when the diagonal cracks at D became wide and eventually the tension strength of steel at the supports was reached.

### 5.1.6 Conclusion experiment

Both frames have the same amount of corner reinforcement but the additional amount of shear reinforcement in PF2 at the internal supports IS2 and IS3 (figure 34 (c)) leads to a more spreading crack pattern at the region near corner D. In contrary with PF1 where the cracks are concentrated at corner D. This stress concentration in PF1 leads to earlier failure of corner D which results in a brittle behavior. PF2 failed like a mechanism since corner D failed after the mechanism was formed.

The main conclusion from this experiment is that corner D determines a ductile or brittle failure of the reinforced concrete frame. Ductile when the corner can resist the stress concentrations and is able to redistribute the internal forces and a brittle failure when corner D fails to redistribute the internal forces.

## 5.2 Level I reliability method: local design resistance experiment Seraj et al. (1995)

A local safety approach according to the Eurocode 2 (NEN-EN 1992 -1-1, 2011) is used to roughly indicate which and where a specific failure mode starts to develop. The local safety approach described in the Eurocode 2 is only meant to determine the design resistance of an element against a certain failure mode.

The portal frame from the experiment of Seraj et al. (1995) is designed with mean material values. This leads to the mean resistance of the structure, which is able to resist a vertical load $F_v = 24$ kN and a horizontal load of $F_h = 20$ kN. The design resistance of several sections is too low according to the Eurocode 2. The design can be improved with a higher reinforcement ratio, higher concrete class or adapting the dimensions of the frame. However the main focus of this study is to determine the real resistance of the structure. Since the local safety approach in Eurocode 2 is conservative it is unlikely that the portal frame cannot resist the vertical and horizontal force.

### 5.2.1 Determination of the internal forces (linear elastic calculation)

To perform a local safety evaluation the linear elastic moments, shear- and normal forces should be determined. The linear elastic calculations are performed with the software package Matrix Frame 5.3. The results are shown in figure 41.

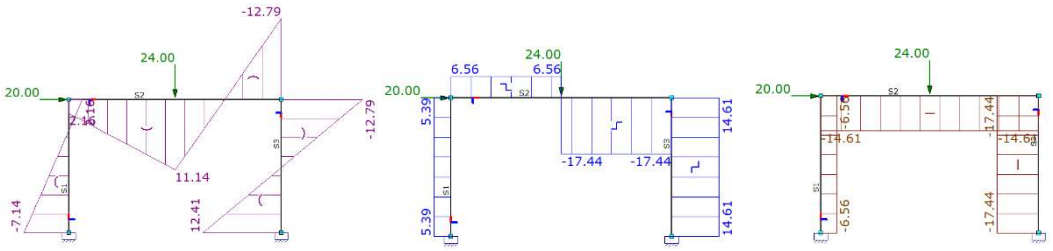


*Figure 41. Linear elastic moment, shear force and normal force diagram (kNm).*

The elements will be numbered from left to right, which is shown in figure 20. The maximal internal forces for each element are summarized in table 6.

*Table 6. Internal forces.*

| | $M_E$ (kNm) | $V_E$ (kN) | $N_E$ (kN) |
|---|---|---|---|
| Element 1 | 7.1 | 5.4 | 6.6 |
| Element 2 | 12.8 | 17.4 | 14.6 |
| Element 3 | 12.8 | 14.6 | 17.4 |

### 5.2.2 Determination of the resistance (ULS)

The bending moment resistance, the shear resistance with and without shear reinforcement is determined in the ultimate limit state (ULS) for each element in the portal frame. The results are presented here and the calculations can be found in Appendix C2.

#### *5.2.2.1 Bending moment capacity (ULS)*

The bending moment capacity $M_{Rd}$ is determined in accordance to Eurocode 2 (NEN-EN 1992 -1-1, 2011). The normal force in the portal frame elements leads to a higher bending moment capacity compared with an element without a normal force. However this positive effect of the normal force on the bending moment resistance is neglected, which is a conservative assumption. The bending moment capacity for each element according to the Eurocode 2 is presented in table 7. In element 2 and 3 a plastic hinge will develop since redistribution of forces is possible in a statically indeterminate portal frame.

*Table 7. Design bending moment capacity (EC2).*

| EC2 | $M_{Rd}$ (kNm) | $M_E$ (kNm) | UC (-) |
|---|---|---|---|
| Element 1 | 10.0 | 7.1 | 0.71 |
| Element 2 | 12.6 | 12.8 | 1.02 |
| Element 3 | 10.0 | 12.8 | 1.28 |

Since the frame is designed using mean material values the mean bending moment capacity $M_{Rm}$ of the elements is also calculated and given in table 8. However it is necessary to mention that the mean bending moment capacity does not lead to an intended reliability index of $\beta_R = 3.04$.

*Table 8. Mean bending moment capacity.*

| Mean | $M_{Rm}$ (kNm) | $M_E$ (kNm) | UC (-) |
|---|---|---|---|
| Element 1 | 12.9 | 7.1 | 0.55 |
| Element 2 | 16.2 | 12.8 | 0.79 |
| Element 3 | 12.9 | 12.8 | 0.99 |

#### *5.2.2.2 Shear capacity (ULS)*

##### Elements without shear reinforcement

The design value for the shear resistance $V_{Rd,C}$ is determined according to the EC2 with the empirical formula (C.6). The calculations are given in appendix C.2.2.2. The shear resistance for elements without shear reinforcement is dependent on the normal force in the specific element. Therefore each element has a different shear resistance. The design shear capacity $V_{Rd,C}$ and the minimum shear capacity $V_{Rd,C,min}$ of the elements is presented in table 9. Element 2 and 3 need shear reinforcement according to EC2.

*Table 9. Design shear capacity without shear reinforcement (EC2).*

| EC2 | $V_{Rd,C,min}$ (kN) | $V_{Rd,C}$ (kN) | $V_E$ (kN) | UC (-) |
|---|---|---|---|---|
| Element 1 | 6.2 | 10.7 | 5.36 | 0.50 |
| Element 2 | 8.6 | 13.3 | 17.45 | 1.21 |
| Element 3 | 7.7 | 12.2 | 14.64 | 1.20 |

The mean shear capacity $V_{Rm,C}$ and the minimum mean shear resistance $V_{Rm,C,min}$ can be determined by using formula (C.6) and set the partial safety factor to $\gamma_c = 1.0$. The results are given in table 10. All unity checks are below zero. This indicates that no shear reinforcement is needed when there is no deviation from the mean value.

*Table 10. Mean shear capacity without shear reinforcement.*

| Mean | $V_{Rm,C,min}$ (kN) | $V_{Rm,C}$ (kN) | $V_E$ (kN) | UC (-) |
|---|---|---|---|---|
| Element 1 | 6.9 | 15.6 | 5.36 | 0.34 |
| Element 2 | 9.4 | 18.9 | 17.45 | 0.92 |
| Element 3 | 8.3 | 17.1 | 14.64 | 0.86 |

### Elements with shear reinforcement

For members with vertical shear reinforcement, the shear capacity is the smallest value of $V_{Rd,S}$ and $V_{Rd,max}$, the maximum tensile force in the stirrups and the maximum compression force in the compression chord, respectively. The calculation according to the EC2 can be found in appendix C.2.2.2 and the results are presented in table 11.

*Table 11. Design shear resistance with shear reinforcement (EC2).*

| EC2 | $V_{Rd,S}$ (kN) | $V_{Rd,max}$ (kN) | $V_E$ (kN) | UC (-) |
|---|---|---|---|---|
| Element 1 | 7.0 | 33.4 | 5.36 | 0.76 |
| Element 2 | 8.6 | 42.0 | 17.45 | 2.02 |
| Element 3 | 7.0 | 35.0 | 14.64 | 2.08 |

There is not enough shear reinforcement to prevent a shear failure according to the Eurocode 2.

#### *5.2.2.3 Plastic analysis (ULS)*

The Eurocode 2 (NEN-EN 1992 -1-1, 2011) is not exactly clear about the rotational capacity of a reinforced concrete corner connection. The Eurocode 2 does only mention some restrictions for the rotational capacity of a statically indeterminate beam. Therefore it is not clear if the corner is ductile enough to form a full plastic hinge. A plastic upper bound analysis for a portal frame which forms a plastic mechanism can be made but it is most likely that the corner D failed earlier which lead to a lower structural resistance.

An attempt will be made to simulate the failure mode of the experiment, where a partially plastic mechanism was formed. The forming of a plastic mechanism is possible if there is enough rotational capacity for the corners of the frame to form a plastic hinge. Most likely the rotational capacity of corner D is too low and the corner will fail, which lead to a partially plastic hinge. First the structural resistance of a full plastic mechanism with plastic hinges in A, C, D and E will be determined. The horizontal force is assumed to be known $F_h = 20$ kN. An upper bound of the vertical collapse load $F_v$ is determined with virtual work according to the following equation:

$$\sum F\ \delta u = \sum M_R\ \delta\theta \tag{5.1}$$

where:

$$\sum F\ \delta u = M_{Rm,1}\ \theta + M_{Rm,2}\ (\theta + \theta) + M_{Rm,3}\ (\theta + \theta) + M_{Rm,3}\ \theta \tag{5.1a}$$

$$\sum M_R\ \delta\theta = 1.725\ F_h\ \theta + 1.3715\ F_v\ \theta. \tag{5.1b}$$

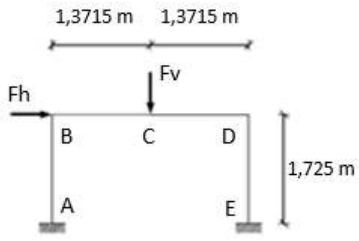


*Figure 42. Portal frame dimensions and load.*

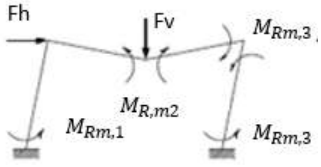


*Figure 43. combined mechanism.*

The mean bending moment resistance $M_{Rm}$ of the several elements is determined in chapter 3.2.1. Equations (5.1a) and (5.2b) are derived for the combined mechanism shown in figure 43. The structural resistance of this full plastic mechanism is:

$F_v = 20$ kN, $F_h = 38.5$ kN.

The structural resistance is much higher than obtained in the experiment of Seraj et al. (1995). This indicates that corner D is not able to form a full plastic hinge. The mean experimental structural resistance can be found in Appendix E.1:

$F_v = 20$ kN, $F_h = 31.0$ kN.

The experimental structural resistance can be used to calculate the real bending moment capacity of corner D with the virtual work equation (5.1). The maximum bending moment resistance of corner D is $0.7\ M_{Rm,3}$. The real bending moment capacity of corner D strongly depends on the case. This effect is also described in chapter 5.3.3, where the failure of the NLFE model from the experiment of the reinforced portal frame is described.

### 5.2.3 Conclusion local design resistance

The local safety approach (the partial factor method) in the Eurocode 2, leads to a structural resistance which is much lower than the mean resistance, since design material values are used. This is needed to obtain a reliability level of at least $\beta_R = 3.04$. The design shear resistance of the elements is too low and a shear failure should happen. However the experimental results in chapter 5.1 show a totally different failure mode, namely the forming of a partially plastic mechanism in combination with the failure of corner D.

A more realistic structural behavior is obtained when the partial safety factors are excluded from the analyses such that the mean resistance of the elements is obtained. Now the shear resistance of the elements is enough to form a partially plastic mechanism in combination with the failure of corner D.

## 5.3 NLFE analyses of experiment Seraj et al. (1995)

The load carrying capacity of the reinforced concrete frame is modelled with the use of the non-linear finite element software package: Diana FEA 10.1. The model is made based on the Guidelines for non-linear finite element analysis of reinforced concrete structures (Hendriks, de Boer, & Belletti, 2017).

### 5.3.1 Geometry and mesh

The experiment of Seraj et al. (1995) is simulated with a NLFE model. The designs of the frames PF1 and PF2 can be found in figure 33.The reinforced concrete frame is modelled with four plane stress elements over the height (4 e.o.h.) and embedded reinforcement. There is chosen for 4 e.o.h. while the Guidelines for NLFE analyses (Hendriks, de Boer, & Belletti, 2017) suggest that at least 6 e.o.h. should be used. The reason for this deviation is a reduction of the computational time and stress concentration in the corner D (Appendix D.4).

There is chosen for a two dimensional model, since the frame is very slender and three dimensional effects can be neglected. The geometry, mesh and applied load is shown in the figures below. Only the geometry, mesh and applied load are shown for PF2. PF1 is modelled in a similar way only the reinforcement design is different (figure 33 and Appendix D.1.2.1).

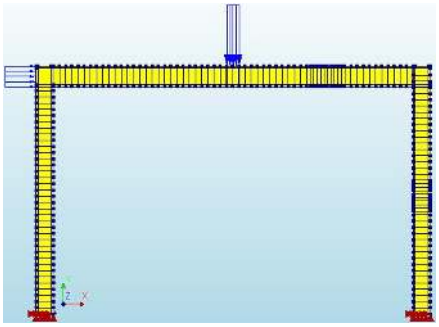

*Figure 44. Geometry, reinforcement and applied load PF2.*

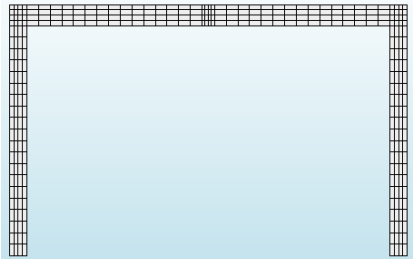

*Figure 45. Mesh concrete (plane stress elements).*

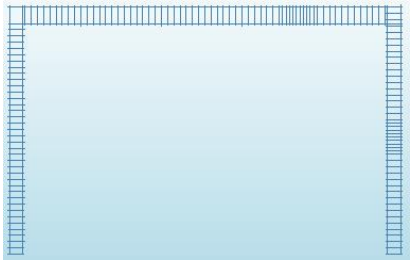

*Figure 46. Mesh embedded reinforcement (bar elements).*

The boundary conditions are shown in figure 44. The columns have fixed translations in the x, y direction and a fixed rotation around the z-axis. Furthermore there is no additional corner reinforcement placed which is shown in figure 46 since the amount of reinforcement is unknown and the design helps only for an opening moment and the governing failure mode is due to a closing moment (right corner D).

### 5.3.2 Non-linear finite element models

The element types, constitutive models used in the non-linear finite element model are shown in appendix D.2. The material parameters used in the NLFE analysis are based on the values given by Seraj et al. (1995) and the unknown material parameters have been calculated according to the Model Code 2010 (fib, 2012). The material parameters are derived in Appendix B. The values used in the NLFE analysis are the mean values in Appendix B.3. The convergence norm applied in the model is a combination of a force and energy norm. The convergence tolerance for the force and energy norm is 0.01 and 0.001, respectively.

### 5.3.2 Load paths for PF1 and PF2

The loading path is constructed in such a manner that simulates the loading path described by the experiment (Seraj, Kotsovos, & Pavlovic, 1995). The additional load due to the sway effect of the frame is calculated by Seraj et al. (1995). For both portal frames tested during the experiment this additional vertical load is different due to different deformation. The additional vertical load starts when a horizontal load of $F_h = 15$ kN is applied. When this horizontal force is applied on the frame there is additional vertical deformation visible which is only explicable due to the additional vertical load (Appendix E1, figure E1 (a)). The additional vertical load $F_{v,sway}$ is calibrated in such a way that when a horizontal load $F_h = 20$ kN is applied on the model, the additional vertical load has reached the collapse load from the experiment.

In the tables 12 and 13 the loading paths are shown. First the vertical load $F_v = 24$ kN is applied with load increments of 10 percent. Secondly the horizontal load is applied till $F_h = 15$ kN. Finally the last load combination is applied which is a combination of the horizontal force $F_h$ and $F_{v,sway}$. The last load combination is applied till failure of the structure.

*Table 12. Load path PF1.*

| PF1 | | | | |
|---|---|---|---|---|
| Equilibrium Iteration | Maximum number of iterations | Load-steps | Line search | Load combination |
| Regular NR | 400 | 0.1(10) | yes | Fv = 24 kN |
| Regular NR | 800 | 0.05(15) | yes | Fh = 20 kN |
| Secant (Quasi-Newton) | 1000 | 0.05(4) 0.01(100)<br>Till failure | yes | Fv = 20 kN<br>Fh (sway) = 18 kN |

*Table 13. Load path PF2.*

| PF2 | | | | |
|---|---|---|---|---|
| Equilibrium Iteration | Maximum number of iterations | Load-steps | Line search | Load combination |
| Regular NR | 400 | 0.1(10) | yes | Fv = 24 kN |
| Regular NR | 800 | 0.05(15) | yes | Fh = 20 kN |
| Secant (Quasi-Newton) | 1000 | 0.05(4) 0.01(100)<br>Till failure | yes | Fv = 20 kN<br>Fh (sway) = 40 kN |

### 5.3.3 Structural failure of the portal frames

The failure modes of the NLFE model of PF2 are presented below. PF1 have comparable failure modes. Several elements have to fail before the structural system fails since the portal frame is statically indeterminate. First the concrete compressive strut in closing corner D (right corner) fails partially (figure 47 and 48). In fact the softening behavior of the parabolic concrete compression diagram (figure 49) is used to redistribute the internal forces to the other parts of the portal frame.

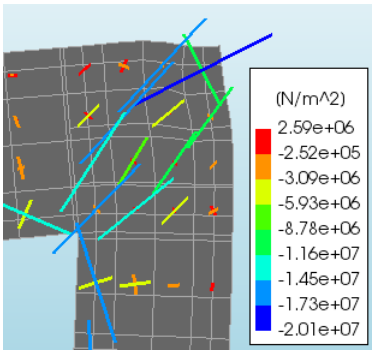


*Figure 47. Principle stresses before partial failure concrete compressive strut corner D (load-step 20).*

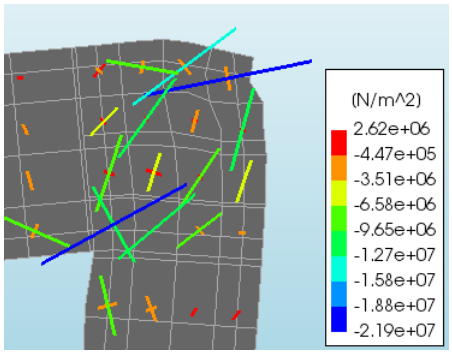


*Figure 48. Principle stresses after partial failure concrete compressive strut corner D (load-step 21).*

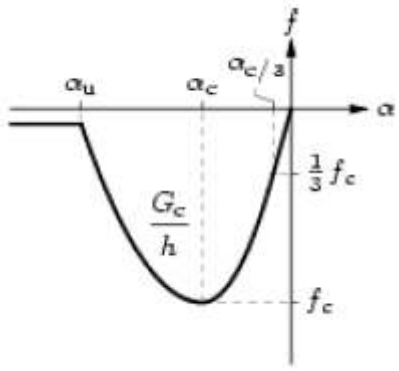


*Figure 49. Parabolic compression diagram concrete (Hendriks, de Boer, & Belletti, 2017).*

Due to the softening behavior of the concrete in corner D the maximum moment capacity of corner D is reached. Composed line elements are included in the NLFE model. This elements can integrate the stresses over the height of the element to determine the moment distribution at a certain position. In figure 51 the moment distribution is shown directly after the failure of the concrete compressive strut (load-step 22). Figure 50 shows the moment distribution before failure of the structural system (load-step 29). The moment capacity of corner D is reached after load-step 22 and cannot increase any more.

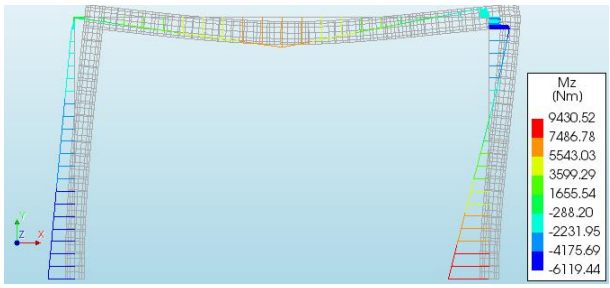


*Figure 51. Moment distribution composed line elements after failure of the concrete compressive strut (load-step 22).*

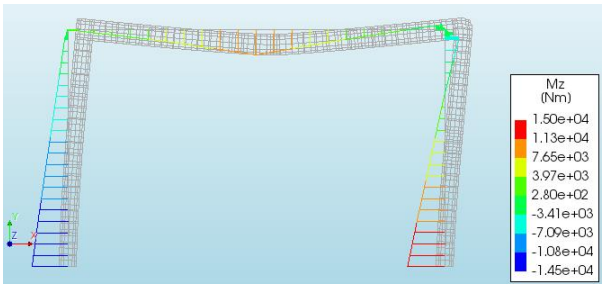


*Figure 50. Moment distribution composed line elements before the structural system failure (load-step 29).*

The failure of the structural system occors after the forming of plastic hinges at midspan C (load-step 23), the bottom of the left and the right column (load-step 29). The forming of the plastic hinges occurs after the yielding of the reinforcement. This is shown in figure 52 and 53. The partial failure of corner D and the forming of the plastic hinges at location A, C and E lead to a mechanism and eventually to the failure of the structural system.

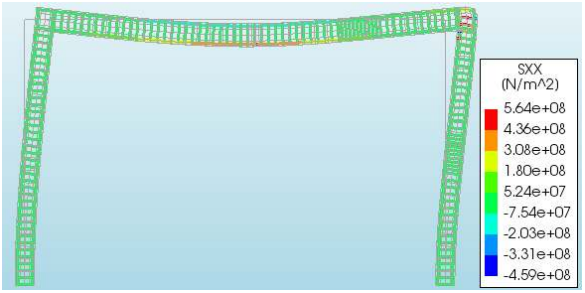


*Figure 52. Yielding of the steel reinforcement at midspan C (load-step 23).*

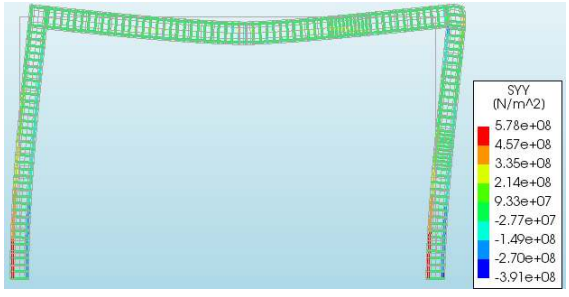


*Figure 53. Yielding of the steel reinforcement at location A and E (load-step 28).*

### 5.3.4 Comparison results NLFE analysis and experiment Seraj et al. (1995)

The non-linear finite element models for PF1 and PF2 are different due to a different reinforcement design and other load paths. The load carrying capacity of the two non-linear finite element models and the load obtained from the experiment can be found in table 14 and 15.

*Table 14. Results NLFE analysis, experiment and model uncertainty for PF1.*

| Model uncertainty PF1 | | | |
|---|---|---|---|
| Direction | F experiment (N) | F NLFE analysis (N) | F(experiment) / F(NLFE analysis) |
| Vertical | 28500 | 28140 | 1.013 |
| Horizontal | 20000 | 19600 | 1.020 |
| Mean | | | 1.016 |

*Table 15. Results NLFE analysis, experiment and model uncertainty for PF2.*

| Model uncertainty PF2 | | | |
|---|---|---|---|
| Direction | F experiment (N) | F NLFE analysis (N) | F(experiment) / F(NLFE analysis) |
| Vertical | 33680 | 32400 | 1.040 |
| Horizontal | 19950 | 19200 | 1.039 |
| Mean | | | 1.039 |

According to Engen (2017), the experimental outcome of different experiments can be compared to the NLFE analysis results when the same solution strategy is used. The following formula for the model uncertainty is applicable in this case:

$$\theta_m = \frac{1}{n} \sum_i^n \left(\frac{R_{exp}}{R_{NLFEA}}\right)_i \tag{2.1}$$

where:

$n = 2$ is the total number of different experiments;

$R_{exp}$ experimental outcome;

$R_{NLFEA}$ results from NLFE analysis.

For this case the model uncertainty for the total load is $\theta_m = \frac{1}{2}\ (1.016 + 1.039) = 1.028$ and the coefficient of variation $V_m = 0.01$ based on the results of PF1 and PF2. These are not very realistic values since just two different experiments have been performed.

The deformational response of the non-linear finite element model is compared with the experimental results in Appendix E.2. Also the measured strain of the reinforcement is compared with the strain found with NLFE analysis at several locations. The stiffness of the model is higher than the experimental results. This is the main reason for the differences in experimental and modelling results.

# 6 Uncertainties in the reinforced concrete frame designs

The uncertainties in the reinforced concrete frame designs can be divided in physical uncertainties (chapter 6.1) and model uncertainties (chapter 6.2).

## 6.1 Physical uncertainties

The physical uncertainties can subsequently divided into: material uncertainties, geometrical uncertainties and loading uncertainties.

### 6.1.1 Material uncertainties

The concrete used in portal frame design 1 and 2 is concrete strength class C30. In portal frame design 3 the concrete strength class C40 is used. The steel grade is the same in the three portal frame designs.

#### *6.1.1.1 Concrete*

The concrete material parameters such as the compressive strength $f_c$, tensile strength $f_{ct}$, the modulus of elasticity $E_c$, the fracture energy $G_f$ and the compressive fracture energy $G_c$ are based on experimental test. Therefore all concrete material can be represented by continuous stochastic variables with a certain distribution type. In this thesis the following concrete variables are used: $f_c, f_{ct}, E_c, G_f$ and $G_c$. All stochastic variables can be described with the following stochastic parameters: distribution type, mean value and coefficient of variation. All concrete variables are lognormal distributed since all values are higher than zero (unlike the normal distribution) and it is an accurate approach for low and high coefficients of variation (Torrent, 1978). The variables that have a large influence on the structural capacity are assumed to be stochastic. The most important stochastic variables are: $f_c, f_{ct}, E_c$ and $G_f$ (table 16 and 17). The compressive fracture energy $G_c$ is assumed to be fully dependent on the fracture energy $G_f$ according to equation (B.8) in Appendix B.1.

*Table 16. Stochastic properties concrete C30.*

| Concrete C30 | | | | | |
|---|---|---|---|---|---|
| Variable | fc (MPa) | fct (MPa) | Ec (MPa) | Gf (Nm/m2) | Gc |
| Mean | 38 | 2.869 | 33550.6 | 140.5 | 35125.6 |
| Standard deviation | 5.7 | 0.430 | 5703.6 | 28.1 | - |
| distribution | LN | LN | LN | LN | Fully dependent on the fracture energy Model Code 2010 (fib, 2012) |

*Table 17. Stochastic properties concrete C40.*

| Concrete C40 | | | | | |
|---|---|---|---|---|---|
| Variable | fc (MPa) | fct (MPa) | Ec (MPa) | Gf | Gc |
| Mean | 48 | 3.509 | 36267.6 | 146.5 | 36634.2 |
| Standard deviation | 7.2 | 0.526 | 6165.5 | 29.3 | - |
| distribution | LN | LN | LN | LN | Fully dependent on the fracture energy Model Code 2010 (fib, 2012) |

The coefficient of variation is $V_{f_c} = 0.15$ (Schlune (2011) and Pimentel et al. (2009)), $V_{f_{ct}} = 0.15$, $V_{E_c} = 0.17$ and $V_{G_f} = 0.2$ (Strauss, Zimmermann, Lehký, Novák, & Kersner, 2014) for the concrete compressive strength, concrete tensile strength, modulus of elasticity and fracture energy, respectively. The coefficient of variation is an important factor in the safety analysis. In literature

many different values can be found. Selecting the right values for a certain case is of great importance to perform a valid safety assessment.

According to the Model Code 2010 (fib, 2012), the material parameters of concrete can all be determined based on the compressive strength of concrete. The relations between the material parameters of concrete are shown in Appendix B.1. Full correlation $\rho = 1$ is assumed between the concrete material parameters. The concrete compressive strength of the portal frame can be related to the other concrete material parameters and calculated with the formulas shown in Appendix B.1. This can be used to perform a safety assessment where full correlation is assumed. The correlation between the concrete variables will be discussed in chapter 6.1.1.3.

### *6.1.1.2 Reinforcement steel*

The stochastic material properties of the reinforcement steel are given in table 18 and table 19. The yield strength of the longitudinal reinforcement $f_{y,l}$ is assumed to be lognormally distributed with a coefficient of variation $V_{f_{y,l}} = 0.05$ according to Schlune (2011), Pimentel et al. (2014) and Faber & Vrouwenvelder (2001). The steel tensile strength $f_{t,l}$ of the longitudinal reinforcement is assumed to be fully dependent on the yield strength according to equation (B.11) in Appendix B.2. The modulus of elasticity $E_s$ and the yield strain $\epsilon_{sy}$ of the reinforcement steel is assumed to be deterministic.

*Table 18. Stochastic properties longitudinal reinforcement.*

| Longitudinal reinforcement | | | | |
|---|---|---|---|---|
| Variable | fy,l (MPa) | ft (MPa) | Es (MPa) | ϵsy |
| Mean | 560 | 680 | 200000 | 0.0028 |
| Standard deviation | 28 | - | - | - |
| Distribution | LN | Fully dependent on yield strength fy,l Model Code 2010 (fib, 2012) | Deterministic | Deterministic |

The shear reinforcement material values are assumed to be deterministic since the portal frame designs are not sensitive for a shear failure mode when a global safety approach is used (see chapter 4.4).

*Table 19. Stochastic properties shear reinforcement.*

| Shear reinforcement | | | | |
|---|---|---|---|---|
| Variable | fy,s (MPa) | ft (MPa) | Es (MPa) | ϵsy |
| Mean | 460 | 510 | 200000 | 0.0023 |
| Standard deviation | - | - | - | - |
| Distribution | Determininistic | Deterministic | Deterministic | Deterministic |

### *6.1.1.3 Correlation material properties*

All concrete material properties are dependent correlated variables. The correlation between the concrete compressive strength $f_c$, the tensile strength $f_{ct}$ and the modulus of elasticity $E_c$ is determined by Octar et al. (1996), which are presented in table 20. In literature there is not much information about the correlation between $f_c$, $f_{ct}$, $E_c$ and the concrete fracture energy $G_f$. Zimmermann et al. (2016) found the correlation factor $\rho_{G_f,f_{ct}} = 0.8$ between the fracture energy and the tensile strength for concrete up to C30/37. The following correlation factors are determined by Keršner et al. (2007): $\rho_{G_f,f_c} = 0.714$ and $\rho_{G_f,E_c} = 0.657$ for the correlation between the fracture

energy with the concrete compressive strength and the modulus of elasticity. The longitudinal reinforcement is independent and uncorrelated from the concrete material properties (table 20).

*Table 20. Correlation matrix.*

| Correlation Matrix | | | | | |
|---|---|---|---|---|---|
| Variable | fc | fct | Ec | Gf | fy,l |
| fc | 1 | 0.932 | 0.772 | 0.714 | 0 |
| fct | 0.932 | 1 | 0.684 | 0.8 | 0 |
| Ec | 0.772 | 0.684 | 1 | 0.657 | 0 |
| Gf | 0.714 | 0.8 | 0.657 | 1 | 0 |
| fy,l | 0 | 0 | 0 | 0 | 1 |

According to chapter 2.5 the correlated lognormal variables can be transformed to correlated normal distributed variables $\ln(\boldsymbol{X})$ with mean $\boldsymbol{\mu_L}$ and standard deviation $\boldsymbol{\sigma_L}$. After that the correlated normally distributed variables $\boldsymbol{X}$ can be transformed to uncorrelated standard normally distributed variables $\boldsymbol{U}$ using a transformation matrix $\boldsymbol{T}$. The matrix $\boldsymbol{T}$ is found using Cholesky decomposition of the correlation matrix $\boldsymbol{\rho}$ (table 20). This is shown in Appendix F.1. The result of the transformation is given below:

$$\boldsymbol{X} = \boldsymbol{\mu_L} + \boldsymbol{DTU}$$

$$\begin{bmatrix} X_{f_c} \\ X_{f_{ct}} \\ X_{E_c} \\ X_{G_f} \\ X_{f_{y,l}} \end{bmatrix} = \begin{bmatrix} \mu_{L,f_c} \\ \mu_{L,f_{ct}} \\ \mu_{L,E_c} \\ \mu_{L,G_f} \\ \mu_{L,f_{y,l}} \end{bmatrix} + \begin{bmatrix} U_{f_c}\,\sigma_{L,f_c} \\ (0.932\,U_{f_c} + 0.362\,U_{f_{ct}})\,\sigma_{L,f_{ct}} \\ \left(0.772\,U_{f_c} - 0.098\,U_{f_{ct}} + 0.628\,U_{E_c}\right)\sigma_{L,E_c} \\ \left(0.714\,U_{f_c} + 0.371\,U_{f_{ct}} + 0.226\,U_{E_c} + 0.549\,U_{G_f}\right)\sigma_{L,G_f} \\ U_{f_{y,l}}\,\sigma_{L,F_{y,l}} \end{bmatrix} \tag{6.1}$$

However it is questionable if this approach of assuming five distribution functions with their corresponding correlation coefficients is a good approximation of the real material behavior. This is because the correlation coefficients between all concrete properties are hard to determine since the properties are determined separately.

A better approach is the use of the relation between the concrete properties as described in the Model Code 2010 (fib, 2012) and which are presented in Appendix B.1. These relations assume full correlation between the concrete properties $\rho = 1$ because all concrete parameters are depending on the concrete compressive strength. This assumption seems to be valid since the correlation coefficients as presented in table 20 are rather high. It is certainly better than assuming independent concrete properties, where $\rho = 0$ or correlation values which are almost impossible to determine. The correlation matrix for fully dependent concrete properties is shown is table 21.

*Table 21. Full correlation matrix.*

| Full correlation Matrix | | | | | | |
|---|---|---|---|---|---|---|
| Variable | fc | fct | Ec | Gf | Gc | fy,l |
| fc | 1 | 1 | 1 | 1 | 1 | 0 |
| fct | 1 | 1 | 1 | 1 | 1 | 0 |
| Ec | 1 | 1 | 1 | 1 | 1 | 0 |
| Gf | 1 | 1 | 1 | 1 | 1 | 0 |
| Gc | 1 | 1 | 1 | 1 | 1 | 0 |
| fy,l | 0 | 0 | 0 | 0 | 0 | 1 |

The same transformation from $\boldsymbol{X}$ to $\boldsymbol{U}$ according to chapter 2.5 can be done for full correlation between the concrete properties. The transformation is shown in Appendix F.2.

$$\boldsymbol{X} = \boldsymbol{\mu_L} + \boldsymbol{DTU}$$

$$\begin{bmatrix} X_{f_c} \\ X_{f_{ct}} \\ X_{E_c} \\ X_{G_f} \\ X_{G_c} \\ X_{f_{y,l}} \end{bmatrix} = \begin{bmatrix} \mu_{L,f_c} \\ \mu_{L,f_{ct}} \\ \mu_{L,E_c} \\ \mu_{L,G_f} \\ \mu_{L,G_c} \\ \mu_{L,f_{y,l}} \end{bmatrix} + \begin{bmatrix} U_{f_c}\ \sigma_{L,f_c} \\ U_{f_c}\ \sigma_{L,f_{ct}} \\ U_{f_c}\ \sigma_{L,E_c} \\ U_{f_c}\ \sigma_{L,G_f} \\ U_{f_c}\ \sigma_{L,G_c} \\ U_{f_{y,l}}\ \sigma_{L,f_{y,l}} \end{bmatrix} \tag{6.2}$$

Equation (6.2) shows that all concrete properties are fully dependent on the concrete compressive strength. The only uncertainty here is the coefficient of variation $V = \sigma/\mu$ of the other concrete properties, namely: the coefficient of variation of the concrete tensile strength $V_{f_{ct}}$, the modulus of elasticity $V_{E_c}$, the fracture energy $V_{G_f}$ and the compressive fracture energy $V_{g_c}$. The value of the coefficient of variation is strongly dependent on the case and several different values are used in literature.

Therefore the best way to deal with the correlated concrete properties is the use of the relations between the concrete properties as described in the Model Code 2010 (fib, 2012) and which are presented in Appendix B.1. The coefficients of variations: $V_{f_{ct}}$, $V_{E_c}$, $V_{G_f}$ and $V_{g_c}$ are in fact hidden in the empirical formulas presented in Appendix B.1. All concrete properties are related to the concrete compressive strength $f_c$. So only the coefficient of variation of the concrete compressive strength $V_{fc}$ is needed to determine the value of all other concrete properties and the coefficient of variation of the steel yield strength $V_{f_y}$ to determine the steel properties.

### 6.1.1.4 *Summary of stochastic material variables used in the safety assessment*

The chosen stochastic variables to represent the material uncertainties are the concrete compressive strength $f_c$ and the yield strength of the longitudinal reinforcement $f_{y,l}$. All other concrete properties are related to the concrete compressive strength using the relations according to the Model Code 2010 (fib, 2012) presented in Appendix B.1.

*Table 22.Stochastic properties concrete C30 used for the global safety assessment in chapter 7.*

| Concrete C30 | | | | | |
|---|---|---|---|---|---|
| Variable | fc (MPa) | fct (MPa) | Ec (MPa) | Gf | Gc |
| Mean | 38 | 2.869 | 33550.6 | 140.5 | 35125.6 |
| Standard deviation | 5.7 | - | - | - | - |
| distribution | LN | Fully dependent on the compressive strength fc according to the Model Code 2010 (fib, 2012) | | | |

*Table 23. Stochastic properties concrete C40 used for the global safety assessment in chapter 7.*

| Concrete C40 | | | | | |
|---|---|---|---|---|---|
| Variable | fc (MPa) | fct (MPa) | Ec (MPa) | Gf | Gc |
| Mean | 48 | 3.509 | 36267.6 | 146.5 | 36634.2 |
| Standard deviation | 7.2 | - | - | - | - |
| distribution | LN | Fully dependent on the compressive strength fc according to the Model Code 2010 (fib, 2012) | | | |

The yield strength of the longitudinal reinforcement $f_{y,l}$ is related to the steel tensile strength $f_t$ using the relation according to the Model Code 2010 (fib, 2012) presented in Appendix B.3 equation (B.11). The stochastic steel material properties are the same as described in chapter 6.1.1.2.

*Table 24. Stochastic longitudinal reinforcement used for the global safety assessment in chapter 7.*

| Longitudinal reinforcement | | | | |
|---|---|---|---|---|
| Variable | fy,l (MPa) | ft (MPa) | Es (MPa) | ϵsy |
| Mean | 560 | 680 | 200000 | 0.0028 |
| Standard deviation | 28 | - | - | - |
| Distribution | LN | Fully dependent on yield strength fy,l Model Code 2010 (fib, 2012) | Deterministic | Deterministic |

## 6.1.2 Geometrical uncertainties

The rotational capacity of corner D is mainly dependent on the used material values and the geometrical values. The material uncertainties are already discussed in chapter 6.1.1. The geometrical uncertainties will be discussed here. The most important geometrical uncertainty is the cross-sectional area of a longitudinal reinforcement bar $A_s$ since this parameter has a large influence on the rotational capacity of corner D. This uncertainty will be discussed in chapter 6.1.2.1. Other geometrical properties are of less importance and will be discussed shortly in chapter 6.1.2.2.

### 6.1.2.1 Corner reinforcement detailing

The cross-sectional area of a longitudinal reinforcement bar is made with a certain accuracy. Therefore the cross-sectional area can be seen as a stochastic variable. Due to fabrication the coefficient of variation of the cross-sectional area of the longitudinal reinforcement is assumed to be $V_{A_s} = 0.02$ (Faber & Vrouwenvelder, 2001).

The corner reinforcement can be placed in several ways. A few examples can be found in chapter 4.1. The structural resistance of the corner is different for each reinforcement layout (Johansson, 2000). Also for corners with the same reinforcement layout a certain spread in the structural resistance and ductility will be obtained. Several corner reinforcement layouts were tested with a high and a low reinforcement ratio by Johansson (2000) and Plos (1994). The results are presented in figure 54. Figure 54 clearly indicates the uncertainty in the structural resistance and the ductility of a reinforced concrete corner.

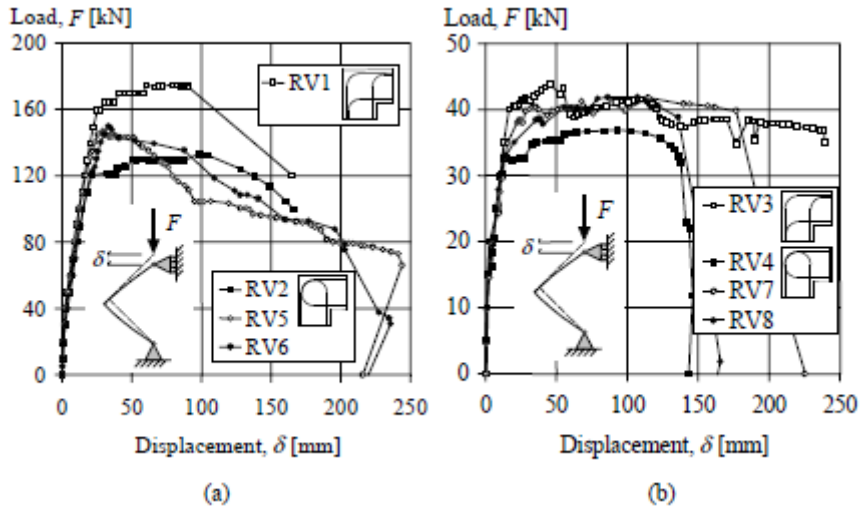


*Figure 54. Load-displacement relations for the frame corners subjected to a closing moment: high reinforcement ratio (a) and low reinforcement ratio (b). Specimens RV1 to RV4 were tested by Plos (1994) and RV5 to RV8 by Johansson (2000).*

Normally this uncertainty is implemented in the model uncertainty since the reinforcement detailing is exactly known. However, in case of a reassessment of an existing structure this is not always known. Specific reinforcement detailing plans may be missing or the reinforcement is not placed exactly according to the reinforcement plan. For instance some information was missing for the two experiments used in chapter 5. The amount of longitudinal reinforcement and shear reinforcement was exactly known and shown on the drawings. However the corner reinforcement detailing was only shown on a picture (figure 35). In order to implement this uncertainty the cross-sectional area $A_s$ of the longitudinal reinforcement is chosen to be a stochastic variable were a larger coefficient of variation $V_{A_s} = 0.10$ is assumed because this parameter has a large influence on the rotational capacity of the corner. The cross-sectional area $A_s$ in fact represent the uncertainty in the reinforcement detailing. Especially in the region of corner D, where the influence of the tensile area $A_s$ on the rotational capacity is rather high.

Summarizing the geometrical uncertainty of the longitudinal reinforcement will be implemented in the following two cases:

- The cross sectional area of the longitudinal reinforcement due to fabrication processes is assumed to be a normally stochastic variable. The estimated coefficient of variation of the cross-sectional area of the longitudinal reinforcement is $V_{A_S} = 0.02$ (Faber & Vrouwenvelder, 2001).
- The cross-sectional area of the longitudinal reinforcement is assumed to be normally distributed to implement the uncertainty of the reinforcement detailing. The coefficient of variation is assumed to be $V_{A_S} = 0.10$. This uncertainty should reflect the uncertainty in the reinforcement detailing and therefore the uncertainty of the resistance and ductility of the corner.

#### *6.1.2.2 Geometrical properties*

The geometrical properties of the reinforced concrete frame are for instance: the height of the frame, the span of the frame, the element height, the element width, etc. The geometrical properties of the portal frame are chosen to be deterministic except for the cross-sectional area $A_s$ of the longitudinal reinforcement as explained in chapter 6.1.2.1. The cross-sectional area of the shear reinforcement is also chosen to be deterministic since this has a relatively low influence on the structural resistance of the portal frame.

### 6.1.3 Loading uncertainties

The safety of the reinforced concrete frame is only checked for the resistance side. The implicit limit state function is defined as (chapter 1.2.1):

$$G(\boldsymbol{X}) = R(\boldsymbol{X}) - R_{SF}.$$

where the load is defined as $R_{SF}$, which is the structural resistance of the non-linear finite element model according to the corresponding safety format. Thus the load $R_{SF}$ is a deterministic value in this approach and the safety of the structure is only estimated from the resistance side of the limit state.

## 6.2 Model uncertainties

The model uncertainties are derived in chapter 5.3.3 with the use of the results of the experiment from Seraj et al. (1995). This experiment is more or less comparable to the NLFE model that will be used for the global safety assessment of portal frame design 1, 2 and 3. The loading is slightly different but in absence of better experimental results this is the best approach to make an estimation of the model uncertainty. The model uncertainty is the ratio between the experimental results and the model results. The model uncertainty $\theta_m = 1.028$ and the coefficient of variation $V_m = 0.01$ are determined in chapter 5.3.3 based on two experiments.

The model uncertainty that will be used in the global safety assessment is $\theta_m = 1.0$. This is a safe assumption since the results of the NLFE model is slightly lower compared to the experimental results. The coefficient of variation of the model uncertainty $V_m$ is neglected since the number of experiments is too low to make a justified assumption. However some of the effects which could results in a larger model uncertainty are described by the uncertainty in the corner reinforcement detailing. This uncertainty is implemented in chapter 6.1.2.1.

# 7 Safety assessment reinforced concrete frame designs

## 7.1 Level II reliability method: local safety evaluation using explicit limit state functions

A local safety evaluation of the portal frame designs is not performed since there is no analytical model available to take into account the rotational capacity and therefore the ductility of corner D. This should be incorporated in combination with the forming of the plastic hinges at location A, C and E. A practical approach would be to analyze the combined mechanism (chapter 5.2.2.3), where corner D is a partial plastic hinge. Still the amount of plasticity in corner D is case dependent and has to be assessed in an analytical model. Therefore only a global safety evaluation will be performed in chapter 7.2.

## 7.2 Level II reliability method: global safety evaluation using an implicit limit state function

The reliability level $\beta_R$ and the probability of failure of the safety formats can be determined with the following implicit limit state function (Blomfors, Engen, & Plos, Evaluation of safety formats for non-linear finite element analyses of statically indeterminate concrete structures subjected to different load paths, 2016):

$$G(\boldsymbol{X}) = R(\boldsymbol{X}) - R_{SF} \tag{7.1}$$

where $R(\boldsymbol{X})$ is the total resistance of a NLFE analysis using stochastic variables $\boldsymbol{X}$ and $R_{SF}$ is the total resistance of the NLFE model according to the corresponding safety format $R_{SF}$. The measure of the total structural resistance is chosen to be the sum of the vertical and horizontal load (Blomfors, Engen, & Plos, Evaluation of safety formats for non-linear finite element analyses of statically indeterminate concrete structures subjected to different load paths, 2016). The measure of the structural resistance is not a real physical quantity. However, this is not needed since this quantity is only used to determine a possible failure of the portal frame. The model uncertainty $\theta_m$ of the NLFE model is assumed to be 1.0 and therefore not implemented in the LSF. This implicit limit state function will be used to perform a global safety assessment of the design resistance according to the safety formats. For each portal frame design only the safety format with the highest probability of failure will be assed. If the reliability index $\beta_R \geq 3.04$, the other safety formats are assumed to be safe. For each design the safety format with the highest global design resistance, i.e. highest probability of failure, can be found in table 2 (chapter 4.4).

The chosen stochastic variables to perform a safety assessment are based on the rotational capacity of corner D. The simplest way to vary the rotational capacity of the corner is to vary the yield strength $f_y$ of the steel and the concrete compressive strength $f_c$. Therefore Case 1 is defined as: a global safety assessment using only stochastic variables: $f_y$ and $f_c$. In fact case 1 is a global safety assessment where there is no geometrical uncertainty implemented in the reinforcement detailing. The advantage of two stochastic variables is that the implicit LSF function derived from the response surface can be plotted.

A more advanced way to vary the rotational capacity is to implement to cross-sectional area $A_s$ of the longitudinal reinforcement as a stochastic variable. This leads to a global safety assessment where $f_y$, $f_c$ and $A_s$ are the chosen as stochastic variables to vary the rotational capacity of corner D. Two additional cases are defined. Case 2: rotational capacity corner D with geometrical uncertainty

in the reinforcement detailing due to fabrication of the longitudinal reinforcement. Case 3 is defined as the rotational capacity of corner D with uncertainty in the detailing of the longitudinal corner reinforcement. The difference between case 2 and case 3 is the coefficient of variation of the cross-sectional area of the longitudinal reinforcement, which is: $V_{A_s} = 0.02$ and $V_{A_s} = 0.10$ for case 2 and 3, respectively.

### 7.2.1 Case 1: rotational capacity corner D without geometrical reinforcement uncertainty

The simplest way to vary the rotational capacity of the corner is to vary the yield strength of the steel and the concrete compressive strength. The stochastic variables $\boldsymbol{X}$ used in the global safety assessment of Case 1 are: $f_y$ and $f_c$.

#### *7.2.1.1 Design 1*

The safety format with the highest global design resistance, i.e. highest probability of failure, for design 1 is the ECOV method. The total global design resistance according to the ECOV method is: $R_{SF} = 36.1$ kN. This leads to the following implicit LSF:

$$G(\boldsymbol{X}) = R(\boldsymbol{X}) - 36.1. \tag{7.2}$$

The response surface to replace the actual LSF is constructed according to the approach of Zhao and Qiu (2013). This approach is discussed in chapter 2.4.2. A detailed calculation of the response surface is presented in Appendix G.1.1. The used python scripts to run the NLFE analyses and to process the results can be found in Appendix H. The structural response of the NLFE model shows a large spread in the results. Therefore there is chosen to use more sample points to create the response surface than $2n + 1$ sample points recommended by Zhao and Qiu (2013). The center of gravity of all sample points is around the initial design point. Subsequently the design point $\boldsymbol{X}_{1,*}$ is obtained with FORM. This first obtained design point $\boldsymbol{X}_{1,*}$ is used in a NLFE analysis to determine $G(\boldsymbol{X}_{1,*})$. This results is added to update the response surface. Again the FORM is used to determine the second design point design point $\boldsymbol{X}_{2,*}$. This procedure is repeated until convergence is achieved. The response surface is presented in the real and standard normal space in figure 55 and 56, respectively. The LSF function derived from the response surface is also presented in real and standard normal space in figures 59 and 60, respectively. The real design point is denoted with $\boldsymbol{X}_*$ and is presented below. The reliability index is $\beta_R = 5.26$. So the safety formats can be used safely for design 1.

$$\boldsymbol{X}_* = \begin{bmatrix} 441.5 \\ 26.7 \end{bmatrix} \qquad \boldsymbol{U}_* = \begin{bmatrix} -4.73 \\ -2.30 \end{bmatrix} \qquad \beta_R = 5.26 \qquad \alpha_R = \begin{bmatrix} 0.900 \\ 0.437 \end{bmatrix}$$

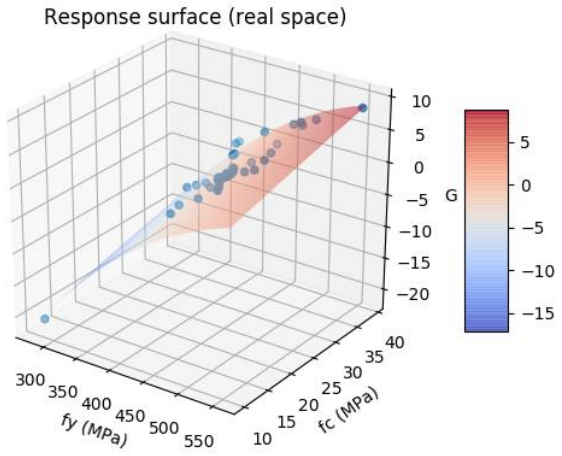


*Figure 55. Design 1: response surface (real space).*

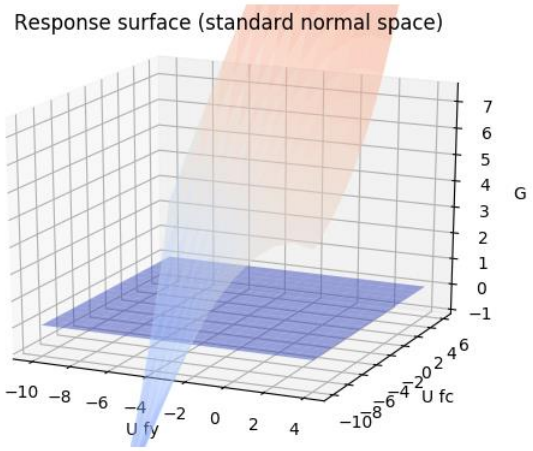


*Figure 56. Design 1: response surface (standard normal space).*

The rotational capacity of corner D has a large influence on the structural resistance and therefore on the result of the LSF. The structural resistance of NLFE analyses with sample points close to each other can differ significantly. The spreading of the results is shown in figure 57 and 58.

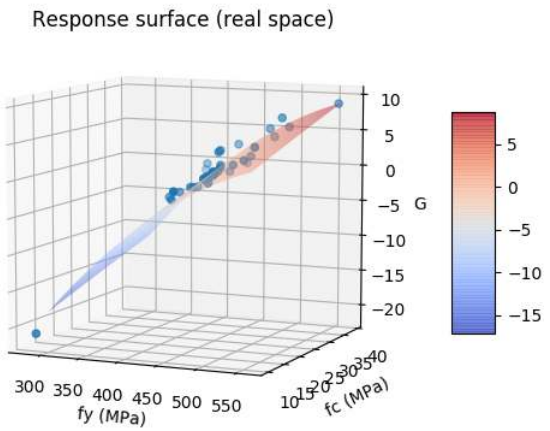


*Figure 57. Design 1: response surface (real space). The spreading of the results of the implicit LSF is clearly visible.*

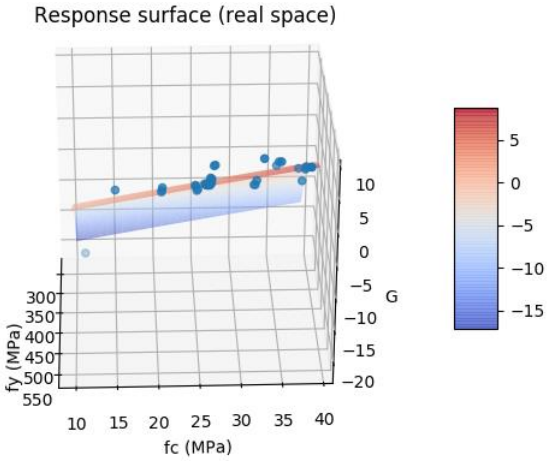


*Figure 58. Design 1: response surface (real space). The spreading of the results of the implicit LSF is clearly visible.*

The shape of the response surface is only an approximation in the region of the used sample points i.e. the region near the design point. In this case all sample points are positioned in the third quadrant of a graph with standard normal variables (figure 60). Therefore the parts of the LSF in the other quadrants should be neglected. The only reason that this parts of the graph are presented in figure 60 is to show that sometimes a design point can be found in a region where hardly any sample point are used after performing the FORM. If this is the case additional sample points should be used near the approximated design point to create a more accurate response surface.

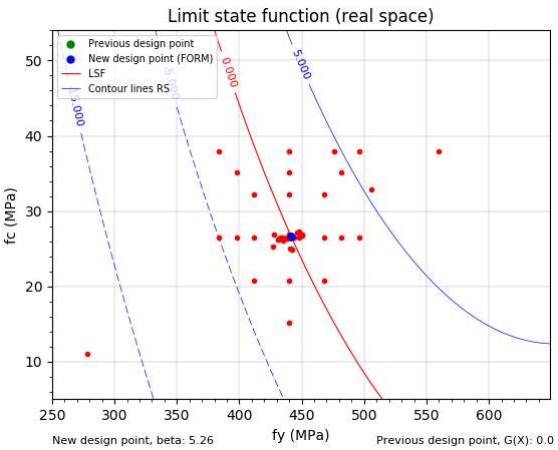


*Figure 59. Design 1: limit state function (real space). Previous design point lies below the new obtained design point.*

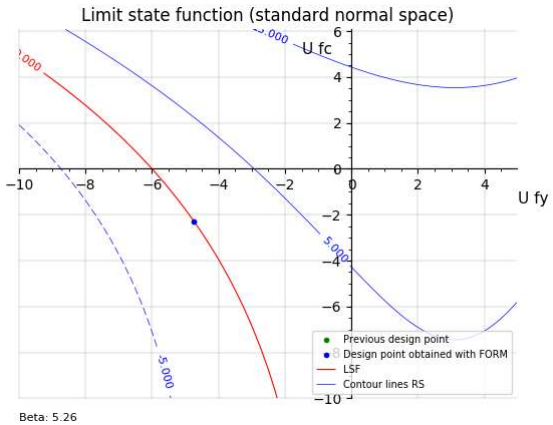


*Figure 60. Design 1: limit state function (standard normal space). The limit state function is only accurately described by sample points (not visible) in the third quadrant.*

### 7.2.1.2 Design 2

The safety format with the highest global design resistance, i.e. highest probability of failure, for design 2 is the PFm. The total global design resistance according to the PFm is: $R_{SF} = 43.7$ kN. This leads to the following implicit LSF:

$$G(\boldsymbol{X}) = R(\boldsymbol{X}) - 43.7. \tag{7.3}$$

The initital design point is found using the straight line appoach by Zhoa and Qiu (2013). This approach can be found in Appendix G.1.2. Around the initial design point four sets of sample points with $f = 0.5; 1.0; 1.5; 2.0$ are used to determine the response surface. The sample points are shown in figure 61 and 63.

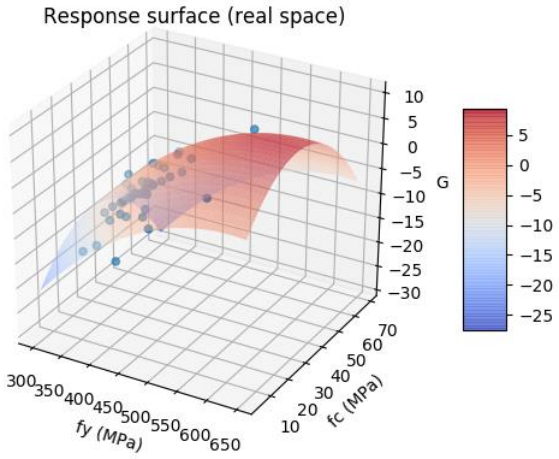


*Figure 61. Design 2: response surface (real space).*

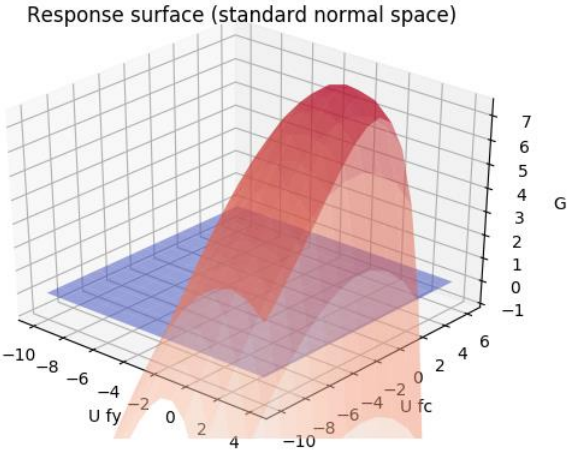


*Figure 62. Design 2: response surface (standard normal space).*

After applying the FORM a design point is found in the region, which is not described by the chosen sample points. This is shown in figure 63 and 64.

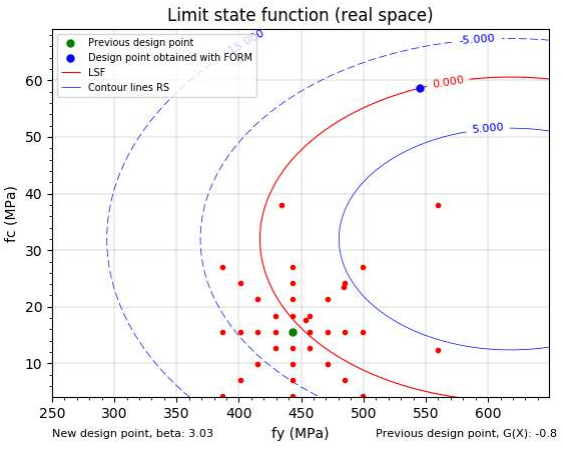


*Figure 63. Design 2: limit state function (real space). Design point obtained with the FORM lies in a region, which is not described accurately by the sample points.*

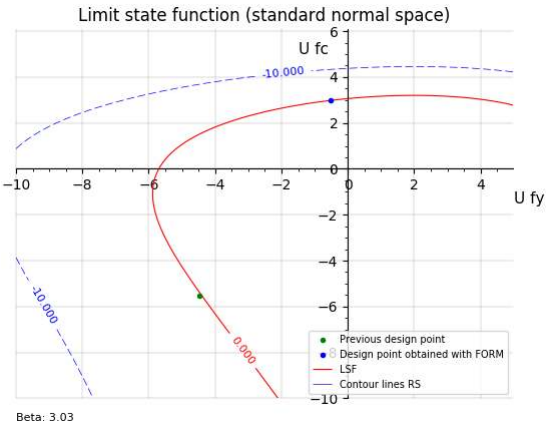


*Figure 64. Design 2: limit state function (standard normal space). The limit state function is only accurately described by sample points (not visible) in the third quadrant. Therefore the obtained design point is not realistic.*

Additional sample points with a high concrete compressive strength coordinates are added to have a better approximation of the response surface in the region of the added sample points. Otherwise an incorrect design point is obtained. The updated response surface is presented in figures 65 till 68.

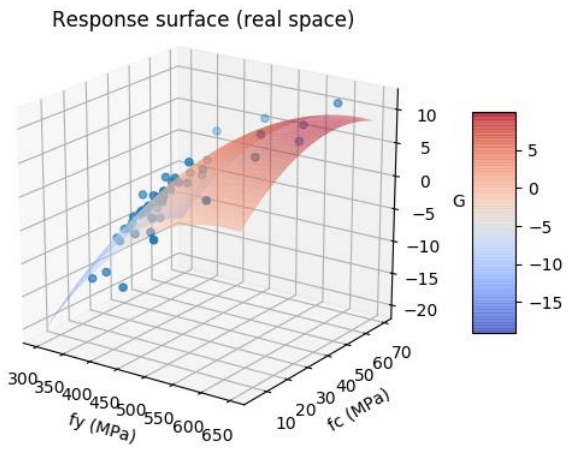


*Figure 65. Design 2: updated response surface (real space) in order to find the real design point.*

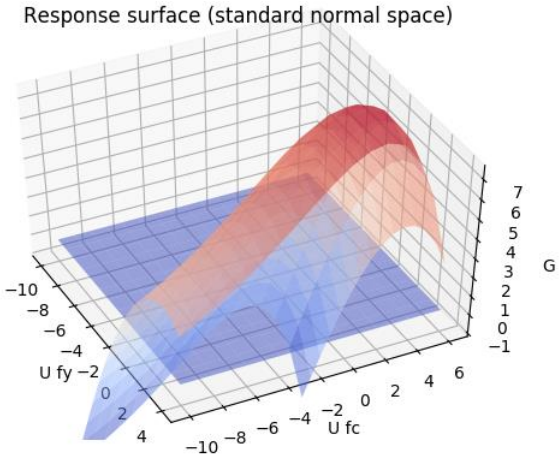


*Figure 66. Design 2: updated response surface (standard normal space) in order to find the real design point.*

The rotational capacity of corner D has a large influence on the structural resistance and therefore on the result of the LSF. The structural resistance of NLFE analyses with sample points close to each other can differ significantly. The spreading of the results is shown in figure 67 and 68.

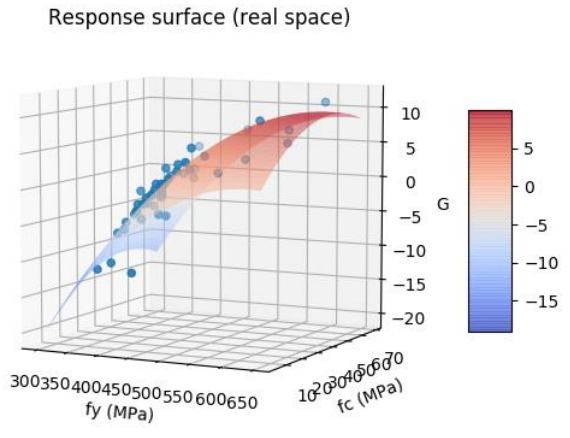


*Figure 67. Design 2: updated response surface (real space). The spreading of the results of the implicit LSF is clearly visible.*

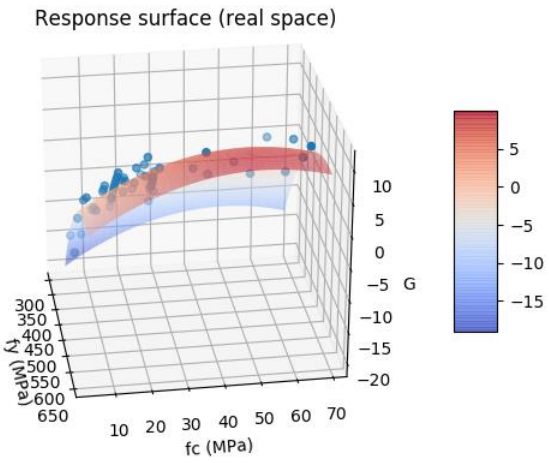


*Figure 68. Design 2: updated response surface (real space). The spreading of the results of the implicit LSF is clearly visible.*

The updated LSF is presented in figure 69 and 70. The obtained design point, reliability index and sensitivity factors are presented below.

$$\boldsymbol{U}_* = \begin{bmatrix} -5.29 \\ -2.25 \end{bmatrix} \qquad \boldsymbol{X}_* = \begin{bmatrix} 429.3 \\ 26.9 \end{bmatrix} \qquad \beta_R = 5.75 \qquad \alpha_R = \begin{bmatrix} 0.920 \\ 0.391 \end{bmatrix}$$

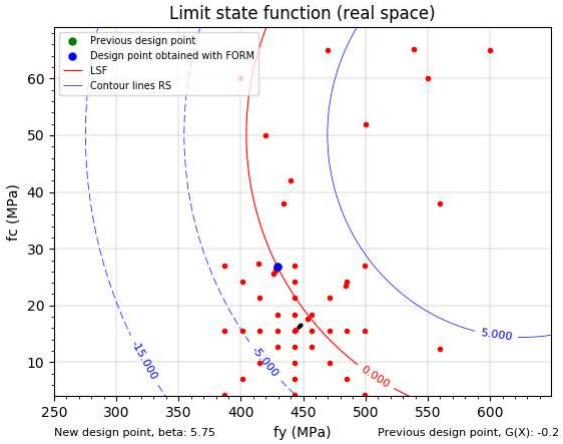


*Figure 69. Design 2: updated limit state function (real space). Previous design point lies below the new obtained design point.*

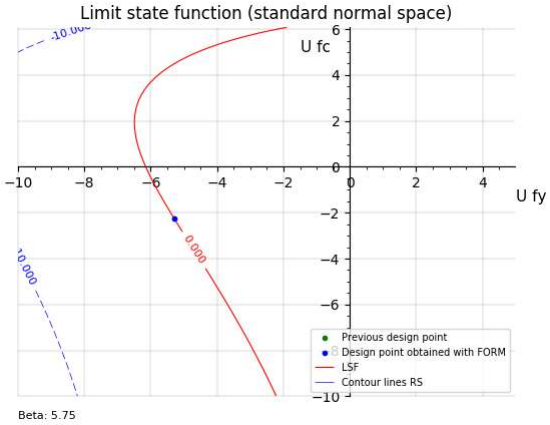


*Figure 70. Design 2: updated limit state function (standard normal space).*

### 7.2.1.3 Design 3

The safety format with the highest global design resistance, i.e. highest probability of failure, for design 3 is the PFm. The total global design resistance according to the PFm is: $R_{SF} = 37.0$ kN. This leads to the following implicit LSF:

$$G(\boldsymbol{X}) = R(\boldsymbol{X}) - 37.0. \tag{7.4}$$

The obtained response surface in the real and in the standard normal space are shown below.

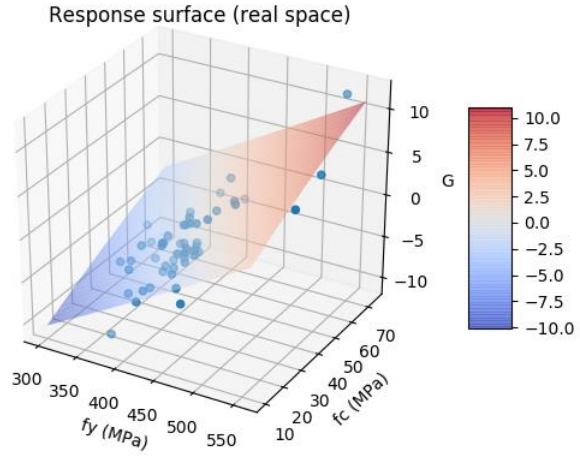


*Figure 71. Design 3: response surface (real space).*

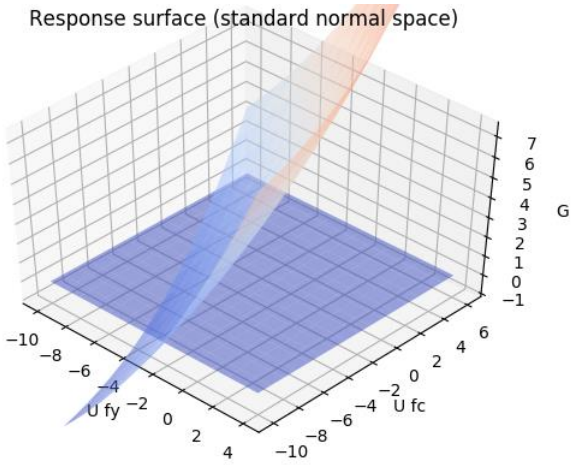


*Figure 72. Design 3: response surface (standard normal space).*

The higher strength class C40 used in design 3 leads to a portal frame, which is very sensitive for a ductile or a brittle failure depending on the rotational capacity of corner D. This results in a large spreading of the obtained structural resistance for sample points close to each other. Therefore the fit of the response surface is not very accurate which is shown in figure 73 and 74.

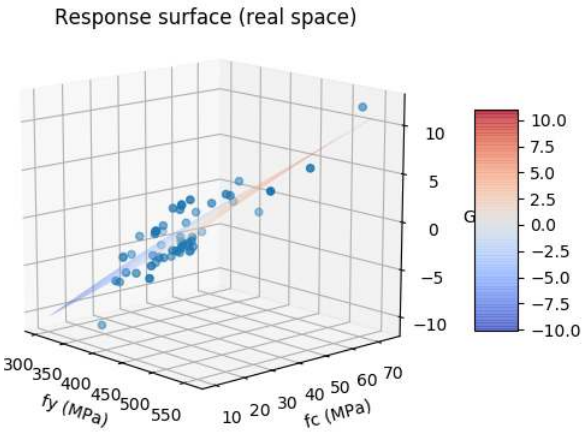


*Figure 73. Design 3: response surface (real space). A lot of spreading in sample points close to each other results in a bad fit of the response surface.*

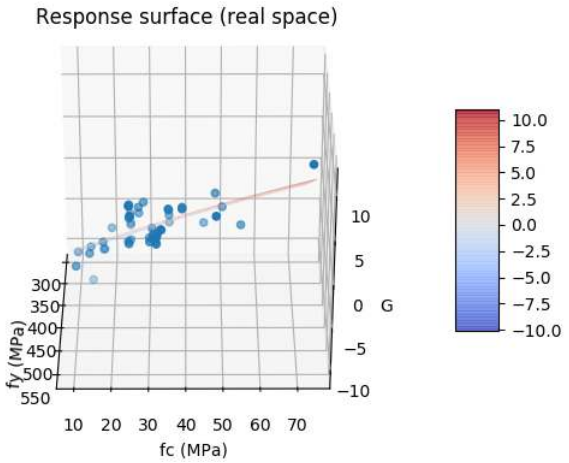


*Figure 74. Design 3: response surface (standard normal space). A lot of spreading in sample points close to each other results in a bad fit of the response surface.*

However after adding a lot of sample points and using the FORM method a good approximation of the real design point can be made. The real design point $\boldsymbol{X}_*$ is given below. The reliability index is $\beta_R = 5.37$ so therefore the safety formats can safely be used for design 3.

$$\boldsymbol{U}_* = \begin{bmatrix} -4.71 \\ -2.57 \end{bmatrix} \qquad \boldsymbol{X}_* = \begin{bmatrix} 442.0 \\ 32.35 \end{bmatrix} \qquad \beta_R = 5.37 \qquad \alpha_R = \begin{bmatrix} 0.878 \\ 0.479 \end{bmatrix}$$

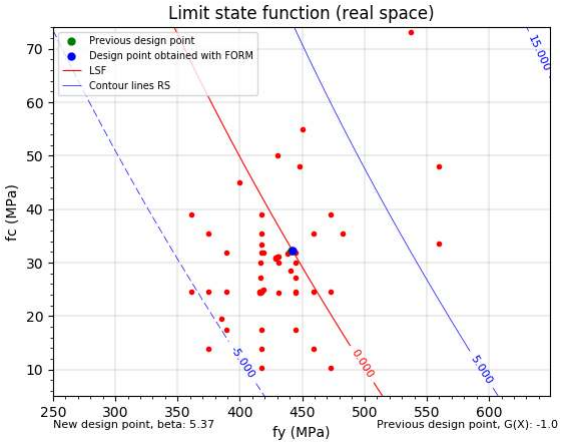


*Figure 75. Design 3: limit state function (real space). Previous design point lies below the new obtained design point.*

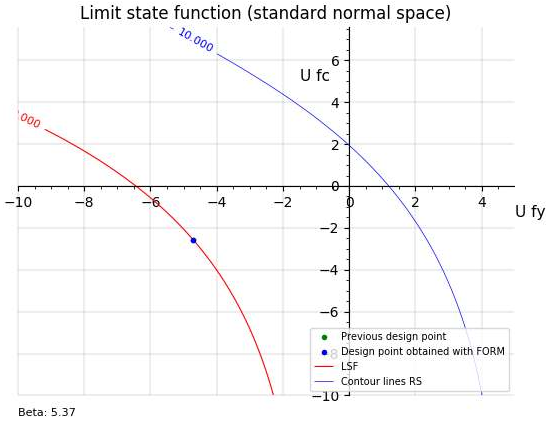


*Figure 76. Design 3: limit state function (standard normal space).*

#### *7.2.1.4 Discussion used method by Zhao and Qiu (2013) to obtain the response surface*

Various issues that arise in obtaining a response surface according to the method proposed by Zhao and Qiu (2013) are discussed on the basis of a few examples.

##### Obtaining the control point $\boldsymbol{X}_c$

Creating a response surface, for a reinforced concrete portal frame, with the use of the control point (Zhao & Qiu, 2013) is not always a useful approach in order to reduce the number of NLFE analyses needed to find the real design point. Normally the control point is found for a problem with $n$ stochastic variables by performing $n+1$ NLFE analyses. The mean material values are used in the first NLFE analysis and for the $n$ other NLFE analyses for one of the stochastic variables a low strength value is used. This done by subtracting $f$ times the standard deviation from one of the stochastic variables. For the other variables the mean values are used. Mostly $f = 3$ is used because it should be close to the real design point. However the rotational capacity can be influenced positively when a lower concrete compressive strength is used because the Young's modulus of concrete will be lower according to the relation (B.9). The concrete is able to resist a larger deformation and since the mean steel values are also used in this analysis the structural resistance could be higher than a NLFE analysis with mean material values. This leads to an unrealistic control point and new NLFE analyses should be performed with a larger $f$ where the structural resistance of the portal frame is lower than the load found with mean material values.

For portal frame design 1 the factor $f = 3$ could be used without any problems. For design 2 and 3 this factor led to an unrealistic control point. This will be shown in the examples below.

- Design 2:

  The results of the first three NLFE analyses to obtain the control point with $f = 3$ are presented below:

  resistance NLFE analysis with $\overline{\boldsymbol{X}} = \begin{bmatrix} f_{y,mean} \\ f_{c,mean} \end{bmatrix} = \begin{bmatrix} 560 \\ 38 \end{bmatrix}$: $F_v = 37.1$ and $F_h = 15.7$;

  resistance NLFE analysis with $\boldsymbol{X} = \begin{bmatrix} f_{y,mean} - f\sigma_{f_y} \\ f_{c,mean} \end{bmatrix}$: $F_v = 31.4$ and $F_h = 15.7$;

  resistance NLFE analysis with $\boldsymbol{X} = \begin{bmatrix} f_{y,mean} \\ f_{c,mean} - f\sigma_{f_c} \end{bmatrix}$: $F_v = 37.6$ and $F_h = 15.7$.

  The resistance of the NLFE analysis with low concrete material values is actually higher than the resistance of a NLFE analysis with mean material values due to a ductile and brittle failure mode, respectively. The low concrete values (lower stiffness) has a positive influence on the rotational capacity of corner D. If these results are used to calculate the control point with equation (2.34) the following result is obtained: $\boldsymbol{X}_c = \begin{bmatrix} f_y \\ f_c \end{bmatrix} = \begin{bmatrix} 423.7 \\ 42.3 \end{bmatrix}$. The mean value of the concrete compressive strength is $f_{c,mean} = 38$ MPa. The direction in which the initial design point is being sought is on a straight line between $\overline{\boldsymbol{X}}$ and $\boldsymbol{X}_c$. Thus the initial design point is being sought in the direction of concrete values higher than the mean strength. This could be the case but some experience with performing NLFE analyses for this problem led to the conclusion that this approach deviates significantly from the real design point. Therefore a larger factor $f = 4.5$ is used to obtain the control point.

- Design 3:

  For design 3 a more realistic control point $\boldsymbol{X}_c$ can be found when the factor $f = 3$ is used. However using this control point led to divergence of the obtained first iteration point $\boldsymbol{X}_{\boldsymbol{M}_1}$ according to equation (2.35). This is shown on the basis of the results of 4 NLFE analyses that are used to obtain the first iteration point $\boldsymbol{X}_{\boldsymbol{M}_1}$:

  resistance NLFE analysis with $\bar{\boldsymbol{X}} = \begin{bmatrix} f_{y,mean} \\ f_{c,mean} \end{bmatrix} = \begin{bmatrix} 560 \\ 48 \end{bmatrix}$: $F_v = 28.3$ and $F_h = 15.7$;

  resistance NLFE analysis with $\boldsymbol{X} = \begin{bmatrix} f_{y,mean} - f\sigma_{f_y} \\ f_{c,mean} \end{bmatrix}$: $F_v = 26.7$ and $F_h = 15.7$;

  resistance NLFE analysis with $\boldsymbol{X} = \begin{bmatrix} f_{y,mean} \\ f_{c,mean} - f\sigma_{f_c} \end{bmatrix}$: $F_v = 26.6$ and $F_h = 15.7$;

  resistance NLFE analysis with $\boldsymbol{X}_c = \begin{bmatrix} 502.6 \\ 29.9 \end{bmatrix}$: $F_v = 26.7$ and $F_h = 15.7$.

  According to equation (2.35) the first iteration point should be $\boldsymbol{X}_{\boldsymbol{M}_1} = \begin{bmatrix} 308.8 \\ -31.0 \end{bmatrix}$. To avoid this divergence a factor $f = 4$ is used to find the initial design point.

### The influence of the factor $f$ on the initial design point

Another problem with the control point is to estimate the factor $f$ because this factor has an influence on the weight factors $w_i$ and therefore the direction of the straight line between $\bar{\boldsymbol{X}}$ and $\boldsymbol{X}_c$ that is used to obtain the initial design point. A wrongly chosen factor $f$ could lead to a large deviation from the initial to the real design point. An example of this can be found in figure 77. A lot of additional NLFE analyses are needed to obtain the real design point.

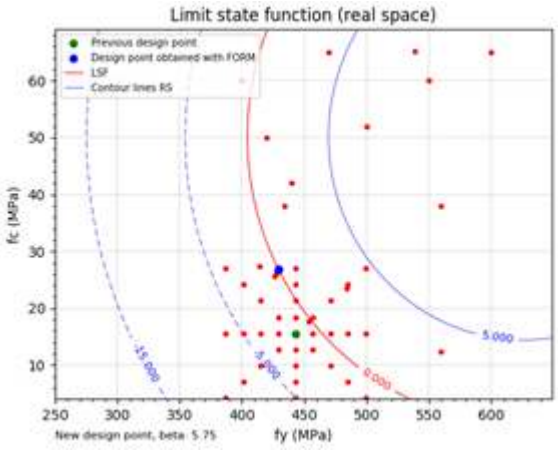


*Figure 77. Design 2: deviation initial design point from real design point due to a wrongly chosen f-factor.*

### Exact calculation of the response surface not possible

The exact calculation of the coefficients $\boldsymbol{b}$ of the response surface by using $2n + 1$ NLFE analyses suggested by Zhao & Qiu (2013) does not lead to correct results since there is a relatively large spreading of the NLFE results. This spreading is mainly caused due to difference in rotational capacity for the several combinations of used material values in the NLFE analyses. Therefore it is better to use more sample points and make use of a least squares approach to fit a response surface to the results. Also the initial founded design point can deviate a lot from the real design point due a badly chosen $f$-factor. This results in wrongly chosen $2n + 1$ points to create the response surface.

### 7.2.2 Case 2: rotational capacity corner D with reinforcement uncertainty due to fabrication

A more advanced way to vary the rotational capacity of the corner is to vary the yield strength of the steel, the concrete compressive strength and the cross-sectional area of the longitudinal reinforcement. The stochastic variables $\boldsymbol{X}$ used in the global safety assessment of Case 1 are: $f_y$, $f_c$ and $A_s$. The coefficient of variation used for the cross-sectional area of the longitudinal reinforcement is $V_{A_s} = 0.02$ for case 2. The results are presented below. The calculations can be found in Appendix G.2.

#### *7.2.2.1 Design 1*

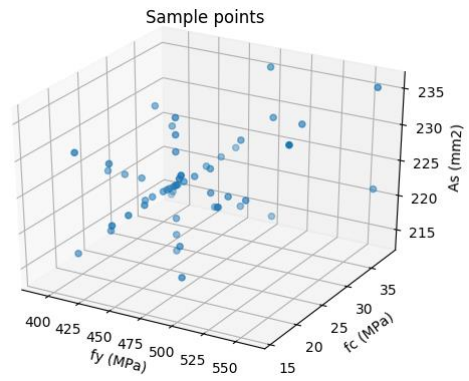


*Figure 78. Design 1: sample points 3D.*

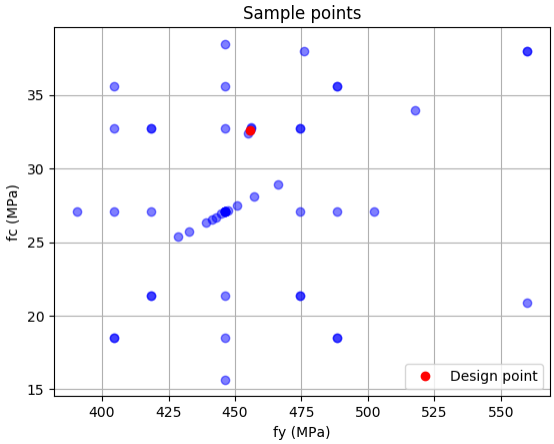


*Figure 79. Design 1: sample points 2D.*

$$\boldsymbol{U}_* = \begin{bmatrix} -4.09 \\ -0.93 \\ -3.85 \end{bmatrix} \qquad \boldsymbol{X}_* = \begin{bmatrix} 455.96 \\ 32.7 \\ 217.5 \end{bmatrix} \qquad \beta_R = 5.69 \qquad \alpha_R = \begin{bmatrix} 0.718 \\ 0.163 \\ 0.677 \end{bmatrix}$$

#### 7.2.2.2 Design 2

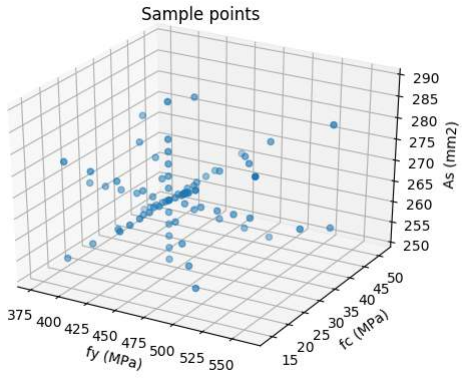


*Figure 80. Design 2: sample points 3D.*

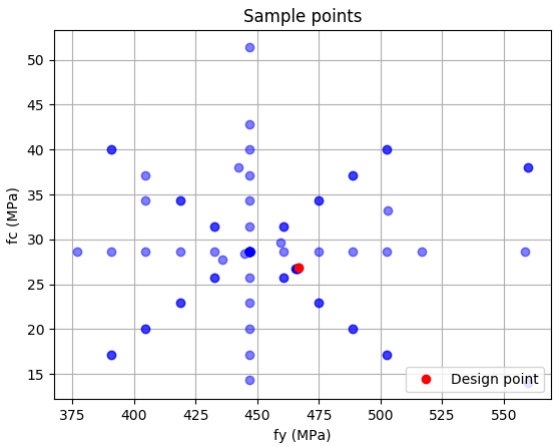


*Figure 81. Design 2: sample points 2D.*

$$\boldsymbol{U}_* = \begin{bmatrix} -3.615 \\ -2.259 \\ -2.736 \end{bmatrix} \qquad \boldsymbol{X}_* = \begin{bmatrix} 466.9 \\ 26.8 \\ 269.5 \end{bmatrix} \qquad \beta_R = 5.07 \qquad \alpha_R = \begin{bmatrix} 0.714 \\ 0.446 \\ 0.540 \end{bmatrix}$$

### 7.2.2.3 Design 3

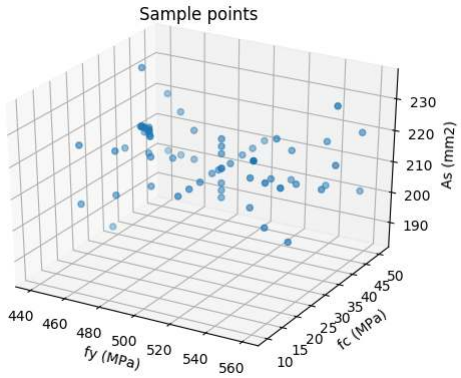


*Figure 82. Design 3: sample points 3D.*

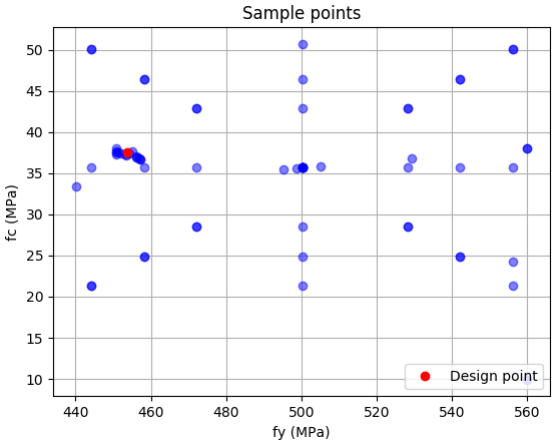


*Figure 83. Design 3: sample points 2D.*

$$\boldsymbol{U}_* = \begin{bmatrix} -4.191 \\ -1.571 \\ -4.015 \end{bmatrix} \qquad \boldsymbol{X}_* = \begin{bmatrix} 453.6 \\ 37.6 \\ 216.7 \end{bmatrix} \qquad \beta_R = 6.01 \qquad \alpha_R = \begin{bmatrix} 0.697 \\ 0.261 \\ 0.668 \end{bmatrix}$$

### 7.2.3 Case 3: rotational capacity corner D with uncertainty in the reinforcement detailing

A more advanced way to vary the rotational capacity of the corner is to vary the yield strength of the steel, the concrete compressive strength and the cross-sectional area of the longitudinal reinforcement. The stochastic variables $\boldsymbol{X}$ used in the global safety assessment of Case 1 are: $f_y$, $f_c$ and $A_s$. The coefficient of variation used for the cross-sectional area of the longitudinal reinforcement is $V_{A_s} = 0.10$ for case 3. The results are presented below. The calculations can be found in Appendix G.3.

#### *7.2.3.1 Design 1*

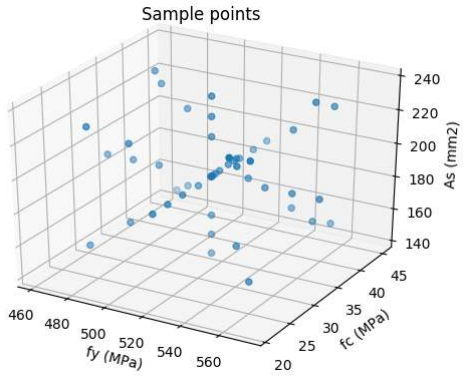


*Figure 84. Design 1: sample points 3D.*

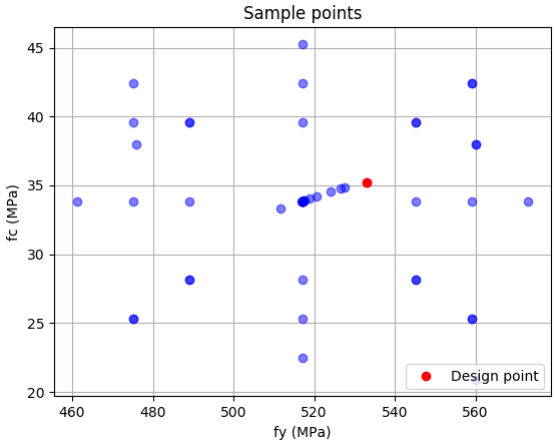


*Figure 85. Design 1: sample points 2D.*

$$\boldsymbol{U}_* = \begin{bmatrix} -0.97 \\ -0.43 \\ -1.94 \end{bmatrix} \qquad \boldsymbol{X}_* = \begin{bmatrix} 532.9 \\ 35.2 \\ 189.9 \end{bmatrix} \qquad \beta_R = 2.21 \qquad \alpha_R = \begin{bmatrix} 0.438 \\ 0.195 \\ 0.878 \end{bmatrix}$$

#### *7.2.3.2 Design 2*

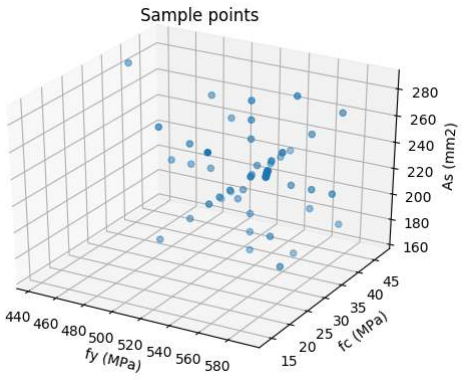


*Figure 86. Design 2: sample points 3D.*

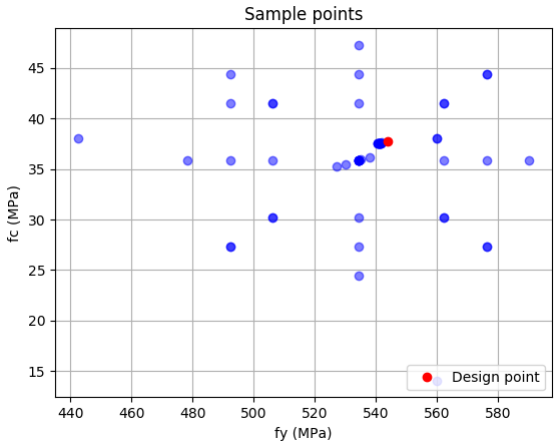


*Figure 87. Design 2: sample points 2D.*

$$\boldsymbol{U}_* = \begin{bmatrix} -0.6418 \\ 0.000596 \\ -2.0851 \end{bmatrix} \qquad \boldsymbol{X}_* = \begin{bmatrix} 541.6 \\ 37.6 \\ 225.7 \end{bmatrix} \qquad \beta_R = 2.18 \qquad \alpha_R = \begin{bmatrix} 0.294 \\ -0.00027 \\ 0.956 \end{bmatrix}$$

### 7.2.3.3 Design 3

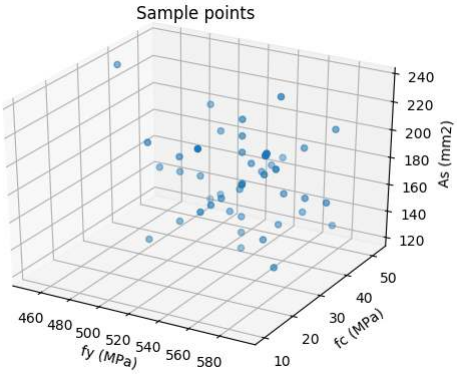


*Figure 88. Design 3: sample points 3D.*

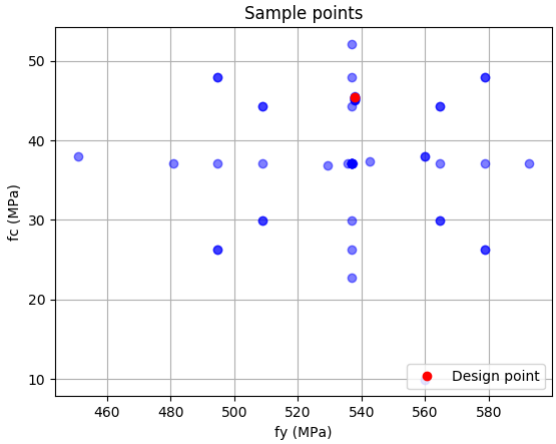


*Figure 89. Design 3: sample points 2D.*

$$\boldsymbol{U}_* = \begin{bmatrix} -0.79 \\ -0.30 \\ -2.34 \end{bmatrix} \qquad \boldsymbol{X}_* = \begin{bmatrix} 537.7 \\ 45.4 \\ 180.5 \end{bmatrix} \qquad \beta_R = 2.49 \qquad \alpha_R = \begin{bmatrix} 0.317 \\ 0.120 \\ 0.941 \end{bmatrix}$$

### 7.2.4 Summary of the results obtained from the global safety assessment

The results of the global safety assessment are presented below. The conclusions are presented in chapter 9.1.

*Table 25. Results obtained from the global safety assessment. The design point in the real space, the sensitivity factors and the design point in the standard normal space.*

| Portal frame designs | Case 1: fy and fc | Case 2: fy, fc and As with Vas=0.02 | Case 3: fy, fc and As with Vas=0.10 |
|---|---|---|---|

| Portal frame designs | Case 1 | | | Case 2 | | | | Case 3 | | | |
|---|---|---|---|---|---|---|---|---|---|---|---|
| | $\beta_R$ | fy (Mpa) | fc (Mpa) | $\beta_R$ | fy (Mpa) | fc (Mpa) | As ($mm^2$) | $\beta_R$ | fy (Mpa) | fc (Mpa) | As ($mm^2$) |
| Design 1 | 5.26 | 441.48 | 26.67 | 5.69 | 455.96 | 32.72 | 217.47 | 2.21 | 532.89 | 35.24 | 189.88 |
| Design 2 | 5.75 | 429.29 | 26.87 | 5.07 | 466.87 | 26.83 | 269.50 | 2.18 | 541.65 | 37.58 | 225.65 |
| Design 3 | 5.37 | 442.00 | 32.35 | 6.01 | 453.64 | 37.55 | 216.70 | 2.49 | 537.73 | 45.40 | 180.53 |

| Portal frame designs | Case 1 | | | Case 2 | | | | Case 3 | | | |
|---|---|---|---|---|---|---|---|---|---|---|---|
| | $\beta_R$ | α fy | α fc | $\beta_R$ | α fy | α fc | α As | $\beta_R$ | α fy | α fc | α As |
| Design 1 | 5.26 | 0.90 | 0.44 | 5.69 | 0.72 | 0.16 | 0.68 | 2.21 | 0.44 | 0.20 | 0.88 |
| Design 2 | 5.75 | 0.92 | 0.39 | 5.07 | 0.71 | 0.45 | 0.54 | 2.18 | 0.29 | 0.00 | 0.96 |
| Design 3 | 5.37 | 0.88 | 0.48 | 6.01 | 0.70 | 0.26 | 0.67 | 2.49 | 0.32 | 0.12 | 0.94 |

| Portal frame designs | Case 1 | | | Case 2 | | | | Case 3 | | | |
|---|---|---|---|---|---|---|---|---|---|---|---|
| | $\beta_R$ | U fy | U fc | $\beta_R$ | U fy | U fc | U As | $\beta_R$ | U fy | U fc | U As |
| Design 1 | 5.26 | -4.73 | -2.30 | 5.69 | -4.09 | -0.93 | -3.85 | 2.21 | -0.97 | -0.43 | -1.94 |
| Design 2 | 5.75 | -5.30 | -2.25 | 5.07 | -3.62 | -2.26 | -2.74 | 2.18 | -0.64 | 0.00 | -2.09 |
| Design 3 | 5.37 | -4.71 | -2.57 | 6.01 | -4.19 | -1.57 | -4.01 | 2.49 | -0.79 | -0.30 | -2.34 |

*Table 26. The sensitivity factors containing the information about the steel parameters are combined in order to make a comparison possible between case 1, case 2 and case 3.*

| Portal frame designs | Case 1 | | | Case 2 | | | Case 3 | | |
|---|---|---|---|---|---|---|---|---|---|
| | $\beta_R$ | α fy | α fc | $\beta_R$ | α fy and As | α fc | $\beta_R$ | α fy and As | α fc |
| Design 1 | 5.26 | 0.8996 | 0.43669 | 5.69 | 0.9866 | 0.1631 | 2.21 | 0.9808 | 0.1951 |
| Design 2 | 5.75 | 0.92 | 0.39 | 5.07 | 0.8950 | 0.4460 | 2.18 | 1.0000 | 0.0003 |
| Design 3 | 5.37 | 0.87785 | 0.47894 | 6.01 | 0.9653 | 0.2613 | 2.49 | 0.9927 | 0.1205 |

# 8 Conclusions and suggestion for further work

In chapter 8.1 the conclusions of this thesis will be presented. Suggestions for further work will be given in chapter 8.2.

## 8.1 Conclusions

The evaluation of safety assessment methods is performed according to figure 90. First the conclusions will be given in chapter 8.1.1 based on the results of the case study of the three reinforced concrete frame designs. Secondly the conclusions based on the used methods are provided in chapter 8.1.2.

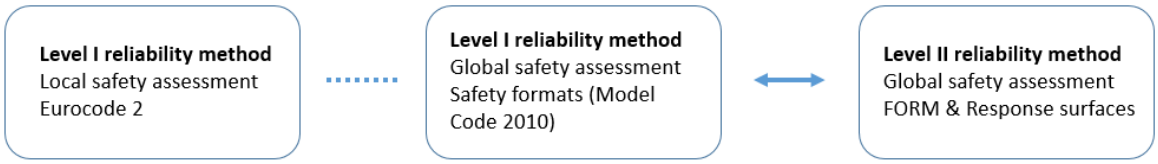


*Figure 90. Schematic representation of the used safety assessment methods*

### 8.1.1 Conclusions about the case study of a reinforced concrete frame

#### *8.1.1.1 Level I: local and global safety assessment of the reinforced concrete frame designs.*

A comparison of the obtained failure modes in the reinforced concrete frame designs and the obtained structural resistance is made and the conclusions are presented below.

##### Eurocode 2

The local safety assessment according to the Eurocode 2 shows that the individual elements of the portal frame designs 1, 2 and 3 can resist the external loads $F_v = 18.8$ kN and $F_h = 17.7$ kN. The columns and the beam of the portal frame are designed in such a way that these elements can resist the linear elastic bending moment, shear- and normal forces. The shear resistance of the single elements determines the structural resistance of the three portal frame designs. The shear resistance is the same for each design since the same shear reinforcement ratio is used. However a more detailed analysis should be carried out in the corner regions by means of strut and tie models to determine the bending moment resistance of the corner. Especially the compressive strut in the corner region exposed to a closing moment could influence the structural resistance of the three portal frame designs.

##### Safety formats (Model Code 2010)

The results of the global design resistance obtained with the safety formats can be found in table 27. The used calculations can be found in chapter 4.4. The concrete portal frame designs can fail in a ductile or a brittle manner depending on the used material values. A brittle failure is obtained when corner D fails before a partial plastic mechanism is obtained with plastic hinges at location A, C and E. A ductile failure is obtained when a partial plastic mechanism lead to the failure of the frame. This failure behavior is also indicated in table 27.

*Table 27. Non-linear finite element analysis (NLFEA), design resistance safety format (SF) included model uncertainty $\gamma_{Rd}$ and used global resistance factor $\gamma_R$.*

| | NLFEA | Failure | $\gamma_R$ | $\gamma_{Rd}$ | SF | NLFEA | Failure | | Failure | $\gamma_R$ | $\gamma_{Rd}$ | SF | NLFEA | Failure | SF |
|---|---|---|---|---|---|---|---|---|---|---|---|---|---|---|---|
| Design 1 | Mean GRF | | | | GRFm | mean | | characteristic | | | | ECOV | PFm | | design |
| Fv (kN) | 26.00 | Brittle | 1.2 | 1.06 | 17.08 | 28.80 | Ductile | 25.30 | Ductile | 1.16 | 1.06 | 20.40 | 19.20 | Ductile | 19.20 |
| Fh (kN) | 15.70 | | | | 15.70 | 15.70 | | 15.70 | | | | 15.70 | 15.70 | | 15.70 |
| Design 2 | Mean GRF | | | | GRFm | mean | | characteristic | | | | ECOV | PFm | | design |
| Fv (kN) | 35.60 | Ductile | 1.2 | 1.06 | 24.63 | 33.10 | Brittle | 30.60 | Ductile | 1.10 | 1.06 | 26.09 | 28.00 | Ductile | 28.00 |
| Fh (kN) | 15.70 | | | | 15.70 | 15.70 | | 15.70 | | | | 15.70 | 15.70 | | 15.70 |
| Design 3 | Mean GRF | | | | GRFm | mean | | characteristic | | | | ECOV | PFm | | design |
| Fv (kN) | 27.60 | Ductile | 1.2 | 1.06 | 18.34 | 28.30 | Brittle | 25.20 | Ductile | 1.14 | 1.06 | 20.58 | 21.30 | Ductile | 21.30 |
| Fh (kN) | 15.70 | | | | 15.70 | 15.70 | | 15.70 | | | | 15.70 | 15.70 | | 15.70 |

The following conclusions can be made based on table 27:

- The global resistance factor $\gamma_R$ derived according to the ECOV method is low compared to the global resistance factor defined in the GRF method. This difference is remarkable because a NLFE analysis with mean GRF material values is usually lower than a NLFE analysis with mean material values. Therefore the design resistance obtained with the GRFm is often much lower than the design resistance obtained with the ECOV method.
- The highest longitudinal reinforcement ratio is used in design 2. The structural resistance of design 2 obtained with a NLFE analysis is higher for the analysis with mean GRF material values compared to the analysis with mean material values. The yield strength of both material values is almost the same (Appendix B.2). However the concrete material values used in NLFE analysis with mean GRF values is much lower compared to the mean concrete material values. The mean GRF material values show a more favorable ductile failure compared to the brittle failure obtained from the NLFE analysis with mean material values. This more favorable ductile failure, i.e. more rotational capacity of corner D, leads to a higher structural resistance. However the design resistance obtained with the ECOV method is still higher compared to the design resistance obtained with the GRF method. This is due to the relatively high global resistance factor $\gamma_R = 1.2$ used in the GRF method.
- The lowest global resistance factor $\gamma_R = 1.10$ for the ECOV method is obtained when the results of the NLFE analysis with mean material values shows a brittle failure and the result of the NLFE analysis with characteristic material values show a ductile failure. The global resistance factor is relatively low but also the mean resistance is relatively low due to the brittle failure. Therefore the structural design resistance of the ECOV method can still be safe.
- The GRF method is in all cases the most conservative safety format due to the relatively high global safety factor $\gamma_R = 1.2$.
- The least conservative safety format for design 1 is the ECOV method. This is caused by a ductile failure in the NLFE analysis with mean and characteristic material values.
- The results of the least conservative safety formats for design 2 and 3 are obtained with the PFm. The model uncertainty and the partial material factors are already included in the

design material values. The design values used in the NLFE analysis are low compared to the material values used in the other methods, but the low concrete material values have a positive influence on the ductile behavior of the frame design and in most cases a larger structural resistance is obtained when a ductile failure is observed.

#### Comparison Eurocode 2 and Safety Formats (Model code 2010)

The real failure mode of the reinforced portal frame design for the defined load situation is a compressive strut failure in the frame corner due to a closing moment followed by the formation of three plastic hinges at location A, C and E. A detailed analysis of a strut and tie model of the concrete frame corner could lead to a lower design resistance compared to the local element resistance where a shear failure is obtained. Therefore the safety formats can improve the design resistance of the reinforced concrete frame since this approach makes redistribution of the concrete compressive strut possible. The least conservative safety formats already show in table 3 that there is some additional vertical capacity. This could probably be higher since the design resistance obtained from a strut and tie model according to the Eurocode 2 could lead to a lower local design resistance.

### *8.1.1.2 Level II: global safety assessment by means of the FORM & response surfaces*

A level II global reliability analysis is performed to determine the reliability level $\beta_R$ of the least conservative safety formats. Response surfaces were constructed for the least conservative safety formats and the FORM is used to determine the reliability level. Three cases with specified uncertainties were defined. Case 1 and 2 are the cases where is assumed that the detailing is known. For case 1 there is assumed that there is no geometrical uncertainty and for case 2 there is assumed that there is some geometrical uncertainty in the longitudinal reinforcement. Fabrication of geometrical reinforcement leads to a coefficient of variation of the cross-sectional area of the longitudinal reinforcement $V_{As} = 0.02$. However, in case of a reassessment of an existing structure the reinforcement detailing is not always known. Specific reinforcement detailing plans may be missing or the reinforcement is not placed exactly according to the reinforcement plan. Especially the specific detailing type in the corner region can be of significant importance as explained in chapter 6.1.2. Therefore case 3 is defined, where this uncertainty in the reinforcement detailing will be reflected in a larger coefficient of variation $V_{As} = 0.10$.

In this thesis the safety of the methods used in the Eurocode 2 has not been assessed by means of a FORM analysis, since this is already done in the past and could be find in literature. The reliability level is assumed to be $\beta_R > 3.04$.

#### Comparison of the FORM & response surfaces with the safety formats (Model Code 2010)

##### Detailing type is exactly known

In the cases 1 an 2 where the detailing is exactly known the reliability index is always higher than $\beta_R > 3.04$ for design 1, 2 and 3. This is shown in table 25. The lowest obtained reliability level is obtained in case 2 for design 2, where the reliability index is $\beta_R = 5.07$. This indicates that there is some margin to compensate for the model uncertainty derived from the two experiments is $\theta_m = 1.028$ and the coefficient of variation $V_m = 0.01$, which was neglected in the level II global reliability analysis. Even a compensation for a higher coefficient of variation $V_m$, which could be the result from more experiments should be possible.

In fact the assumed model uncertainty in the safety formats of $y_{Rd} = 1.06$ is already compensating for this uncertainties. It should be noted that the model uncertainty derived from the experiment is defined as $\theta_m = \frac{R_{exp}}{R_{NLFEA}}$ (Engen, 2017) is the inverse of $\gamma_{Rd} = \frac{R_{NLFE}}{R_{exp}}$. Therefore the obtained model

uncertainty $\theta_m$ is in this case a positive influence since $\frac{1}{\theta_m} = 0.972$. However the coefficient of variation can still lead to a negative influence on the structural resistance.

#### Detailing type is not exactly known

In case 3 the reinforcement detailing is not exactly known. This uncertainty is implemented in a larger coefficient of variation of the cross-sectional area of the longitudinal reinforcement $V_{As} = 0.10$. Table 25 shows that in each of the three portal frame designs the reliability level $\beta_R < 3.04$. In this case the model uncertainty of $\gamma_{Rd} = 1.06$ is certainly not sufficient for the unknown detailing type. The safety formats should compensate for the unknown detailing type by using a higher model uncertainty $\gamma_{Rd}$. The model uncertainty $\gamma_{Rd}$ needed for this case can be determined using an inverse approach. The design resistance obtained from the safety formats $R_{SF}$ should be lowered using a slightly larger model uncertainty. The obtained response surfaces will be a bit higher and therefore the reliability index will be higher. This iterative process should be repeated until the obtained reliability index is equal to 3.04. In case of the PFm it is more work to obtain the design resistance with a higher model uncertainty, since the model uncertainty is implemented in the partial safety factor $\gamma_M$ (equation (3.9)). The model uncertainty $\gamma_{Rd}$ that should be used instead of $\gamma_{Rd} = 1.06$ has not been determined yet. However, the determination of the model uncertainty that should be used in the safety formats is only useful for a situation where the uncertainties are estimated in a better way. The uncertainties should be based on more experimental results.

In case of a reassessment of an existing structure the exact reinforcement design is not always known. For instance specific reinforcement detailing plans may be missing or the reinforcement is not placed according to the reinforcement plan. The assumed uncertainty is case 3 is still not that high and the safety formats already fail to reach the intended reliability level. Therefore the safety formats should be used with a certain caution when they are used to reassess a concrete structure.

### 8.1.2 Conclusions about the safety assessment methods

#### *8.1.2.1 Comparison multiple loads in the safety formats (Model code 2010) and Eurocode 2*

The safety formats are not clear on how to determine the structural design resistance of a structure with multiple loads placed in a certain order and different load directions. For instance, in this case the vertical load is applied first on the structure, after that the horizontal load is applied on the structure and subsequently the structural resistance is obtained by increasing the vertical load until failure. There is chosen to put all the safety in the vertical resistance and the horizontal resistance is not reduced. This is done to compare the structural resistance of several portal frame designs where only the vertical resistance of the portal frame is different. Therefore the safety that could be implemented in order to reduce the horizontal resistance is also subtracted from vertical resistance. The results of the level II global safety assessment lead to a safe reliability index (case 1 and 2), which means that the used approach is safe. There could also be chosen to obtain the structural resistance of the portal frame by reducing the vertical and horizontal resistance, which is probably the most logical choice in case that the loads are applied at the same time. Or a less safe structural resistance can be obtained by only reducing the vertical resistance without applying some additional reduction in order to compensate for the not reduced horizontal resistance. However when the partial factor method is used it is always clear on how to reduce the structural resistance since the last applied load determines the structural design resistance because there is no global resistance factor used. Another aspect is that the loading order can have an influence on the structural resistance of the structure (Blomfors, Global Safety Assesment of Concrete Structures using Nonlinear Finite Element Analysis, 2014). An assumption of a realistic loading order should be made to obtain a realistic design resistance.

The loading order in a local safety assessment method according to the Eurocode 2 does not matter since the loads are present at the same time. Also the assumed resistance models do not take into account different loading orders. Furthermore there is no global resistance factor used so there is no problem in defining a constant horizontal load that the structure should be able to resist.

#### *8.1.2.2 Composed line elements used in the NLFE model*

The NLFE model of the statically indeterminate reinforced concrete portal frame is made with plane stress elements in combination with integrated composed line elements. Composed line elements are incorporated in Diana 10.1, which could integrate the internal stresses over the height of a cross-section in order to produce a bending moment distribution. Especially for a statically indeterminate structure this could help in order to find the plastic hinges that are formed in the portal frame. Initially there was expected a plastic hinge in corner D of the portal frame. However, the bending moment distribution determined from the composed line elements showed that the bending moment capacity of corner D was in fact really low. After thoroughly investigating the corner region there was found that the internal compressive strut has failed and therefore the formation of a plastic hinge was not possible. The linear elastic (or plastic moment distribution) obtained from a local design approach and the bending moment distribution using a global design approach can be compared much easier with the use of composed line elements.

#### *8.1.2.3 FORM & Response surfaces*

In theory creating a response surface in combination with the FORM should be an accurate method to determine the reliability index of a structure by means of a NLFE model. However in practice there are a lot of issues to discuss. First of all the settings in the used NLFE package. Most of the settings that should be used are described in detail in the Guidelines for Non-Linear Finite Element Analysis of Concrete Structures (Hendriks, de Boer, & Belletti, 2017). In order to obtain the structural resistance of the portal frame the last load-step were the convergence criterion is fulfilled should be checked in order to be certain that the structure has failed. Things like convergence criteria, number of iterations and load-step sizes can still have an influence on the results. This is one of the reason that the safety assessment could not be automated. Some other issues will be described below and are more case dependent. These issues are also described with a few examples in chapter 7.2.1.4.

##### Obtaining the control point $\boldsymbol{X}_c$

To obtain the control point a factor $f$ should be chosen in order to assess the individual influence of the stochastic variables. A factor $f = 3$ is recommended but this led to an unrealistic design point in some of the cases. The control point can be obtained by performing a NLFE analysis with the mean values of the stochastic variables and some NLFE analyses where the mean values are used in combination with one reduced stochastic variable to determine the individual influence of that variable on the structural resistance. The reduction of the stochastic variable is obtained by subtracting $f$ times the standard deviation from the mean value. For portal frame design 2 and 3 a brittle failure was obtained after performing a NLFE analysis with mean material values. The analyses with reduced concrete material values with $f = 3$ led to ductile failure mode with even a higher structural resistance. This led to an unrealistic control point and a larger value of $f$ should be used to obtain a more realistic control point. The best way to estimate the factor $f$ is to start with a NLFE analysis with mean material values and subsequently performing several NLFE analyses with an increasing $f$-factor to obtain low concrete material values until a lower structural resistance is obtained than the mean resistance. After that the NLFE analyses for the other uncertainties can be performed with the correct $f$-factor. In this way a lot of time can be saved.

### The influence of the factor $f$ on the initial design point

The factor $f$ have a lot of influence on the control point that is obtained and therefore the direction of the straight line between $\overline{\boldsymbol{X}}$ and $\boldsymbol{X}_c$ on which the initial design point is found. The factor $f$ is basically an initial guess and a correct choice can only be verified when the real design point is found. A wrong choice could lead in much more effort to find the real design point since the real design point is far away from the initial design point.

### Exact calculation of the response surface not recommended

In the theory a response surface should be created with $2n$+1 sample points. Basically $2n$ sample points around the initial design point. This lead to an exact calculation of the response surface i.e. the response surface goes exactly through the sample points. However due to the brittle and ductile failure modes that could be obtained there is always the danger of a response surface that not describes the real behavior of the structure. Therefore a least squares approach is used with more sample points. However using too many sample points is also not recommended since the obtained response surface is hardly changing after adding an intended design point.

An exact calculation of the response surface is only possible when you are certain that the initial design point is very close to the real design points and therefore again strongly dependent on the initial choice of the factor $f$.

### Poor description of the response surface in the zones without sample points can lead to divergence

Another problem with creating a response surface is the poor description of the zones without sample points. A situation could occur where the region of the real design point is described very accurately, but after applying the FORM a design point outside the zone which is described by sample point could be obtained i.e. a divergence of the iteration process has been occurred. An example of this can be found in chapter 7.2.1.2. A solution to the problem is adding some sample points in this region.

## 8.2 Suggestions for further work

- A prediction model to determine whether a reinforced concrete corner fails in a brittle or ductile manner and what is the influence on the structural resistance based on several detailing types and material properties. A lot of experiments should be used to determine the model uncertainty.
- Optimize the reinforcement detailing in the reinforced concrete corner such that a full plastic hinge can develop in the corner region. This could have a large effect on the structural resistance obtained with the safety formats and therefore on the reliability index.
- Better ways to determine the control point $\boldsymbol{X}_c$ probably based on more than $n + 1$ NLFE analyses where not only one material parameter is reduced by the factor $f$ but make use of combinations to obtain a more realistic structural behavior close to unsafe region. In this way the initial design point should be much better predicted and convergence will be achieved faster.

# References


Allaix, D. L., Carbone, V. I., & Mancini, G. (2013). Global Safety format for non-linear analysis of reinforced concrete structures. *Structural Concrete*.

Blomfors, M. (2014). *Global Safety Assesment of Concrete Structures using Nonlinear Finite Element Analysis.* Master Thesis, Chalmers University of Technology, Göteborg.

Blomfors, M., Engen, M., & Plos, M. (2016). Evaluation of safety formats for non-linear finite element analyses of statically indeterminate concrete structures subjected to different load paths. *Structural Concrete*.

Bucher, C., & Bourgund, U. (1990). A fast and effiecient response surface approach for structural reliability problems. *Structural Safety*.

Cervenka, V. (2013). Global safety formats in fib Model Code 2010 for design of concrete structures. *11th international Probabilistic Workshop.* Brno: Cervenka Consulting.

De Vuyst , S. (2018). *https://en.wikipedia.org/wiki/Log-normal_distribution*. Retrieved from https://en.wikipedia.org/wiki/Log-normal_distribution

Eklund, H., Skorve, A., & Strand, A. (2017). *Reliability assesment of concrete structures using non-linear finite element analyses.* Master Thesis, Norwegian University of Science and Technology.

Engen, M. (2017). *Aspects of design of reinforced concrete structures using non-linear finite element analyses.* Doctoral thesis, Norwegian University of Science and Technology.

Faber, M., & Vrouwenvelder, T. (2001). *Probabilistic Model Code.* Joint Committee on Structural Safety (JCSS).

fib. (2012). *Model Code 2010.* International Federation for Structural Concrete (fib).

Hendriks, M., de Boer, A., & Belletti, B. (2017). *Guidelines for Nonlinear Finite Element Analysis of Concrete Structures.* Rijkswaterstaat Centre for Infrastructure. Report RTD:1016-1:2017.

Johansson, M. (2000). *Structural Behaviour in Concrete Frame Corners of Civil Defence Shelters.* Göteborg: Chalmers University of Technology.

Jonkman, S., Steenbergen, R., Morales-Nápoles, O., Vrouwenvelder, A., & Vrijling, J. (2016). *Probabilistic Design: Risk and reliability analysis in Civil Engineering (CIE4130).* Delft: TU Delft.

Kersner, Z., Lehky, D., Drahomir, n., Elias, J., Strauss, A., Hoffman, S., . . . Bergmeister, K. (2007). Determination of fracture-mechanical parameters for reliability calculation. *5th International Probabilistic Workshop.* Ghent.

NEN-EN 1990. ( 2011). *Basis of Structural Design.*

NEN-EN 1992 -1-1. (2011). *Eurocode 2: Design of concrete structures - Part 1-1: General rules and rules for buildings.*

Octar, O. N., Moral, H., & Tasdemir, M. A. (1996). Factors determining the correlations between concrete properties. *Cement and Concrete Research*.

Pimentel, M., Eugen, B., & Figueiras, J. (2014). Safety examination of excisting concrete structures using the global resistance safety factor concept. *Engineering Structures*.

Plos, M. (1994). Splicing of Reinforcement in Frame Corner - Experimental Studies. *Nordic Concrete Research*.

Rajashekhar, M. R., & Ellingwood, B. R. (1993). A new look at the response surface approach for reliability analysis. *Structural Safety*.

Schlune, H. (2011). *Safety Evaluation of Concrete Structures with Nonlinear Analysis.* Thesis for the degree of doctor of philosophy, Chalmers University of Technology, Gothenburg.

Schlune, H., Plos, M., & Gylltoft, K. (2011). Safety formats for nonlinear analysis tested on concrete beams subjected to shear forces and bending moments. *Elsevier*.

Schneider, J. (2006). *Introduction to safety and Reliability of structures.* Zürich: IABSE.

Seraj, S. M., Kotsovos, M. D., & Pavlovic, M. N. (1995). Application of the compressive-force path concept in the design of reinforced concrete indeterminate structure: A pilot study. *Structural Engineering & Mechanics*.

Sørensen, J. D. (2004). *Notes in Structural Reliability Theory and risk Analysis.* Aalborg: Aalborg University.

Strauss, A., Zimmermann, T., Lehký, D., Novák, D., & Kersner, Z. (2014). Stochastic fracture-mechanical parameters for the performance-based design of concrete structures. *Structural Concrete*.

Torrent, R. (1978). The log-normal distribution: A better fitness for the results of mechanical testing of materials. *Materials and Structures*.

Walraven, J. (1988). Staafwerkmodellen als basis voor het detailleren van betonconstructies. *Cement*.

Walraven, J., & Fennis, S. (2013). *Gewapend Beton (CTB2220).* Delft: TU Delft.

Zhao, W., & Qiu, Z. (2013). An efficient response surface method and its application to structural reliability and reliability-based optimization. *Finite Elements in Analysis and Design*.

Zimmermann, T., Lehký, D., & Strauss, A. (2016). Correlation among selected fracture-mechanical parameters of concrete obtained from experiments and inverse analyses. *Structural Concrete 17*.

# Appendices

# Appendix A Background theory of the safety formats

## A.1 Material input values in the GRFm safety format

This safety format determines the design resistance $R_d$ with a NLFE analysis with the input of mean GRF material parameters with the same (scaled) global resistance factor for each material. Figure A1 shows the probability density function (PDF) of steel and concrete. The global resistance factor is related to the mean variable.

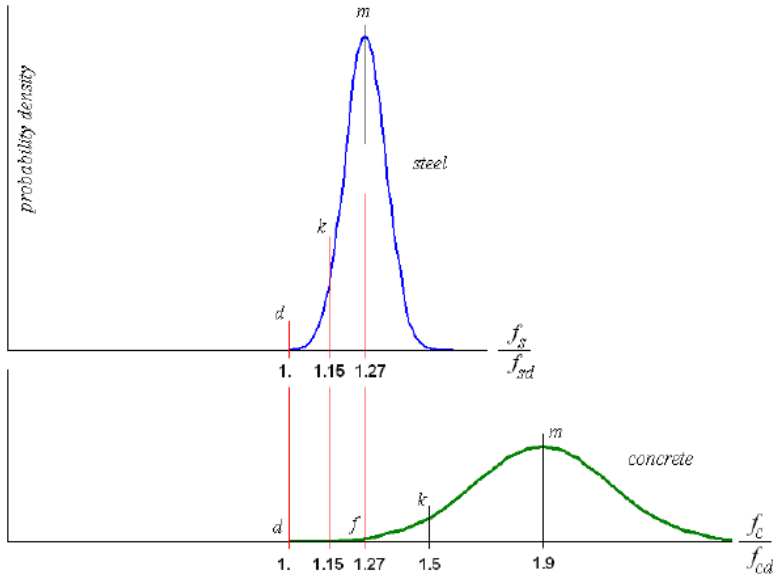


*Figure A1. Probabilistic definition of mean (m), characteristic (k) and design (d) values for steel and concrete failure and the reduced concrete strength (f) (Cervenka, 2013).*

The global resistance factor of steel is:

$$\gamma_{GL}^{steel} = \frac{f_{sm}}{f_{sd}} = \frac{1.1\, f_{sd}\, \gamma_s}{f_{sd}} = 1.27 \qquad \text{(A.1)}$$

where:

$f_{sm} = \frac{1.27}{1.15} f_{yk} = 1.1\, f_{yk} = 1.1\, f_{sd}\, \gamma_s$ is the mean strength of steel (see figure A1 for factors);

$f_{sd}$ is the design strength of steel;

$\gamma_s = 1.15$ is the partial safety factor for the characteristic strength of steel.

The global resistance factor of concrete is:

$$\gamma_{GL}^{concrete} = \frac{f_{cm}}{f_{cd}} = \frac{f_{cd}\, \gamma_c\, 1.27}{f_{cd}} = 1.9 \qquad \text{(A.2)}$$

where:

$f_{cm} = \frac{f_{cd}\, \gamma_c \frac{1.9}{1.5}}{f_{cd}}$ is the mean concrete compressive strength (figure A1);

$f_{cd}$ is the design concrete compressive strength;

$\gamma_c = 1.5$ is the partial safety factor for the characteristic strength of concrete.

In order to have the same global resistance factors for steel and concrete, the mean concrete compressive strength is reduced to get a lower global resistance factor for concrete $\gamma_{GL}^{concrete}$.

Figure A1 shows a reduced value for the mean concrete compressive strength $f_{cm}^{GRF}$ at location $(f)$, $\frac{f_c}{f_{cd}} = 1.27$ on the horizontal axis (instead of $f_{cm}$ at location$(m)$, $\frac{f_c}{f_{cd}} = 1.9$ on the horizontal axis).

The new reduced mean concrete strength can be derived according to:

$$f_{cm}^{GRF} = \frac{1.1\,\gamma_s}{\gamma_c} f_{ck} \tag{A.3}$$

The new mean concrete compressive strength $f_{cm}^{GRF}$ is lower than the characteristic concrete compressive strength $f_{ck}$. This leads to the required additional safety for concrete when it is compared to steel. The global resistance factor for steel $\gamma_{GL}^{steel}$ is now per definition the same as the new obtained global resistance factor for concrete $\gamma_{GL}^{concrete}$. The global resistance factor $\gamma_{GL}$is defined as:

$$\gamma_{GL} = \gamma_{GL}^{steel} = \gamma_{GL}^{concrete} = \frac{f_{ym}^{GRF}}{f_{cd}} = \frac{0.85\,f_{ck}}{\frac{f_{ck}}{1.5}} = 1.27 \tag{A.4}$$

$$\gamma_{GL} = \gamma_R\,\gamma_{Rd} \tag{A.5}$$

where:

$\gamma_R = 1.2$ is the partial factor of the resistance;

$\gamma_{Rd} = 1.06$ is the model uncertainty.

From equation (A.5) follows that the partial factor of the resistance $\gamma_R = 1.2$. The input values for the NLFE analysis for steel and concrete can be derived from (A.1) and (A.3) which leads to the following formulas:

$$f_{ym}^{GRF} = 1.1\,f_{yk}, \tag{A.6}$$

$$f_{cm}^{GRF} = 0.85\,f_{ck}. \tag{A.7}$$

## A.2 Global resistance factor ECOV safety format

Probabilistic studies indicate a log-normal distribution function (fib, 2012) for the resistance of a reinforced concrete beam. The random distribution can be described by a two-parameter (the mean resistance $R_m$ and coefficient of variation $V_R$ of the resistance) log-normal distribution with the lower bound at the origin (fib, 2012).

The random variable $R \sim LN(R_m, \sigma_m^2)$ is log-normal distributed then its natural logarithm $Y = \ln(R)$ is normally distributed with the mean $\mu$ and the standard deviation $\sigma$.

$$R \sim LN(R_m, \sigma_m^2) \tag{A.8}$$

$$Y = \ln(R) \sim N(\mu(Y), \sigma(Y)^2) \tag{A.9}$$

$$Y = \ln(R) = \mu(Y) + \sigma(Y)Z \tag{A.10}$$

$$R = e^{\mu(Y)+\sigma(Y)Z} \tag{A.11}$$

where: $Z \sim N(0,1)$

The expected value $E(R)$ can be estimated with (Jonkman, Steenbergen, Morales-Nápoles, Vrouwenvelder, & Vrijling, 2016):

$$E(R) = e^{E(Y)+\frac{1}{2}\sigma^2(Y)} \approx e^{E(Y)} \qquad \text{only valid if: } \sigma(Y) \ll E(Y) \qquad \text{(A.12)}$$

where:
$E(R) = R_m$
$E(Y) = \mu(Y)$;
$\sigma(y) = \sqrt{Var(y)}$.

This leads to the following approximation:

$$R_m \approx e^{\mu(Y)}. \qquad \text{(A.13)}$$

The standard deviation $\sigma(R)$ can be estimated with (Jonkman, Steenbergen, Morales-Nápoles, Vrouwenvelder, & Vrijling, 2016):

$$\sigma(R) = E(X)\sqrt{e^{\sigma^2(Y)-1}} \approx E(R)\sigma(Y) \qquad \text{only valid if: } \sigma(Y) \ll E(Y) \qquad \text{(A.14)}$$

where:
$\sigma(R) = \sigma_m$
$E(X) = R_m$
$\sigma(Y) = \sqrt{Var(y)}$.

The coefficient of variation $V_R$ is defined as:

$$V_R = \frac{\sigma_m}{\mu_R} = \frac{\sigma(R)}{E(R)} \approx \frac{E(R)\sigma(Y)}{E(R)} \approx \sigma(Y). \qquad \text{(A.15)}$$

The characteristic value of the resistance can be calculated according to:

$$P(R < R_k) = 0.05 \qquad \text{(A.16)}$$

Substitute (A.11), (A.13) and (A.15) in equation (A.16):

$$P\left(e^{\mu(Y)+\sigma(Y)Z} < R_k\right) = P(\ln(R_m) + \sigma(Y)Z < \ln(R_k)) = P\left(Z < \frac{\ln(R_k)-\ln(R_m)}{V_R}\right) = 0.05.$$

$$\frac{\ln\left(\frac{R_k}{R_m}\right)}{V_R} = -1.65 \qquad \text{(A.17)}$$

An acceptable approximation of the characteristic resistance is:

$$R_k = R_m\, e^{-1.65\, V_R} \qquad \text{(A.18)}$$

where:
$R_m$ is the mean resistance;
$V_R$ is the coefficient of variation.

The coefficient of variation can be estimated for a failure probability of 0.05 by rearranging formula (A.18):

$$V_R = \frac{1}{1.65}\ln\left(\frac{R_m}{R_k}\right). \qquad \text{(A.19)}$$

The global resistance factor is defined as:

$$\gamma_R = \frac{R_m}{R_d} = \frac{R_m}{R_m\, e^{-\alpha_R\, \beta\, V_R}} = e^{\alpha_R\, \beta\, V_R} = e^{3.04\, V_R} \qquad \text{(A.20)}$$

where:

| | |
|---|---|
| $R_m$ | is the mean resistance obtained from NLFE analysis with mean input parameters; |
| $R_k$ | is the characteristic resistance obtained from a NLFE analysis with characteristic input parameters; |
| $\alpha_R = 0.8$ | is the sensitivity factor (dominant strength parameter); |
| $\beta = 3.8$ | is the reliability index; |
| $V_R$ | is the coefficient of variation. |

# Appendix B Material properties

## B.1 Concrete material properties by Model Code 2010 (fib, 2012)

Mean compressive strength:

$f_{cm} = f_{ck} + \Delta f$ where: $\Delta f = 8$ MPa (B.1)

Characteristic compressive strength:

$f_{ck}$ (B.2)

Design compressive strength:

$f_{cd} = \alpha_{cc} \frac{f_{ck}}{\gamma_c}$ where: $\alpha_{cc} = 1.0$ and $\gamma_c = 1.5$ (B.3)

Mean tensile strength:

$f_{ctm} = 0.3\, f_{ck}^{2/3}$ (B.4)

Characteristic tensile strength:

$f_{ctk,min} = 0.7\, f_{ctm}$ (B.5)

Design tensile strength:

$f_{ctd} = \frac{f_{ctk,min}}{\gamma_c}$ (B.6)

Fracture energy:

$G_F = 73\, f_{cm}^{0.18}$ (B.7)

Compressive fracture energy:

$G_C = 250\, G_F$ (B.8)

Young's modulus after 28 days:

$E_{ci} = E_{co} \left(\frac{f_{cm}}{10}\right)^{1/3}$ where: $E_{co} = 21500$ MPa (B.9)

## B.2 Material input values for the different safety formats Model Code 2010

The material input values for the safety formats calculated according to Guidelines for NLFE analyses of Concrete Structures (Hendriks, de Boer, & Belletti, 2017) are shown in the table B1, B2 and B3.

Density reinforced concrete:
$\rho = 2500$ kg/m$^3$

Partial safety factor concrete:
$\gamma_c = 1.5$

The young's modulus of reinforcing steel:
$E_s = 200000$ MPa.

Partial safety factor steel:
$\gamma_s = 1.15$

*Table B1. Material input values for the safety formats: concrete C30.*

| **Concrete** | | | | | | |
|---|---|---|---|---|---|---|
| **C30** | fc | (MPa) | fct | (MPa) | Ec | (MPa) |
| Mean Measured | fcm | 38 | fctm | 2.896 | Eci | 33550.6 |
| Characteristic | fck | 30 | fck, min | 2.028 | Eci | 31008.4 |
| Mean GRF | fcm,GRF | 25.5 | fctm, GRF | 2.599 | Eci | 29373.2 |
| Design | fcd | 20 | fctd | 1.352 | Eci | 27088.3 |
| | | | | | | |
| **C30** | v | | GF | (Nmm/mm2) | Gc | (Nmm/mm2) |
| Mean Measured | variable | | GF | 140.5 | Gc | 35125.6 |
| Characteristic | variable | | GF | 134.6 | Gc | 33662.4 |
| Mean GRF | variable | | GF | 130.8 | Gc | 32691.9 |
| Design | variable | | GF | 125.2 | Gc | 31293.1 |

*Table B2. Material input values for the safety formats: concrete C40.*

| **Concrete** | | | | | | |
|---|---|---|---|---|---|---|
| **C40** | fc | (MPa) | fct | (MPa) | Ec | (MPa) |
| Mean Measured | fcm | 48 | fctm | 3.509 | Eci | 36267.6 |
| Characteristic | fck | 40 | fck, min | 2.456 | Eci | 34129.1 |
| Mean GRF | fcm,GRF | 34 | fctm, GRF | 3.149 | Eci | 32329.4 |
| Design | fcd | 26.7 | fctd | 1.637 | Eci | 29814.5 |
| | | | | | | |
| **C40** | v | | GF | (Nmm/mm2) | Gc | (Nmm/mm2) |
| Mean Measured | variable | | GF | 146.5 | Gc | 36634.2 |
| Characteristic | variable | | GF | 141.8 | Gc | 35451.4 |
| Mean GRF | variable | | GF | 137.7 | Gc | 34429.4 |
| Design | variable | | GF | 131.8 | Gc | 32956.2 |

*Table B3. Material input values for the safety formats: longitudinal reinforcement.*

| **Longitudinal reinforcement** | | | | | | |
|---|---|---|---|---|---|---|
| **Steel** | fy | (MPa) | ft | (MPa) | ϵsy | |
| Mean Measured | fym | 560 | ftm | 680 | ϵsy | 0.0028 |
| Characteristic | fyk | 507 | ftk | 616 | ϵyk | 0.0025 |
| Mean GRF | fym,GRF | 558 | ftk, GRF | 677 | ϵym, GRF | 0.0028 |
| Design | fyd | 441 | ftd | 536 | ϵcd | 0.0022 |

*Table B3. Material input values for the safety formats: shear reinforcement.*

| **Shear reinforcement** | | | | | | |
|---|---|---|---|---|---|---|
| **Steel** | fy | (MPa) | ft | (MPa) | ϵsy | (-) |
| Mean Measured | fym | 460 | ftm | 510 | ϵsy | 0.0023 |
| Characteristic | fyk | 417 | ftk | 462 | ϵyk | 0.0021 |
| Mean GRF | fym,GRF | 458 | ftk, GRF | 508 | ϵym, GRF | 0.0023 |
| Design | fyd | 362 | ftd | 402 | ϵcd | 0.0018 |

The mean, characteristic and design concrete strength can be calculated according to Appendix B.1. The mean GRF values can be calculated according to Appendix A.1 and Appendix B.1.

The mean values of steel yield strength $f_{ym}$ and tensile strength $f_{tm}$ where measured in the experiment. To obtain the characteristic values of the yield strength $f_{yk}$ a lognormal distribution is assumed with a coefficient of variation ranging from 0.05 to 0.1. The coefficient of variation $V_s = 0.6$ is assumed to be a good intermediate value (Hendriks, de Boer, & Belletti, 2017). The characteristic yield strength is determined by a probability of 0.05 of the lognormal distribution:

$$f_{ck} = f_{cm}\, e^{-1.65\, V_s} \tag{B.10}$$

Furthermore the steel tensile strength is calculated with:

$$f_{ti} = f_{yi}\, A \qquad \text{where: } A = \frac{f_{tm}}{f_{ym}} \tag{B.11}$$

The main design characteristics are given below:

| | | | |
|---|---|---|---|
| Design 1: | longitudinal reinforcement: | 3Ø10 | $A_{s,l} = 3\,(0.25\,\pi\,10^2) = 235.62$ mm² |
| | shear reinforcement | 2Ø1.5 | $A_{s,s} = 2\,(0.25\,\pi\,1.5^2) = 3.53$ mm² |
| | concrete strength class | C30 | |
| Design 2: | longitudinal reinforcement | 3Ø11 | $A_{s,l} = 3\,(0.25\,\pi\,10^2) = 285.1$ mm² |
| | shear reinforcement | 2Ø1.5 | $A_{s,s} = 2\,(0.25\,\pi\,1.5^2) = 3.53$ mm² |
| | concrete strength class | C30 | |
| Design 3: | longitudinal reinforcement: | 3Ø10 | $A_{s,l} = 3\,(0.25\,\pi\,10^2) = 235.62$ mm² |
| | shear reinforcement | 2Ø1.5 | $A_{s,s} = 2\,(0.25\,\pi\,1.5^2) = 3.53$ mm² |
| | concrete strength class | C40 | |

## B.3 Material values used in the experiment Seraj et al. (1995)

Concrete:
$f_{cm,cube} = 48$ MPa (on test day)
$f_{cm,cilinder} \approx 0.8 \cdot 48 \approx 38$ MPa

Longitudinal reinforcement:
$f_{ym} = 560$ MPa and $f_{tm} = 680$ MPa — 3Ø10 $A_s = 3\,(0.25\,\pi\,10^2)$ mm² (PF1 and PF2)

Shear reinforcement:
$f_{ym} = 460$ MPa and $f_{tm} = 510$ MPa — 2Ø1.5 $A_s = 2\,(0.25\,\pi\,1.5^2)$ mm² (PF1 and PF2)
3Ø1.5 $A_s = 3\,(0.25\,\pi\,1.5^2)$ mm² (PF2)

# Appendix C Level I reliability method: local design resistance (Eurocode 2)

To perform a local safety evaluation according to the Eurocode 2 (NEN-EN 1992 -1-1, 2011) a distinction between the several elements is necessary. Therefore the elements will be numbered from left to right. This leads to the following element numbering: the left column (AB), beam (BD) and the right column (DE) are labeled as element 1, element 2 and element 3, respectively. The element numbering is shown in figure C1.

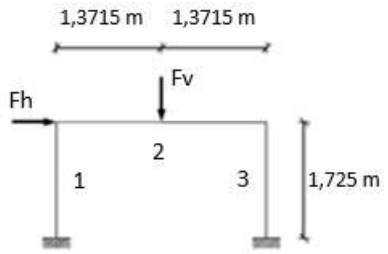


*Figure C1. Element numbering.*

## C.1 local design resistance portal frame design 1, 2 & 3

The local design resistance of the elements of portal frame design 1 will be worked out in this appendix. Using the same approach the design resistance of the elements of portal frame design 2 and 3 can be found. Only the results will be presented in chapter C.1.3.

### C.1.1 Design 1: determination of the internal forces (linear elastic calculation)

The moment capacities of the elements can be determined using a local element approach for both columns $M_{R,1} = M_{R,3}$ and the beam $M_{R,2}$ of the frame. In this calculation there is chosen for a simplified moment capacity without a compressive normal force and in only tension reinforcement is considered. The moment capacities can be derived from the equilibrium of a section:

$$N_s = N_c \tag{C.1}$$

where: $N_s = A_s\, f_y$ and $N_c = \frac{3}{4} x_u\, f_{cd}\, b$. From equation (C.1) $x_u$ can be solved and the internal lever arm for both elements can be calculated:

$$z_1 = d_1 - 0.39\, x_u \tag{C.2a}$$
$$z_2 = d_2 - 0.39\, x_u \tag{C.2b}$$

The moment capacities can be determined with the following formulas:

$$M_{R,1} = A_s\, f_y\, z_1 \tag{C.3a}$$
$$M_{R,2} = A_s\, f_y\, z_2. \tag{C.3b}$$

After substituting all deterministic variables given in chapter 4.2.1 in the following equations can be derived:

$$M_{R,1} = \frac{31.8\, f_y\, f_c - 0.32\, f_y^2}{f_c}\ \text{(Nm)} \tag{C.4a}$$
$$M_{R,2} = \frac{25.9\, f_y\, f_c - 0.32\, f_y^2}{f_c}\ \text{(Nm)}. \tag{C.4b}$$

The bending moment resistance of portal frame design 1 is calculated with the following Maple script presented in figure C2. An example is given for the bending moment resistance for element 1, which lead to a bending moment resistance of $M_{Rd,1} = 10.0$ kNm. The bending moment resistance of element 2 and 3 are calculated in the same manner and are equal to $M_{Rd,2} = 12.6$ kNm and $M_{Rd,3} = 10.0$ kNm.

```
restart :
# Moment capacity for elements with the following material values and height:
fc := 20 : fy := 441 : h := 125 :
# Constants:
b := 90 : c := 15 : As := 3·0.25·Pi·10^2 : eps_cu3 := 3.5·10^-3 : Es := 200000 :
eps_sy := evalf(fy/Es) :
# Horizontal equilibrium:
H := Nc + Ns_compr − Ns :
Nc := 0.75·b·xu·fc :
Ns_compr := (xu − c)/xu ·eps_cu3·As·Es :
Ns := fy·As :
sol := solve([H], [xu]) :
assign(sol[1]);
xu;
                                  25.80714589                              (1)

# Check assumption (only yielding in bottom reinforcement): eps_s>0.0028
eps_s_compr := (xu − c)/xu · eps_cu3;
                        eps_s_compr := 0.001465679730                      (2)
eps_c_top := eps_cu3;
                        eps_c_top := 0.003500000000                        (3)
eps_s := (h − c − xu)/xu · eps_cu3;
                        eps_s := 0.01141834865                             (4)
# assumption correct
# Moment capacity MR(Nm):
MR := (Nc·(1/2·h − 7/18·xu) + Ns_compr·(1/2·h − c) + Ns·(1/2·h − c))·10^-3;
                        MR := 10044.21691                                  (5)
```

*Figure C2. Portal frame design 1: bending moment resistance element 1.*

The bending moment resistance of each element is needed to determine the linear elastic moment, shear and normal force distribution, since the portal frame is statically indeterminate. The moment, shear and normal force distribution is determined with the Maple script presented in figure C3. Therefore the governing bending moment resistance of element 3 (corner D) is used: $M_{Rd,3} = 10.0$ kNm and the fact that the horizontal wind load is known $F_h = 15.7$ kN. The maximum external vertical and horizontal force $F_v$ and $F_h$ is also determined with the Maple script presented in figure C3.

```
restart :
# Statically undetermined structure with 5 unkowns: Ma, Mb, Me, theta
    and Fv (5 equations needed to solve)
# Constants
l1 := 1.725 : l2 := 2.743 : b := 90 : h1 := 250 : h2 := 300 : fm := 38 :
    Ec := fm / (1.75·10^-3) :
# Not the real EI since the reinforcement is not included but it's only
    meant for the EI ratio between the columns and the beam
EI1 := evalf( 1/12 · b/1000 · (h1/1000)^3 ) · Ec :
EI2 := evalf( 1/12 · b/1000 · (h2/1000)^3 ) · Ec :
# The characterisic moment capacity of the column is decisive and is
    found at location d:
Md := 10044.21691
                        Md := 10044.21691                    (1)
assign(sol) :
Fh := 15681.83475
                        Fh := 15681.83475                    (2)
# Angle conditions (5 equations to solve the unkowns):
eq1 := phi_A = 0 :
eq2 := phi_B_AB = phi_B_BD :
eq3 := phi_D_BD = phi_D_DE :
eq4 := phi_E = 0 :
eq5 := Ma + Mb + Md + Me = Fh·l1 :

# Shear forces:
V[AB] := (M[A] + M[B]) / l1 ; V[BC] := (M[C] − M[B]) / (1/2 · l2) ;
V[CD] := (M[C] + M[D]) / (1/2 · l2) ; V[DE] := (M[D] + M[E]) / l1 ;
                        V_AB := 4205.514037
                        V_BC := 5133.852532
                        V_CD := 13684.34917
                        V_DE := 11476.32071                  (4)
# where:
phi_A := + 1/3 · Ma·l1/EI1 − 1/6 · Mb·l1/EI1 − theta :
phi_B_AB := + 1/3 · Mb·l1/EI1 − 1/6 · Ma·l1/EI1 − theta :
phi_B_BD := − 1/3 · Mb·l2/EI2 + 1/6 · Md·l2/EI2 − 1/16 · Fv·l2^2/EI2 :
phi_D_BD := − 1/3 · Md·l2/EI2 + 1/6 · Mb·l2/EI2 + 1/16 · Fv·l2^2/EI2 :
phi_D_DE := + 1/3 · Md·l1/EI1 − 1/6 · Me·l1/EI1 − theta :
phi_E := + 1/3 · Me·l1/EI1 − 1/6 · Md·l1/EI1 − theta :
sol1 := solve( [eq1, eq2, eq3, eq4, eq5], [Ma, Mb, Me, theta, Fv] ) :
assign(sol1) :
# Moments and external loads:
M[A] := Ma; M[B] := Mb; M[C] := − (−Mb + Md)/2 + 1/4 · Fv·l2;
M[D] := Md; M[E] := Me; Fv := Fv; Fh := Fh; LF := Fv/Fh;
                        M_A := 5571.722478
                        M_B := 1682.789235
                        M_C := 8723.867982
                        M_D := 10044.21691
                        M_E := 9752.436317
                        Fv := 18818.20170
                        Fh := 15681.83475
                        LF := 1.200000000                    (3)

# Reaction forces:
R_A_H := V[AB]; R_A_V := (Fv · 1/2 · l2 − Fh·l1 + Ma + Me) / l2 ;
R_E_H := V[DE]; R_E_V := (Fh·l1 + Fv · 1/2 · l2 − Ma − Me) / l2 ;
                        R_A_H := 4205.514037
                        R_A_V := 5133.852526
                        R_E_H := 11476.32071
                        R_E_V := 13684.34917                 (5)
# Normal forces:
N[AB] := R_A_V; N[BD] := Fh − V[AB]; N[DE] := R_E_V;
                        N_AB := 5133.852526
                        N_BD := 11476.32071
                        N_DE := 13684.34917                  (6)
```

*Figure C3. Maple script to determine the external load Fv and Fh of portal frame design 1.*

The maximum external load on the structure is: $F_v = 18.8$ kN and $F_h = 15.7$ kN according to a linear elastic moment distribution. This results in the following internal forces as presented in table C1.

*Table C1. Internal forces resulting from Fv and Fh*

| Design 1 | $M_E$ (kNm) | $V_E$ (kN) | $N_E$ (kN) |
|---|---|---|---|
| Element 1 | 5.58 | 4.22 | 5.12 |
| Element 2 | 10.04 | 13.68 | 11.48 |
| Element 3 | 10.04 | 11.48 | 13.68 |

## C.1.2 Design 1: determination of the resistance

### *C.1.2.1 Bending moment resistance (ULS)*

The local safety evaluation for the bending moment resistance of portal frame design 1 is performed in table C2. The bending moment resistance and the bending moment due to the external forces is determined in Appendix C.1.1.

*Table C2. Local safety evaluation (unity checks (UC)) for the linear elastic bending moment resistance.*

| EC2: Design 1 | $M_{Rd}$ (kNm) | $M_E$ (kNm) | UC (-) |
|---|---|---|---|
| Element 1 | 10.0 | 5.6 | 0.56 |
| Element 2 | 12.6 | 10.0 | 0.79 |
| Element 3 | 10.0 | 10.0 | 1.00 |

### *C.1.2.2 Shear resistance (ULS)*

The general check for the shear resistance is defined as (NEN-EN 1992 -1-1, 2011):

$V_E < V_{Rd,C}$ no shear reinforcement is needed, otherwise: (C.5a)

$V_E < V_{Rd,S}$. (C.5b)

#### Elements without shear reinforcement

Shear capacity elements without shear reinforcement (NEN-EN 1992 -1-1, 2011)

$$V_{Rd,C} = \{C_{Rd,C}\ k\ (100\ \rho_l\ f_{ck})^{1/3} + k_1\ \sigma_{cp}\} b_w\ d \quad \text{(C.6a)}$$

with a minimum of

$$V_{Rd,C,min} = \{v_{min} + k_1\ \sigma_{cp}\}\ b_w\ d \quad \text{(C.6b)}$$

where:

| | |
|---|---|
| $f_{ck}$ | characteristic concrete strength; |
| $C_{Rd,C} = \frac{0.18}{\gamma_c}$ | empirical factor ($\gamma_c = 1.5$); |
| $k = 1 + \sqrt{\frac{200}{d}} \leq 2.0$ | with $d$ in mm; |
| $\rho_l = \frac{A_{sl}}{b_w\ d} \leq 0.02$ | longitudinal reinforcement ratio; |
| $A_{sl}$ | is the area of tensile reinforcement; |
| $b_w$ | is the smallest with of the cross-section in the tensile area; |
| $\sigma_{cp} = \frac{N_{Ed}}{A_c} < 0.2\ f_{cd}$ | compressive stresses due to the normal force in the portal frame; |
| $N_{Ed}$ | is the normal force in the portal frame; |
| $Ac$ | is the area of the concrete cross-section; |
| $k1 = 0.15$ | empirical factor; |
| $v_{min} = 0.035\ k^{3/2}\ f_{ck}^{1/2}$ | empirical formula for minimum shear stresses. |

*Table C3. Design 1: calculation shear resistance elements without shear reinforcement.*

| EC2: Elements without shear reinforcement | | | | | | | | |
|---|---|---|---|---|---|---|---|---|
| Element 1 | | | Element 2 | | | Element 3 | | |
| V | 4220.00 | N | V | 13680.00 | N | V | 11480.00 | N |
| v | 0.53 | | v | 0.53 | | v | 0.53 | |
| V < | 52272.00 | N | V < | 64152.00 | N | V < | 52272.00 | N |
| h | 125.00 | mm | h | 150.00 | mm | h | 125.00 | mm |
| bw | 90.00 | mm | bw | 90.00 | mm | bw | 90.00 | mm |
| c | 15.00 | mm | c | 15.00 | mm | c | 15.00 | mm |
| d | 110.00 | mm | d | 135.00 | mm | d | 110.00 | mm |
| Ac | 11250.00 | mm2 | Ac | 13500.00 | mm2 | Ac | 11250.00 | mm2 |
| Crd,c | 0.12 | | Crd,c | 0.12 | | Crd,c | 0.12 | |
| k | 2.35 | < 2 | k | 2.22 | < 2 | k | 2.35 | < 2 |
| k | 2.00 | | k | 2.00 | | k | 2.00 | |
| v min | 0.54 | N/mm2 | v min | 0.54 | N/mm2 | v min | 0.54 | N/mm2 |
| Asl | 235.62 | mm2 | Asl | 235.62 | mm2 | Asl | 235.62 | mm2 |
| ρl | 0.02 | < 0.02 | ρl | 0.02 | < 0.02 | ρl | 0.02 | < 0.02 |
| σcp | 0.46 | N/mm2 | σcp | 0.85 | N/mm2 | σcp | 1.22 | N/mm2 |
| k1 | 0.15 | | k1 | 0.15 | | k1 | 0.15 | |
| V Rd, c, min | 6043.79 | N | V Rd, c, min | 8137.74 | N | V Rd, c, min | 7173.71 | N |
| V Rd, c | 10532.86 | N | V Rd, c | 12848.79 | N | V Rd, c | 11662.78 | N |
| UC | 0.40 | | UC | 1.06 | | UC | 0.98 | |

The calculations and the results of the local safety evaluation (unity check) are presented in table C3 and C4.

*Table C4. Local safety evaluation (unity checks (UC)) for the shear resistance without shear reinforcement.*

| EC2: design 1 | $V_{Rd,C,min}$ (kN) | $V_{Rd,C}$ (kN) | $V_E$ (kN) | UC (-) |
|---|---|---|---|---|
| Element 1 | 6.0 | 10.5 | 4.21 | 0.40 |
| Element 2 | 8.1 | 12.8 | 13.68 | 1.06 |
| Element 3 | 7.2 | 11.7 | 11.48 | 0.98 |

### Elements with shear reinforcement

Shear capacity for elements with shear reinforcement (NEN-EN 1992 -1-1, 2011)

$$V_{Rd,S} = \frac{A_{sw}}{s} z f_{ywd} \cot\theta \quad \text{(C.7a)}$$

and

$$V_{Rd,max} = \alpha_{cw} b_w z v \frac{f_{cd}}{\cot\theta + \tan\theta} \quad \text{(C.7b)}$$

where:

| | |
|---|---|
| $s$ | is the spacing of the stirrups; |
| $f_{ywd}$ | is the design yield strength of the shear reinforcement; |
| $v = 0.6\left[1 - \frac{f_{ck}}{250}\right]$ | is a strength reduction factor for concrete cracked in shear; |
| $\alpha_{cw} = 1 + \frac{\sigma_{cp}}{f_{cd}}$ | is a coeffiecient taking account of the state of stress in the compression chord (for $0 < \sigma_{cp} < 0.25\, f_{cd}$). |

*Table C5. Design 1: calculation shear resistance elements with shear reinforcement.*

| EC2: Elements with shear reinforcement | | | | | | | | |
|---|---|---|---|---|---|---|---|---|
| Element 1 | | | Element 2 | | | Element 3 | | |
| θ | 21.80 | | θ | 21.80 | | θ | 21.80 | |
| cot θ | 2.50 | | cot θ | 2.50 | | cot θ | 2.50 | |
| Asw | 3.53 | mm2 | Asw | 3.53 | mm2 | Asw | 3.53 | mm2 |
| s | 45.00 | mm | s | 45.00 | mm | s | 45.00 | mm |
| z | 99.00 | mm | z | 121.50 | mm | z | 99.00 | mm |
| α cw | 1.02 | | α cw | 1.04 | | α cw | 1.06 | |
| tan θ | 0.40 | | tan θ | 0.40 | | tan θ | 0.40 | |
| V Rd, max | 33181.27 | N | V Rd, max | 41509.36 | N | V Rd, max | 34415.55 | N |
| V Rd, s | 7043.05 | N | V Rd, s | 8643.75 | N | V Rd, s | 7043.05 | N |
| UC s | 0.60 | | UC | 1.58 | | UC | 1.63 | |
| Ucmax | 0.13 | | Ucmax | 0.33 | | Ucmax | 0.33 | |

The calculations and results of the local safety evaluation (unity check) are presented in table C5 and C6. According to this local safety evaluation element 2 and 3 does not have enough shear reinforcement, but according to the calculation for elements without shear reinforcement, this is not needed since $V_E < V_{Rd,C}$.

*Table C6. Local safety evaluation (unity checks (UC)) for the shear resistance with shear reinforcement.*

| EC2: design 1 | $V_{Rd,S}$ (kN) | $V_{Rd,max}$ (kN) | $V_E$ (kN) | UC (-) |
|---|---|---|---|---|
| Element 1 | 7.0 | 33.2 | 4.21 | 0.60 |
| Element 2 | 8.6 | 41.5 | 13.68 | 1.58 |
| Element 3 | 7.0 | 34.4 | 11.48 | 1.63 |

#### *C.1.2.3 Strut and tie model*

A detailed analysis of the detailing in the corner region should be performed by means of a strut and tie model. This could influence the structural resistance of the portal frame.

#### *C.1.2.4 Plastic analysis*

There is no reason to perform a plastic analysis for a portal frame which forms a plastic mechanism since the frame already has been collapsed due to a shear failure.

### C.1.3 Summary results portal frame design 1, 2 and 3

Portal frame design 1, 2 and 3 are provided with only the minimum required shear reinforcement and as a consequence the shear resistance is determined by $V_E = V_{Rd,C}$ since $V_{Rd,C} > V_{Rd,S}$.

All portal frame designs are supposed to resist a horizontal and vertical load of based on shear resistance of the portal frame designs:

$F_v = 18.8$ kN and $F_h = 15.7$ kN.

A detailed analysis of the corner region by means of a strut and tie model has not been performed. The bending moment resistance of the corners can have an influence on the structural resistance of the portal frame. This could possibly reduce the resistance of the portal frame.

The critical local safety evaluations for all portal frame designs where the shear resistance determines the structural resistance of the three portal frame designs are presented in chapter C.1.3.1.

#### *C.1.3.1 Shear resistance elements without shear reinforcement*

The local safety evaluation of the governing failure mode of portal frame design 1, 2 and 3 is presented in the table C7.

*Table C7. Local safety evaluation for the shear resistance without shear reinforcement.*

| Shear resistance | | | | |
|---|---|---|---|---|
| Design 1 | VRd,C,min (kN) | VRd,C (kN) | VE (kN) | UC (-) |
| Element 1 | 6.0 | 10.5 | 4.21 | 0.40 |
| Element 2 | 8.1 | 12.8 | 13.68 | 1.06 |
| Element 3 | 7.2 | 11.7 | 11.48 | 0.98 |
| Design 2 | VRd,C,min (kN) | VRd,C (kN) | VE (kN) | UC (-) |
| Element 1 | 6.0 | 11.2 | 4.21 | 0.4 |
| Element 2 | 8.1 | 13.6 | 13.68 | 1.0 |
| Element 3 | 7.2 | 12.3 | 11.48 | 0.9 |
| Design 3 | VRd,C,min (kN) | VRd,C (kN) | VE (kN) | UC (-) |
| Element 1 | 6.9 | 11.5 | 4.21 | 0.37 |
| Element 2 | 9.2 | 14.0 | 13.68 | 0.98 |
| Element 3 | 8.0 | 12.7 | 11.48 | 0.91 |

### *C.1.3.2 Bending moment resistance*

The bending moment resistance $M_{Rd}$ and the corresponding horizontal and vertical force $F_v$ and $F_h$, for a situation when there is no shear failure, is presented in table C8 and C9. This is only the case when enough shear reinforcement is used according to Eurocode 2.

*Table C8. Bending moment resistance portal frame design 1, 2 and 3.*

| EC2 | Design 1 | Design 2 | Design 3 |
|---|---|---|---|
| | $M_{Rd}$ (kNm) | $M_{Rd}$ (kNm) | $M_{Rd}$ (kNm) |
| Element 1 | 10.0 | 12.1 | 10.1 |
| Element 2 | 12.6 | 15.3 | 12.7 |
| Element 3 | 10.0 | 12.1 | 10.1 |

*Table C9. Design resistance according to the Eurocode 2 using a local safety approach.*

| EC2 | Design 1 | Design 2 | Design 3 |
|---|---|---|---|
| Fv (kN) | 18.8 | 28.1 | 19.2 |
| Fh (kN) | 15.7 | 15.7 | 15.7 |

## C.2 Local design resistance experiment Seraj et al. (1995)

### C.2.1 Determination of the internal forces (linear elastic calculation)

To perform a local safety evaluation the linear elastic moments, shear- and normal forces should be determined. The linear elastic calculations are performed with the software package Matrix Frame 5.3. The results are shown in figure C4.

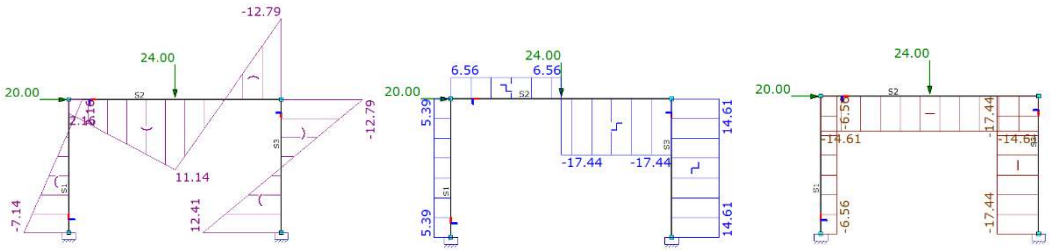


*Figure C4. Linear elastic moment, shear force and normal force diagram (kNm).*

The linear elastic moments, shear forces and normal forces in the sections A, B, C, D and E are also calculated with the Maple script below.

```
restart :
# Statically undetermined structure with 5 unkowns: Ma, Mb, Md, Me and
    theta (5 equations needed to solve):
External loads :
Fv := 24000 : Fh := 20000 :
# Not the real EI since the reinforcement is not included but it's only
    meant for the EI ratio between the columns and the beam
l1 := 1.725 : l2 := 2.743 : b := 90 : h1 := 250 : h2 := 300 : fm := 38 :
    Ec := fm / (1.75·10^-3) :
EI1 := evalf( (1/12)·(b/1000)·((h1/1000)^3) )·Ec :
EI2 := evalf( (1/12)·(b/1000)·((h2/1000)^3) )·Ec :
# Angle conditions (5 equations to solve the unkowns):
eq1 := phi_A = 0 :
eq2 := phi_B_AB = phi_B_BD :
eq3 := phi_D_BD = phi_D_DE :
eq4 := phi_E = 0 :
eq5 := Ma + Mb + Md + Me = Fh·l1 :
phi_A := + (1/3)·(Ma·l1/EI1) − (1/6)·(Mb·l1/EI1) − theta :
phi_B_AB := + (1/3)·(Mb·l1/EI1) − (1/6)·(Ma·l1/EI1) − theta :
phi_B_BD := − (1/3)·(Mb·l2/EI2) + (1/6)·(Md·l2/EI2) − (1/16)·(Fv·l2^2/EI2) :
phi_D_BD := − (1/3)·(Md·l2/EI2) + (1/6)·(Mb·l2/EI2) + (1/16)·(Fv·l2^2/EI2) :
phi_D_DE := + (1/3)·(Md·l1/EI1) − (1/6)·(Me·l1/EI1) − theta :
phi_E := + (1/3)·(Me·l1/EI1) − (1/6)·(Md·l1/EI1) − theta :
sol := solve([eq1, eq2, eq3, eq4, eq5], [Ma, Mb, Md, Me, theta]) :
assign(sol) :
```

```
# Moments:
M[A] := Ma; M[B] := Mb; M[C] := −(−Mb + Md)/2 + (1/4)·Fv·l2;
M[D] := Md; M[E] := Me;
                    M_A := 7105.957394
                    M_B := 2146.163714
                    M_C := 11126.08074
                    M_D := 12810.00224
                    M_E := 12437.87666
# Shear forces:
V[AB] := (M[A] + M[B])/l1; V[BC] := (M[C] − M[B])/((1/2)·l2);
V[CD] := (M[C] + M[D])/((1/2)·l2); V[DE] := (M[D] + M[E])/l1;
                    V_AB := 5363.548468
                    V_BC := 6547.515148
                    V_CD := 17452.48486
                    V_DE := 14636.45154
# Normal forces:
N[AB] := R_A_V; N[BD] := Fh − V[AB]; N[DE] := R_E_V;
                    N_AB := 6547.515148
                    N_BD := 14636.45153
                    N_DE := 17452.48485
```

*Figure C5. Linear elastic calculation critical moment, shear force and normal force distribution*

The governing moment, shear force and normal force are presented in table C10.

*Table C10. Critical moment, shear force and normal force for element 1, 2 and 3.*

| | $M_E$ (kNm) | $V_E$ (kN) | $N_E$ (kN) |
|---|---|---|---|
| Element 1 | 7.1 | 5.4 | 6.6 |
| Element 2 | 12.8 | 17.4 | 14.6 |
| Element 3 | 12.8 | 14.6 | 17.4 |

## C.2.2 Determination of the resistance

### *C.2.2.1 Bending moment resistance (ULS)*

The design bending moment resistance according to Eurocode 2 is determined with formulas (C.1) to (C.4). The results are presented in the table below.

*Table C11. Design bending moment capacity (EC2).*

| EC2 | $M_{Rd}$ (kNm) | $M_E$ (kNm) | UC (-) |
|---|---|---|---|
| Element 1 | 10.0 | 7.1 | 0.71 |
| Element 2 | 12.6 | 12.8 | 1.02 |
| Element 3 | 10.0 | 12.8 | 1.28 |

The mean bending moment resistance is determined with formulas (C.1) to (C.4), where the design material values are replaced with mean material values. The results are presented in the table below.

*Table C12. Mean bending moment capacity.*

| Mean | $M_{Rm}$ (kNm) | $M_E$ (kNm) | UC (-) |
|---|---|---|---|
| Element 1 | 12.9 | 7.1 | 0.55 |
| Element 2 | 16.2 | 12.8 | 0.79 |
| Element 3 | 12.9 | 12.8 | 0.99 |

### *C.2.2.2 Shear resistance (ULS)*

The general check for the shear resistance is defined as (NEN-EN 1992 -1-1, 2011): $V_E < V_{Rd,C}$, for elements without shear reinforcement, otherwise: $V_E < V_{Rd,S}$.

#### Elements without shear reinforcement

The design shear resistance according to Eurocode 2 is determined with equation (C.6). The calculations are presented in table C13 and summarized in table C14.

*Table C13. Calculation shear resistance elements without shear reinforcement.*

| EC2: Elements without shear reinforcement | | | | | | | | |
|---|---|---|---|---|---|---|---|---|
| Element 1 | | | Element 2 | | | Element 3 | | |
| VEd | 5363.50 | N | VEd | 17452.50 | N | VEd | 14635.50 | N |
| v | 0.53 | | v | 0.53 | | v | 0.53 | |
| V < | 52272.00 | N | V < | 64152.00 | N | V < | 52272.00 | N |
| h | 125.00 | mm | h | 150.00 | mm | h | 125.00 | mm |
| bw | 90.00 | mm | bw | 90.00 | mm | bw | 90.00 | mm |
| c | 15.00 | mm | c | 15.00 | mm | c | 15.00 | mm |
| d | 110.00 | mm | d | 135.00 | mm | d | 110.00 | mm |
| Ac | 11250.00 | mm2 | Ac | 13500.00 | mm2 | Ac | 11250.00 | mm2 |
| Crd,c | 0.12 | | Crd,c | 0.12 | | Crd,c | 0.12 | |
| k | 2.35 | < 2 | k | 2.22 | < 2 | k | 2.35 | < 2 |
| k | 2.00 | | k | 2.00 | | k | 2.00 | |
| v min | 0.54 | N/mm2 | v min | 0.54 | N/mm2 | v min | 0.54 | N/mm2 |
| Asl | 235.62 | mm2 | Asl | 235.62 | mm2 | Asl | 235.62 | mm2 |
| ρl | 0.02 | < 0.02 | ρl | 0.02 | < 0.02 | ρl | 0.02 | < 0.02 |
| σcp | 0.58 | N/mm2 | σcp | 1.08 | N/mm2 | σcp | 1.55 | N/mm2 |
| k1 | 0.15 | | k1 | 0.15 | | k1 | 0.15 | |
| V Rd, c, min | 6232.22 | N | V Rd, c, min | 8563.87 | N | V Rd, c, min | 7671.68 | N |
| V Rd, c | 10721.29 | N | V Rd, c | 14412.07 | N | V Rd, c | 12160.75 | N |
| UC | 0.50 | | UC | 1.21 | | UC | 1.20 | |

*Table C14. Design shear capacity without shear reinforcement (EC2).*

| EC2 | $V_{Rd,C,min}$ (kN) | $V_{Rd,C}$ (kN) | $V_E$ (kN) | UC (-) |
|---|---|---|---|---|
| Element 1 | 6.2 | 10.7 | 5.36 | 0.50 |
| Element 2 | 8.6 | 13.3 | 17.45 | 1.21 |
| Element 3 | 7.7 | 12.2 | 14.64 | 1.20 |

The mean shear capacity $V_{Rm,C}$ and the minimum mean shear resistance $V_{Rm,C,min}$ can be determined by using equation (C.6) and set the partial safety factor to $\gamma_c = 1.0$. The results are given in table C15. All unity checks are below zero. This indicates that no shear reinforcement is needed when there is no deviation from the mean value.

*Table C15. Mean shear capacity without shear reinforcement.*

| Mean | $V_{Rm,C,min}$ (kN) | $V_{Rm,C}$ (kN) | $V_E$ (kN) | UC (-) |
|---|---|---|---|---|
| Element 1 | 6.9 | 15.6 | 5.36 | 0.34 |
| Element 2 | 9.4 | 18.9 | 17.45 | 0.92 |
| Element 3 | 8.3 | 17.1 | 14.64 | 0.86 |

## Elements with shear reinforcement

The design resistance of elements with shear reinforcement according to the Eurocode 2 is determined with equation (C.7). The calculations are presented in table C16 and the results are summarized in table C17.

*Table C16. Calculation shear resistance elements with shear reinforcement.*

| EC2: Elements with shear reinforcement | | | | | | | | |
|---|---|---|---|---|---|---|---|---|
| Element 1 | | | Element 2 | | | Element 3 | | |
| θ | 21.80 | | θ | 21.80 | | θ | 21.80 | |
| cot θ | 2.50 | | cot θ | 2.50 | | cot θ | 2.50 | |
| Asw | 3.53 | mm2 | Asw | 3.53 | mm2 | Asw | 3.53 | mm2 |
| s | 45.00 | mm | s | 45.00 | mm | s | 45.00 | mm |
| z | 99.00 | mm | z | 121.50 | mm | z | 99.00 | mm |
| α cw | 1.03 | | α cw | 1.05 | | α cw | 1.08 | |
| tan θ | 0.40 | | tan θ | 0.40 | | tan θ | 0.40 | |
| V Rd, max | 33387.11 | N | V Rd, max | 41974.84 | N | V Rd, max | 34959.51 | N |
| V Rd, s | 7043.05 | N | V Rd, s | 8643.75 | N | V Rd, s | 7043.05 | N |
| UC s | 0.76 | | UC s | 2.02 | | UC s | 2.08 | |
| Ucmax | 0.16 | Ucmax | Ucmax | 0.42 | | Ucmax | 0.42 | |

*Table C17. Design shear resistance with shear reinforcement (EC2).*

| EC2 | $V_{Rd,S}$ (kN) | $V_{Rd,max}$ (kN) | $V_E$ (kN) | UC (-) |
|---|---|---|---|---|
| Element 1 | 7.0 | 33.4 | 5.36 | 0.76 |
| Element 2 | 8.6 | 42.0 | 17.45 | 2.02 |
| Element 3 | 7.0 | 35.0 | 14.64 | 2.08 |

The mean shear resistance is not calculated since the mean shear capacity for element without shear reinforcement is sufficient.

#### *C.2.2.3 Strut and tie model*

A detailed analysis of the detailing in the corner region should be performed by means of a strut and tie model. This could influence the structural resistance of the portal frame.

#### *C.2.2.4 Plastic analysis*

A plastic analysis is not performed since it is unsure if the corner has enough rotational capacity to form a plastic hinge. Experimental results show earlier corner failure, which means that there is not enough rotational capacity.

# Appendix D Non-linear Finite element models

## D.1 Geometry mesh

The reinforced concrete frame is modelled with 4 plane stress elements over the height (4 e.o.h.) and embedded reinforcement. There is chosen for 4 e.o.h. while the Guidelines for NLFE analyses (Hendriks, de Boer, & Belletti, 2017) suggest that at least 6 e.o.h. should be used. The reason for this deviation is a reduction of the computational time and stress concentration in the corner D (Appendix E.2.4).

There is chosen for a two dimensional model, since the frame is very slender and three dimensional effects can be neglected. The geometry, mesh and reinforcement detailing will be presented in the next chapters. The boundary conditions are shown in figure D1. The columns have fixed translations in the x, y direction and a fixed rotation around the z-axis.

### D.1.1 Portal frame design 1, 2 and 3

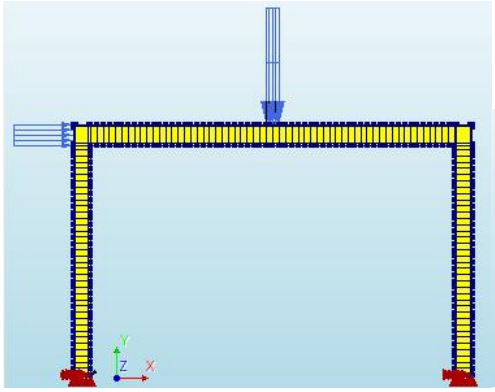

*Figure D1. Geometry, reinforcement and applied load safety format.*

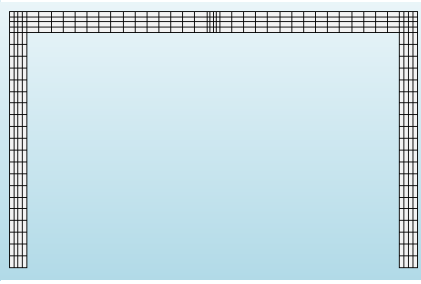

*Figure D2. Mesh concrete (plane stress elements).*

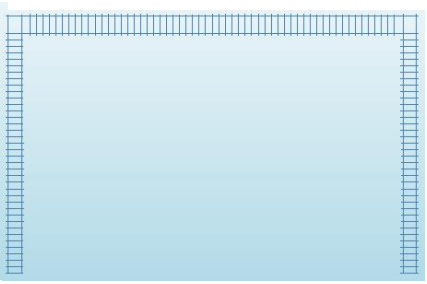

*Figure D3. Mesh embedded reinforcement (bar elements).*

### D.1.2 Experiment Seraj et al. (1995)

#### *D.1.2.1 PF1*

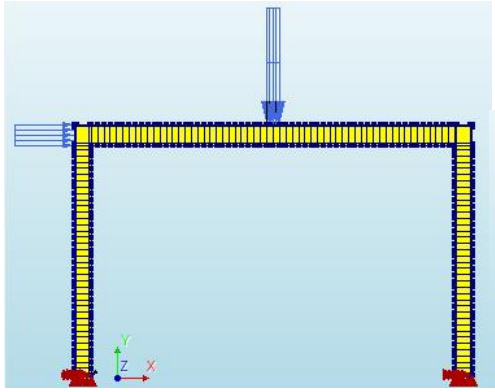

*Figure D4. Geometry, reinforcement and applied load PF1.*

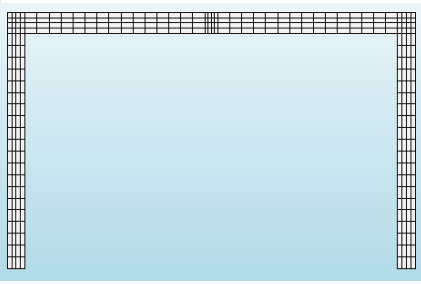

*Figure D5. Mesh concrete (plane stress elements).*

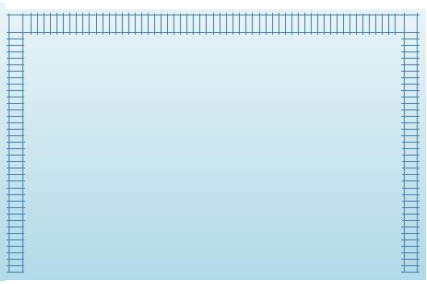

*Figure D6. Mesh embedded reinforcement (bar elements).*

### *D.1.2.2 PF2*

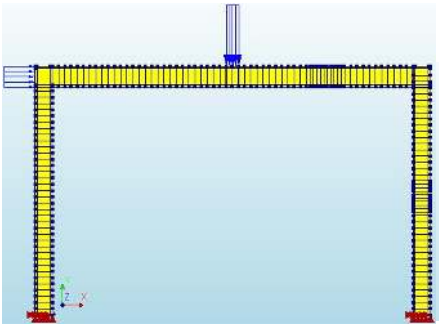

*Figure D7. Geometry, reinforcement and applied load PF2.*

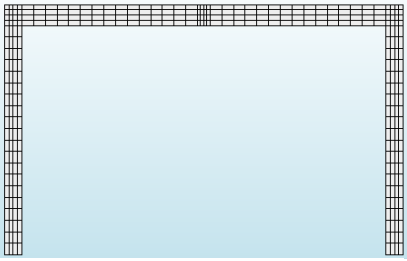

*Figure D8. Mesh concrete (plane stress elements).*

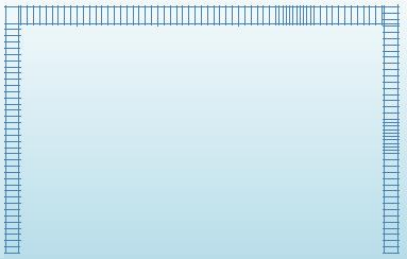

*Figure D9. Mesh embedded reinforcement (bar elements).*

## D.2 NLFE models

All NLFE models are in accordance with the Guidelines for Non-Linear Finite Element Analysis of concrete Structures (Hendriks, de Boer, & Belletti, 2017). The element types, constitutive models used in the NLFE models are shown in table D1 and D2. The convergence norm applied in the model is a combination of a force and energy norm. The convergence tolerance for the force and energy norm is 0.01 and 0.001, respectively.

*Table D1. Concrete: element type and constitutive model used in Diana FEA 10.1.*

| Concrete | |
|---|---|
| Finite Element | |
| Element type | plane stress element CQ16M |
| Interpolation scheme | Quadratic |
| Integration scheme | Full (2x2 point Gauss) |
| Constitutive Modelling | |
| Model | Total strain based fixed crack model |
| Crack orientation | Fixed |
| Crack bandwidth specification | Rots |
| Shear behaviour | Constant |
| Shear retention | 0.1 |
| Tensile behavior | Exponential softening |
| Poisson's ratio reduction | Damaged based |
| Compressive behavior | Parabolic |
| Reduction due to lateral cracking | Vecchio and Collins 1993 |
| Lower bound reduction curve | 0 |
| Stress confinement model | Selby and Vecchio |

*Table D2. Reinforcement steel: element type and constitutive model used in Diana FEA 10.1.*

| Reinforcement Steel | |
|---|---|
| Finite Element | |
| Embedded reinforcement | Bar element |
| Constitutive Modelling | |
| Model | Elastic plastic model with hardening |
| Plastic hardening | Plastic strain-yield stress |
| Hardening hypotheses | Strain hardening |
| Hardening type | Isotropic hardening |

## D.3 Load path

The loading path is different for each NLFE model and will be presented in the tables below.

### D.3.1 Portal frame design 1, 2 and 3

First the load determined according to the local design resistance, $F_v = 18.8$ kN and $F_h = 15.7$ kN is applied on the structure. After that the vertical load will increased till failure of the portal frame. In this way the additional 'hidden' capacity of a portal frame design is found. The loading order is presented in table D3. First the vertical load $F_v$ is applied on the structure, subsequently the horizontal load $F_h$ is applied and finally the vertical load $F_h$ is increased till failure of the portal frame. The load is applied in load-steps, which represents the percentage of the total load (see table D3).

*Table D3. Load path safety format.*

| Load path safety formats | | | | |
|---|---|---|---|---|
| Equilibrium Iteration | Maximum number of iterations | Load-steps | Line search | Load combination |
| Regular NR | 800 | 0.1(10) | yes | Fv = 18.8 kN |
| Regular NR | 800 | 0.05(20) | yes | Fh = 15.7 kN |
| Secant (Quasi-Newton) | 1000 | 0.01(1000)<br>Till failure | yes | Fv = 10.0 kN |

### D.3.2 Experiment Seraj et al. (1995)

The derivation of the load path that is used in the NLFE model for PF1 and PF2 is described in chapter 5.3.2. The loading order is presented in the tables D4 and D5.

#### *D.3.2.1 Portal frame 1 (PF1)*

*Table D4. Load path PF1.*

| PF1 | | | | |
|---|---|---|---|---|
| Equilibrium Iteration | Maximum number of iterations | Load-steps | Line search | Load combination |
| Regular NR | 400 | 0.1(10) | yes | Fv = 24 kN |
| Regular NR | 800 | 0.05(15) | yes | Fh = 20 kN |
| Secant (Quasi-Newton) | 1000 | 0.05(4)<br>0.01(100)<br>Till failure | yes | Fv = 20 kN<br>Fh (sway) = 18 kN |

#### *D.3.2.2 Portal frame 2 (PF2)*

*Table D5. Load path PF2.*

| PF2 | | | | |
|---|---|---|---|---|
| Equilibrium Iteration | Maximum number of iterations | Load-steps | Line search | Load combination |
| Regular NR | 400 | 0.1(10) | yes | Fv = 24 kN |
| Regular NR | 800 | 0.05(15) | yes | Fh = 20 kN |
| Secant (Quasi-Newton) | 1000 | 0.05(4)<br>0.01(100)<br>Till failure | yes | Fv = 20 kN<br>Fh (sway) = 40 kN |

# Appendix E Experiment Seraj et al. (1995)

## E.1 Experimental Results

### E.1.1 Load carrying capacity

The collapse load of PF1 and PF2 can be found in table E1. The total vertical load carrying capacity is the sum of the applied vertical load and the additional vertical load due to the sway effect. The total horizontal load is the measured horizontal load during the experiment.

*Table E1. Total load carrying capacity PF1 and PF2 from experiment (Seraj, Kotsovos, & Pavlovic, 1995).*

| Results experiment | | | |
|---|---|---|---|
| Design | Fv (kN) | Fh (kN) | Failure mode |
| PF1 | 28.5 | 20 | Partially corner D failure and three plastic hinges |
| PF2 | 33.68 | 19.95 | Partially corner D failure and three plastic hinges |

The results of the experiment are shown in figure E1.

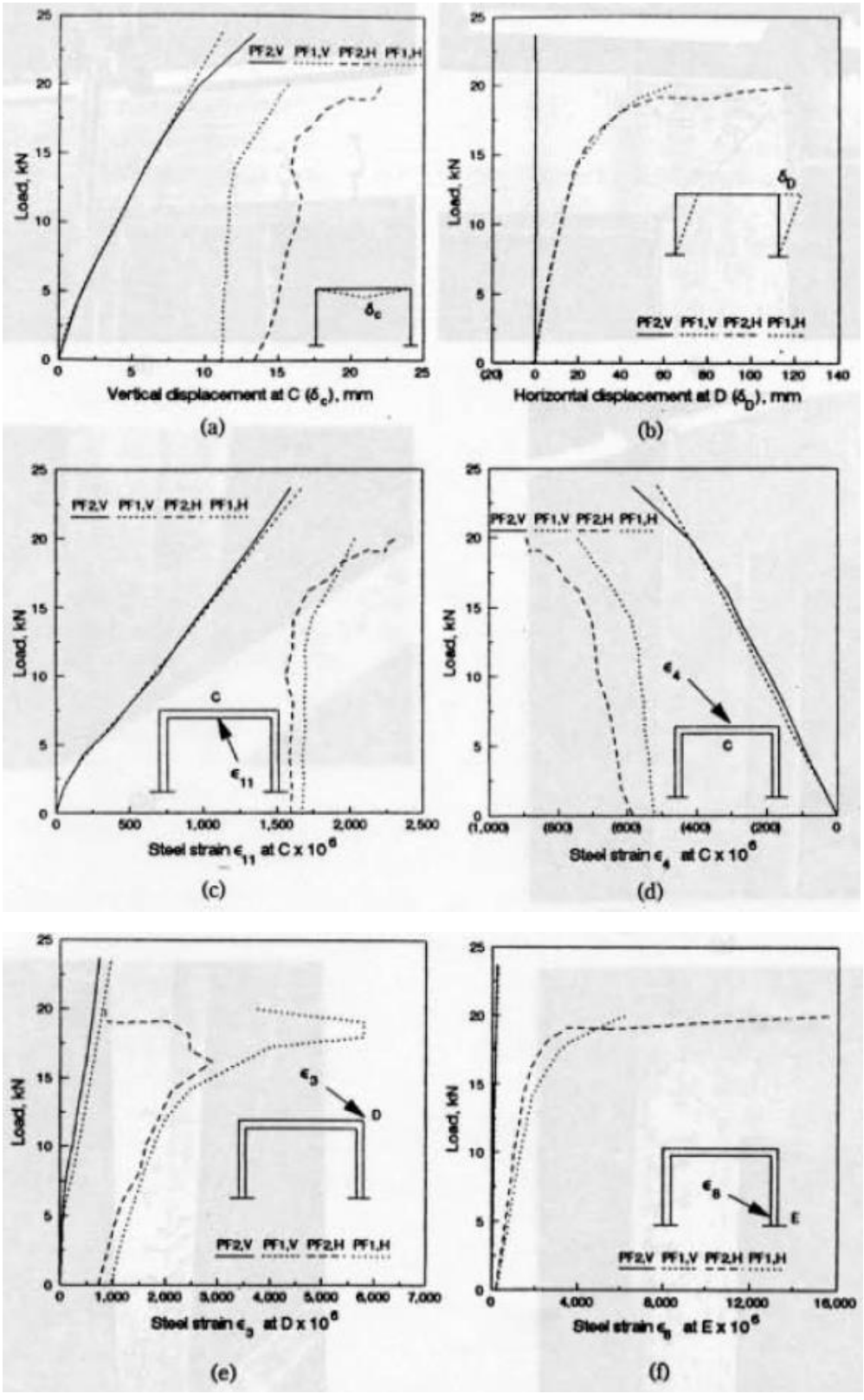


*Figure E1. Load versus, vertical displacement (a), horizontal displacement (b), steel strain ϵ11 (c), steel strain ϵ 4 (d), steel strain ϵ3 (e) and steel strain ϵ8 (e) due to vertical loading Fv and combined vertical Fv,sway and horizontal loading Fh. (Seraj, Kotsovos, & Pavlovic, 1995).*

### E.1.2 Crack pattern PF1 and PF2 (Seraj, Kotsovos, & Pavlovic, 1995)

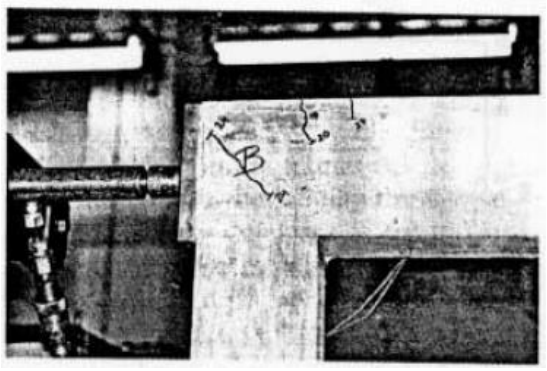


*Figure E2. PF1 and PF2: location B.*

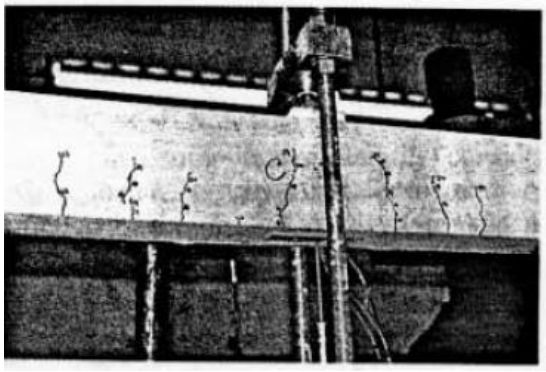


*Figure E3. PF1 and PF2: location C.*


*Figure E4. PF1: location D.*


*Figure E5. PF2: location D.*

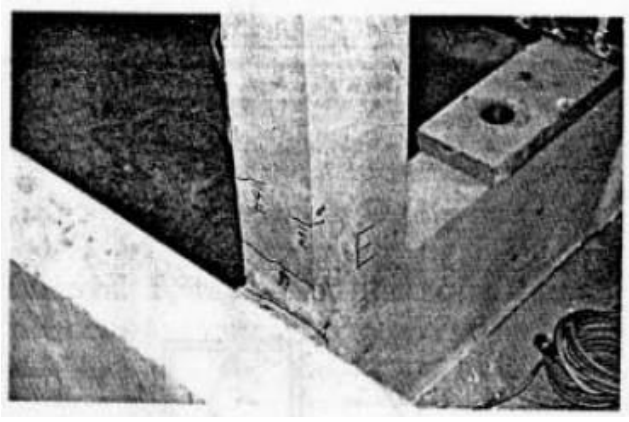


*Figure E6. PF1: location E.*

*Figure E7. PF2: location E.*

## E.2 Results NLFE analyses experiment Seraj et al. (1995)

### E.2.1 Vertical and horizontal deformation experiment PF1 and PF2

The vertical and horizontal deformation of PF1 and PF2 resulting from the experiment are shown in the figures below.

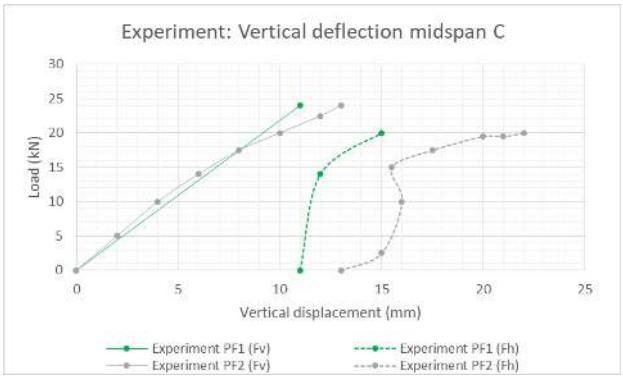


*Figure E8. Vertical deflection experiment (Seraj, Kotsovos, & Pavlovic, 1995).*

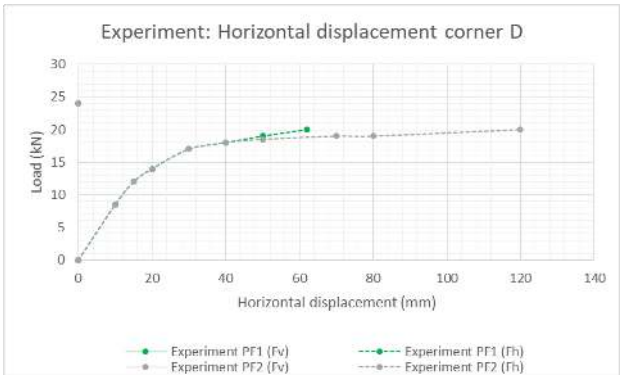


*Figure E9. Horizontal displacement experiment (Seraj, Kotsovos, & Pavlovic, 1995).*

### E.2.2 Vertical and horizontal deformation NLFE analyses PF1 and PF2

The results of the NLFE analyses for PF1 and PF2 are shown in the figures below.

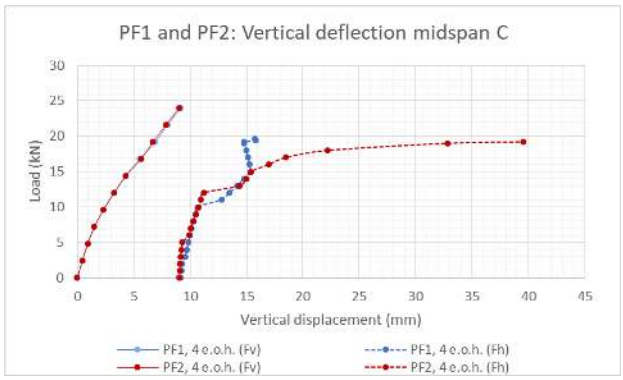


*Figure E10. Vertical deflection FF1 and PF2.*

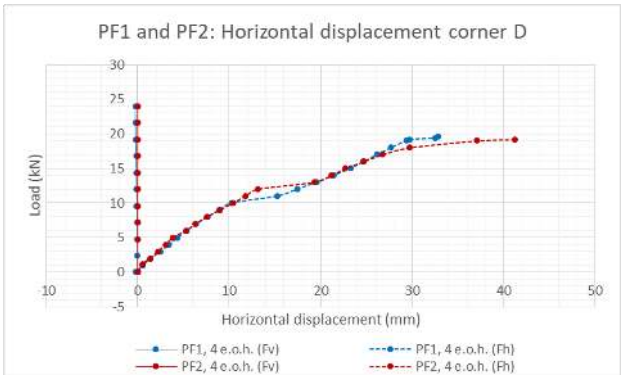


*Figure E11. Horizontal displacement FF1 and PF2.*

### E.2.3 Results PF1 and PF2 and experiment (Seraj, Kotsovos, & Pavlovic, 1995)

The results of the experiment (Seraj, Kotsovos, & Pavlovic, 1995) and the NLFE analysis are shown in the graphs below. The graphs show the comparison for PF1 and PF2 on the left and right side, respectively. The straight lines shows the displacement or strain due to the vertical load and the dashed lines shows the displacement or strain due to the horizontal load. The stiffness of the non-linear finite element model differs from the experimental results. This results in a different initial displacement or strain (caused by the vertical load) of the NLFE analysis and the experimental results when the horizontal load is applied.

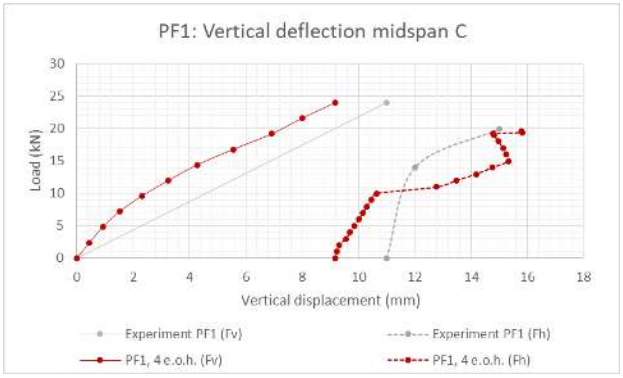


*Figure E12. PF1: vertical deflection C.*

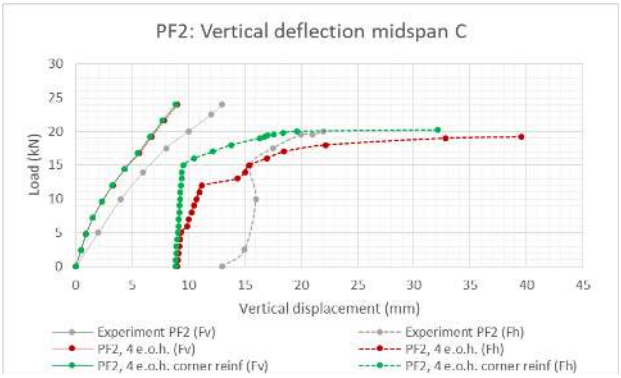


*Figure E13. PF2: vertical deflection C.*

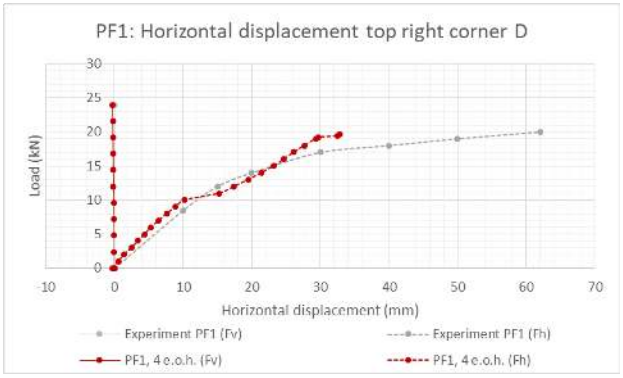


*Figure E14. PF1: horizontal displacement D.*

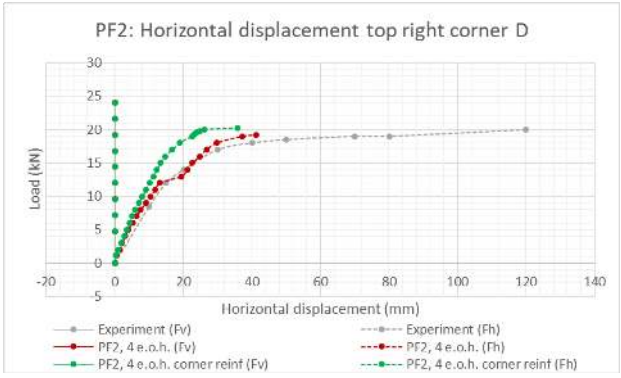


*Figure E15. PF2: horizontal displacement D.*

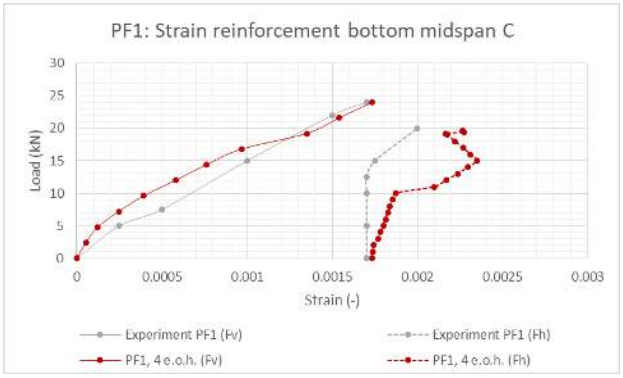


*Figure E16. PF1: bottom strain reinforcement C.*

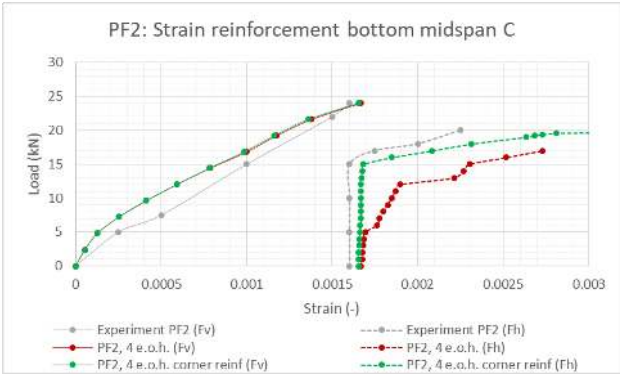


*Figure E17. PF2: bottom strain reinforcement C.*

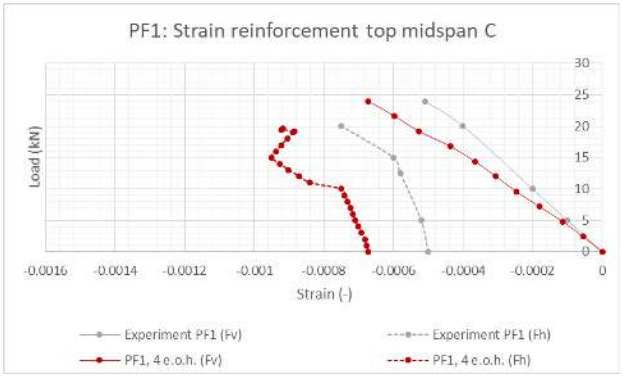


*Figure E18. PF1: top strain reinforcement C.*

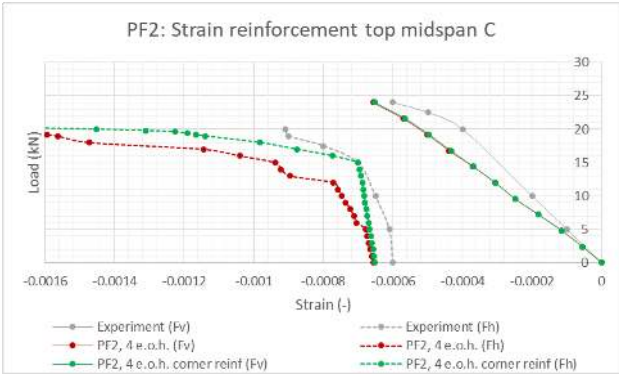


*Figure E19. PF2: top strain reinforcement C.*

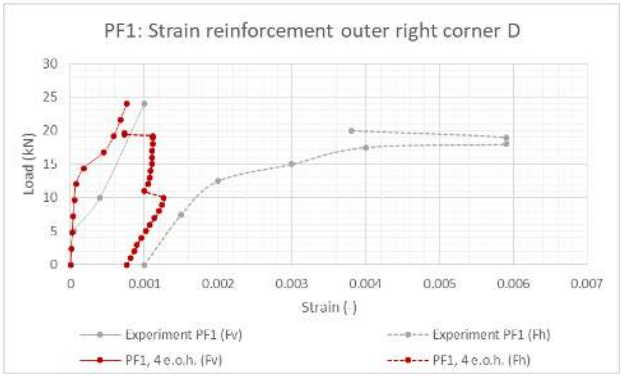


*Figure E20. PF1: strain reinforcement outer right corner D.*

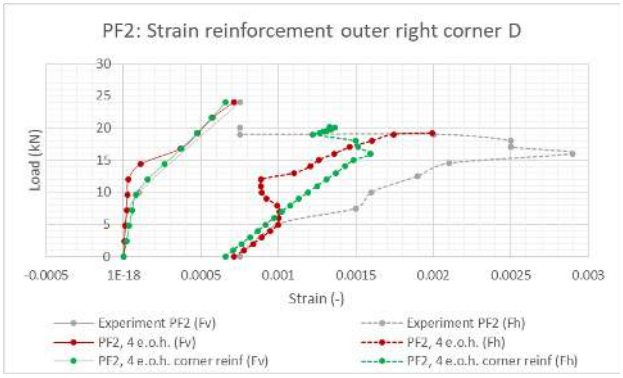


*Figure E21. PF2: strain reinforcement outer right corner D.*

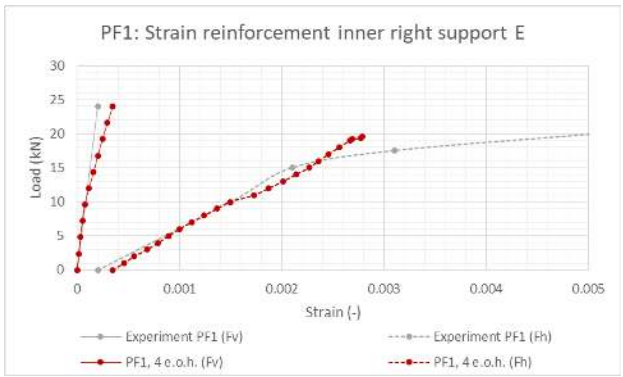


*Figure E22. PF1: strain reinforcement inner right support E.*

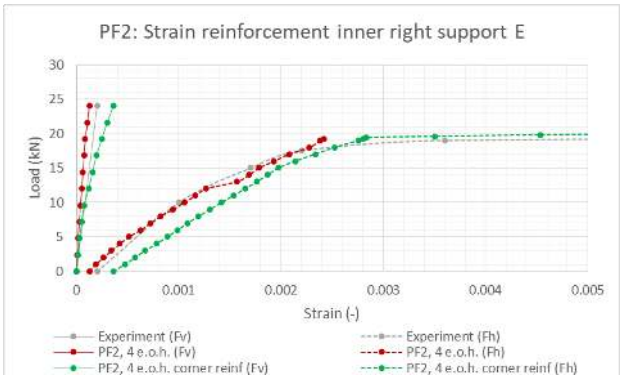


*Figure E23. PF2: strain reinforcement inner right support E.*

### E.2.4 Mesh refinement

The results of a coarse and a fine mesh for PF2 are given in the graphs below. The number of elements over the height of the beam is 4 (4 e.o.h.) and 6 (6 e.o.h.) for the coarse and the fine mesh, respectively. The coarse mesh leads to a loading capacity closer to the experimental results (table E1). Also the computational time is less, which is an important criterion since many NLFE analyses have to be performed in order to do a safety assessment.

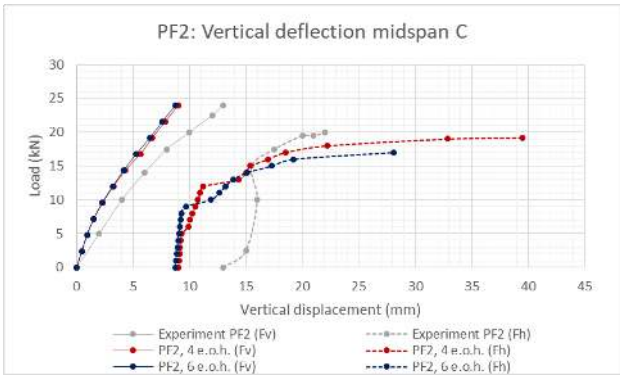


*Figure E24. PF2: vertical deflection C (coarse and fine mesh).*

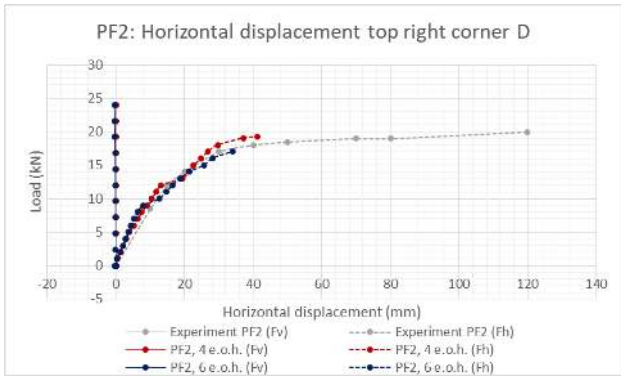


*Figure E25. PF2: horizontal displacement D (coarse and fine mesh).*

The fine mesh leads to earlier corner failure since the stress concentration will be higher. This is shown in figure E24 and E25 where a jump in the graph is visible for $F_h = 12$ kN and $F_h = 9$ kN for

the coarse and the fine mesh, respectively. Even if a corner radius (minimum corner radius is 4ϕ (NEN-EN 1992 -1-1, 2011)) is applied for the fine mesh. The results are shown below.

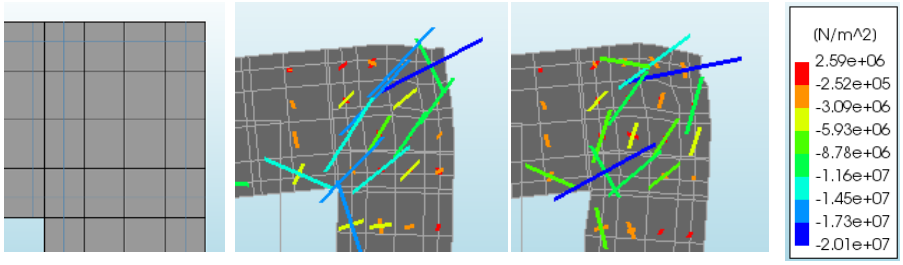


*Figure E26. Coarse mesh: Left: mesh and reinforcement, middle: before partial failure (load-factor 0.5) and right: after partial failure (load-factor 0.55)*

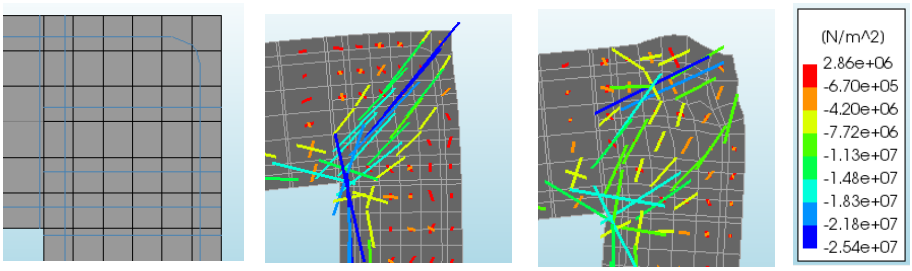


*Figure E27. Coarse mesh: Left: mesh and reinforcement with minimum corner radius 4φ, middle: before partial failure (load-factor 0.4) and right: after partial failure (load-factor 0.5)*

For the total load carrying capacity it is not needed to make a very accurate model of the corner. This could be done in a detailed analyses but that is not the scope of this thesis. Since the design of a corner with a finer mesh performs only worse and the computational time is higher, there is chosen for a coarse mesh with 4 e.o.h.

*Table E2. Results experiment PF2 and NLFE analyses: coarse and fine mesh.*

| Results NLFE analyses (4 e.o.h. and 6 e.o.h.) and PF2 (experiment) | | |
|---|---|---|
| | Fv (N) | Fh (N) |
| PF2 (experiment) | 33680 | 19950 |
| NLFE analysis (4 e.o.h.) | 23400 | 19200 |
| NLFE analysis (6 e.o.h.) | 28000 | 17000 |

# Appendix F Transformation to standard normal variables

## F.1 Correlation matrix concrete and reinforcement steel

According to chapter 2.5.2 the correlated lognormal variables can be transformed to correlated normal distributed variables $\boldsymbol{X}$ with the mean $\boldsymbol{\mu_L}$ and the standard deviation $\boldsymbol{\sigma_L}$.

*Table F1. Transformation to normal correlated variables.*

| Concrete and reinforcement steel | | | | | |
|---|---|---|---|---|---|
| Variable | fc (MPa) | fct (MPa) | Ec (MPa) | Gf (Nmm/mm2) | fy,l (MPa) |
| μ | 38.00 | 2.87 | 33550.60 | 140.50 | 560.00 |
| σ | 5.70 | 0.43 | 5703.60 | 28.10 | 28.00 |
| Distribution | LN | LN | LN | LN | LN |
| μL | 3.63 | 1.04 | 10.41 | 4.93 | 6.33 |
| σL | 0.15 | 0.15 | 0.17 | 0.20 | 0.05 |
| Distribution | N | N | N | N | N |

After that the correlated normally distributed variables $\boldsymbol{X}$ can be transformed to uncorrelated standard normally distributed variables $\boldsymbol{U}$ using a transformation matrix $\boldsymbol{T}$. The matrix $\boldsymbol{T}$ is found using Cholesky decomposition of the correlation matrix $\boldsymbol{\rho} = \boldsymbol{T}\boldsymbol{T}^T$. Matrix $\boldsymbol{T}$ is found with the following Maple script:

```
rho := Matrix([[1, 0.932, 0.772, 0.714, 0, 0], [0.932, 1, 0.684, 0.8, 0, 0], [0.772, 0.684, 1, 0.657, 0, 0], [0.714, 0.8, 0.657, 1, 0, 0], [0, 0, 0, 0, 1, 0], [0, 0, 0, 0, 0, 1]]);

T := Matrix(n) :
s1 := 0 : s2 := 0 :
for k from 1 to n do
for i from 1 to n do


if i = k then

for j from 1 to (k − 1) do
s1 := T[k, j]^2 + s1;
end do;
T[k, i] := sqrt(rho[k, k] − s1);
s1 := 0;

elif k ≥ i then

for j from 1 to (i − 1) do

s2 := T[i, j]·T[k, j] + s2;

end do;

T[k, i] := (rho[k, i] − s2)/T[i, i];
s2 := 0;


else
T[i, j] := 0;

end if

end do
end do
T := T;
```

*Figure F1. Maple script: Cholesky decomposition*

$$\boldsymbol{\rho} = \begin{bmatrix} 1 & 0.932 & 0.772 & 0.714 & 0 \\ 0.932 & 1 & 0.684 & 0.8 & 0 \\ 0.772 & 0.684 & 1 & 0.657 & 0 \\ 0.714 & 0.8 & 0.657 & 1 & 0 \\ 0 & 0 & 0 & 0 & 1 \end{bmatrix}$$

$$\boldsymbol{T} = \begin{bmatrix} 1 & 0 & 0 & 0 & 0 \\ 0.932 & 0.362 & 0 & 0 & 0 \\ 0.772 & -0.098 & 0.628 & 0 & 0 \\ 0.714 & 0.371 & 0.226 & 0.549 & 0 \\ 0 & 0 & 0 & 0 & 1 \end{bmatrix}$$

$$\boldsymbol{D} = \begin{bmatrix} \sigma_{L,1} & 0 & 0 & 0 & 0 \\ 0 & \sigma_{L,2} & 0 & 0 & 0 \\ 0 & 0 & \sigma_{L,3} & 0 & 0 \\ 0 & 0 & 0 & \sigma_{L,4} & 0 \\ 0 & 0 & 0 & 0 & \sigma_{L,5} \end{bmatrix}$$

The transformation from the correlated normally distributed variables $\boldsymbol{X}$ to the uncorrelated standard normally distributed variables $\boldsymbol{U}$ can be expressed as:

$$\boldsymbol{X} = \boldsymbol{\mu_L} + \boldsymbol{DTU}$$

$$\begin{bmatrix} X_{f_c} \\ X_{f_{ct}} \\ X_{E_c} \\ X_{G_f} \\ X_{f_{y,l}} \end{bmatrix} = \begin{bmatrix} \mu_{L,f_c} \\ \mu_{L,f_{ct}} \\ \mu_{L,E_c} \\ \mu_{L,G_f} \\ \mu_{L,f_{y,l}} \end{bmatrix} + \begin{bmatrix} U_{f_c}\,\sigma_{L,f_c} \\ (0.932\,U_{f_c} + 0.362\,U_{f_{ct}})\,\sigma_{L,f_{ct}} \\ (0.772\,U_{f_c} - 0.098\,U_{f_{ct}} + 0.628\,U_{E_c})\,\sigma_{L,E_c} \\ (0.714\,U_{f_c} + 0.371\,U_{f_{ct}} + 0.226\,U_{E_c} + 0.549\,U_{G_f})\,\sigma_{L,G_f} \\ U_{f_{y,l}}\,\sigma_{L,F_{y,l}} \end{bmatrix} \quad \text{(F.1)}$$

## F.2 Full correlation between concrete properties

The correlation matrix for concrete and reinforcement when full correlation between the concrete properties is assumed is:

$$\boldsymbol{\rho} = \begin{bmatrix} 1 & 1 & 1 & 1 & 1 & 0 \\ 1 & 1 & 1 & 1 & 1 & 0 \\ 1 & 1 & 1 & 1 & 1 & 0 \\ 1 & 1 & 1 & 1 & 1 & 0 \\ 1 & 1 & 1 & 1 & 1 & 0 \\ 0 & 0 & 0 & 0 & 0 & 1 \end{bmatrix}.$$

Cholesky decomposition is not possible since the matrix $\boldsymbol{\rho}$ is not positive definitive but it is easy to see that $\boldsymbol{\rho} = \boldsymbol{TT}^T$ leads to the following transformation Matrix:

$$\boldsymbol{T} = \begin{bmatrix} 1 & 0 & 0 & 0 & 0 & 0 \\ 1 & 0 & 0 & 0 & 0 & 0 \\ 1 & 0 & 0 & 0 & 0 & 0 \\ 1 & 0 & 0 & 0 & 0 & 0 \\ 1 & 0 & 0 & 0 & 0 & 0 \\ 0 & 0 & 0 & 0 & 0 & 1 \end{bmatrix}.$$

The $\boldsymbol{D}$ matrix with only the standard deviation on the diagonal terms. The transformation from the correlated normally distributed variables $\boldsymbol{X}$ to the uncorrelated standard normally distributed variables $\boldsymbol{U}$ is again expressed as:

$$\boldsymbol{X} = \boldsymbol{\mu_L} + \boldsymbol{DTU}$$

$$\begin{bmatrix} X_{f_c} \\ X_{f_{ct}} \\ X_{E_c} \\ X_{G_f} \\ X_{G_c} \\ X_{f_{y,l}} \end{bmatrix} = \begin{bmatrix} \mu_{L,f_c} \\ \mu_{L,f_{ct}} \\ \mu_{L,E_c} \\ \mu_{L,G_f} \\ \mu_{L,G_c} \\ \mu_{L,f_{y,l}} \end{bmatrix} + \begin{bmatrix} U_{f_c}\,\sigma_{L,f_c} \\ U_{f_c}\,\sigma_{L,f_{ct}} \\ U_{f_c}\,\sigma_{L,E_c} \\ U_{f_c}\,\sigma_{L,G_f} \\ U_{f_c}\,\sigma_{L,G_c} \\ U_{f_{y,l}}\,\sigma_{L,f_{y,l}} \end{bmatrix} \quad \text{(F.2)}$$

# Appendix G Level II Reliability Method: Global Safety evaluation

## G.1 Case 1: rotational capacity corner D without geometrical reinforcement uncertainty

The global safety assessment of portal frame design 1, 2 and 3 is performed and extensively discussed below.

### G.1.1 Design 1

The safety format with the highest global design resistance, i.e. highest probability of failure, for design 1 is the ECOV method. The global design resistance according to the ECOV method is: $R_{SF} = 36.1$ kN. This leads to the following implicit LSF:

$$G(\boldsymbol{X}) = R(\boldsymbol{X}) - 36.1.$$

The response surface is constructed according to the approach of Zhao and Qiu (2013). The theory of the method is explained in detail in chapter 2.4.2. The number of stochastic variables for Case 1 is: $n = 2$. The first step is to perform three NLFE analyses to calculate the control point $\boldsymbol{X}_c$. Therefore NLFE analyses with mean $\overline{\boldsymbol{X}}$, low steel $\boldsymbol{X}_{f_y} = \overline{\boldsymbol{X}} - f\boldsymbol{\sigma}$ and low concrete $\boldsymbol{X}_{f_c} = \overline{\boldsymbol{X}} - f\boldsymbol{\sigma}$ material values are performed. The coordinates of the three points are shown in figure G1.

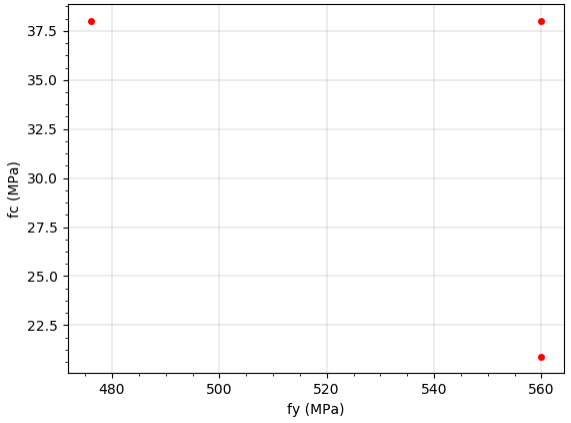


*Figure G1. The n+1 selected experimental points: mean $\overline{\boldsymbol{X}}$, low steel $\boldsymbol{X}_{f_y}$ and low concrete $\boldsymbol{X}_{f_c}$ material values.*

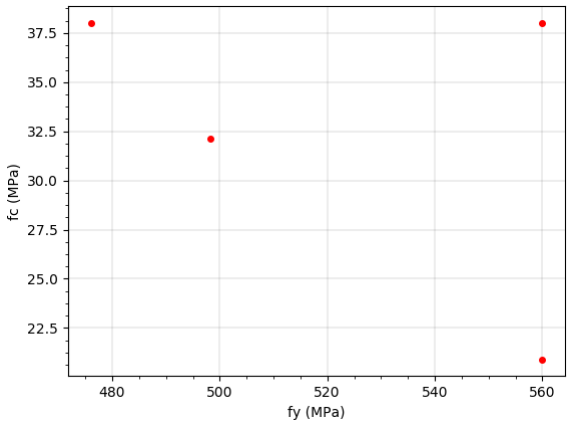


*Figure G2. The control point $\boldsymbol{X}_c$ in the real space is added.*

**<u>The control point $\boldsymbol{X}_c$ is calculated below:</u>**

<u>step 1:</u>

select $n + 1$ experimental points:

$$\overline{\boldsymbol{X}} = \begin{bmatrix} \mu_{f_y} \\ \mu_{f_c} \end{bmatrix}, \qquad \boldsymbol{X}_{f_y} = \begin{bmatrix} \mu_{f_y} - f\sigma_{f_y} \\ \mu_{f_c} \end{bmatrix}, \qquad \boldsymbol{X}_{f_c} = \begin{bmatrix} \mu_{f_y} \\ \mu_{f_c} - f\sigma_{f_c} \end{bmatrix}, \quad \text{where } f = 3.$$

<u>step 2:</u>

$G(\overline{\boldsymbol{X}}) = 8.9$

$G(\boldsymbol{X}_{f_y}) = 3.8$

$G(\boldsymbol{X}_{f_c}) = 6.9$

<u>step 3:</u>

$F(\boldsymbol{X}_{f_y}) = G(\overline{\boldsymbol{X}}) - G(\boldsymbol{X}_{f_y}) = 5.1$

$F(\boldsymbol{X}_{f_c}) = G(\overline{\boldsymbol{X}}) - G(\boldsymbol{X}_{f_c}) = 2.0$

<u>step 4:</u>

$$w_1 = \frac{F(\boldsymbol{X}_{f_y})}{F(\boldsymbol{X}_{f_y}) + F(\boldsymbol{X}_{f_c})} = 0.72$$

$$w_2 = \frac{F(\boldsymbol{X}_{f_c})}{F(\boldsymbol{X}_{f_y}) + F(\boldsymbol{X}_{f_c})} = 0.28$$

step 5:

The control point in the standard normal space is determined below. First the log-normal distributed variables are transformed to standard normal variables according to chapter 2.5.1.

$\sigma_{f_y} = 28$ MPa, $\mu_{f_y} = 560$ MPa,

$\sigma_{f_{y,L}} = \sqrt{\ln\left(\frac{\sigma_{f_y}^2}{\mu_{f_y}^2} + 1\right)} = 0.05$ MPa, $\mu_{f_{y,L}} = \ln \mu_{f_y} - \frac{1}{2}\,\sigma_{f_{y,L}}^2 = 6.327$ MPa

$\sigma_{f_c} = 5.7$ MPa, $\mu_{f_c} = 38$ MPa,

$\sigma_{f_{c,L}} = \sqrt{\ln\left(\frac{\sigma_{f_c}^2}{\mu_{f_c}^2} + 1\right)} = 0.149$ MPa, $\mu_{f_{c,L}} = \ln \mu_{f_c} - \frac{1}{2}\,\sigma_{f_{c,L}}^2 = 3.626$ MPa

$$\boldsymbol{U}_1 = \begin{bmatrix} \frac{\ln(\mu_{f_y} - f\sigma_{f_y}) - \mu_{f_{y,L}}}{\sigma_{f_{y,L}}} \\ \frac{\ln(\mu_{f_c}) - \mu_{f_{c,L}}}{\sigma_{f_{c,L}}} \end{bmatrix}, \qquad \boldsymbol{U}_2 = \begin{bmatrix} \frac{\ln(\mu_{f_y}) - \mu_{f_{y,L}}}{\sigma_{f_{y,L}}} \\ \frac{\ln(\mu_{f_c - f\,\sigma_{f_{c,L}}}) - \mu_{f_{c,L}}}{\sigma_{f_{c,L}}} \end{bmatrix}$$

The control point in the standard normal space:

$$\boldsymbol{U}_c = \sum_{i=1}^{n} w_i\, \boldsymbol{U}_i = \begin{bmatrix} -2.31 \\ -1.05 \end{bmatrix}$$

**The response surface and the real desing point are determined using the following steps:**

step 1:

The control point in the real space:

$$\boldsymbol{X}_c = \begin{bmatrix} \exp(-2.31\,\sigma_{f_{y,L}} + \mu_{f_{y,L}}) \\ \exp(-1.05\,\sigma_{f_{c,L}} + \mu_{f_{c,L}}) \end{bmatrix} = \begin{bmatrix} 498.3 \\ 32.1 \end{bmatrix} \quad \text{and} \quad G(\boldsymbol{X_c}) = -1.3$$

Wrong iteratation method used so the results of the NLFE analysis is not valid $G(\boldsymbol{X_c}) = -1.3$ and will not be used in the response surface to obtain the design point. The results of the NLFE analyses is $G(\boldsymbol{X_c}) = 5.3$ when the right iteration method was used. However the coordinates of the design points are still valid so the procedure to find the initial design point can still go on. The coordinates of the control point are shown in figure G2.

Step 2:

1. Based on the control point $\boldsymbol{X}_c$ and $G(\boldsymbol{X_c})$ the first iteration point is calculated according to:
   $\boldsymbol{X}_{M1} = \overline{\boldsymbol{X}} + (\boldsymbol{X_C} - \overline{\boldsymbol{X}})\frac{G(\overline{\boldsymbol{X}})}{G(\overline{\boldsymbol{X}}) - G(\boldsymbol{X_C})}$.

   $\boldsymbol{X}_{M1} = \begin{bmatrix} 506.2 \\ 32.8 \end{bmatrix}$, $G(\boldsymbol{X}_{M1}) = 7.2$, $\left|\frac{G(\boldsymbol{X}_{M1})}{G(\overline{\boldsymbol{X}})}\right| = 0.8 < 0.01$

2. No convergence, so the second iteration point is calculated with:
   $\boldsymbol{X}_{M_{i+1}} = \boldsymbol{X}_{M_i} + (\boldsymbol{X}_{M_{i-1}} - \boldsymbol{X}_{M_i})\frac{G(\boldsymbol{X}_{M_i})}{G(\boldsymbol{X}_{M_i}) - G(\boldsymbol{X}_{M_{i-1}})}$.

$$\boldsymbol{X}_{M2} = \begin{bmatrix} 278.1 \\ 11.1 \end{bmatrix}, \qquad G(\boldsymbol{X}_{M2}) = -21.0, \qquad \left|\frac{G(\boldsymbol{X}_{M2})}{G(\bar{\boldsymbol{X}})}\right| = 2.36 < 0.01$$

The first two iteration point are added in the figures G3 and G4, respectively.

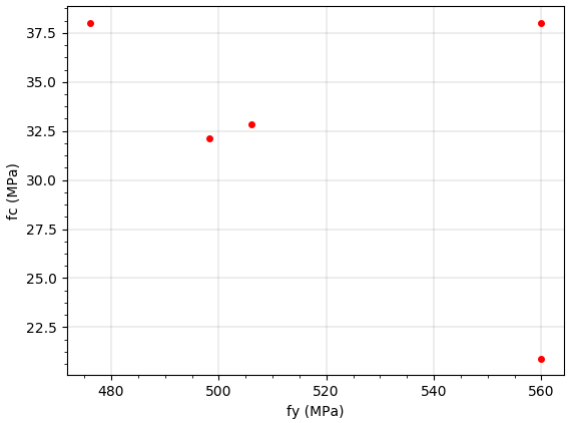


*Figure G3. The first iteration point $\boldsymbol{X}_{M1}$ is added.*

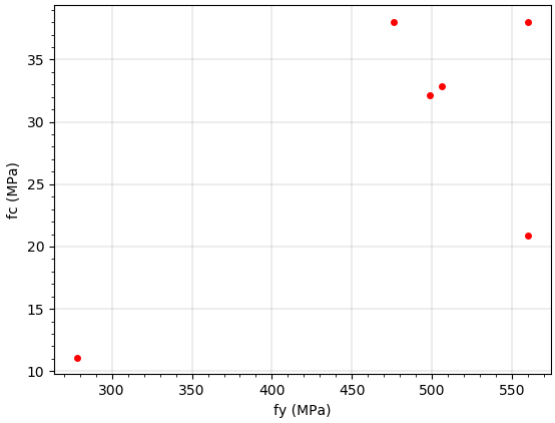


*Figure G4. The second iteration point $\boldsymbol{X}_{M2}$ is added.*

3. No convergence, so the third iteration point is calculated with:

$$\boldsymbol{X}_{M_{i+1}} = \boldsymbol{X}_{M_i} + \left(\boldsymbol{X}_{M_{i-1}} - \boldsymbol{X}_{M_i}\right)\frac{G(\boldsymbol{X}_{M_i})}{G\left(\boldsymbol{X}_{M_i}\right) - G(\boldsymbol{X}_{M_{i-1}})}.$$

$$\boldsymbol{X}_{M3} = \begin{bmatrix} 448.0 \\ 27.3 \end{bmatrix}, \qquad G(\boldsymbol{X}_{M3}) = 3.0, \qquad \left|\frac{G(\boldsymbol{X}_{M3})}{G(\bar{\boldsymbol{X}})}\right| = 0.34 < 0.01$$

4. No convergence, so the fourth iteration point is calculated with:

$$\boldsymbol{X}_{M_{i+1}} = \boldsymbol{X}_{M_i} + \left(\boldsymbol{X}_{M_{i-1}} - \boldsymbol{X}_{M_i}\right)\frac{G(\boldsymbol{X}_{M_i})}{G\left(\boldsymbol{X}_{M_i}\right) - G(\boldsymbol{X}_{M_{i-1}})}.$$

$$\boldsymbol{X}_{M4} = \begin{bmatrix} 426.8 \\ 25.3 \end{bmatrix}, \qquad G(\boldsymbol{X}_{M4}) = -1.9, \qquad \left|\frac{G(\boldsymbol{X}_{M4})}{G(\bar{\boldsymbol{X}})}\right| = 0.22 < 0.01$$

5. No convergence, so the fifth iteration point is calculated with:

$$\boldsymbol{X}_{M_{i+1}} = \boldsymbol{X}_{M_i} + \left(\boldsymbol{X}_{M_{i-1}} - \boldsymbol{X}_{M_i}\right)\frac{G(\boldsymbol{X}_{M_i})}{G\left(\boldsymbol{X}_{M_i}\right) - G(\boldsymbol{X}_{M_{i-1}})}.$$

$$\boldsymbol{X}_{M5} = \begin{bmatrix} 435.1 \\ 26.1 \end{bmatrix}, \qquad G(\boldsymbol{X}_{M5}) = -0.6, \qquad \left|\frac{G(\boldsymbol{X}_{M5})}{G(\bar{\boldsymbol{X}})}\right| = 0.067 < 0.01$$

6. No convergence, so the sixth iteration point is calculated with:

$$\boldsymbol{X}_{M_{i+1}} = \boldsymbol{X}_{M_i} + \left(\boldsymbol{X}_{M_{i-1}} - \boldsymbol{X}_{M_i}\right)\frac{G(\boldsymbol{X}_{M_i})}{G\left(\boldsymbol{X}_{M_i}\right) - G(\boldsymbol{X}_{M_{i-1}})}.$$

$$\boldsymbol{X}_{M6} = \begin{bmatrix} 438.9 \\ 26.4 \end{bmatrix}, \qquad G(\boldsymbol{X}_{M6}) = -0.4, \qquad \left|\frac{G(\boldsymbol{X}_{M6})}{G(\bar{\boldsymbol{X}})}\right| = 0.04 < 0.01$$

7. No convergence, so the seventh iteration point is calculated with:

$$\boldsymbol{X}_{M_{i+1}} = \boldsymbol{X}_{M_i} + \left(\boldsymbol{X}_{M_{i-1}} - \boldsymbol{X}_{M_i}\right)\frac{G(\boldsymbol{X}_{M_i})}{G\left(\boldsymbol{X}_{M_i}\right) - G(\boldsymbol{X}_{M_{i-1}})}.$$

$$\boldsymbol{X}_{M7} = \begin{bmatrix} 446.4 \\ 27.2 \end{bmatrix}, \qquad G(\boldsymbol{X}_{M7}) = 2.8, \qquad \left|\frac{G(\boldsymbol{X}_{M7})}{G(\bar{\boldsymbol{X}})}\right| = 0.31 < 0.01$$

8. No convergence, so the eighth iteration point is calculated with:

$$\boldsymbol{X}_{M_{i+1}} = \boldsymbol{X}_{M_i} + \left(\boldsymbol{X}_{M_{i-1}} - \boldsymbol{X}_{M_i}\right)\frac{G(\boldsymbol{X}_{M_i})}{G\left(\boldsymbol{X}_{M_i}\right) - G(\boldsymbol{X}_{M_{i-1}})}.$$

$$\boldsymbol{X}_{M8} = \begin{bmatrix} 439.8 \\ 26.5 \end{bmatrix}, \qquad G(\boldsymbol{X}_{M8}) = -0.3, \qquad \left|\frac{G(\boldsymbol{X}_{M8})}{G(\overline{\boldsymbol{X}})}\right| = 0.03 < 0.01$$

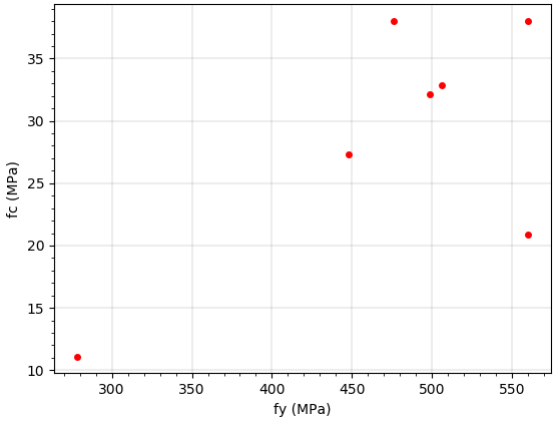


*Figure G5. Iteration point $\boldsymbol{X}_{M3}$ is added.*

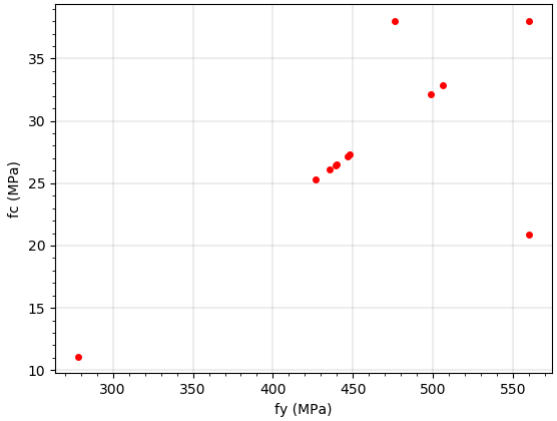


*Figure G6. Iteration point $\boldsymbol{X}_{M4}$, $\boldsymbol{X}_{M5}$, $\boldsymbol{X}_{M6}$, $\boldsymbol{X}_{M7}$ and $\boldsymbol{X}_{M8}$ are added.*

9. No convergence, so the ninth iteration point is calculated with:

$$\boldsymbol{X}_{M_{i+1}} = \boldsymbol{X}_{M_i} + \left(\boldsymbol{X}_{M_{i-1}} - \boldsymbol{X}_{M_i}\right)\frac{G(\boldsymbol{X}_{M_i})}{G\left(\boldsymbol{X}_{M_i}\right) - G(\boldsymbol{X}_{M_{i-1}})}.$$

$$\boldsymbol{X}_{M9} = \begin{bmatrix} 440.4 \\ 26.6 \end{bmatrix}, \qquad G(\boldsymbol{X}_{M9}) = -0.4, \qquad \left|\frac{G(\boldsymbol{X}_{M9})}{G(\overline{\boldsymbol{X}})}\right| = 0.04 < 0.01$$

10. No convergence, so the tenth iteration point is calculated with:

$$\boldsymbol{X}_{M_{i+1}} = \boldsymbol{X}_{M_i} + \left(\boldsymbol{X}_{M_{i-1}} - \boldsymbol{X}_{M_i}\right)\frac{G(\boldsymbol{X}_{M_i})}{G\left(\boldsymbol{X}_{M_i}\right) - G(\boldsymbol{X}_{M_{i-1}})}.$$

$$\boldsymbol{X}_{M10} = \begin{bmatrix} 437.9 \\ 26.3 \end{bmatrix}, \qquad G(\boldsymbol{X}_{M10}) = -0.5, \qquad \left|\frac{G(\boldsymbol{X}_{M10})}{G(\overline{\boldsymbol{X}})}\right| = 0.06 < 0.01$$

Divergence of the design point in the ninth and tenth iteration. $X_{M8}$ is closest to convergence and will be selected as initial design point.

<u>step 3:</u>

Select $2n + 1$ experimental points, where the center point is $\boldsymbol{X}_{M8}$: $\boldsymbol{X}_i = \boldsymbol{X}_{M8} \pm f\boldsymbol{\sigma}$, where $f = 1$, because the center point should be close to the real design point. This led to the following sample points and corresponding limit state functions:

$$\boldsymbol{X}_1 = \begin{bmatrix} 439.8 \\ 26.5 \end{bmatrix} \qquad G(\boldsymbol{X}_1) = -0.3$$
$$\boldsymbol{X}_2 = \begin{bmatrix} 467.8 \\ 26.5 \end{bmatrix} \qquad G(\boldsymbol{X}_2) = 1.2$$
$$\boldsymbol{X}_3 = \begin{bmatrix} 439.8 \\ 32.2 \end{bmatrix} \qquad G(\boldsymbol{X}_3) = -0.6$$
$$\boldsymbol{X}_4 = \begin{bmatrix} 411.8 \\ 26.5 \end{bmatrix} \qquad G(\boldsymbol{X}_4) = -2.2$$
$$\boldsymbol{X}_5 = \begin{bmatrix} 439.8 \\ 20.8 \end{bmatrix} \qquad G(\boldsymbol{X}_5) = -1.3$$

The rotational capacity of corner D has a lot of influence on the structural resistance. Some experience of using the NLFE model led to the conclusion that the ratio of the concrete strength and the steel yield strength has a large influence on the structural resistance. This ratio determines the rotational capacity of the corner and therefore leads to a brittle or ductile failure mode. For this reason convergence is hard to achieve. The best way to estimate the design point is to determine a lot of points around the estimated design point such that the response surface is an accurate approximation of the actual LSF.

Calculation of the design point with the first 5 points is not possible since this leads to an unrealistic shape of the response surface $\overline{G}(\boldsymbol{X})$, especially in the region outside the zone where the sample points are chosen. The response surface will be determined in step 4. Therefore some additional points will be added to create a more realistic response surface.

The additional cross points for are:

$\boldsymbol{X}_i = \boldsymbol{X}_{M8} \pm f\boldsymbol{\sigma}$, with $f = 1.0$

$\boldsymbol{X}_6 = \begin{bmatrix} 467.8 \\ 32.2 \end{bmatrix}$ $G(\boldsymbol{X}_6) = 1.7$

$\boldsymbol{X}_7 = \begin{bmatrix} 411.8 \\ 32.2 \end{bmatrix}$ $G(\boldsymbol{X}_7) = -2.2$

$\boldsymbol{X}_8 = \begin{bmatrix} 411.8 \\ 20.8 \end{bmatrix}$ $G(\boldsymbol{X}_8) = -3.2$

$\boldsymbol{X}_9 = \begin{bmatrix} 467.8 \\ 20.8 \end{bmatrix}$ $G(\boldsymbol{X}_9) = 0.8$

The additional points along the axes are:

$\boldsymbol{X}_i = \boldsymbol{X}_{M8} \pm f\boldsymbol{\sigma}$, with $f = 1.5$

$\boldsymbol{X}_{10} = \begin{bmatrix} 481.8 \\ 26.5 \end{bmatrix}$ $G(\boldsymbol{X}_{10}) = 1.9$

$\boldsymbol{X}_{11} = \begin{bmatrix} 439.8 \\ 35.1 \end{bmatrix}$ $G(\boldsymbol{X}_{11}) = 2.9$

$\boldsymbol{X}_{12} = \begin{bmatrix} 397.8 \\ 26.5 \end{bmatrix}$ $G(\boldsymbol{X}_{12}) = -3.0$

$\boldsymbol{X}_{13} = \begin{bmatrix} 439.8 \\ 17.8 \end{bmatrix}$ $G(\boldsymbol{X}_{13}) = 0.8$

$\boldsymbol{X}_i = \boldsymbol{X}_{M8} \pm f\boldsymbol{\sigma}$, with $f = 2.0$

$\boldsymbol{X}_{18} = \begin{bmatrix} 495.8 \\ 26.5 \end{bmatrix}$ $G(\boldsymbol{X}_{18}) = 3.8$

$\boldsymbol{X}_{19} = \begin{bmatrix} 439.8 \\ 37.9 \end{bmatrix}$ $G(\boldsymbol{X}_{19}) = -0.1$

$\boldsymbol{X}_{20} = \begin{bmatrix} 383.8 \\ 26.5 \end{bmatrix}$ $G(\boldsymbol{X}_{20}) = -3.8$

$\boldsymbol{X}_{21} = \begin{bmatrix} 439.8 \\ 15.1 \end{bmatrix}$ $G(\boldsymbol{X}_{21}) = -1.1$

The additional cross points are:

$\boldsymbol{X}_i = \boldsymbol{X}_{M8} \pm f\boldsymbol{\sigma}$, with $f = 1.5$

$\boldsymbol{X}_{14} = \begin{bmatrix} 481.8 \\ 35.1 \end{bmatrix}$ $G(\boldsymbol{X}_{14}) = 5.3$

$\boldsymbol{X}_{15} = \begin{bmatrix} 397.8 \\ 35.1 \end{bmatrix}$ $G(\boldsymbol{X}_{15}) = -0.1$

$\boldsymbol{X}_{16} = \begin{bmatrix} 397.8 \\ 18.0 \end{bmatrix}$ $G(\boldsymbol{X}_{16}) = -1.6$

$\boldsymbol{X}_{17} = \begin{bmatrix} 481.8 \\ 18.0 \end{bmatrix}$ $G(\boldsymbol{X}_{17}) = 0.1$

$\boldsymbol{X}_i = \boldsymbol{X}_{M8} \pm f\boldsymbol{\sigma}$, with $f = 2.0$

$\boldsymbol{X}_{22} = \begin{bmatrix} 495.8 \\ 37.9 \end{bmatrix}$ $G(\boldsymbol{X}_{22}) = 5.3$

$\boldsymbol{X}_{23} = \begin{bmatrix} 383.8 \\ 37.9 \end{bmatrix}$ $G(\boldsymbol{X}_{23}) = -1.4$

$\boldsymbol{X}_{24} = \begin{bmatrix} 383.8 \\ 15.1 \end{bmatrix}$ $G(\boldsymbol{X}_{24}) = -4.6$

$\boldsymbol{X}_{25} = \begin{bmatrix} 495.8 \\ 15.1 \end{bmatrix}$ $G(\boldsymbol{X}_{25}) = 2.8$

Also the ten iteration points $\boldsymbol{X}_{Mi}$, the control point $\boldsymbol{X}_c$ and the first three points $\overline{\boldsymbol{X}}$, $\boldsymbol{X}_{f_y}$ and $\boldsymbol{X}_{f_c}$ are used to create a realistic response surface.

<u>step 4:</u>
The response surface can be formed after determining the unknown coefficients (see chapter 2.4.1). A least squares approach is used to determine the unknown coefficients (which leads to an exact results if the number of unknown coefficients is equal to the number of sample points). The unknown coefficients can be determined according to:

$$\boldsymbol{b} = (\boldsymbol{A}^T\boldsymbol{A})^{-1}\boldsymbol{A}^T\boldsymbol{G}.$$

Now the response surface $\overline{G}(\boldsymbol{X})$ can be obtained according to the following equation:

$$\overline{G}(\boldsymbol{X}) = \boldsymbol{A}\boldsymbol{b}$$

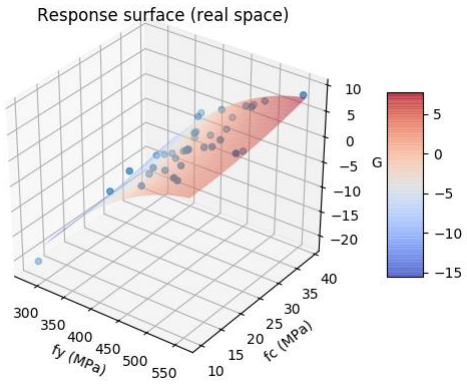


*Figure G7. Response surface (real space).*

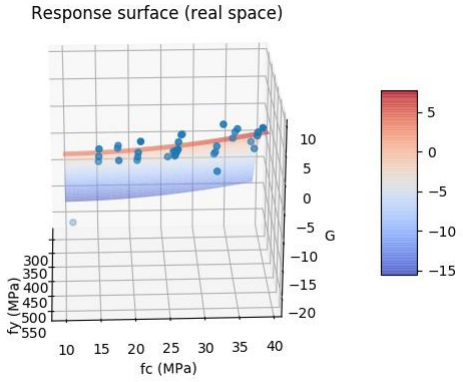


*Figure G8. Response surface (real space).*

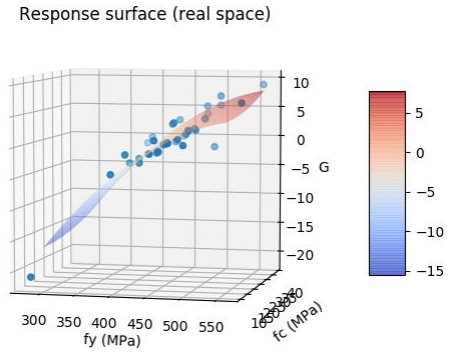


*Figure G9. Response surface (real space).*

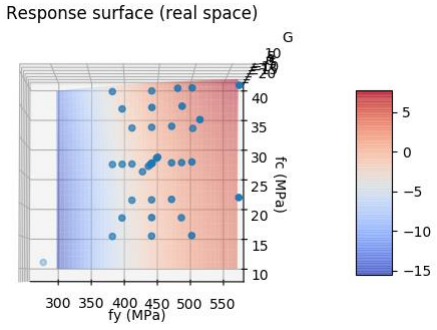


*Figure G10. Response surface (real space).*

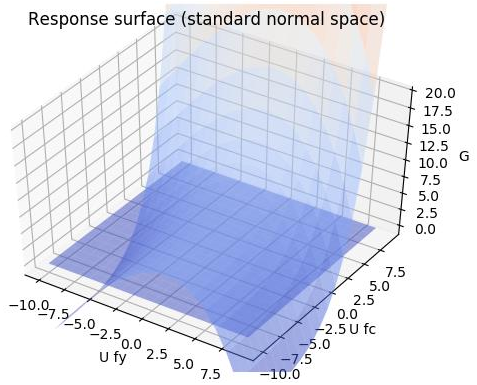


*Figure G11. Response surface (standard normal space).*

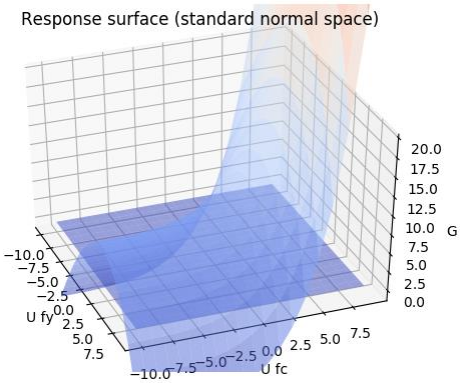


*Figure G12. Response surface (standard normal space).*

However this response surface led to divergence after using the FORM in order to obtain the real design point. A design point with a larger reliability index than the initial design point was found. The initial design point led to the following results:

$$\boldsymbol{X}_{M8} = \begin{bmatrix} 439.8 \\ 26.5 \end{bmatrix} \qquad \boldsymbol{U}_{M8} = \begin{bmatrix} -4.73 \\ -2.30 \end{bmatrix} \qquad \beta_{inititial} = 5.34 \qquad G(\boldsymbol{X}_{M8}) = -0.3.$$

The first iteration using the FORM in order to obtain the real design led to the following results:

$$\boldsymbol{X}_{1,*} = \begin{bmatrix} 434.5 \\ 28.8 \end{bmatrix} \qquad \boldsymbol{U}_{1,*} = \begin{bmatrix} -5.05 \\ -1.79 \end{bmatrix} \qquad \beta_{1,R} = 5.36 \qquad G\left(\boldsymbol{X}_{1,*}\right) = 3.1.$$

The results are graphically presented in figure G13 and G14. Immediately can be seen that there is no failure in the first obtained design point since $G\left(\boldsymbol{X}_{1,*}\right) > 0$. When more iteration were used to obtain the real design point only higher values of the reliability index were obtained. This could not be the case since the initial design point $\boldsymbol{X}_{M8}$ led to a failure of the structure $G(\boldsymbol{X}_{M8}) < 0$ with a lower reliability index.

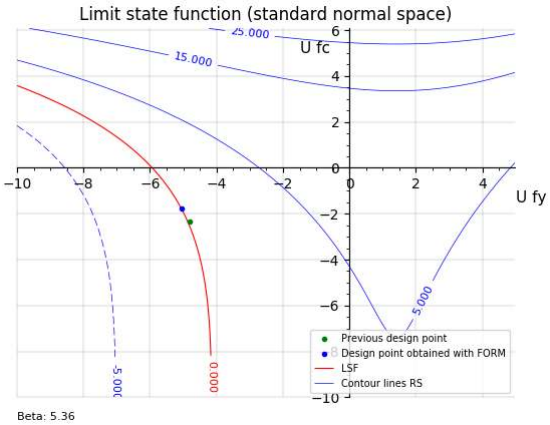


*Figure G13. Limit state function (standard normal space).*

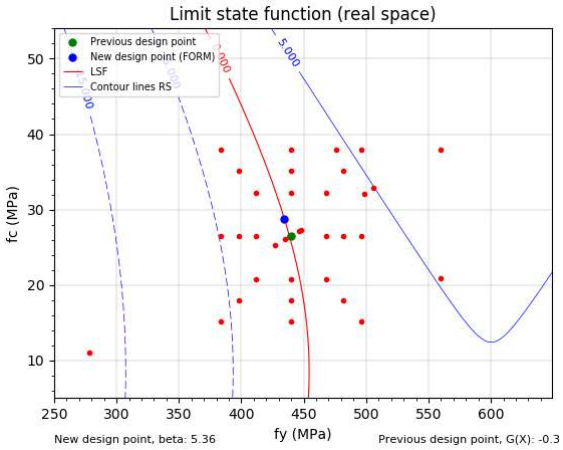


*Figure G14. Limit state function (real space) and sample points.*

To overcome this divergence the results of the implicit limit state function $\bar{G}(\boldsymbol{X})$ with relatively large outcomes compared to the real design point were not used to create the response surface since this points influence the shape of the response surface in the region of the design point too much. The adopted response surface could be used to find the real design point $\boldsymbol{X}_*$. This led to the following response surface, which is shown in the figures G13 till G18. The difference of the shape of the new and the old response surface is best noticeable by comparing figures G11 and G12 with G17 and G18, where the response surface is presented in the standard normal space.

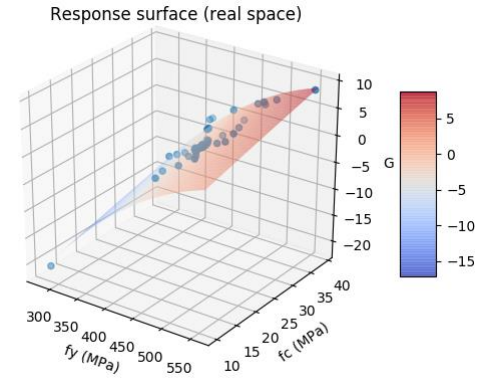


*Figure G13. Response surface (real space).*

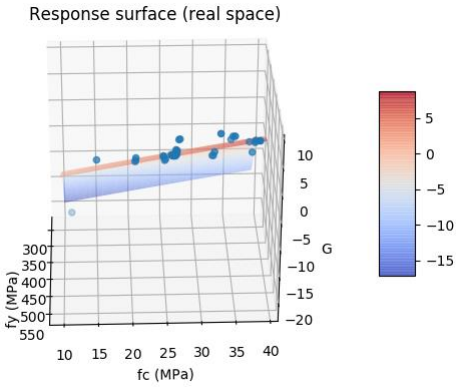


*Figure G14. Response surface (real space).*

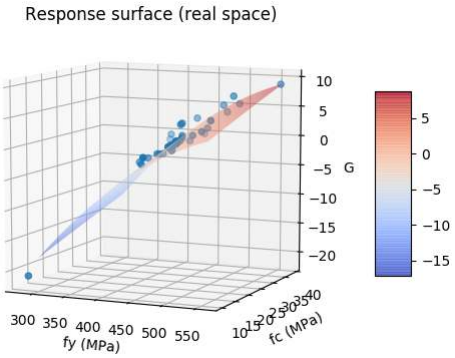


*Figure G15. Response surface (real space).*

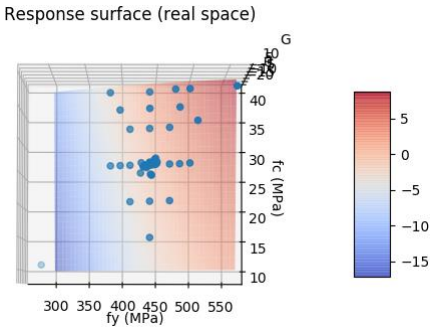


*Figure G16. Response surface (real space).*

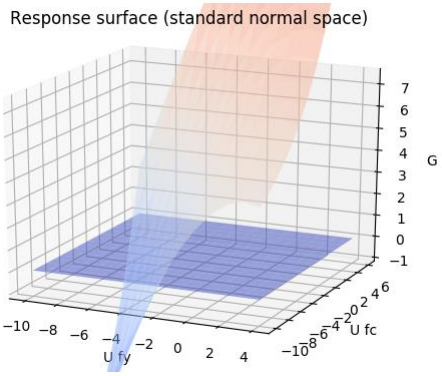


*Figure G17. Response surface (real space).*

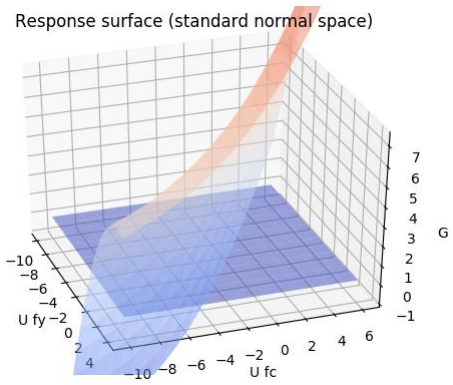


*Figure G18. Response surface (real space).*

Step 5:

The design point is determined after several iterations using the FORM in combination with the obtained response surface of step 4. This is shown figures G19 and G20. The coordinates of the design point in the standard normal space $\boldsymbol{U}_*$, the coordinates in of the design point in the real space $\boldsymbol{X}_*$, the reliability index $\beta_R$ and the sensitivity factors $\alpha_R$ are:

$$\boldsymbol{X}_* = \begin{bmatrix} 441.5 \\ 26.7 \end{bmatrix} \qquad \boldsymbol{U}_* = \begin{bmatrix} -4.73 \\ -2.30 \end{bmatrix} \qquad \beta_R = 5.26 \qquad \alpha_R = \begin{bmatrix} 0.900 \\ 0.437 \end{bmatrix}.$$

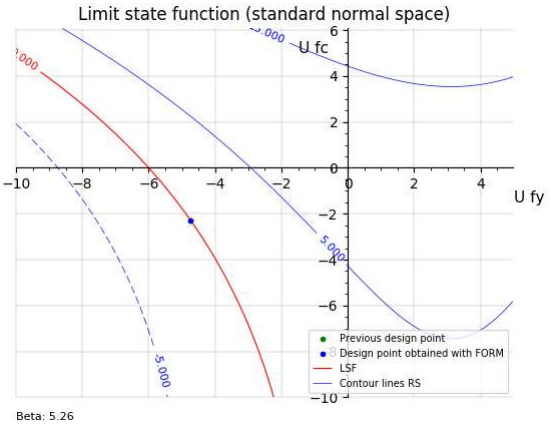


*Figure G19. Limit state function (standard normal space).*

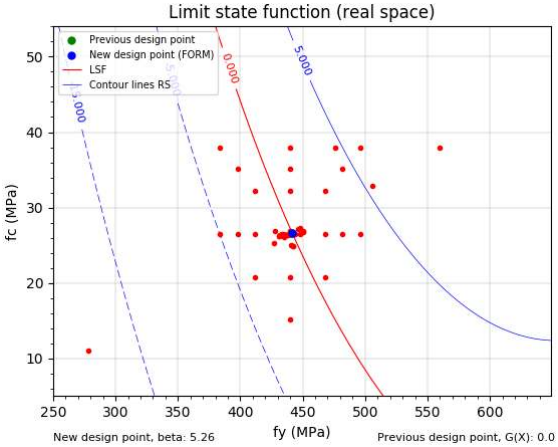


*Figure G20. Limit state function (real space) and sample points.*

### G.1.2 Design 2

The safety format with the highest global design resistance, i.e. highest probability of failure, for design 2 is the PFm. The total global design resistance according to the PFm is: $R_{SF} = 43.7$ kN. This leads to the following implicit LSF:

$$G(\boldsymbol{X}) = R(\boldsymbol{X}) - 43.7.$$

The response surface is constructed according to the approach of Zhao and Qiu (2013). The first step is to perform three NLFE analyses to calculate the control point $\boldsymbol{X}_c$. Therefore NLFE analyses with mean $\overline{\boldsymbol{X}}$, low steel $\boldsymbol{X}_{f_y} = \overline{\boldsymbol{X}} - f\boldsymbol{\sigma}$ and low concrete $\boldsymbol{X}_{f_c} = \overline{\boldsymbol{X}} - f\boldsymbol{\sigma}$ material values are performed. For this case $f = 4.5$ because otherwise the influence of the individual stochastic variables on the failure load is not correctly expressed by the weight factors $w_i$. However this is an indication i.e. an intitial guess so the correct factor of $f$ cannot be predicted in advance. A discussion on choosing the factor $f$ can be found in chapter 7.2.1.4.

**The control point $\boldsymbol{X_c}$ is calculated below:**

step 1:
select $n + 1$ experimental points:

$$\overline{\boldsymbol{X}} = \begin{bmatrix}\mu_{f_y}\\ \mu_{f_c}\end{bmatrix}, \qquad \boldsymbol{X}_{f_y} = \begin{bmatrix}\mu_{f_y} - f_1\sigma_{f_y}\\ \mu_{f_c}\end{bmatrix}, \quad f_1 = 4.5 \qquad \boldsymbol{X}_{f_c} = \begin{bmatrix}\mu_{f_y}\\ \mu_{f_c} - f_2\sigma_{f_c}\end{bmatrix}, \quad f_2 = 4.5.$$

step 2:

$$G(\overline{\boldsymbol{X}}) = 9.1$$

$$G(\boldsymbol{X}_{f_y}) = 1.1$$

$$G(\boldsymbol{X}_{f_c}) = 3.1$$

step 3:

$$F(\boldsymbol{X}_{f_y}) = G(\overline{\boldsymbol{X}}) - G(\boldsymbol{X}_{f_y}) = 8.0$$

$$F(\boldsymbol{X}_{f_c}) = G(\overline{\boldsymbol{X}}) - G(\boldsymbol{X}_{f_c}) = 6.0$$

step 4:

$$w_1 = \frac{F(\boldsymbol{X}_{f_y})}{F(\boldsymbol{X}_{f_y}) + F(\boldsymbol{X}_{f_c})} = 0.57$$

$$w_2 = \frac{F(\boldsymbol{X}_{f_c})}{F(\boldsymbol{X}_{f_y}) + F(\boldsymbol{X}_{f_c})} = 0.43$$

step 5:

$\sigma_{f_y} = 28$ MPa, $\quad \mu_{f_y} = 560$ MPa,

$$\sigma_{f_y,L} = \sqrt{\ln\left(\frac{\sigma_{f_y}^2}{\mu_{f_y}^2} + 1\right)} = 0.05 \text{ MPa}, \qquad \mu_{f_y,L} = \ln \mu_{f_y} - \frac{1}{2}\,\sigma_{f_y,L}^2 = 6.327 \text{ MPa}$$

$\sigma_{f_c} = 7.2$ MPa, $\quad \mu_{f_c} = 38$ MPa,

$$\sigma_{f_c,L} = \sqrt{\ln\left(\frac{\sigma_{f_c}^2}{\mu_{f_c}^2} + 1\right)} = 0.149 \text{ MPa}, \qquad \mu_{f_c,L} = \ln \mu_{f_c} - \frac{1}{2}\,\sigma_{f_c,L}^2 = 3.626 \text{ MPa}$$

$$\boldsymbol{U}_1 = \begin{bmatrix}\frac{\ln(\mu_{f_y} - f\sigma_{f_y}) - \mu_{f_y,L}}{\sigma_{f_y,L}}\\ \frac{\ln(\mu_{f_c}) - \mu_{f_c,L}}{\sigma_{f_c,L}}\end{bmatrix}, \qquad \boldsymbol{U}_2 = \begin{bmatrix}\frac{\ln(\mu_{f_y}) - \mu_{f_y,L}}{\sigma_{f_y,L}}\\ \frac{\ln(\mu_{f_c - f\,\sigma_{f_c,L}}) - \mu_{f_c,L}}{\sigma_{f_c,L}}\end{bmatrix}$$

The control point in the standard normal space:

$$\boldsymbol{U}_c = \sum_{i=1}^{n} w_i\,\boldsymbol{U}_i = \begin{bmatrix}-2.89\\ -3.15\end{bmatrix}$$

**The response surface and the real desing point are determined using the following steps:**

step 1:

The control point in the real space:

$$\boldsymbol{X}_c = \begin{bmatrix} \exp(-2.89\ \sigma_{f_y,L} + \mu_{f_y,L}) \\ \exp(-3.15\ \sigma_{f_c,L} + \mu_{f_c,L}) \end{bmatrix} = \begin{bmatrix} 484.1 \\ 23.5 \end{bmatrix} \quad \text{and} \quad G(\boldsymbol{X_c}) = 2.6$$

step 2:

The initial design point is found with the same approach as for design 1 using the control point.

step 3 and 4 (a):

Around the initial design point four sets of sample points with $f = 0.5; 1.0; 1.5; 2.0$ are used to determine the response surface. The sample points are shown in figure G21 and G23.

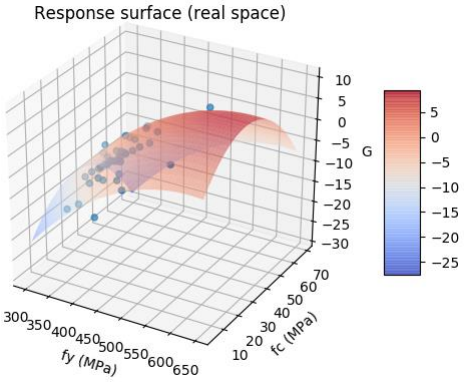


*Figure G21. Design 2: response surface (real space).*

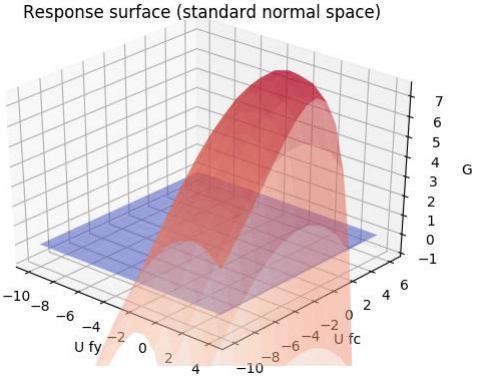


*Figure G22. Design 2: response surface (standard normal space).*

step 5 (a):

After using the FORM a design point is found in the region which is not described by the chosen sample points. This is shown in figure G23 and G24. Therefore additional sample points were added and the response surface is modified. Therfore step 3 and 4 has been perormed again.

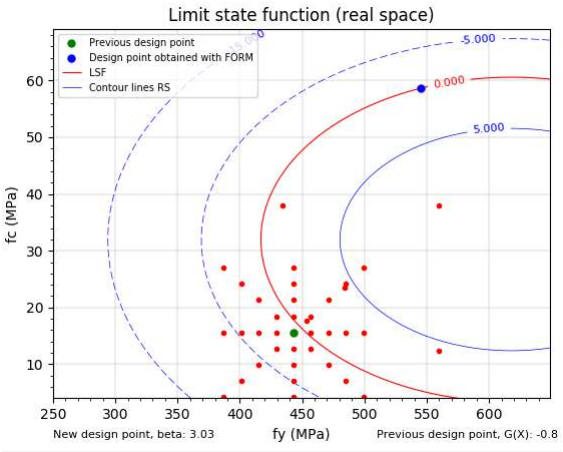


*Figure G23. Design 2: limit state function (real space). Design point obtained with the FORM lies in a region, which is not described accurately by the sample points.*

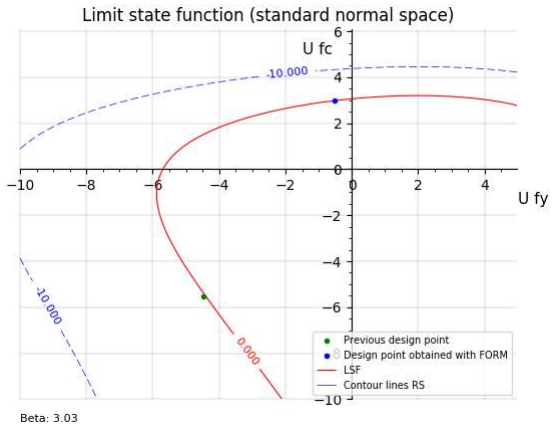


*Figure G24. Design 2: limit state function (standard normal space). The limit state function is only accurately described by sample points (not visible in this figure)) in the third quadrant. Therefore the obtained design point is not realistic.*

step 3 and 4 (b):

Additional sample points with a high concrete compressive strength are added to have a better approximation of the response surface in the region of the added sample points. Otherwise an incorrect design point is obtained. The updated response surface is presented in figures G25 till G28.

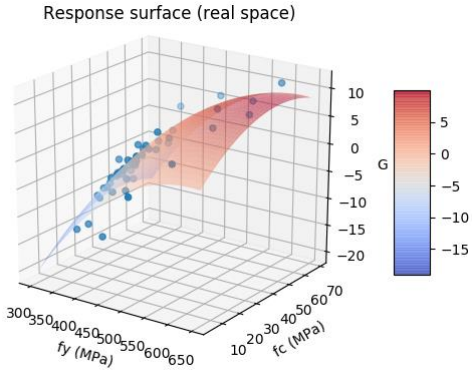


*Figure G25. Design 2: updated response surface (real space) in order to find the real design point.*

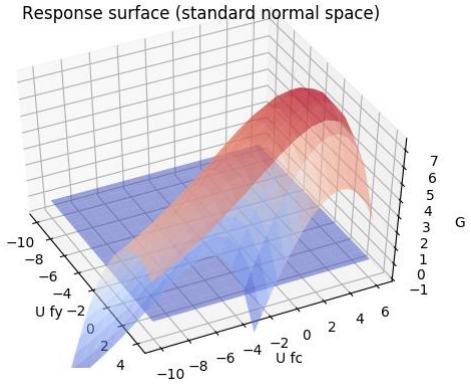


*Figure G26. Design 2: updated response surface (standard normal space) in order to find the real design point.*

The rotational capacity of corner D has a large influence on the structural resistance and therefore on the result of the LSF. The structural resistance of NLFE analyses with sample points close to each other can differ significantly. The spreading of the results is shown in figure G27 and G28.

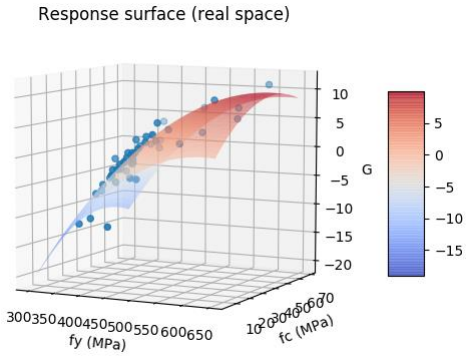


*Figure G27. Design 2: updated response surface (real space). The spreading of the results of the implicit LSF is clearly visible.*

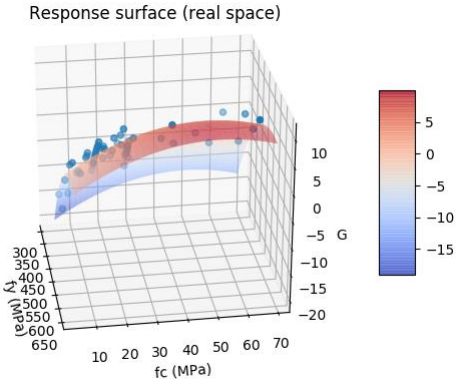


*Figure G28. Design 2: updated response surface (real space). The spreading of the results of the implicit LSF is clearly visible.*

step 5 (b):

The design point is determined after several iterations using the FORM in combination with the obtained response surface of step 4. This is shown figures G29 and G30. The coordinates of the design point in the standard normal space $\boldsymbol{U}_*$, the coordinates in of the design point in the real space $\boldsymbol{X}_*$, the reliability index $\beta_R$ and the sensitivity factors $\alpha_R$ are:

$$\boldsymbol{U}_* = \begin{bmatrix} -5.29 \\ -2.25 \end{bmatrix} \qquad \boldsymbol{X}_* = \begin{bmatrix} 429.3 \\ 26.9 \end{bmatrix} \qquad \beta_R = 5.75 \qquad \alpha_R = \begin{bmatrix} 0.920 \\ 0.391 \end{bmatrix}.$$

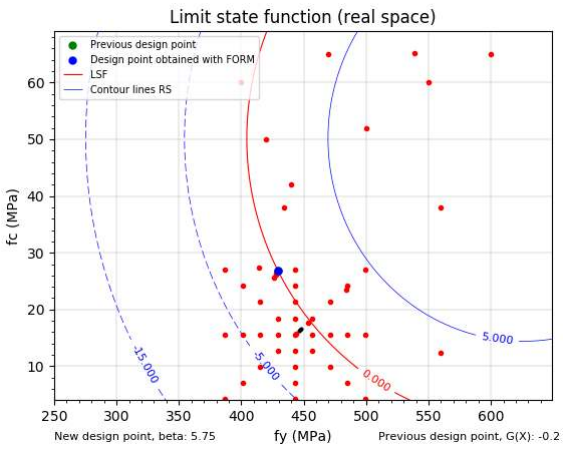


*Figure G29. Design 2: updated limit state function (real space). Previous design point lies below the new obtained design point.*

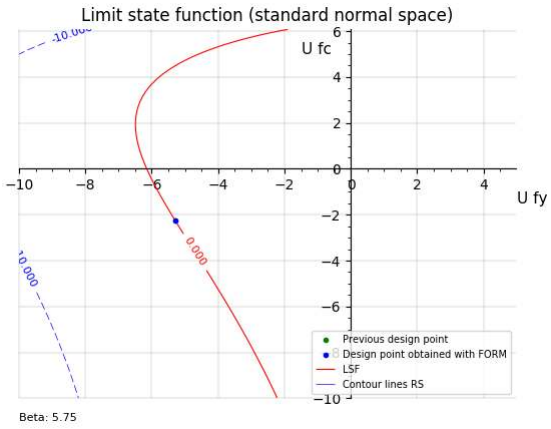


*Figure G30. Design 2: updated limit state function (standard normal space).*

### G.1.3 Design 3

The safety format with the highest global design resistance, i.e. highest probability of failure, for design 3 is the PFm. The total global design resistance according to the PFm is: $R_{SF} = 37.0$ kN. This leads to the following implicit LSF:

$$G(\boldsymbol{X}) = R(\boldsymbol{X}) - 37.0.$$

The response surface is constructed according to the approach of Zhao and Qiu (2013). The first step is to perform three NLFE analysis to calculate the control point $\boldsymbol{X}_c$. Therefore NLFE analyses with mean $\overline{\boldsymbol{X}}$, low steel $\boldsymbol{X}_{f_y} = \overline{\boldsymbol{X}} - f\boldsymbol{\sigma}$ and low concrete $\boldsymbol{X}_{f_c} = \overline{\boldsymbol{X}} - f\boldsymbol{\sigma}$ material values are performed. For this case $\boldsymbol{f}$=4.0 because otherwise the influence of the individual stochastic variables on the failure load is not correctly expressed by the weight factors $w_i$.

**The control point $\boldsymbol{X}_c$ is calculated below:**

step 1:

select $n + 1$ experimental points:

$$\overline{\boldsymbol{X}} = \begin{bmatrix}\mu_{f_y}\\ \mu_{f_c}\end{bmatrix}, \qquad \boldsymbol{X}_{f_y} = \begin{bmatrix}\mu_{f_y} - f_1\sigma_{f_y}\\ \mu_{f_c}\end{bmatrix}, \quad f_1 = 4.0 \qquad \boldsymbol{X}_{f_c} = \begin{bmatrix}\mu_{f_y}\\ \mu_{f_c} - f_2\sigma_{f_c}\end{bmatrix}, \quad f_2 = 4.0$$

step 2:

$$G(\overline{\boldsymbol{X}}) = 7.0$$

$$G(\boldsymbol{X}_{f_y}) = 4.0$$

$$G(\boldsymbol{X}_{f_c}) = 5.5$$

step 3:

$$F(\boldsymbol{X}_{f_y}) = G(\overline{\boldsymbol{X}}) - G(\boldsymbol{X}_{f_y}) = 3.0$$

$$F(\boldsymbol{X}_{f_c}) = G(\overline{\boldsymbol{X}}) - G(\boldsymbol{X}_{f_c}) = 1.5$$

step 4:

$$w_1 = \frac{F(\boldsymbol{X}_{f_y})}{F(\boldsymbol{X}_{f_y}) + F(\boldsymbol{X}_{f_c})} = 0.66$$

$$w_2 = \frac{F(\boldsymbol{X}_{f_c})}{F(\boldsymbol{X}_{f_y}) + F(\boldsymbol{X}_{f_c})} = 0.33$$

step 5:

$\sigma_{f_y} = 28$ MPa, $\mu_{f_y} = 560$ MPa,

$$\sigma_{f_y,L} = \sqrt{\ln\left(\frac{\sigma_{f_y}^2}{\mu_{f_y}^2} + 1\right)} = 0.05 \text{ MPa}, \qquad \mu_{f_y,L} = \ln \mu_{f_y} - \frac{1}{2}\sigma_{f_y,L}^2 = 6.327 \text{ MPa}$$

$\sigma_{f_c} = 5.7$ MPa, $\mu_{f_c} = 48$ MPa,

$$\sigma_{f_c,L} = \sqrt{\ln\left(\frac{\sigma_{f_c}^2}{\mu_{f_c}^2} + 1\right)} = 0.149 \text{ MPa}, \qquad \mu_{f_c,L} = \ln \mu_{f_c} - \frac{1}{2}\sigma_{f_c,L}^2 = 3.871 \text{ MPa}$$

$$\boldsymbol{U}_1 = \begin{bmatrix}\frac{\ln(\mu_{f_y} - f\sigma_{f_y}) - \mu_{f_y,L}}{\sigma_{f_y,L}}\\ \frac{\ln(\mu_{f_c}) - \mu_{f_c,L}}{\sigma_{f_c,L}}\end{bmatrix}, \qquad \boldsymbol{U}_2 = \begin{bmatrix}\frac{\ln(\mu_{f_y}) - \mu_{f_y,L}}{\sigma_{f_y,L}}\\ \frac{\ln(\mu_{f_c} - f\,\sigma_{f_c,L}) - \mu_{f_c,L}}{\sigma_{f_c,L}}\end{bmatrix}$$

The control point in the standard normal space:

$$\boldsymbol{U}_c = \sum_{i=1}^{n} w_i\,\boldsymbol{U}_i = \begin{bmatrix}-2.95\\ -1.97\end{bmatrix}$$

**The response surface and the real desing point are determined using the following steps:**

step 1:

The control point in the real space:

$$\boldsymbol{X}_c = \begin{bmatrix} \exp(-2.95\ \sigma_{f_y,L} + \mu_{f_y,L}) \\ \exp(-1.97\ \sigma_{f_c,L} + \mu_{f_c,L}) \end{bmatrix} = \begin{bmatrix} 482.6 \\ 35.4 \end{bmatrix} \quad \text{and} \quad G(\boldsymbol{X_c}) = 3.9$$

step 2:

The initial design point is found with the same approach as in design 1 using the control point.

step 3:

Select extra points around the intitial design points to create the response surface using the same approach as for design 1.

step 4:

The response surface for the selected points in step 3 is determined below.

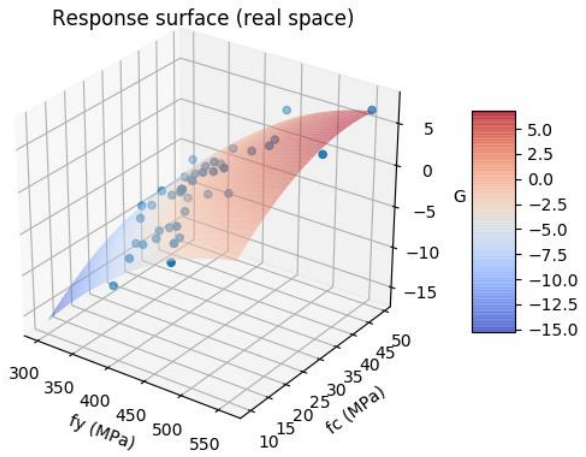


*Figure G31. Response surface (real space).*

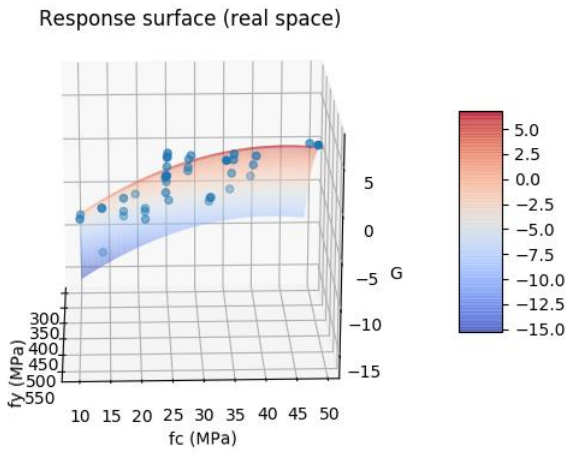


*Figure G32. Response surface (real space).*

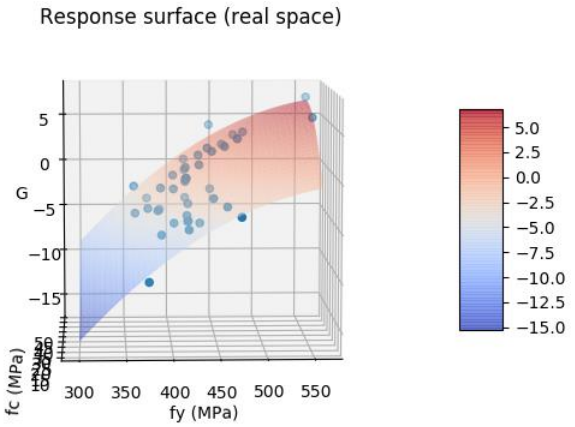


*Figure G33. Response surface (real space).*

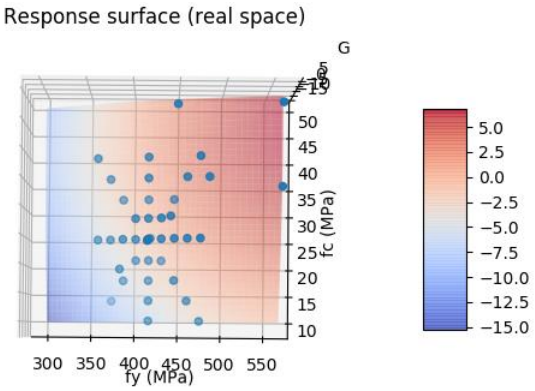


*Figure G34. Response surface (real space).*

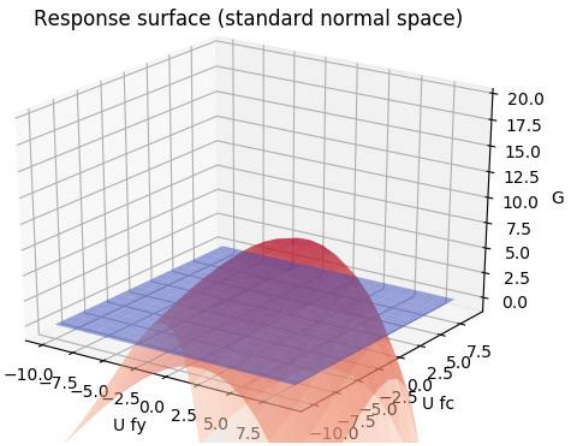


*Figure G35. Response surface (standard normal space).*

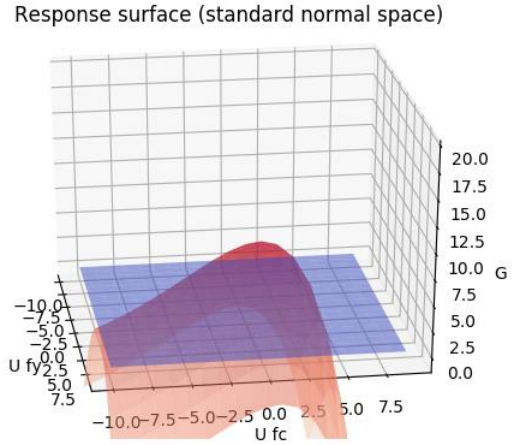


*Figure G36. Response surface (standard normal space).*

Step 5:

The design point is determined using a FORM in combination with the obtained response surface in step 4.

1. Now FORM is used to obtain the first iteration of the design point. This is shown figures G37 and G38. The coordinates of the design point in the standard normal space $\boldsymbol{U}_{1,*}$, the coordinates in of the design point in the real space $\boldsymbol{X}_{1,*}$ the reliability index $\beta_{1,R}$ and the sensitivity factors $\alpha_{1,R}$ are:

$$\boldsymbol{U}_{1,*} = \begin{bmatrix} -5.65 \\ -3.45 \end{bmatrix} \qquad \boldsymbol{X}_{1,*} = \begin{bmatrix} 421.7 \\ 28.4 \end{bmatrix} \qquad \beta_{1,R} = 6.62 \qquad \alpha_{1,R} = \begin{bmatrix} 0.853 \\ 0.521 \end{bmatrix}$$

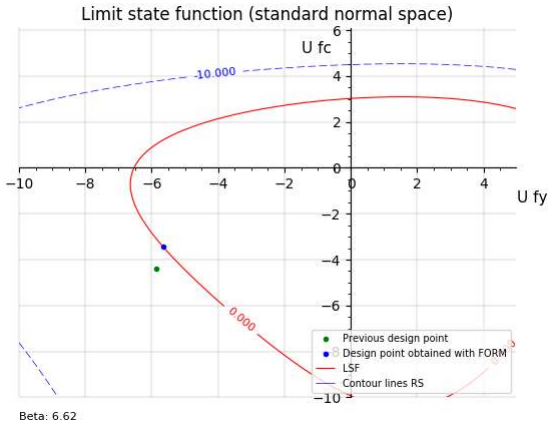


*Figure G37. Limit state function (standard normal space).*

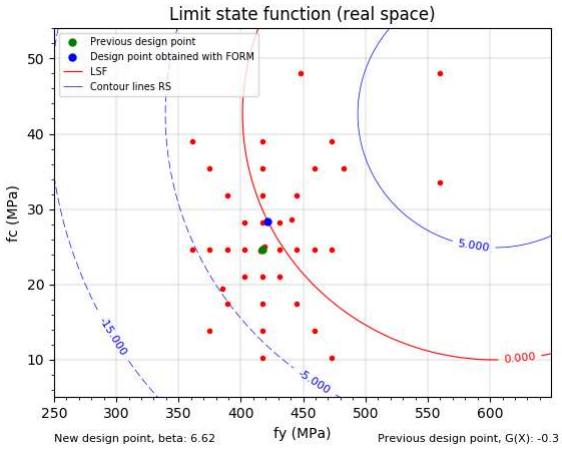


*Figure G38. Limit state function (real space).*

2. However there is still no convergence of the design point since $\bar{G}(\boldsymbol{X}_{1,*}) = 2.7$. Therefore several iteration were performed. The response surface has changed due to the added sample points and is given below.

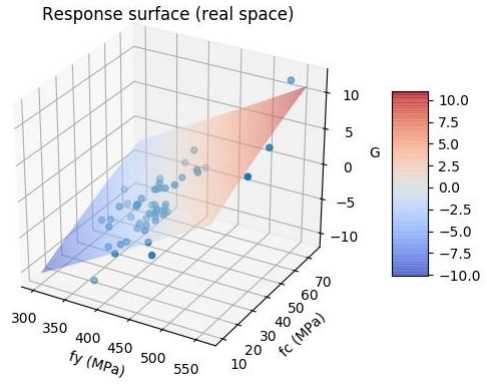


*Figure G38. Design 3: response surface (real space).*

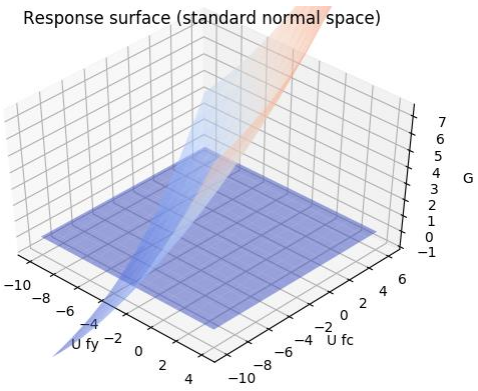


*Figure G39. Design 3: response surface (standard normal space).*

The higher strength class C40 used in design 3 leads to a portal frame, which is very sensitive for a ductile or a brittle failure depending on the rotational capacity of corner D. This results in a large spreading of the obtained structural resistance for sample points close to each other. Therefore the fit of the response surface is not very accurate which is shown in figure G40 and G41.

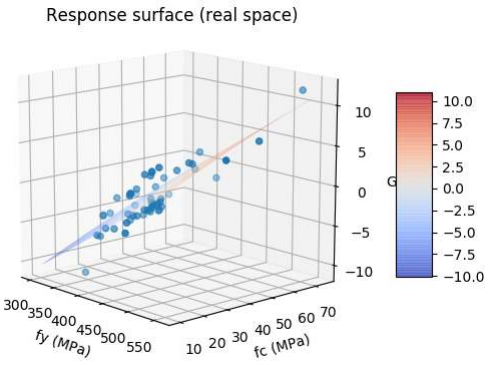


*Figure G40. Design 3: response surface (real space). A lot of spreading in sample points close to each other results in a bad fit of the response surface.*

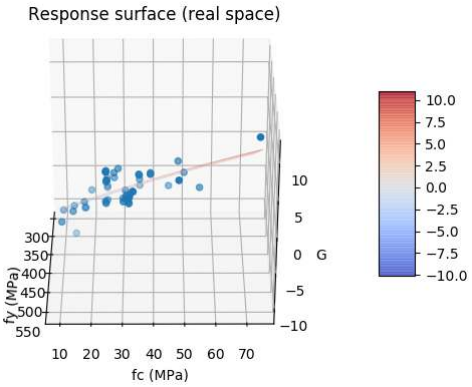


*Figure G41. Design 3: response surface (standard normal space). A lot of spreading in sample points close to each other results in a bad fit of the response surface.*

The design point is determined after several iterations using the FORM. This is shown figures G42 and G43. The coordinates of the design point in the standard normal space $\boldsymbol{U}_*$, the coordinates in of the design point in the real space $\boldsymbol{X}_*$, the reliability index $\beta_R$ and the sensitivity factors $\alpha_R$ are:

$$\boldsymbol{U}_* = \begin{bmatrix} -4.71 \\ -2.57 \end{bmatrix} \qquad \boldsymbol{X}_* = \begin{bmatrix} 442.0 \\ 32.35 \end{bmatrix} \qquad \beta_R = 5.37 \qquad \alpha_R = \begin{bmatrix} 0.878 \\ 0.479 \end{bmatrix}$$

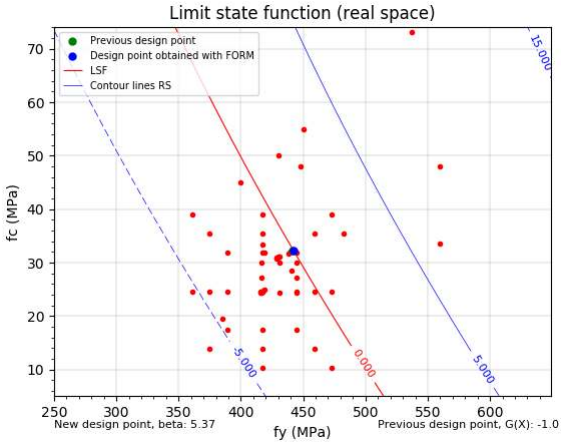


*Figure G42. Design 3: limit state function (real space). Previous design point lies below the new obtained design point.*

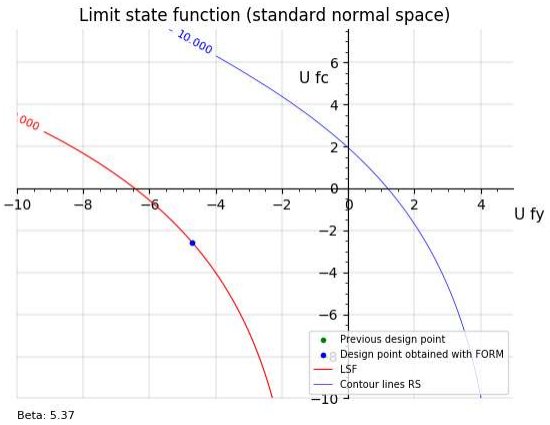


*Figure G43. Design 3: limit state function (standard normal space).*

## G.2 Case 2: rotational capacity corner D with reinforcement uncertainty due to fabrication

### G.2.1 Design 1

The safety format with the highest global design resistance, i.e. highest probability of failure, for design 1 is the ECOV method. The global design resistance according to the ECOV method is: $R_{SF} = 36.1$ kN. This leads to the following implicit LSF:

$$G(\boldsymbol{X}) = R(\boldsymbol{X}) - 36.1.$$

The response surface is constructed according to the approach of Zhao and Qiu (2013). The theory of the method is explained in detail in chapter 2.4.2. The number of stochastic variables for Case 2 is: $n = 2$. The first step is to perform three NLFE analysis to calculate the control point $\boldsymbol{X}_c$. Therefore NLFE analyses with mean $\overline{\boldsymbol{X}}$, low steel $\boldsymbol{X}_{f_y} = \overline{\boldsymbol{X}} - f\boldsymbol{\sigma}$, low concrete $\boldsymbol{X}_{f_c} = \overline{\boldsymbol{X}} - f\boldsymbol{\sigma}$ and a low cross-sectional area $\boldsymbol{X}_{A_s} = \overline{\boldsymbol{X}} - f\boldsymbol{\sigma}$ values are performed, where $f = 3$ is chosen. The results are presented below.

**The control point $\boldsymbol{X}_c$ is calculated below:**

step 1:
select $n + 1$ experimental points:

$$\overline{\boldsymbol{X}} = \begin{bmatrix} \mu_{f_y} \\ \mu_{f_c} \\ \mu_{A_s} \end{bmatrix}, \quad \boldsymbol{X}_{f_y} = \begin{bmatrix} \mu_{f_y} - f\sigma_{f_y} \\ \mu_{f_c} \\ \mu_{A_s} \end{bmatrix}, \quad \boldsymbol{X}_{f_c} = \begin{bmatrix} \mu_{f_y} \\ \mu_{f_c} - f\sigma_{f_c} \\ \mu_{A_s} \end{bmatrix} \quad \text{and} \quad \boldsymbol{X}_{A_s} = \begin{bmatrix} \mu_{f_y} \\ \mu_{f_c} \\ \mu_{A_s} - f\sigma_{A_s} \end{bmatrix}.$$

step 2:

$G(\overline{\boldsymbol{X}}) = 8.9$

$G(\boldsymbol{X}_{f_y}) = 3.8$

$G(\boldsymbol{X}_{f_c}) = 6.9$

$G(\boldsymbol{X}_{A_s}) = 5.4$

step 3:

$F(\boldsymbol{X}_{f_y}) = G(\overline{\boldsymbol{X}}) - G(\boldsymbol{X}_{f_y}) = 5.1$

$F(\boldsymbol{X}_{f_c}) = G(\overline{\boldsymbol{X}}) - G(\boldsymbol{X}_{f_c}) = 2.0$

$F(\boldsymbol{X}_{A_s}) = G(\overline{\boldsymbol{X}}) - G(\boldsymbol{X}_{A_s}) = 3.5$

step 4:

$$w_1 = \frac{F(\boldsymbol{X}_{f_y})}{F(\boldsymbol{X}_{f_y}) + F(\boldsymbol{X}_{f_c}) + F(\boldsymbol{X}_{A_s})} = 0.48$$

$$w_2 = \frac{F(\boldsymbol{X}_{f_c})}{F(\boldsymbol{X}_{f_y}) + F(\boldsymbol{X}_{f_c}) + F(\boldsymbol{X}_{A_s})} = 0.19$$

$$w_3 = \frac{F(\boldsymbol{X}_{A_s})}{F(\boldsymbol{X}_{f_y}) + F(\boldsymbol{X}_{f_c}) + F(\boldsymbol{X}_{A_s})} = 0.33$$

step 5:
The control point in the standard normal space is determined below. First the log-normal distributed variables are transformed to standard normal variables according to chapter 2.5.1.

$\sigma_{f_y} = 28$ MPa, $\mu_{f_y} = 560$ MPa,

$\sigma_{f_y,L} = \sqrt{\ln\left(\frac{\sigma_{f_y}^2}{\mu_{f_y}^2} + 1\right)} = 0.05$ MPa, $\mu_{f_y,L} = \ln \mu_{f_y} - \frac{1}{2}\sigma_{f_y,L}^2 = 6.327$ MPa

$\sigma_{f_c} = 5.7$ MPa, $\mu_{f_c} = 38$ MPa,

$\sigma_{f_c,L} = \sqrt{\ln\left(\frac{\sigma_{f_c}^2}{\mu_{f_c}^2} + 1\right)} = 0.149$ MPa, $\mu_{f_c,L} = \ln \mu_{f_c} - \frac{1}{2}\sigma_{f_c,L}^2 = 3.626$ MPa

$\sigma_{A_s} = 4.712$ mm$^2$ $\mu_{A_s} = 235.62$ mm$^2$,

$$\boldsymbol{U}_1 = \begin{bmatrix} \frac{\ln(\mu_{f_y} - f\sigma_{f_y}) - \mu_{f_{y,L}}}{\sigma_{f_{y,L}}} \\ \frac{\ln(\mu_{f_c}) - \mu_{f_{c,L}}}{\sigma_{f_{c,L}}} \\ \frac{\mu_{A_S} - \mu_{A_S}}{\sigma_{A_S}} \end{bmatrix}, \quad \boldsymbol{U}_2 = \begin{bmatrix} \frac{\ln(\mu_{f_y}) - \mu_{f_{y,L}}}{\sigma_{f_{y,L}}} \\ \frac{\ln(\mu_{f_c - f\,\sigma_{f_c,L}}) - \mu_{f_{c,L}}}{\sigma_{f_{c,L}}} \\ \frac{\mu_{A_S} - \mu_{A_S}}{\sigma_{A_S}} \end{bmatrix} \quad \text{and} \quad \boldsymbol{U}_3 = \begin{bmatrix} \frac{\ln(\mu_{f_y}) - \mu_{f_{y,L}}}{\sigma_{f_{y,L}}} \\ \frac{\ln(\mu_{f_c - f\,\sigma_{f_c,L}}) - \mu_{f_{c,L}}}{\sigma_{f_{c,L}}} \\ \frac{\mu_{A_S} - f\,\mu_{A_S}}{\sigma_{A_S}} \end{bmatrix}$$

The control point in the standard normal space:

$$\boldsymbol{U}_c = \sum_{i=1}^{n} w_i\, \boldsymbol{U}_i = \begin{bmatrix} -1.54 \\ -0.68 \\ -0.99 \end{bmatrix}$$

**The response surface and the real desing point are determined using the following steps:**

step 1:
The control point in the real space:

$$\boldsymbol{X}_c = \begin{bmatrix} \exp(-1.54\,\sigma_{f_{y,L}} + \mu_{f_{y,L}}) \\ \exp(-0.68\,\sigma_{f_{c,L}} + \mu_{f_{c,L}}) \\ -0.99\,\sigma_{A_S} + \mu_{A_S} \end{bmatrix} = \begin{bmatrix} 517.9 \\ 33.9 \\ 231.0 \end{bmatrix} \quad \text{and} \quad G(\boldsymbol{X_c}) = 5.6$$

step 2:

The initial design point is found with the same approach as shown in Case 1 using the control point.

step 3, 4 and 5:

Around the initial design point four sets of sample points with $f = 1.0; 1.5; 2.0$ are used to determine the response surface. After the initial design point was found several iteration where performed in comination with the FORM to obtain the real design point.

$$\boldsymbol{U}_* = \begin{bmatrix} -4.09 \\ -0.93 \\ -3.85 \end{bmatrix} \qquad \boldsymbol{X}_* = \begin{bmatrix} 455.96 \\ 32.7 \\ 217.5 \end{bmatrix} \qquad \beta_R = 5.69 \qquad \alpha_R = \begin{bmatrix} 0.718 \\ 0.163 \\ 0.677 \end{bmatrix}$$

### G.2.2 Design 2

The safety format with the highest global design resistance, i.e. highest probability of failure, for design 2 is the PFm method. The total global design resistance according to the PFm is: $R_{SF} = 43.7$ kN. This leads to the following implicit LSF:

$$G(\boldsymbol{X}) = R(\boldsymbol{X}) - 43.7.$$

The response surface is constructed according to the approach of Zhao and Qiu (2013). The theory of the method is explained in detail in chapter 2.4.2. The number of stochastic variables for Case 2 is: $n = 2$. The first step is to perform three NLFE analysis to calculate the control point $\boldsymbol{X}_c$. Therefore NLFE analyses with mean $\overline{\boldsymbol{X}}$, low steel $\boldsymbol{X}_{f_y} = \overline{\boldsymbol{X}} - f\boldsymbol{\sigma}$, low concrete $\boldsymbol{X}_{f_c} = \overline{\boldsymbol{X}} - f\boldsymbol{\sigma}$ and a low cross-sectional area $\boldsymbol{X}_{A_s} = \overline{\boldsymbol{X}} - f\boldsymbol{\sigma}$ values are performed, where $f = 4.2$ is chosen. The results are presented below.

**The control point $\boldsymbol{X}_c$ is calculated below:**

step 1:
select $n + 1$ experimental points:

$$\overline{\boldsymbol{X}} = \begin{bmatrix} \mu_{f_y} \\ \mu_{f_c} \\ \mu_{A_s} \end{bmatrix}, \qquad \boldsymbol{X}_{f_y} = \begin{bmatrix} \mu_{f_y} - f\sigma_{f_y} \\ \mu_{f_c} \\ \mu_{A_s} \end{bmatrix}, \quad \boldsymbol{X}_{f_c} = \begin{bmatrix} \mu_{f_y} \\ \mu_{f_c} - f\sigma_{f_c} \\ \mu_{A_s} \end{bmatrix} \quad \text{and} \quad \boldsymbol{X}_{A_s} = \begin{bmatrix} \mu_{f_y} \\ \mu_{f_c} \\ \mu_{A_s} - f\sigma_{A_s} \end{bmatrix}.$$

step 2:

$G(\overline{\boldsymbol{X}}) = 9.1$

$G(\boldsymbol{X}_{f_y}) = 1.6$

$G(\boldsymbol{X}_{f_c}) = 6.9$

$G(\boldsymbol{X}_{A_s}) = 2.4$

step 3:

$F(\boldsymbol{X}_{f_y}) = G(\overline{\boldsymbol{X}}) - G(\boldsymbol{X}_{f_y}) = 7.5$

$F(\boldsymbol{X}_{f_c}) = G(\overline{\boldsymbol{X}}) - G(\boldsymbol{X}_{f_c}) = 2.2$

$F(\boldsymbol{X}_{A_s}) = G(\overline{\boldsymbol{X}}) - G(\boldsymbol{X}_{A_s}) = 7.2$

step 4:

$$w_1 = \frac{F(\boldsymbol{X}_{f_y})}{F(\boldsymbol{X}_{f_y}) + F(\boldsymbol{X}_{f_c}) + F(\boldsymbol{X}_{A_s})} = 0.46$$

$$w_2 = \frac{F(\boldsymbol{X}_{f_c})}{F(\boldsymbol{X}_{f_y}) + F(\boldsymbol{X}_{f_c}) + F(\boldsymbol{X}_{A_s})} = 0.13$$

$$w_3 = \frac{F(\boldsymbol{X}_{A_s})}{F(\boldsymbol{X}_{f_y}) + F(\boldsymbol{X}_{f_c}) + F(\boldsymbol{X}_{A_s})} = 0.41$$

step 5:
The control point in the standard normal space is determined below. First the log-normal distributed variables are transformed to standard normal variables according to chapter 2.5.1.

$\sigma_{f_y} = 28$ MPa,

$\mu_{f_y} = 560$ MPa,

$$\sigma_{f_y,L} = \sqrt{\ln\left(\frac{\sigma_{f_y}^2}{\mu_{f_y}^2} + 1\right)} = 0.05 \text{ MPa},$$

$$\mu_{f_y,L} = \ln \mu_{f_y} - \frac{1}{2}\sigma_{f_y,L}^2 = 6.327 \text{ MPa}$$

$\sigma_{f_c} = 7.2$ MPa,

$\mu_{f_c} = 38$ MPa,

$$\sigma_{f_c,L} = \sqrt{\ln\left(\frac{\sigma_{f_c}^2}{\mu_{f_c}^2} + 1\right)} = 0.149 \text{ MPa},$$

$$\mu_{f_c,L} = \ln \mu_{f_c} - \frac{1}{2}\sigma_{f_c,L}^2 = 3.626 \text{ MPa}$$

$\sigma_{A_s} = 5.701$ mm²

$\mu_{A_s} = 285.1$ mm²,

$$\boldsymbol{U}_1 = \begin{bmatrix} \frac{\ln(\mu_{f_y} - f\sigma_{f_y}) - \mu_{f_{y,L}}}{\sigma_{f_{y,L}}} \\ \frac{\ln(\mu_{f_c}) - \mu_{f_{c,L}}}{\sigma_{f_{c,L}}} \\ \frac{\mu_{A_S} - \mu_{A_S}}{\sigma_{A_S}} \end{bmatrix}, \quad \boldsymbol{U}_2 = \begin{bmatrix} \frac{\ln(\mu_{f_y}) - \mu_{f_{y,L}}}{\sigma_{f_{y,L}}} \\ \frac{\ln(\mu_{f_c - f\,\sigma_{f_{c,L}}}) - \mu_{f_{c,L}}}{\sigma_{f_{c,L}}} \\ \frac{\mu_{A_S} - \mu_{A_S}}{\sigma_{A_S}} \end{bmatrix} \quad \text{and} \quad \boldsymbol{U}_3 = \begin{bmatrix} \frac{\ln(\mu_{f_y}) - \mu_{f_{y,L}}}{\sigma_{f_{y,L}}} \\ \frac{\ln(\mu_{f_c - f\,\sigma_{f_{c,L}}}) - \mu_{f_{c,L}}}{\sigma_{f_{c,L}}} \\ \frac{\mu_{A_S} - f\,\mu_{A_S}}{\sigma_{A_S}} \end{bmatrix}$$

The control point in the standard normal space:

$$\boldsymbol{U}_c = \sum_{i=1}^{n} w_i\, \boldsymbol{U}_i = \begin{bmatrix} -2.13 \\ -0.82 \\ -1.72 \end{bmatrix}$$

**<u>The response surface and the real desing point are determined using the following steps:</u>**

<u>step 1:</u>
The control point in the real space:

$$\boldsymbol{X}_c = \begin{bmatrix} \exp(-2.13\,\sigma_{f_{y,L}} + \mu_{f_{y,L}}) \\ \exp(-0.82\,\sigma_{f_{c,L}} + \mu_{f_{c,L}}) \\ -1.72\,\sigma_{A_s} + \mu_{A_s} \end{bmatrix} = \begin{bmatrix} 502.8 \\ 33.3 \\ 275.3 \end{bmatrix} \quad \text{and} \quad G(\boldsymbol{X_c}) = 4.9$$

<u>step 2:</u>

The initial design point is found with the same approach as shown in Case 1 using the control point.

<u>step 3, 4 and 5:</u>

Around the initial design point four sets of sample points with $f = 1.0; 1.5; 2.0$ are used to determine the response surface. After the initial design point was found several iteration where performed in comination with the FORM to obtain the real design point.

$$\boldsymbol{U}_* = \begin{bmatrix} -3.615 \\ -2.259 \\ -2.736 \end{bmatrix} \qquad \boldsymbol{X}_* = \begin{bmatrix} 466.9 \\ 26.8 \\ 269.5 \end{bmatrix} \qquad \beta_R = 5.07 \qquad \alpha_R = \begin{bmatrix} 0.714 \\ 0.446 \\ 0.540 \end{bmatrix}$$

### G.2.3 Design 3

The safety format with the highest global design resistance, i.e. highest probability of failure, for design 3 is the PFm method. The total global design resistance according to the PFm is: $R_{SF} = 37.0$ kN. This leads to the following implicit LSF:

$$G(\boldsymbol{X}) = R(\boldsymbol{X}) - 37.0.$$

The response surface is constructed according to the approach of Zhao and Qiu (2013). The theory of the method is explained in detail in chapter 2.4.2. The number of stochastic variables for Case 2 is: $n = 2$. The first step is to perform three NLFE analysis to calculate the control point $\boldsymbol{X}_c$. Therefore NLFE analyses with mean $\overline{\boldsymbol{X}}$, low steel $\boldsymbol{X}_{f_y} = \overline{\boldsymbol{X}} - f\boldsymbol{\sigma}$, low concrete $\boldsymbol{X}_{f_c} = \overline{\boldsymbol{X}} - f\boldsymbol{\sigma}$ and a low cross-sectional area $\boldsymbol{X}_{A_s} = \overline{\boldsymbol{X}} - f\boldsymbol{\sigma}$ values are performed, where $f = 3.9$ is chosen. The results are presented in the below.

**The control point $\boldsymbol{X}_c$ is calculated below:**

step 1:
select $n + 1$ experimental points:

$$\overline{\boldsymbol{X}} = \begin{bmatrix} \mu_{f_y} \\ \mu_{f_c} \\ \mu_{A_s} \end{bmatrix}, \quad \boldsymbol{X}_{f_y} = \begin{bmatrix} \mu_{f_y} - f\sigma_{f_y} \\ \mu_{f_c} \\ \mu_{A_s} \end{bmatrix}, \quad \boldsymbol{X}_{f_c} = \begin{bmatrix} \mu_{f_y} \\ \mu_{f_c} - f\sigma_{f_c} \\ \mu_{A_s} \end{bmatrix} \quad \text{and} \quad \boldsymbol{X}_{A_s} = \begin{bmatrix} \mu_{f_y} \\ \mu_{f_c} \\ \mu_{A_s} - f\sigma_{A_s} \end{bmatrix}.$$

step 2:

$G(\overline{\boldsymbol{X}}) = 7.0$

$G(\boldsymbol{X}_{f_y}) = 4.1$

$G(\boldsymbol{X}_{f_c}) = 6.6$

$G(\boldsymbol{X}_{A_s}) = -0.8$

step 3:

$F(\boldsymbol{X}_{f_y}) = G(\overline{\boldsymbol{X}}) - G(\boldsymbol{X}_{f_y}) = 2.9$

$F(\boldsymbol{X}_{f_c}) = G(\overline{\boldsymbol{X}}) - G(\boldsymbol{X}_{f_c}) = 0.4$

$F(\boldsymbol{X}_{A_s}) = G(\overline{\boldsymbol{X}}) - G(\boldsymbol{X}_{A_s}) = 7.8$

step 4:

$$w_1 = \frac{F(\boldsymbol{X}_{f_y})}{F(\boldsymbol{X}_{f_y}) + F(\boldsymbol{X}_{f_c}) + F(\boldsymbol{X}_{A_s})} = 0.26$$

$$w_2 = \frac{F(\boldsymbol{X}_{f_c})}{F(\boldsymbol{X}_{f_y}) + F(\boldsymbol{X}_{f_c}) + F(\boldsymbol{X}_{A_s})} = 0.04$$

$$w_3 = \frac{F(\boldsymbol{X}_{A_s})}{F(\boldsymbol{X}_{f_y}) + F(\boldsymbol{X}_{f_c}) + F(\boldsymbol{X}_{A_s})} = 0.70$$

step 5:
The control point in the standard normal space is determined below. First the log-normal distributed variables are transformed to standard normal variables according to chapter 2.5.1.

$\sigma_{f_y} = 28$ MPa,

$\mu_{f_y} = 560$ MPa,

$$\sigma_{f_y,L} = \sqrt{\ln\left(\frac{\sigma_{f_y}^2}{\mu_{f_y}^2} + 1\right)} = 0.05 \text{ MPa},$$

$$\mu_{f_y,L} = \ln \mu_{f_y} - \frac{1}{2}\sigma_{f_y,L}^2 = 6.327 \text{ MPa}$$

$\sigma_{f_c} = 5.7$ MPa,

$\mu_{f_c} = 48$ MPa,

$$\sigma_{f_c,L} = \sqrt{\ln\left(\frac{\sigma_{f_c}^2}{\mu_{f_c}^2} + 1\right)} = 0.149 \text{ MPa},$$

$$\mu_{f_c,L} = \ln \mu_{f_c} - \frac{1}{2}\sigma_{f_c,L}^2 = 3.871 \text{ MPa}$$

$\sigma_{A_s} = 4.712$ mm$^2$

$\mu_{A_s} = 235.62$ mm$^2$,

$$\boldsymbol{U}_1 = \begin{bmatrix} \frac{\ln(\mu_{f_y} - f\sigma_{f_y}) - \mu_{f_{y,L}}}{\sigma_{f_{y,L}}} \\ \frac{\ln(\mu_{f_c}) - \mu_{f_{c,L}}}{\sigma_{f_{c,L}}} \\ \frac{\mu_{A_S} - \mu_{A_S}}{\sigma_{A_S}} \end{bmatrix}, \quad \boldsymbol{U}_2 = \begin{bmatrix} \frac{\ln(\mu_{f_y}) - \mu_{f_{y,L}}}{\sigma_{f_{y,L}}} \\ \frac{\ln(\mu_{f_c - f\,\sigma_{f_{c,L}}}) - \mu_{f_{c,L}}}{\sigma_{f_{c,L}}} \\ \frac{\mu_{A_S} - \mu_{A_S}}{\sigma_{A_S}} \end{bmatrix} \quad \text{and} \quad \boldsymbol{U}_3 = \begin{bmatrix} \frac{\ln(\mu_{f_y}) - \mu_{f_{y,L}}}{\sigma_{f_{y,L}}} \\ \frac{\ln(\mu_{f_c - f\,\sigma_{f_{c,L}}}) - \mu_{f_{c,L}}}{\sigma_{f_{c,L}}} \\ \frac{\mu_{A_S} - f\,\mu_{A_S}}{\sigma_{A_S}} \end{bmatrix}$$

The control point in the standard normal space:

$$\boldsymbol{U}_c = \sum_{i=1}^{n} w_i\, \boldsymbol{U}_i = \begin{bmatrix} -1.11 \\ -1.70 \\ -2.74 \end{bmatrix}$$

**The response surface and the real desing point are determined using the following steps:**

step 1:
The control point in the real space:

$$\boldsymbol{X}_c = \begin{bmatrix} \exp(-1.11\,\sigma_{f_{y,L}} + \mu_{f_{y,L}}) \\ \exp(-1.70\,\sigma_{f_{c,L}} + \mu_{f_{c,L}}) \\ -2.74\,\sigma_{A_s} + \mu_{A_s} \end{bmatrix} = \begin{bmatrix} 529.1 \\ 36.8 \\ 222.7 \end{bmatrix} \quad \text{and} \quad G(\boldsymbol{X_c}) = 5.2$$

step 2:

The initial design point is found with the same approach as shown in Case 1 using the control point.

step 3, 4 and 5:

Around the initial design point four sets of sample points with $f = 1.0; 1.5; 2.0$ are used to determine the response surface. After the initial design point was found several iteration where performed in comination with the FORM to obtain the real design point.

$$\boldsymbol{U}_* = \begin{bmatrix} -4.191 \\ -1.571 \\ -4.015 \end{bmatrix} \qquad \boldsymbol{X}_* = \begin{bmatrix} 453.6 \\ 37.6 \\ 216.7 \end{bmatrix} \qquad \beta_R = 6.01 \qquad \alpha_R = \begin{bmatrix} 0.697 \\ 0.261 \\ 0.668 \end{bmatrix}$$

## G.3 Case 3: rotational capacity corner D with uncertainty in the reinforcement detailing

### G.3.1 Design 1

The safety format with the highest global design resistance, i.e. highest probability of failure, for design 1 is the ECOV method. The global design resistance according to the ECOV method is: $R_{SF} = 36.1$ kN. This leads to the following implicit LSF:

$$G(\boldsymbol{X}) = R(\boldsymbol{X}) - 36.1.$$

The response surface is constructed according to the approach of Zhao and Qiu (2013). The theory of the method is explained in detail in chapter 2.4.2. The number of stochastic variables for Case 2 is: $n = 2$. The first step is to perform three NLFE analysis to calculate the control point $\boldsymbol{X}_c$. Therefore NLFE analyses with mean $\overline{\boldsymbol{X}}$, low steel $\boldsymbol{X}_{f_y} = \overline{\boldsymbol{X}} - f\boldsymbol{\sigma}$, low concrete $\boldsymbol{X}_{f_c} = \overline{\boldsymbol{X}} - f\boldsymbol{\sigma}$ and a low cross-sectional area $\boldsymbol{X}_{A_s} = \overline{\boldsymbol{X}} - f\boldsymbol{\sigma}$ values are performed, where $f = 3$ is chosen. The results are presented in the below.

**The control point $\boldsymbol{X}_c$ is calculated below:**

step 1:
select $n + 1$ experimental points:

$$\overline{\boldsymbol{X}} = \begin{bmatrix} \mu_{f_y} \\ \mu_{f_c} \\ \mu_{A_s} \end{bmatrix}, \quad \boldsymbol{X}_{f_y} = \begin{bmatrix} \mu_{f_y} - f\sigma_{f_y} \\ \mu_{f_c} \\ \mu_{A_s} \end{bmatrix}, \quad \boldsymbol{X}_{f_c} = \begin{bmatrix} \mu_{f_y} \\ \mu_{f_c} - f\sigma_{f_c} \\ \mu_{A_s} \end{bmatrix} \quad \text{and} \quad \boldsymbol{X}_{A_s} = \begin{bmatrix} \mu_{f_y} \\ \mu_{f_c} \\ \mu_{A_s} - f\sigma_{A_s} \end{bmatrix}.$$

step 2:

$G(\overline{\boldsymbol{X}}) = 8.9$

$G(\boldsymbol{X}_{f_y}) = 3.8$

$G(\boldsymbol{X}_{f_c}) = 6.9$

$G(\boldsymbol{X}_{A_s}) = 2.1$

step 3:

$F(\boldsymbol{X}_{f_y}) = G(\overline{\boldsymbol{X}}) - G(\boldsymbol{X}_{f_y}) = 5.1$

$F(\boldsymbol{X}_{f_c}) = G(\overline{\boldsymbol{X}}) - G(\boldsymbol{X}_{f_c}) = 2.0$

$F(\boldsymbol{X}_{A_s}) = G(\overline{\boldsymbol{X}}) - G(\boldsymbol{X}_{A_s}) = 6.8$

step 4:

$$w_1 = \frac{F(\boldsymbol{X}_{f_y})}{F(\boldsymbol{X}_{f_y}) + F(\boldsymbol{X}_{f_c}) + F(\boldsymbol{X}_{A_s})} = 0.37$$

$$w_2 = \frac{F(\boldsymbol{X}_{f_c})}{F(\boldsymbol{X}_{f_y}) + F(\boldsymbol{X}_{f_c}) + F(\boldsymbol{X}_{A_s})} = 0.14$$

$$w_3 = \frac{F(\boldsymbol{X}_{A_s})}{F(\boldsymbol{X}_{f_y}) + F(\boldsymbol{X}_{f_c}) + F(\boldsymbol{X}_{A_s})} = 0.49$$

step 5:
The control point in the standard normal space is determined below. First the log-normal distributed variables are transformed to standard normal variables according to chapter 2.5.1.

$\sigma_{f_y} = 28$ MPa, $\quad \mu_{f_y} = 560$ MPa,

$$\sigma_{f_y,L} = \sqrt{\ln\left(\frac{\sigma_{f_y}^2}{\mu_{f_y}^2} + 1\right)} = 0.05 \text{ MPa}, \quad \mu_{f_y,L} = \ln \mu_{f_y} - \frac{1}{2}\sigma_{f_y,L}^2 = 6.327 \text{ MPa}$$

$\sigma_{f_c} = 5.7$ MPa, $\quad \mu_{f_c} = 38$ MPa,

$$\sigma_{f_c,L} = \sqrt{\ln\left(\frac{\sigma_{f_c}^2}{\mu_{f_c}^2} + 1\right)} = 0.149 \text{ MPa}, \quad \mu_{f_c,L} = \ln \mu_{f_c} - \frac{1}{2}\sigma_{f_c,L}^2 = 3.626 \text{ MPa}$$

$\sigma_{A_s} = 23.56$ mm$^2$ $\quad \mu_{A_s} = 235.62$ mm$^2$,

$$\boldsymbol{U}_1 = \begin{bmatrix} \frac{\ln\left(\mu_{f_y} - f\sigma_{f_y}\right) - \mu_{f_y,L}}{\sigma_{f_y,L}} \\ \frac{\ln(\mu_{f_c}) - \mu_{f_c,L}}{\sigma_{f_c,L}} \\ \frac{\mu_{A_s} - \mu_{A_s}}{\sigma_{A_s}} \end{bmatrix}, \quad \boldsymbol{U}_2 = \begin{bmatrix} \frac{\ln\left(\mu_{f_y}\right) - \mu_{f_y,L}}{\sigma_{f_y,L}} \\ \frac{\ln\left(\mu_{f_c - f\,\sigma_{f_c,L}}\right) - \mu_{f_c,L}}{\sigma_{f_c,L}} \\ \frac{\mu_{A_s} - \mu_{A_s}}{\sigma_{A_s}} \end{bmatrix} \quad \text{and} \quad \boldsymbol{U}_3 = \begin{bmatrix} \frac{\ln\left(\mu_{f_y}\right) - \mu_{f_y,L}}{\sigma_{f_y,L}} \\ \frac{\ln\left(\mu_{f_c - f\,\sigma_{f_c,L}}\right) - \mu_{f_c,L}}{\sigma_{f_c,L}} \\ \frac{\mu_{A_s} - f\,\mu_{A_s}}{\sigma_{A_s}} \end{bmatrix}$$

The control point in the standard normal space:

$$\boldsymbol{U}_c = \sum_{i=1}^{n} w_i\, \boldsymbol{U}_i = \begin{bmatrix} -1.17 \\ -0.50 \\ -1.47 \end{bmatrix}$$

**The response surface and the real desing point are determined using the following steps:**

step 1:
The control point in the real space:

$$\boldsymbol{X}_c = \begin{bmatrix} \exp(-1.17\,\sigma_{f_y,L} + \mu_{f_y,L}) \\ \exp(-0.50\,\sigma_{f_c,L} + \mu_{f_c,L}) \\ -1.47\sigma_{A_s} + \mu_{A_s} \end{bmatrix} = \begin{bmatrix} 527.6 \\ 34.9 \\ 201.0 \end{bmatrix} \quad \text{and} \quad G(\boldsymbol{X_c}) = 1.6$$

step 2:

The initial design point is found with the same approach as shown in Case 1 using the control point.

step 3, 4 and 5:

Around the initial design point four sets of sample points with $f = 1.0; 1.5; 2.0$ are used to determine the response surface. After the initial design point was found several iteration where performed in comination with the FORM to obtain the real design point.

$$\boldsymbol{U}_* = \begin{bmatrix} -0.97 \\ -0.43 \\ -1.94 \end{bmatrix} \qquad \boldsymbol{X}_* = \begin{bmatrix} 532.9 \\ 35.2 \\ 189.9 \end{bmatrix} \qquad \beta_{2,R} = 2.21 \qquad \alpha_R = \begin{bmatrix} 0.438 \\ 0.195 \\ 0.878 \end{bmatrix}$$

### G.3.2 Design 2

The safety format with the highest global design resistance, i.e. highest probability of failure, for design 2 is the PFm method. The total global design resistance according to the PFm is: $R_{SF} = 43.7$ kN. This leads to the following implicit LSF:

$$G(\boldsymbol{X}) = R(\boldsymbol{X}) - 43.7.$$

The response surface is constructed according to the approach of Zhao and Qiu (2013). The theory of the method is explained in detail in chapter 2.4.2. The number of stochastic variables for Case 2 is: $n = 2$. The first step is to perform three NLFE analysis to calculate the control point $\boldsymbol{X}_c$. Therefore NLFE analyses with mean $\overline{\boldsymbol{X}}$, low steel $\boldsymbol{X}_{f_y} = \overline{\boldsymbol{X}} - f\boldsymbol{\sigma}$, low concrete $\boldsymbol{X}_{f_c} = \overline{\boldsymbol{X}} - f\boldsymbol{\sigma}$ and a low cross-sectional area $\boldsymbol{X}_{A_s} = \overline{\boldsymbol{X}} - f\boldsymbol{\sigma}$ values are performed, where $f = 4.2$ is chosen. The results are presented below.

**The control point $\boldsymbol{X}_c$ is calculated below:**

step 1:
select $n + 1$ experimental points:

$$\overline{\boldsymbol{X}} = \begin{bmatrix} \mu_{f_y} \\ \mu_{f_c} \\ \mu_{A_s} \end{bmatrix}, \qquad \boldsymbol{X}_{f_y} = \begin{bmatrix} \mu_{f_y} - f\sigma_{f_y} \\ \mu_{f_c} \\ \mu_{A_s} \end{bmatrix}, \quad \boldsymbol{X}_{f_c} = \begin{bmatrix} \mu_{f_y} \\ \mu_{f_c} - f\sigma_{f_c} \\ \mu_{A_s} \end{bmatrix} \quad \text{and} \quad \boldsymbol{X}_{A_s} = \begin{bmatrix} \mu_{f_y} \\ \mu_{f_c} \\ \mu_{A_s} - f\sigma_{A_s} \end{bmatrix}.$$

step 2:

$G(\overline{\boldsymbol{X}}) = 9.1$

$G(\boldsymbol{X}_{f_y}) = 1.6$

$G(\boldsymbol{X}_{f_c}) = 6.9$

$G(\boldsymbol{X}_{A_s}) = -10.3$

step 3:

$F(\boldsymbol{X}_{f_y}) = G(\overline{\boldsymbol{X}}) - G(\boldsymbol{X}_{f_y}) = 7.5$

$F(\boldsymbol{X}_{f_c}) = G(\overline{\boldsymbol{X}}) - G(\boldsymbol{X}_{f_c}) = 2.2$

$F(\boldsymbol{X}_{A_s}) = G(\overline{\boldsymbol{X}}) - G(\boldsymbol{X}_{A_s}) = 19.4$

step 4:

$$w_1 = \frac{F(\boldsymbol{X}_{f_y})}{F(\boldsymbol{X}_{f_y}) + F(\boldsymbol{X}_{f_c}) + F(\boldsymbol{X}_{A_s})} = 0.26$$

$$w_2 = \frac{F(\boldsymbol{X}_{f_c})}{F(\boldsymbol{X}_{f_y}) + F(\boldsymbol{X}_{f_c}) + F(\boldsymbol{X}_{A_s})} = 0.08$$

$$w_3 = \frac{F(\boldsymbol{X}_{A_s})}{F(\boldsymbol{X}_{f_y}) + F(\boldsymbol{X}_{f_c}) + F(\boldsymbol{X}_{A_s})} = 0.67$$

step 5:
The control point in the standard normal space is determined below. First the log-normal distributed variables are transformed to standard normal variables according to chapter 2.5.1.

$\sigma_{f_y} = 28$ MPa,

$\mu_{f_y} = 560$ MPa,

$$\sigma_{f_{y,L}} = \sqrt{\ln\left(\frac{\sigma_{f_y}^2}{\mu_{f_y}^2} + 1\right)} = 0.05 \text{ MPa},$$

$$\mu_{f_{y,L}} = \ln \mu_{f_y} - \frac{1}{2}\sigma_{f_{y,L}}^2 = 6.327 \text{ MPa}$$

$\sigma_{f_c} = 7.2$ MPa,

$\mu_{f_c} = 38$ MPa,

$$\sigma_{f_{c,L}} = \sqrt{\ln\left(\frac{\sigma_{f_c}^2}{\mu_{f_c}^2} + 1\right)} = 0.149 \text{ MPa},$$

$$\mu_{f_{c,L}} = \ln \mu_{f_c} - \frac{1}{2}\sigma_{f_{c,L}}^2 = 3.626 \text{ MPa}$$

$\sigma_{A_s} = 28.51$ mm²

$\mu_{A_s} = 285.1$ mm²,

$$\boldsymbol{U}_1 = \begin{bmatrix} \frac{\ln(\mu_{f_y} - f\sigma_{f_y}) - \mu_{f_y,L}}{\sigma_{f_y,L}} \\ \frac{\ln(\mu_{f_c}) - \mu_{f_c,L}}{\sigma_{f_c,L}} \\ \frac{\mu_{A_s} - \mu_{A_s}}{\sigma_{A_s}} \end{bmatrix}, \quad \boldsymbol{U}_2 = \begin{bmatrix} \frac{\ln(\mu_{f_y}) - \mu_{f_y,L}}{\sigma_{f_y,L}} \\ \frac{\ln(\mu_{f_c - f\,\sigma_{f_c,L}}) - \mu_{f_c,L}}{\sigma_{f_c,L}} \\ \frac{\mu_{A_s} - \mu_{A_s}}{\sigma_{A_s}} \end{bmatrix} \quad \text{and} \quad \boldsymbol{U}_3 = \begin{bmatrix} \frac{\ln(\mu_{f_y}) - \mu_{f_y,L}}{\sigma_{f_y,L}} \\ \frac{\ln(\mu_{f_c - f\,\sigma_{f_c,L}}) - \mu_{f_c,L}}{\sigma_{f_c,L}} \\ \frac{\mu_{A_s} - f\,\mu_{A_s}}{\sigma_{A_s}} \end{bmatrix}$$

The control point in the standard normal space:

$$\boldsymbol{U}_c = \sum_{i=1}^{n} w_i\, \boldsymbol{U}_i = \begin{bmatrix} -1.19 \\ -0.43 \\ -2.80 \end{bmatrix}$$

**The response surface and the real desing point are determined using the following steps:**

step 1:

The control point in the real space:

$$\boldsymbol{X}_c = \begin{bmatrix} \exp(-1.19\,\sigma_{f_y,L} + \mu_{f_y,L}) \\ \exp(-0.43\,\sigma_{f_c,L} + \mu_{f_c,L}) \\ -2.80\,\sigma_{A_s} + \mu_{A_s} \end{bmatrix} = \begin{bmatrix} 527.0 \\ 36.16 \\ 231.7 \end{bmatrix} \quad \text{and} \quad G(\boldsymbol{X_c}) = -4.5$$

step 2:

The initial design point is found with the same approach as shown in Case 1 using the control point.

step 3, 4 and 5:

Around the initial design point four sets of sample points with $f = 1.0; 1.5; 2.0$ are used to determine the response surface. After the initial design point was found several iteration where performed in comination with the FORM to obtain the real design point.

$$\boldsymbol{U}_* = \begin{bmatrix} -0.6418 \\ 0.000596 \\ -2.0851 \end{bmatrix} \quad \boldsymbol{X}_* = \begin{bmatrix} 541.6 \\ 37.6 \\ 225.7 \end{bmatrix} \quad \beta_{2,R} = 2.18 \quad \alpha_R = \begin{bmatrix} 0.294 \\ -0.00027 \\ 0.956 \end{bmatrix}$$

### G.3.3 Design 3

The safety format with the highest global design resistance, i.e. highest probability of failure, for design 3 is the PFm method. The total global design resistance according to the PFm is: $R_{SF} = 37.0$ kN. This leads to the following implicit LSF:

$$G(\boldsymbol{X}) = R(\boldsymbol{X}) - 37.0.$$

The response surface is constructed according to the approach of Zhao and Qiu (2013). The theory of the method is explained in detail in chapter 2.4.2. The number of stochastic variables for Case 2 is: $n = 2$. The first step is to perform three NLFE analysis to calculate the control point $\boldsymbol{X}_c$. Therefore NLFE analyses with mean $\overline{\boldsymbol{X}}$, low steel $\boldsymbol{X}_{f_y} = \overline{\boldsymbol{X}} - f\boldsymbol{\sigma}$, low concrete $\boldsymbol{X}_{f_c} = \overline{\boldsymbol{X}} - f\boldsymbol{\sigma}$ and a low cross-sectional area $\boldsymbol{X}_{A_s} = \overline{\boldsymbol{X}} - f\boldsymbol{\sigma}$ values are performed, where $f = 3.9$ is chosen. The results are presented below.

**The control point $\boldsymbol{X}_c$ is calculated below:**

step 1:
select $n + 1$ experimental points:

$$\overline{\boldsymbol{X}} = \begin{bmatrix} \mu_{f_y} \\ \mu_{f_c} \\ \mu_{A_s} \end{bmatrix}, \qquad \boldsymbol{X}_{f_y} = \begin{bmatrix} \mu_{f_y} - f\sigma_{f_y} \\ \mu_{f_c} \\ \mu_{A_s} \end{bmatrix}, \quad \boldsymbol{X}_{f_c} = \begin{bmatrix} \mu_{f_y} \\ \mu_{f_c} - f\sigma_{f_c} \\ \mu_{A_s} \end{bmatrix} \quad \text{and} \quad \boldsymbol{X}_{A_s} = \begin{bmatrix} \mu_{f_y} \\ \mu_{f_c} \\ \mu_{A_s} - f\sigma_{A_s} \end{bmatrix}.$$

step 2:

$G(\overline{\boldsymbol{X}}) = 7.0$

$G(\boldsymbol{X}_{f_y}) = 4.1$

$G(\boldsymbol{X}_{f_c}) = 6.6$

$G(\boldsymbol{X}_{A_s}) = -3.8$

step 3:

$F(\boldsymbol{X}_{f_y}) = G(\overline{\boldsymbol{X}}) - G(\boldsymbol{X}_{f_y}) = 2.9$

$F(\boldsymbol{X}_{f_c}) = G(\overline{\boldsymbol{X}}) - G(\boldsymbol{X}_{f_c}) = 0.4$

$F(\boldsymbol{X}_{A_s}) = G(\overline{\boldsymbol{X}}) - G(\boldsymbol{X}_{A_s}) = 10.8$

step 4:

$$w_1 = \frac{F(\boldsymbol{X}_{f_y})}{F(\boldsymbol{X}_{f_y}) + F(\boldsymbol{X}_{f_c}) + F(\boldsymbol{X}_{A_s})} = 0.21$$

$$w_2 = \frac{F(\boldsymbol{X}_{f_c})}{F(\boldsymbol{X}_{f_y}) + F(\boldsymbol{X}_{f_c}) + F(\boldsymbol{X}_{A_s})} = 0.03$$

$$w_3 = \frac{F(\boldsymbol{X}_{A_s})}{F(\boldsymbol{X}_{f_y}) + F(\boldsymbol{X}_{f_c}) + F(\boldsymbol{X}_{A_s})} = 0.77$$

step 5:
The control point in the standard normal space is determined below. First the log-normal distributed variables are transformed to standard normal variables according to chapter 2.5.1.

$\sigma_{f_y} = 28$ MPa,

$\mu_{f_y} = 560$ MPa,

$\sigma_{f_y,L} = \sqrt{\ln\left(\frac{\sigma_{f_y}^2}{\mu_{f_y}^2} + 1\right)} = 0.05$ MPa,

$\mu_{f_y,L} = \ln \mu_{f_y} - \frac{1}{2}\sigma_{f_y,L}^2 = 6.327$ MPa

$\sigma_{f_c} = 5.7$ MPa,

$\mu_{f_c} = 48$ MPa,

$\sigma_{f_c,L} = \sqrt{\ln\left(\frac{\sigma_{f_c}^2}{\mu_{f_c}^2} + 1\right)} = 0.149$ MPa,

$\mu_{f_c,L} = \ln \mu_{f_c} - \frac{1}{2}\sigma_{f_c,L}^2 = 3.871$ MPa

$\sigma_{A_s} = 23.56$ mm$^2$

$\mu_{A_s} = 235.62$ mm$^2$,

$$\boldsymbol{U}_1 = \begin{bmatrix} \frac{\ln(\mu_{f_y} - f\sigma_{f_y}) - \mu_{f_{y,L}}}{\sigma_{f_{y,L}}} \\ \frac{\ln(\mu_{f_c}) - \mu_{f_{c,L}}}{\sigma_{f_{c,L}}} \\ \frac{\mu_{A_S} - \mu_{A_S}}{\sigma_{A_S}} \end{bmatrix}, \quad \boldsymbol{U}_2 = \begin{bmatrix} \frac{\ln(\mu_{f_y}) - \mu_{f_{y,L}}}{\sigma_{f_{y,L}}} \\ \frac{\ln(\mu_{f_c - f\,\sigma_{f_c,L}}) - \mu_{f_{c,L}}}{\sigma_{f_{c,L}}} \\ \frac{\mu_{A_S} - \mu_{A_S}}{\sigma_{A_S}} \end{bmatrix} \quad \text{and} \quad \boldsymbol{U}_3 = \begin{bmatrix} \frac{\ln(\mu_{f_y}) - \mu_{f_{y,L}}}{\sigma_{f_{y,L}}} \\ \frac{\ln(\mu_{f_c - f\,\sigma_{f_c,L}}) - \mu_{f_{c,L}}}{\sigma_{f_{c,L}}} \\ \frac{\mu_{A_S} - f\,\mu_{A_S}}{\sigma_{A_S}} \end{bmatrix}$$

The control point in the standard normal space:

$$\boldsymbol{U}_c = \sum_{i=1}^{n} w_i\, \boldsymbol{U}_i = \begin{bmatrix} -0.87 \\ -1.66 \\ -2.98 \end{bmatrix}$$

**The response surface is determined using the following steps:**

step 1:
The control point in the real space:

$$\boldsymbol{X}_c = \begin{bmatrix} \exp(-0.87\,\sigma_{f_{y,L}} + \mu_{f_{y,L}}) \\ \exp(-1.66\,\sigma_{f_{c,L}} + \mu_{f_{c,L}}) \\ -2.98\,\sigma_{A_S} + \mu_{A_S} \end{bmatrix} = \begin{bmatrix} 529.1 \\ 36.8 \\ 222.7 \end{bmatrix} \quad \text{and} \quad G(\boldsymbol{X_c}) = -2.8$$

step 2:

The initial design point is found with the same approach as shown in Case 1 using the control point.

step 3, 4 and 5:

Around the initial design point four sets of sample points with $f = 1.0; 1.5; 2.0$ are used to determine the response surface. After the initial design point was found several iteration where performed in comination with the FORM to obtain the real design point.

$$\boldsymbol{U}_* = \begin{bmatrix} -0.79 \\ -0.30 \\ -2.34 \end{bmatrix} \qquad \boldsymbol{X}_* = \begin{bmatrix} 537.7 \\ 45.4 \\ 180.5 \end{bmatrix} \qquad \beta_{2,R} = 2.49 \qquad \alpha_R = \begin{bmatrix} 0.317 \\ 0.120 \\ 0.941 \end{bmatrix}$$

# Appendix H Python scripts to perform NLFE analyses and processing results

## H.1 Python script to run NLFE analyses

In the example below a python script is written to perform three NLFE analyses in Diana 10.1. The NLFE models defined in Appendix D are used to change several input parameters.

```
##########################################################################

openProject( "C:/Users/..../ECOV/Three variables/Design 1/Portal Frame.dpf" )

##########################################################################

# parameters shear reinforcement
setParameter( "GEOMET", "Shear reinforcement", "REIEMB/CROSSE", ((2.0*0.25*1.5**2*3.141592654)*10**-6.0) )

##########################################################################

#NLFE analyses
copyAnalysis( "Nonlinear Main", "Nonlinear Main - Copy 1" )
renameAnalysis( "Nonlinear Main - Copy 1", "Main1" )

copyAnalysis( "Nonlinear Main", "Nonlinear Main - Copy 1" )
renameAnalysis( "Nonlinear Main - Copy 1", "Main2" )

copyAnalysis( "Nonlinear Main", "Nonlinear Main - Copy 1" )
renameAnalysis( "Nonlinear Main - Copy 1", "Main3" )
```

*Figure H1. Python code to open a project.*

The input parameters are given below. To run the three different analyses a for loop is used.

```
## Material input parameters

for i in range (3):

    i = i+1
#Mean strength values
    if i==1:
        if loadResults( "Main1", "C:/Users/....ECOV/Three variables/Design 1/Main1.dnb" ):
            loadResults( "Main1", "C:/Users/..../ECOV/Three variables/Design 1/Main1.dnb" )


        else:

        # parameters concrete
            setParameter( "MATERIAL", "Concrete", "LINEAR/ELASTI/YOUNG", (21500*(38/10.0)**(1.0/3.0)*10**6) )
            setParameter( "MATERIAL", "Concrete", "TENSIL/TENSTR", ((0.3*(38.0-8.0)**(2.0/3.0))*10**6) )
            setParameter( "MATERIAL", "Concrete", "TENSIL/GF1",  (73.0*(38.0)**0.18)  )
            setParameter( "MATERIAL", "Concrete", "COMPRS/COMSTR", 38.0e+6 )
            setParameter( "MATERIAL", "Concrete", "COMPRS/GC",  ((73.0*(38.0)**0.18)*250.0)  )
        # parameters longitudinal reinforcement
            setParameter( "MATERIAL", "Longitudinal reinforcement", "PLASTI/HARDI2/KAPSIG",
            [ -0.1138, -6.8e+08, 0, -5.6e+08, 0, 5.6e+08, 0.1138, 6.8e+08 ] )

        # parameters shear reinforcement
            setParameter( "MATERIAL", "Shear reinforcement", "PLASTI/HARDI2/KAPSIG",
            [ -0.1152, -5.1e+08, 0, -4.6e+08, 0, 4.6e+08, 0.1152, 5.1e+08 ] )

        # parameters longitudinal reinforcement
            setParameter( "GEOMET", "As longitudinal reinforcement", "REIEMB/CROSSE",
            ((3.0*0.25*10.0**2*3.141592654)*10**-6.0) )

            generateMesh( [] )

        # analysis
            runSolver( "Main1" )
            i=i-1
```

```
#Low steel strength
    elif i==2:
        if loadResults( "Main2", "C:/Users/..../ECOV/Three variables/Design 1/Main2.dnb" ):
            loadResults( "Main2", "C:/Users/..../ECOV/Three variables/Design 1/Main2.dnb" )


        else:

        # parameters concrete
            setParameter( "MATERIAL", "Concrete", "LINEAR/ELASTI/YOUNG", (21500*(38/10.0)**(1.0/3.0)*10**6) )
            setParameter( "MATERIAL", "Concrete", "TENSIL/TENSTR", ((0.3*(38.0-8.0)**(2.0/3.0))*10**6) )
            setParameter( "MATERIAL", "Concrete", "TENSIL/GF1", (73.0*(38.0)**0.18) )
            setParameter( "MATERIAL", "Concrete", "COMPRS/COMSTR", 38.0e+6 )
            setParameter( "MATERIAL", "Concrete", "COMPRS/GC", ((73.0*(38.0)**0.18)*250.0) )
        # parameters longitudinal reinforcement
            setParameter( "MATERIAL", "Longitudinal reinforcement", "PLASTI/HARDI2/KAPSIG",
            [ -0.1138, -5.78e+08, 0, -4.76e+08, 0, 4.76e+08, 0.1138, 5.78e+08 ] )

        # parameters shear reinforcement
            setParameter( "MATERIAL", "Shear reinforcement", "PLASTI/HARDI2/KAPSIG",
            [ -0.1152, -5.1e+08, 0, -4.6e+08, 0, 4.6e+08, 0.1152, 5.1e+08 ] )

        # parameters longitudinal reinforcement
            setParameter( "GEOMET", "As longitudinal reinforcement", "REIEMB/CROSSE",
            ((3.0*0.25*10.0**2*3.141592654)*10**-6.0) )

            generateMesh( [] )
        # analysis
            runSolver( "Main2" )
            i=i-1
#Low concrete strength
    elif i==3:

        if loadResults( "Main3", "C:/Users/..../ECOV/Three variables/Design 1/Main3.dnb" ):
            loadResults( "Main3", "C:/Users/..../ECOV/Three variables/Design 1/Main3.dnb" )


        else:

        # parameters concrete
            setParameter( "MATERIAL", "Concrete", "LINEAR/ELASTI/YOUNG", (21500*(20.9/10.0)**(1.0/3.0)*10**6) )
            setParameter( "MATERIAL", "Concrete", "TENSIL/TENSTR", ((0.3*(20.9-8.0)**(2.0/3.0))*10**6) )
            setParameter( "MATERIAL", "Concrete", "TENSIL/GF1", (73.0*(20.9)**0.18) )
            setParameter( "MATERIAL", "Concrete", "COMPRS/COMSTR", 20.9e+6 )
            setParameter( "MATERIAL", "Concrete", "COMPRS/GC", ((73.0*(20.9)**0.18)*250.0) )
        # parameters longitudinal reinforcement
            setParameter( "MATERIAL", "Longitudinal reinforcement", "PLASTI/HARDI2/KAPSIG",
            [ -0.1138, -6.8e+08, 0, -5.6e+08, 0, 5.6e+08, 0.1138, 6.8e+08 ] )

        # parameters shear reinforcement
            setParameter( "MATERIAL", "Shear reinforcement", "PLASTI/HARDI2/KAPSIG",
            [ -0.1152, -5.1e+08, 0, -4.6e+08, 0, 4.6e+08, 0.1152, 5.1e+08 ] )

        # parameters longitudinal reinforcement
            setParameter( "GEOMET", "As longitudinal reinforcement", "REIEMB/CROSSE",
            ((3.0*0.25*10.0**2*3.141592654)*10**-6.0) )

            generateMesh( [] )
        # analysis
            runSolver( "Main3" )
            i=i-1
```

*Figure H2. Python code to run 3 NLFE analyses*

The results for the displacement of node 559 (midspan C) of the three analyses are exported to .txt files. This files can be used to obtain the total load carrying capacity.

```
# Results
cases = resultCases('Main1','Output')
table = [ 'Main1', 'Output', 'Total Displacements']
exportResultsToCSV( "C:/Users/..../ECOV/Three variables/Design 1/Results/1.txt", table, cases, [559] )

cases = resultCases('Main2','Output')
table = [ 'Main2', 'Output', 'Total Displacements']
exportResultsToCSV( "C:/Users/..../ECOV/Three variables/Design 1/Results/2.txt", table, cases, [559] )

cases = resultCases('Main3','Output')
table = [ 'Main3', 'Output', 'Total Displacements']
exportResultsToCSV( "C:/Users/..../ECOV/Three variables/Design 1/Results/3.txt", table, cases, [559] )
```

*Figure H3. Python code to export the results to .txt files.*

## H.2 Python script for processing results

The results of the three analyses are imported.

```
#########################################################################
#Import results

# n = number of Analyses
n = 3
Fh = np.zeros(n)
Fv = np.zeros(n)

j = 0
for j in range (n):
    j = j+1

    if j==1:
        data1 = np.genfromtxt('C:/Users/..../ECOV/Three variables/Design 1/Results/1.txt',
        delimiter=',', skip_header = 3,skip_footer = 1)
    elif j==2:
        data1 = np.genfromtxt('C:/Users/..../ECOV/Three variables/Design 1/Results/2.txt',
        delimiter=',', skip_header = 3,skip_footer = 1)
    elif j==3:
        data1 = np.genfromtxt('C:/Users/..../ECOV/Three variables/Design 1/Results/3.txt',
        delimiter=',', skip_header = 3,skip_footer = 1)
```

*Figure H4. Python code to import the results from the .txt files.*

Two arrays are created containing the maximum vertical and horizontal load of each analyses.

```
#########################################################################
# Load carrying capacity

    j=j-1
    case_1 = data1[:,2]
    k1 =len(case_1)-1
    i = 0
    for i in range (k1):
        i=i+1
        if case_1[i]<11:
            Fv1 = data1[i,3]*18818.20170/1000.0
            Fh1 = 0
        elif case_1[i]<71:
            Fh1 = data1[i,3]*15681.83475/1000.0
        else:
            Fv1 = data1[9,3]*18818.20170/1000.0 + data1[i,3]*10000.0/1000.0
            Fh1 = data1[69,3]*15681.83475/1000.0 + data1[i,3]*0.0/1000.0
    Fv[j] = Fv1
    Fh[j] = Fh1
#########################################################################
```

*Figure H5. Python code to store the maximum vertical and horizontal load in an array*

The structural resistance according to the ECOV method is defined below.

```
#########################################################################
#Resistance safety format

#ECOV
Rsf_ECOV = 36.10
#########################################################################
```

*Figure H6. Total structural resistance according to the ECOV method.*

The response surface is determined for Case 1: two stochastic variables, Case 2: three stochastic variables with $V_{A_s}$=0.02 and Case 3: three stochastic variables with $V_{A_s}$=0.10.

### H.2.1 Case 1: rotational capacity corner D without geometrical reinforcement uncertainty

Two stochastic variables: $f_y$ and $f_c$. The control point is determined with the Python code presented in figure H7 based on the results of the NLFE analyses.

```
189 ########################################################################
190 #Approach Zhoa and Qiu (2013)
191
192 #Difference from mean
193 F1 = (Fv[0]+Fh[0]) - (Fv[1]+Fh[1])
194 F2 = (Fv[0]+Fh[0]) - (Fv[2]+Fh[2])
195
196 #Weight factors
197 w1 = F1/(abs(F1+F2))
198 w2 = F2/(abs(F1+F2))
199
200 #Transformation from lognormal to normal
201 mx1 = 560.0;sdx1 = 28.0;sdx_L1 = sqrt(np.log(sdx1**2/(mx1**2)+1));mx_L1 = np.log(mx1)-0.5*sdx_L1**2;
202 mx2 = 38.0; sdx2 = 5.7;sdx_L2 = sqrt(np.log(sdx2**2/(mx2**2)+1));mx_L2 = np.log(mx2)-0.5*sdx_L2**2;
203
204 U1 = np.array([(np.log(560.0-3.0*28.0)-mx_L1)/sdx_L1,(np.log(38.0)-mx_L2)/sdx_L2])
205 U2 = np.array([(np.log(560)-mx_L1)/sdx_L1,(np.log(38.0-3.0*5.7)-mx_L2)/sdx_L2])
206
207 #Control point
208 Uc = np.array([w1*U1[0] + w2*U2[0],w1*U1[1] + w2*U2[1]])
209 Xc = np.array([np.exp(sdx_L1*Uc[0]+mx_L1),np.exp(sdx_L2*Uc[1]+mx_L2)])
210
211 ########################################################################
```

*Figure H7. Python code to determine the control point based on the results of the NLFE analyses.*

The procedure to find the initial design point is explained in Appendix G. Around the initial design points several experimental points are selected to create a response surface. In this example the initial design point is $\boldsymbol{X}_{M8}$. The steel yield strength coordinates are:

```
495 ###################################
496 # Steel
497 fy = np.array([
498
499 Xm8[0],Xm8[0]+28.0,Xm8[0],Xm8[0]-28.0,Xm8[0],
500
501 #Cross points f=1.0
502 Xm8[0]+1.0*28.0,Xm8[0]-1.0*28.0,Xm8[0]-1.0*28.0,Xm8[0]+1.0*28.0,
503
504 #Cross points f=1.5
505 Xm8[0]+1.5*28.0,Xm8[0]-1.5*28.0,Xm8[0]-1.5*28.0,Xm8[0]+1.5*28.0,
506
507 #Cross points f=2
508 Xm8[0]+2.0*28.0,Xm8[0]-2.0*28.0,Xm8[0]-2.0*28.0,Xm8[0]+2.0*28.0,
509
510 #f=2
511 Xm8[0]+2.0*28.0,Xm8[0],Xm8[0]-2.0*28.0,Xm8[0],
512
513 #f=1.5
514 Xm8[0]+1.5*28.0,Xm8[0],Xm8[0]-1.5*28.0,Xm8[0],
515
516 #extra
517 448.5,434.5,420.5,434.5,448.5,420.5,420.5,448.5,434.5,
518
519 #mean
520 560,
521
522 #first two points
523 560-3.0*28.0,
524 560,
525
526 #control point
527 Xc[0],
528
529 #iteration points
530 Xm1[0],Xm2[0],Xm3[0],Xm4[0],Xm5[0],Xm6[0],Xm7[0],Xm8[0],Xm9[0],Xm10[0],
531 ])
532 ###################################
```

*Figure H8. Coordinates steel yield strength corresponding to the used input parameters in the NLFE analyses.*

The concrete compressive strength coordinates are:

```
####################################
# Concrete
fc = np.array([

Xm8[1],Xm8[1],Xm8[1]+5.7,Xm8[1],Xm8[1]-5.7,

#Cross points f=1.0
Xm8[1]+1.0*5.7,Xm8[1]+1.0*5.7,Xm8[1]-1.0*5.7,Xm8[1]-1.0*5.7,

#Cross points f=1.5
Xm8[1]+1.5*5.7,Xm8[1]+1.5*5.7,Xm8[1]-1.5*5.7,Xm8[1]-1.5*5.7,

#Cross points f=2.0
Xm8[1]+2.0*5.7,Xm8[1]+2.0*5.7,Xm8[1]-2.0*5.7,Xm8[1]-2.0*5.7,

#f=2
Xm8[1],Xm8[1]+2.0*5.7,Xm8[1],Xm8[1]-2.0*5.7,

#f=1.5
Xm8[1],Xm8[1]+1.5*5.7,Xm8[1],Xm8[1]-1.5*5.7,

#extra
28.8,31.6,28.8,25.9,31.6,31.6,25.9,25.9,28.8,

#mean
38,

#first two points
38.0,
38.0-3.0*5.7,

#control point
Xc[1],

#iteration points
Xm1[1],Xm2[1],Xm3[1],Xm4[1],Xm5[1],Xm6[1],Xm7[1],Xm8[1],Xm9[1],Xm10[1],
])
####################################
```

*Figure H9. Coordinates concrete compressive strength corresponding to the used input parameters in the NLFE analyses.*

This coordinates are used in Matrix $\boldsymbol{A}$ in order to find the unknown coefficients $\boldsymbol{b}$. Matrix $\boldsymbol{A}$ is given below:

```
####################################
A1 = np.array([
[1.0,fy[0],fc[0],fy[0]**2,fc[0]**2],
[1.0,fy[1],fc[1],fy[1]**2,fc[1]**2],
[1.0,fy[2],fc[2],fy[2]**2,fc[2]**2],
[1.0,fy[3],fc[3],fy[3]**2,fc[3]**2],
[1.0,fy[4],fc[4],fy[4]**2,fc[4]**2],
[1.0,fy[5],fc[5],fy[5]**2,fc[5]**2],
[1.0,fy[6],fc[6],fy[6]**2,fc[6]**2],
[1.0,fy[7],fc[7],fy[7]**2,fc[7]**2],
[1.0,fy[8],fc[8],fy[8]**2,fc[8]**2],
[1.0,fy[9],fc[9],fy[9]**2,fc[9]**2],
[1.0,fy[10],fc[10],fy[10]**2,fc[10]**2],
[1.0,fy[11],fc[11],fy[11]**2,fc[11]**2],
[1.0,fy[12],fc[12],fy[12]**2,fc[12]**2],
[1.0,fy[13],fc[13],fy[13]**2,fc[13]**2],
[1.0,fy[14],fc[14],fy[14]**2,fc[14]**2],
[1.0,fy[15],fc[15],fy[15]**2,fc[15]**2],
[1.0,fy[16],fc[16],fy[16]**2,fc[16]**2],
[1.0,fy[17],fc[17],fy[17]**2,fc[17]**2],
[1.0,fy[18],fc[18],fy[18]**2,fc[18]**2],
[1.0,fy[19],fc[19],fy[19]**2,fc[19]**2],
[1.0,fy[20],fc[20],fy[20]**2,fc[20]**2],
[1.0,fy[21],fc[21],fy[21]**2,fc[21]**2],
[1.0,fy[22],fc[22],fy[22]**2,fc[22]**2],
[1.0,fy[23],fc[23],fy[23]**2,fc[23]**2],
[1.0,fy[24],fc[24],fy[24]**2,fc[24]**2],
[1.0,fy[25],fc[25],fy[25]**2,fc[25]**2],
[1.0,fy[26],fc[26],fy[26]**2,fc[26]**2],
[1.0,fy[27],fc[27],fy[27]**2,fc[27]**2],
[1.0,fy[28],fc[28],fy[28]**2,fc[28]**2],
[1.0,fy[29],fc[29],fy[29]**2,fc[29]**2],
[1.0,fy[30],fc[30],fy[30]**2,fc[30]**2],
[1.0,fy[31],fc[31],fy[31]**2,fc[31]**2],
[1.0,fy[32],fc[32],fy[32]**2,fc[32]**2],
[1.0,fy[33],fc[33],fy[33]**2,fc[33]**2],
[1.0,fy[34],fc[34],fy[34]**2,fc[34]**2],
[1.0,fy[35],fc[35],fy[35]**2,fc[35]**2],
[1.0,fy[36],fc[36],fy[36]**2,fc[36]**2],
[1.0,fy[37],fc[37],fy[37]**2,fc[37]**2],
[1.0,fy[38],fc[38],fy[38]**2,fc[38]**2],
[1.0,fy[39],fc[39],fy[39]**2,fc[39]**2],
[1.0,fy[40],fc[40],fy[40]**2,fc[40]**2],
[1.0,fy[41],fc[41],fy[41]**2,fc[41]**2],
[1.0,fy[42],fc[42],fy[42]**2,fc[42]**2],
[1.0,fy[43],fc[43],fy[43]**2,fc[43]**2],
[1.0,fy[44],fc[44],fy[44]**2,fc[44]**2],
[1.0,fy[45],fc[45],fy[45]**2,fc[45]**2],
[1.0,fy[46],fc[46],fy[46]**2,fc[46]**2],
[1.0,fy[47],fc[47],fy[47]**2,fc[47]**2],
])
####################################
```

*Figure H10. Matrix $\boldsymbol{A}$ based on the coordinates defined in figure H8 and H9.*

The results of the corresponding NLFE anlyses are stored in array $\boldsymbol{G}$:

```
623 ####################################
624
625 G = np.array([
626
627 [Fv[11]+Fh[11]-Rsf_ECOV],
628 [Fv[14]+Fh[14]-Rsf_ECOV],[Fv[15]+Fh[15]-Rsf_ECOV],[Fv[16]+Fh[16]-Rsf_ECOV],[Fv[17]+Fh[17]-Rsf_ECOV],
629
630 #Cross points f=1.0
631 [Fv[26]+Fh[26]-Rsf_ECOV],[Fv[27]+Fh[27]-Rsf_ECOV],[Fv[28]+Fh[28]-Rsf_ECOV],[Fv[29]+Fh[29]-Rsf_ECOV],
632
633 #Cross points f=1.5
634 [Fv[30]+Fh[30]-Rsf_ECOV],[Fv[31]+Fh[31]-Rsf_ECOV],[Fv[32]+Fh[32]-Rsf_ECOV],[Fv[33]+Fh[33]-Rsf_ECOV],
635
636 #Cross points f=2.0
637 [Fv[34]+Fh[34]-Rsf_ECOV],[Fv[35]+Fh[35]-Rsf_ECOV],[Fv[36]+Fh[36]-Rsf_ECOV],[Fv[37]+Fh[37]-Rsf_ECOV],
638
639 #f=2
640 [Fv[18]+Fh[18]-Rsf_ECOV],[Fv[19]+Fh[19]-Rsf_ECOV],[Fv[20]+Fh[20]-Rsf_ECOV],[Fv[21]+Fh[21]-Rsf_ECOV],
641
642 #f=1.5'
643 [Fv[22]+Fh[22]-Rsf_ECOV],[Fv[23]+Fh[23]-Rsf_ECOV],[Fv[24]+Fh[24]-Rsf_ECOV],[Fv[25]+Fh[25]-Rsf_ECOV],
644
645 #extra
646 [Fv[38]+Fh[38]-Rsf_ECOV],
647 [Fv[39]+Fh[39]-Rsf_ECOV],[Fv[40]+Fh[40]-Rsf_ECOV],[Fv[41]+Fh[41]-Rsf_ECOV],[Fv[42]+Fh[42]-Rsf_ECOV],
648 [Fv[43]+Fh[43]-Rsf_ECOV],[Fv[44]+Fh[44]-Rsf_ECOV],[Fv[45]+Fh[45]-Rsf_ECOV],[Fv[46]+Fh[46]-Rsf_ECOV],
649
650 #mean
651 [Fv[0]+Fh[0]-Rsf_ECOV],
652
653 #first two points
654 [Fv[1]+Fh[1]-Rsf_ECOV],
655 [Fv[2]+Fh[2]-Rsf_ECOV],
656
657 #control point
658 [GXc],
659
660 #iteration points
661 [GX1],[GX2],[GX3],[GX4],[GX5],[GX6],[GX7],[GX8],[GX9],[GX10],
662 ])
```

*Figure H11. The results of the implicit LSF $\boldsymbol{G}$ based on the resistance of the NLFE analyses are stored in array $\boldsymbol{G}$.*

The unknown coefficients $\boldsymbol{b}$ can be determined with a least squares approach according to equation (2.27):

```
692 b = np.dot(np.dot(inv(np.dot(np.transpose(A1),A1)),np.transpose(A1)),G)
```

*Figure H12. The matrix $\boldsymbol{A}$ and $\boldsymbol{G}$ are used to calculate the unknown coefficients $\boldsymbol{b}$ according to equation (2.27).*

The response surface $\overline{\boldsymbol{G}}$ based on the NLFE analyses $\boldsymbol{G}$ with input parameters $f_y$ and $f_c$ is given in the standard normal space:

```
701 # Transformation LSF to standard normal space
702 mx1 = 560;sdx1 = 28.0;sdx_L1 = sqrt(np.log(sdx1**2/(mx1**2)+1));mx_L1 = np.log(mx1)-0.5*sdx_L1**2;
703 mx2 = 38; sdx2 = 5.7;sdx_L2 = sqrt(np.log(sdx2**2/(mx2**2)+1));mx_L2 = np.log(mx2)-0.5*sdx_L2**2;
704
705 b0 = np.asscalar(b[0])
706 b1 = np.asscalar(b[1])
707 b2 = np.asscalar(b[2])
708 b3 = np.asscalar(b[3])
709 b4 = np.asscalar(b[4])
710
711 def G(u1,u2):
712         x1 = exp(mx_L1+u1*sdx_L1)
713         x2 = exp(mx_L2+u2*sdx_L2)
714         G =  b0+b1*x1+b2*x2+b3*x1**2+b4*x2**2
715         return G
```

*Figure H13. The response surface $\overline{\boldsymbol{G}}$ defined in the stand normal space.*

To use a FORM, the partial derivatives of the response surface $\overline{\boldsymbol{G}}$: $a_1 = \frac{\partial \bar{G}}{\partial u1}$ and $a_2 = \frac{\partial \bar{G}}{\partial u2}$ are calculated with Maple and added to the python script:

```
718 #Differentiation with Maple:
719 def a1(u1,u2):
720         a1 = 0.9993758450e-1*(exp(0.4996879225e-1*u1+6.326688344))**2*b3+0.4996879225e-1*exp(0.4996879225e-1*u1+6.326688344)*b1
721         return a1
722
723 def a2(u1,u2):
724         a2 = .2983327600*(exp(.1491663800*u2+3.626460856))**2*b4+.1491663800*exp(.1491663800*u2+3.626460856)*b2
725         return a2
```

*Figure H14. Partial derivatives response surface $\overline{\boldsymbol{G}}$.*

Now the FORM is used to determine the design point $\boldsymbol{u}_*$ and the reliability index $\beta_R$ of the response surface $\overline{\boldsymbol{G}}$.

```
#step 1: Guess u0
u = np.array([-5.0,-6.0])
u1 = u[0]
u2 = u[1]
beta1 = np.sqrt(np.dot(u,u))

alpha = np.zeros((2))
u12 = np.zeros((2))

e = 10.0
n = 2

while (e>0.001):

    beta0 = beta1

    #step 2
    gu = G(u1,u2)
    #step 3
    dg1 = a1(u1,u2)
    dg2 = a2(u1,u2)
    dg = np.array([dg1,dg2])
    #step 4
    u =dg*((np.dot(dg,u))-gu)/(np.dot(dg,dg))
    u1 = u[0]
    u2 = u[1]
    #step 5
    beta1 = np.sqrt(np.dot(u,u))
    #print beta1
    #step 6
    e = abs(beta1-beta0)
    beta = beta1
    alpha12_store = dg/(np.sqrt(np.dot(dg,dg)))

for j in range (n):
    alpha[j] = alpha12_store[j]
    u12[j] = u[j]
```

```
print 'beta: '
print beta
print
print 'Phi(-beta): '
print norm.cdf(-beta)
print
print 'alpha1 and alpha2: '
print alpha
print
print 'u1* and u2*: '
print u12
print
mx_L = np.array([mx_L1,mx_L2])
sdx_L = np.array([sdx_L1,sdx_L2])
x12 = np.exp(mx_L+u12*sdx_L)
print 'x1* and x2*: '
print x12
print 'gu: '
print gu
```

*Figure H15. Python code to perform the FORM for stochastic variables in the standard normal space.*

The figures used in appendix G to graphically show the response surface, the sample points and the LSF are made with the following python scripts:

```
##############################################################################
# Response surface (real space)

fig = plt.figure()
ax = fig.gca(projection='3d')
ax.set_xlabel('fy (MPa)')
ax.set_ylabel('fc (MPa)')
ax.set_zlabel('G')
plt.title('Response surface (real space)')


# Make data.
x1 = np.arange(300, 560, 1.0)
x2 = np.arange(10, 40, 1.0)
x1, x2 = np.meshgrid(x1, x2)

#Response surface Main load LF 5
G1 = b[0]+b[1]*x1+b[2]*x2+b[3]*x1**2+b[4]*x2**2

#Sample points
ax.scatter(fy, fc, G, label = 'Sample points')

# Plot the surface.
surf = ax.plot_surface(x1, x2, G1, cmap=cm.coolwarm, alpha=0.5,
                       linewidth=0, antialiased=True,)

# Add a color bar which maps values to colors.
fig.colorbar(surf, shrink=0.5, aspect=5)

plt.show()

##############################################################################
```

*Figure H16. Python code to plot the response surface in the real space.*

```
889 ###############################################################################
890 # Response surface (Standard normal space)
891
892 fig = plt.figure()
893 ax = fig.gca(projection='3d')
894 ax.set_xlabel('U fy')
895 ax.set_ylabel('U fc')
896 ax.set_zlabel('G')
897 plt.title('Response surface (standard normal space)')
898 ax.set_zlim3d(-1,20)
899
900
901 # Make data.
902 u1 = np.arange(-10, 10, 1.0)
903 u2 = np.arange(-10, 10, 1.0)
904 u1, u2 = np.meshgrid(u1, u2)
905 #Response surface standard normal space calculated with Maple
906 g1 = (np.exp(0.4996879225e-1*u1+6.326688344))**2*b3+(np.exp(.1491663800*u2+3.626460856))**2*b4
907 + np.exp(0.4996879225e-1*u1+6.326688344)*b1+np.exp(.1491663800*u2+3.626460856)*b2+b0
908
909 # Plot the surface.
910 surf = ax.plot_surface(u1, u2, g1, cmap=cm.coolwarm, alpha=0.5,linewidth=0, antialiased=True)
911 surf = ax.plot_surface(u1, u2,  0, cmap=cm.coolwarm, alpha=0.5,linewidth=0, antialiased=True)
912
913 plt.show()
914
915 ###############################################################################
```

*Figure H17. Python code to plot the response surface in the standard normal space.*

```
927 ###############################################################################
928 #Plot LSF standard normal space
929
930 delta = 0.025
931 u1 = np.arange(-10.0, 5, delta)
932 u2 = np.arange(-10.0, 6.1, delta)
933 u1, u2 = np.meshgrid(u1, u2)
934
935 g1 = g1 = (np.exp(0.4996879225e-1*u1+6.326688344))**2*b3
936 +(np.exp(.1491663800*u2+3.626460856))**2*b4
937 +np.exp(0.4996879225e-1*u1+6.326688344)*b1
938 +np.exp(.1491663800*u2+3.626460856)*b2+b0
939
940 fig = plt.figure()
941
942 ax = fig.add_subplot(1,1,1)
943 ax.spines['left'].set_position('zero')
944 ax.spines['right'].set_color('none')
945 ax.spines['bottom'].set_position('zero')
946 ax.spines['top'].set_color('none')
947 ax.spines['left'].set_smart_bounds(True)
948 ax.spines['bottom'].set_smart_bounds(True)
949 ax.xaxis.set_ticks_position('bottom')
950 ax.yaxis.set_ticks_position('left')
951 ax.grid()
952 ax.grid(linestyle='-', linewidth='0.1', color='black')
953 ax.minorticks_on()
954 ax.text(5, -1.5, 'U fy' ,color='k', fontsize=11)
955 ax.text(-1.5, 5, 'U fc' ,color='k', fontsize=11)
956 ax.text(-10, -11, 'Beta: ' +str(round(beta,2)) ,color='k', fontsize=8)
```

```
958 levels = np.arange(0,0.25,0.25)
959 levels2 = np.arange(-5,400.0,10)
960 CS1 = plt.contour(u1, u2, g1, linewidths=0.8, colors=('r'), levels=levels)
961 CS2 = plt.contour(u1, u2, g1, linewidths=0.5, colors=('b'), levels=levels2)
962
963 plt.plot(U[0],U[1], 'ro',markersize=3, label='Previous design point')
964 plt.plot(u12[0],u12[1], 'bo',markersize=3, label='Design point obtained with FORM')
965 labels = np.array(['LSF','Contour lines RS'])
966 CS1.collections[0].set_label(labels[0])
967 CS2.collections[1].set_label(labels[1])
968 plt.legend(loc='lower right',fontsize=7)
969
970 plt.clabel(CS1, inline=1, fontsize=8)
971 plt.clabel(CS2, inline=1, fontsize=8)
972 plt.title('Limit state function (standard normal space)')
973
974 plt.show()
975
976 ###############################################################################
```

*Figure H18. Python code to plot the limit state function in the standard normal space. The limit state function is in fact the contour line of the response surface at height 0.*

```
976 ###############################################################################
977 #Plot LSF real space
978
979 # Make data.
980 x1 = np.arange(250, 650, 1.0)
981 x2 = np.arange(5, 55, 1.0)
982 x1, x2 = np.meshgrid(x1, x2)
983
984 #Response surface Main load LF 5
985 G1 = b[0]+b[1]*x1+b[2]*x2+b[3]*x1**2+b[4]*x2**2
986
987 fig = plt.figure()
988 ax = fig.add_subplot(1,1,1)
989 ax.grid()
990 ax.grid(linestyle='-', linewidth='0.1', color='black')
991 ax.minorticks_on()
992 ax.set_xlabel('fy (MPa)')
993 ax.set_ylabel('fc (MPa)')
994
995 levels = np.arange(0,0.25,0.25)
996 levels2 = np.arange(-15,50.0,10)
997 CS1 = plt.contour(x1, x2, G1, linewidths=0.8, colors=('r'), levels=levels)
998 CS2 = plt.contour(x1, x2, G1, linewidths=0.5, colors=('b'), levels=levels2)
999
1000 plt.plot(fy[0],fc[0], 'ro',markersize=5, label='Previous design point')
1001 plt.plot(x12[0],x12[1], 'bo',markersize=5, label='New design point (FORM)')
1002 labels = np.array(['LSF','Contour lines RS'])
1003 CS1.collections[0].set_label(labels[0])
1004 CS2.collections[2].set_label(labels[1])
1005 plt.legend(loc='upper left',fontsize=7)
1006
1007 ax.text(250, -1, 'New design point, beta: ' +str(round(beta,2)) ,color='k', fontsize=8)
1008 ax.text(510, -1, 'Previous design point, G(X): ' +str(round(G[0],2)) ,color='k', fontsize=8)
1009
1010 plt.plot(fy, fc, 'ro',markersize=3)
1011 plt.title('Limit state function (real space)')
1012 plt.clabel(CS1, inline=1, fontsize=8)
1013 plt.clabel(CS2, inline=0.1, fontsize=8)
1014
1015 plt.show()
1016
1017 ###############################################################################
```

*Figure H19. Python code to plot the limit state function in the real space. The limit state function is in fact the contour line of the response surface at height 0.*

### H.2.2 Case 2: rotational capacity corner D with reinforcement uncertainty due to fabrication

Three stochastic variables: $f_y$, $f_c$ and $A_s$. The control point is determined with the Python code presented in figure H20 based on the results of the NLFE analyses.

```
#########################################################################
#Approach Zhoa and Qiu (2013)

#Difference from mean
F1 = (Fv[0]+Fh[0]) - (Fv[1]+Fh[1])
F2 = (Fv[0]+Fh[0]) - (Fv[2]+Fh[2])
F3 = (Fv[0]+Fh[0]) - (Fv[3]+Fh[3])

#Weight factors
w1 = F1/(abs(F1+F2+F3))
w2 = F2/(abs(F1+F2+F3))
w3 = F3/(abs(F1+F2+F3))

#Transformation from lognormal to normal
mx1 = 560.0;sdx1 = 28.0;sdx_L1 = sqrt(np.log(sdx1**2/(mx1**2)+1));mx_L1 = np.log(mx1)-0.5*sdx_L1**2;
mx2 = 38.0; sdx2 = 5.7;sdx_L2 = sqrt(np.log(sdx2**2/(mx2**2)+1));mx_L2 = np.log(mx2)-0.5*sdx_L2**2;
mx3 = 235.619449; sdx3 = mx3*0.02;

U1 = np.array([(np.log(560.0-3.0*28.0)-mx_L1)/sdx_L1,(np.log(38.0)-mx_L2)/sdx_L2,((mx3)-mx3)/sdx3])
U2 = np.array([(np.log(560)-mx_L1)/sdx_L1,(np.log(38.0-3.0*5.7)-mx_L2)/sdx_L2,((mx3)-mx3)/sdx3])
U3 = np.array([(np.log(560)-mx_L1)/sdx_L1,(np.log(38.0)-mx_L2)/sdx_L2,((mx3-3.*sdx3)-mx3)/sdx3])

#Control point
Uc = np.array([w1*U1[0] + w2*U2[0] + w3*U3[0], w1*U1[1] + w2*U2[1]+w3*U3[1], w1*U1[2] + w2*U2[2] + w3*U3[2] ])
Xc = np.array([np.exp(sdx_L1*Uc[0]+mx_L1), np.exp(sdx_L2*Uc[1]+mx_L2), Uc[2]*sdx3+mx3 ])

#########################################################################
```

*Figure H20. Python code to determine the control point based on the NLFE resutls.*

The procedure to find the initial design point is explained in Appendix G. Around the initial design points several experimental points are selected to create a response surface. In this example the initial design point is $X_{M1}$. The steel yield strength $f_y$ coordinates are:

```
####################################
# Steel
fy = np.array([

Xm1[0],

# f=1.0
Xm1[0]+28.0,Xm1[0],Xm1[0],Xm1[0]-28.0,Xm1[0],Xm1[0],
#Cross points f=1.0
Xm1[0]+28.0,Xm1[0]-28.0,Xm1[0]-28.0,Xm1[0]+28.0,Xm1[0]+28.0,Xm1[0]-28.0,Xm1[0]-28.0,Xm1[0]+28.0,

# f=2.0
Xm1[0]+2*28.0,Xm1[0],Xm1[0],Xm1[0]-2*28.0,Xm1[0],Xm1[0],

# f=1.5
Xm1[0]+1.5*28.0,Xm1[0],Xm1[0],Xm1[0]-1.5*28.0,Xm1[0],Xm1[0],
#Cross points f=1.5
Xm1[0]+1.5*28.0,Xm1[0]-1.5*28.0,Xm1[0]-1.5*28.0,Xm1[0]+1.5*28.0,Xm1[0]+1.5*28.0,Xm1[0]-1.5*28.0,Xm1[0]-1.5*28.0,Xm1[0]+1.5*28.0,

#extra
454.85911513,456.17734552,

#mean
560,

#first two points
560-3.0*28.0,560,560,

#control point
Xc[0],

#iteration points
Xm1[0],Xm2[0],Xm3[0],Xm4[0],Xm5[0],Xm6[0],Xm7[0],Xm8[0],Xm9[0],Xm10[0],Xm11[0],

])
####################################
```

*Figure H21. Coordinates steel yield strength corresponding to the used input parameters in the NLFE analyses.*

The concrete compressive strength $f_c$ coordinates are:

```
#####################################
# Concrete
fc = np.array([

Xm1[1],

# f=1.0
Xm1[1],Xm1[1]+5.7,Xm1[1],Xm1[1],Xm1[1]-5.7,Xm1[1],
#Cross points f=1.0
Xm1[1]+5.7,Xm1[1]+5.7,Xm1[1]-5.7,Xm1[1]-5.7,Xm1[1]+5.7,Xm1[1]+5.7,Xm1[1]-5.7,Xm1[1]-5.7,

# f=2.0
Xm1[1],
Xm1[1]+2*5.7,
Xm1[1],
Xm1[1],
Xm1[1]-2*5.7,
Xm1[1],

# f=1.5
Xm1[1],Xm1[1]+1.5*5.7,Xm1[1],Xm1[1],Xm1[1]-1.5*5.7,Xm1[1],
#Cross points f=1.5
Xm1[1]+1.5*5.7,Xm1[1]+5.7,Xm1[1]-1.5*5.7,Xm1[1]-1.5*5.7,Xm1[1]+1.5*5.7,Xm1[1]+1.5*5.7,Xm1[1]-1.5*5.7,Xm1[1]-1.5*5.7,

#extra
32.38530659,32.7999568,

#mean
38,

#first two points
38.0,38.0-3.0*5.7,38.0,

#control point
Xc[1],

#iteration points
Xm1[1],Xm2[1],Xm3[1],Xm4[1],Xm5[1],Xm6[1],Xm7[1],Xm8[1],Xm9[1],Xm10[1],Xm11[1],

])
#####################################
```

*Figure H22. Coordinates concrete compressive strength corresponding to the used input parameters in the NLFE analyses.*

The cross-sectional area $A_s$ of the longitudinal reinforcement coordinates are:

```
#####################################
# As
As = np.array([

Xm1[2],

# f=1.0
Xm1[2],Xm1[2],Xm1[2]+sdx3,Xm1[2],Xm1[2],Xm1[2]-sdx3,
#Cross points f=1.0
Xm1[2]+sdx3,Xm1[2]+sdx3,Xm1[2]+sdx3,Xm1[2]+sdx3,Xm1[2]-sdx3,Xm1[2]-sdx3,Xm1[2]-sdx3,Xm1[2]-sdx3,

# f=2.0
Xm1[2],Xm1[2],Xm1[2]+2*sdx3,Xm1[2],Xm1[2],Xm1[2]-2*sdx3,

# f=1.5
Xm1[2],Xm1[2],Xm1[2]+1.5*sdx3,Xm1[2],Xm1[2],Xm1[2]-1.5*sdx3,
#Cross points f=1.5
Xm1[2]+1.5*sdx3,Xm1[2]+1.5*sdx3,Xm1[2]+1.5*sdx3,Xm1[2]+1.5*sdx3,Xm1[2]-1.5*sdx3,Xm1[2]-1.5*sdx3,Xm1[2]-1.5*sdx3,Xm1[2]-1.5*sdx3,

#extra
217.64278599,217.43310791,

#mean
mx3,

#first two points
mx3,
mx3,
mx3-3.0*sdx3,

#control point
Xc[2],

#iteration points
Xm1[2],Xm2[2],Xm3[2],Xm4[2],Xm5[2],Xm6[2],Xm7[2],Xm8[2],Xm9[2],Xm10[2],Xm11[2],

])
#####################################
```

*Figure H23. Coordinates cross-sectional area longitudinal reinforcement, corresponding to the used input parameters in the NLFE analyses.*

The sample points to create the response surface $\overline{\boldsymbol{G}}$ can be shown graphically with the following python script:

```
################################################################################
# sample points to create the response surface

fig = plt.figure()
ax = fig.gca(projection='3d')
ax.set_xlabel('fy (MPa)')
ax.set_ylabel('fc (MPa)')
ax.set_zlabel('As (mm2)')
plt.title('Sample points')

# Make data.
x1 = np.arange(300, 560, 1.0)
x2 = np.arange(10, 40, 1.0)
x1, x2 = np.meshgrid(x1, x2)

#Sample points
ax.scatter(fy, fc, As, label = 'Sample points')

plt.show()

################################################################################
```

*Figure H24. Python script to plot a graphical representation of the chosen sample points.*

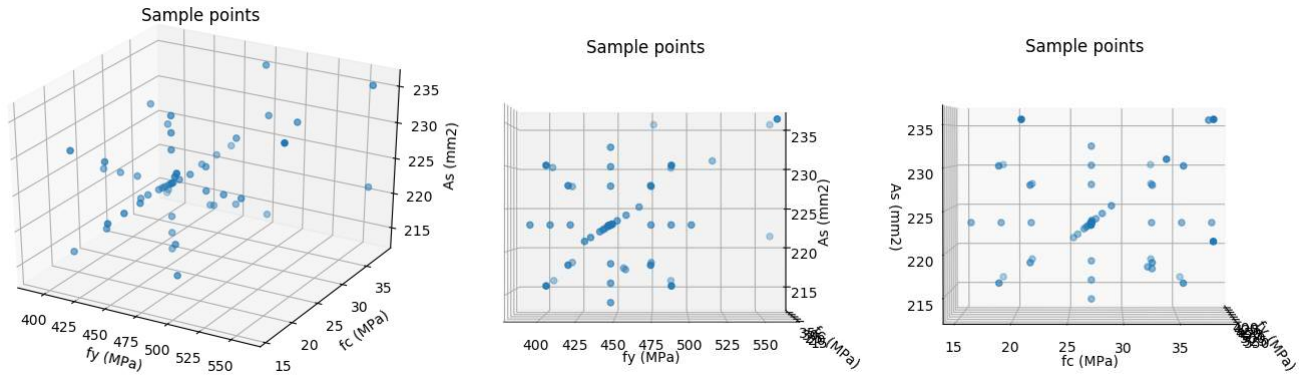


*Figure H25. Graphical representation of the chosen sample points*

This coordinates are used in Matrix $\boldsymbol{A}$ in order to find the unknown coefficients $\boldsymbol{b}$. Matrix $\boldsymbol{A}$ is given below:

```
#####################################
A1 = np.array([
[1.0,fy[0],fc[0],As[0],fy[0]**2,fc[0]**2,As[0]**2],
[1.0,fy[1],fc[1],As[1],fy[1]**2,fc[1]**2,As[1]**2],
[1.0,fy[2],fc[2],As[2],fy[2]**2,fc[2]**2,As[2]**2],
[1.0,fy[3],fc[3],As[3],fy[3]**2,fc[3]**2,As[3]**2],
[1.0,fy[4],fc[4],As[4],fy[4]**2,fc[4]**2,As[4]**2],
[1.0,fy[4],fc[5],As[5],fy[5]**2,fc[5]**2,As[5]**2],
[1.0,fy[6],fc[6],As[6],fy[6]**2,fc[6]**2,As[6]**2],
[1.0,fy[7],fc[7],As[7],fy[7]**2,fc[7]**2,As[7]**2],
[1.0,fy[8],fc[8],As[8],fy[8]**2,fc[8]**2,As[8]**2],
[1.0,fy[9],fc[9],As[9],fy[9]**2,fc[9]**2,As[9]**2],
[1.0,fy[10],fc[10],As[10],fy[10]**2,fc[10]**2,As[10]**2],
[1.0,fy[11],fc[11],As[11],fy[11]**2,fc[11]**2,As[11]**2],
[1.0,fy[12],fc[12],As[12],fy[12]**2,fc[12]**2,As[12]**2],
[1.0,fy[13],fc[13],As[13],fy[13]**2,fc[13]**2,As[13]**2],
[1.0,fy[14],fc[14],As[14],fy[14]**2,fc[14]**2,As[14]**2],
[1.0,fy[15],fc[15],As[15],fy[15]**2,fc[15]**2,As[15]**2],
[1.0,fy[16],fc[16],As[16],fy[16]**2,fc[16]**2,As[16]**2],
[1.0,fy[17],fc[17],As[17],fy[17]**2,fc[17]**2,As[17]**2],
[1.0,fy[18],fc[18],As[18],fy[18]**2,fc[18]**2,As[18]**2],
[1.0,fy[19],fc[19],As[19],fy[19]**2,fc[19]**2,As[19]**2],
[1.0,fy[20],fc[20],As[20],fy[20]**2,fc[20]**2,As[20]**2],
[1.0,fy[21],fc[21],As[21],fy[21]**2,fc[21]**2,As[21]**2],
[1.0,fy[22],fc[22],As[22],fy[22]**2,fc[22]**2,As[22]**2],
[1.0,fy[23],fc[23],As[23],fy[23]**2,fc[23]**2,As[23]**2],
[1.0,fy[24],fc[24],As[24],fy[24]**2,fc[24]**2,As[24]**2],
[1.0,fy[25],fc[25],As[25],fy[25]**2,fc[25]**2,As[25]**2],
[1.0,fy[26],fc[26],As[26],fy[26]**2,fc[26]**2,As[26]**2],
[1.0,fy[27],fc[27],As[27],fy[27]**2,fc[27]**2,As[27]**2],
[1.0,fy[28],fc[28],As[28],fy[28]**2,fc[28]**2,As[28]**2],
[1.0,fy[29],fc[29],As[29],fy[29]**2,fc[29]**2,As[29]**2],
[1.0,fy[30],fc[30],As[30],fy[30]**2,fc[30]**2,As[30]**2],
[1.0,fy[31],fc[31],As[31],fy[31]**2,fc[31]**2,As[31]**2],
[1.0,fy[32],fc[32],As[32],fy[32]**2,fc[32]**2,As[32]**2],
[1.0,fy[33],fc[33],As[33],fy[33]**2,fc[33]**2,As[33]**2],
[1.0,fy[34],fc[34],As[34],fy[34]**2,fc[34]**2,As[34]**2],
[1.0,fy[35],fc[35],As[35],fy[35]**2,fc[35]**2,As[35]**2],
[1.0,fy[36],fc[36],As[36],fy[36]**2,fc[36]**2,As[36]**2],
[1.0,fy[37],fc[37],As[37],fy[37]**2,fc[37]**2,As[37]**2],
[1.0,fy[38],fc[38],As[38],fy[38]**2,fc[38]**2,As[38]**2],
[1.0,fy[39],fc[39],As[39],fy[39]**2,fc[39]**2,As[39]**2],
[1.0,fy[40],fc[40],As[40],fy[40]**2,fc[40]**2,As[40]**2],
[1.0,fy[41],fc[41],As[41],fy[41]**2,fc[41]**2,As[41]**2],
[1.0,fy[42],fc[42],As[42],fy[42]**2,fc[42]**2,As[42]**2],
[1.0,fy[43],fc[43],As[43],fy[43]**2,fc[43]**2,As[43]**2],
[1.0,fy[44],fc[44],As[44],fy[44]**2,fc[44]**2,As[44]**2],
[1.0,fy[45],fc[45],As[45],fy[45]**2,fc[45]**2,As[45]**2],
[1.0,fy[46],fc[46],As[46],fy[46]**2,fc[46]**2,As[46]**2],
[1.0,fy[47],fc[47],As[47],fy[47]**2,fc[47]**2,As[47]**2],
[1.0,fy[48],fc[48],As[48],fy[48]**2,fc[48]**2,As[48]**2],
[1.0,fy[49],fc[49],As[49],fy[49]**2,fc[49]**2,As[49]**2],
[1.0,fy[50],fc[50],As[50],fy[50]**2,fc[50]**2,As[50]**2],
[1.0,fy[51],fc[51],As[51],fy[51]**2,fc[51]**2,As[51]**2],
[1.0,fy[52],fc[52],As[52],fy[52]**2,fc[52]**2,As[52]**2],
])
#####################################
```

*Figure H26. Matrix $\boldsymbol{A}$ based on the coordinates defined in figures H21, H22 and 23.*

The results of the corresponding NLFE anlyses are stored in array $\boldsymbol{G}$:

```
####################################
G = np.array([

#initial design point
[Fv[5]+Fh[5]-Rsf_ECOV],

#f=1.0
[Fv[16]+Fh[16]-Rsf_ECOV],[Fv[17]+Fh[17]-Rsf_ECOV],[Fv[18]+Fh[18]-Rsf_ECOV],
[Fv[19]+Fh[19]-Rsf_ECOV],[Fv[20]+Fh[20]-Rsf_ECOV],[Fv[21]+Fh[21]-Rsf_ECOV],
#Cross points f=1.0
[Fv[22]+Fh[22]-Rsf_ECOV],[Fv[23]+Fh[23]-Rsf_ECOV],[Fv[24]+Fh[24]-Rsf_ECOV],[Fv[25]+Fh[25]-Rsf_ECOV],
[Fv[26]+Fh[26]-Rsf_ECOV],[Fv[27]+Fh[27]-Rsf_ECOV],[Fv[28]+Fh[28]-Rsf_ECOV],[Fv[29]+Fh[29]-Rsf_ECOV],

#f=2.0
[Fv[30]+Fh[30]-Rsf_ECOV],[Fv[31]+Fh[31]-Rsf_ECOV],[Fv[32]+Fh[32]-Rsf_ECOV],
[Fv[33]+Fh[33]-Rsf_ECOV],[Fv[34]+Fh[34]-Rsf_ECOV],[Fv[35]+Fh[35]-Rsf_ECOV],

#f=1.5
[Fv[36]+Fh[36]-Rsf_ECOV],[Fv[37]+Fh[37]-Rsf_ECOV],[Fv[38]+Fh[38]-Rsf_ECOV],
[Fv[39]+Fh[39]-Rsf_ECOV],[Fv[40]+Fh[40]-Rsf_ECOV],[Fv[41]+Fh[41]-Rsf_ECOV],
#Cross points f=1.5
[Fv[42]+Fh[42]-Rsf_ECOV],[Fv[43]+Fh[43]-Rsf_ECOV],[Fv[44]+Fh[44]-Rsf_ECOV],[Fv[45]+Fh[45]-Rsf_ECOV],
[Fv[46]+Fh[46]-Rsf_ECOV],[Fv[47]+Fh[47]-Rsf_ECOV],[Fv[48]+Fh[48]-Rsf_ECOV],[Fv[49]+Fh[49]-Rsf_ECOV],

#extra
[Fv[64]+Fh[64]-Rsf_ECOV],[Fv[65]+Fh[65]-Rsf_ECOV],

#mean
[Fv[0]+Fh[0]-Rsf_ECOV],

#first two points
[Fv[1]+Fh[1]-Rsf_ECOV],[Fv[2]+Fh[2]-Rsf_ECOV],[Fv[3]+Fh[3]-Rsf_ECOV],

#control point
[GXc],

#iteration points
[GX1],[GX2],[GX3],[GX4],[GX5],[GX6],[GX7],[GX8],[GX9],[GX10],[GX11],
])
#########################################################################
```

*Figure H27. The results of the implicit LSF $\boldsymbol{G}$ based on the resistance of the NLFE analyses are stored in array $\boldsymbol{G}$.*

The unknown coefficients $\boldsymbol{b}$ can be determined with a least squares approach according to equation (2.27):

```
b = np.dot(np.dot(inv(np.dot(np.transpose(A1),A1)),np.transpose(A1)),G)
```

*Figure H28. The matrix $\boldsymbol{A}$ and $\boldsymbol{G}$ are used to calculate the unknown coefficients $\boldsymbol{b}$ according to equation (2.27).*

The response surface $\overline{\boldsymbol{G}}$ based on the NLFE analyses $\boldsymbol{G}$ with input parameters $f_y$, $f_c$ and $A_s$ is given in the standard normal space:

```
# Transformation LSF to standard normal space
mx1 = 560;sdx1 = 28.0;sdx_L1 = sqrt(np.log(sdx1**2/(mx1**2)+1));mx_L1 = np.log(mx1)-0.5*sdx_L1**2;
mx2 = 38; sdx2 = 5.7;sdx_L2 = sqrt(np.log(sdx2**2/(mx2**2)+1));mx_L2 = np.log(mx2)-0.5*sdx_L2**2;


b0 = np.asscalar(b[0])
b1 = np.asscalar(b[1])
b2 = np.asscalar(b[2])
b3 = np.asscalar(b[3])
b4 = np.asscalar(b[4])
b5 = np.asscalar(b[5])
b6 = np.asscalar(b[6])

def G(u1,u2,u3):
        x1 = exp(mx_L1+u1*sdx_L1)
        x2 = exp(mx_L2+u2*sdx_L2)
        x3 = mx3+u3*sdx3
        G = b0 + b1*x1 + b2*x2 + b3*x3 + b4*x1**2 + b5*x2**2 + b6*x3**2
        return G
```

*Figure H29. The response surface $\overline{\boldsymbol{G}}$ defined in the stand normal space.*

To use a FORM, the partial derivatives of the response surface $\overline{\boldsymbol{G}}$: $a_1 = \frac{\partial \bar{G}}{\partial u1}$, $a_2 = \frac{\partial \bar{G}}{\partial u2}$ and $a_3 = \frac{\partial \bar{G}}{\partial u3}$ are calculated with Maple and added to the python script:

```
#Differentiation with Maple:
def a1(u1,u2,u3):
        a1 = 0.9993758450e-1*(exp(0.4996879225e-1*u1+6.326688344))**2*b4+0.4996879225e-1*exp(0.4996879225e-1*u1+6.326688344)*b1
        return a1

def a2(u1,u2,u3):
        a2 = .2983327600*(exp(.1491663800*u2+3.626460856))**2*b5+.1491663800*exp(.1491663800*u2+3.626460856)*b2
        return a2

def a3(u1,u2,u3):
        a3 = (9.424777960*(4.712388980*u3+235.6194490))*b6+4.712388980*b3
        return a3
```

*Figure H30. Partial derivatives response surface $\overline{\boldsymbol{G}}$.*

Now the FORM is used to determine the design point $\boldsymbol{u}_*$ and the reliability index $\beta_R$ of the response surface $\overline{\boldsymbol{G}}$.

```
#step 1: Guess u0
u = np.array([-3.0,-3.0,-3.0])
u1 = u[0]
u2 = u[1]
u3 = u[2]
print u
beta1 = np.sqrt(np.dot(u,u))
print beta1
e = 10.0
i=0

alpha = np.zeros((3))
u123 = np.zeros((3))
i = 0
n = 3

while (e>0.0000001):

    beta0 = beta1

    #step 2
    gu = G(u1,u2,u3)
    #step 3
    dg1 = a1(u1,u2,u3)
    dg2 = a2(u1,u2,u3)
    dg3 = a3(u1,u2,u3)
    dg = np.array([dg1,dg2,dg3])
    #step 4
    u =dg*((np.dot(dg,u))-gu)/(np.dot(dg,dg))
    u1 = u[0]
    u2 = u[1]
    u3 = u[2]
    #step 5
    beta1 = np.sqrt(np.dot(u,u))
    #step 6
    e = abs(beta1-beta0)
    beta = beta1
    alpha12_store = dg/(np.sqrt(np.dot(dg,dg)))

for j in range (n):
    alpha[j] = alpha12_store[j]
    u123[j] = u[j]
```

```
print 'beta: '
print beta
print
print 'Phi(-beta): '
print norm.cdf(-beta)
print
print 'alpha1, alpha2 and alpha3: '
print alpha
print
print 'u1*, u2* and u3*: '
print u123
print

u1 = u123[0]
u2 = u123[1]
u3 = u123[2]
x1 = exp(mx_L1+u1*sdx_L1)
x2 = exp(mx_L2+u2*sdx_L2)
x3 = mx3+u3*sdx3
x123 = np.array([x1,x2,x3])

print 'x1* and x2*: '
print x123
print 'gu: '
print gu
```

*Figure H31. Python code to perform the FORM for stochastic variables in the standard normal space.*

### H.2.3 Case 3: rotational capacity corner D with uncertainty in the reinforcement detailing

Basically the same python script is used as for case 2 only a few modifications are made in order to implement a different coefficient of variation $V_{As}$ that is used for case 3.